# THE EXPLORATION OF AN EFFECTIVE MEDICAL COUNTERMEASURE ENHANCING SURVIVAL AND HEMATOPOIETIC RECOVERY AND PREVENTING IMMUNE INSUFFICIENCY IN LETHALLY-IRRADIATED MICE

Tong Wu

Submitted to the faculty of the University Graduate School
in partial fulfillment of the requirements
for the degree
Doctor of Philosophy
in the Department of Cellular and Integrative Physiology,
Indiana University

August 2020

Accepted by the Graduate Faculty of Indiana University, in partial fulfillment of the requirements for the degree of Doctor of Philosophy.

Doctoral Committee

_____
Christie M. Orschell, Ph.D., Chair

_____
David P. Basile, Ph.D.

June 24, 2020

_____
Joseph L. Unthank, Ph.D.

_____
Laura S. Haneline, M.D.

_____
Louis M. Pelus, Ph.D.

_____
Thomas J. MacVittie, Ph.D.

# DEDICATION

To my family, and in memory of my beloved family members that I have lost over these years, thank you for all your support and encouragement.

ACKNOWLEDGEMENT

First and foremost, I would like to thank my mentor Dr. Christie M. Orschell for accepting me in her lab. She has been a preeminent teacher and has provided me with insights and instructions during my academic training. Through the discussion and exchange of views with Christie, I not only received construction feedbacks but also learned the core of scientific attitude, which are of great importance to my future career.

I would like to thank my lab members, Dr. Artur Plett, Dr. Hui Lin Chua, Dr. Sasidhar Vemula, Dr. Rajendran Sellamuthu, Carol Sampson, Hailin Feng, Helen Chin Sinex, and Alexa Fisher; and Pelus lab members, Dr. Andrea Patterson, Dr. Pratibha Singh, Dr. Liqiong Liu and Dr. Hongge Li; and Max Jacobsen in Dr. George E. Sandusky's pathology lab, for their generous helping hands in organizing studies, reviewing manuscript, image processing, sharing immense knowledge and patiently answering my questions, providing technical training and technical assistance.

I would like to thank my committee members, Dr. Louis M. Pelus, Dr. Thomas J. MacVittie, Dr. David P. Basile, Dr. Joseph L. Unthank, and Dr. Laura S. Haneline, for their valuable inputs throughout these studies.

I also want to extend thanks to Dr. Louise Pay for her help in grammatical checking and corrections to the draft of my thesis; Jennifer Stashevsky for her help in Picrosirius red staining; Dr. Laura Wright for her help in measurement of bone marrow volume through micro CT in the bone marrow cytokine analysis.

Thanks Dr. Medhora at Medical College of Wisconsin for supplying lisinopril; Dr. George Cox at Bolder Biotech for supplying all the pegylated hematopoietic growth

factors; and Dr. Zuniga-Pflucker at University of Toronto for providing OP9 and OP9-DL4 cell lines.

Finally, I thank the members of the Flow Cytometry Resource Facility (FCRF) of the IU Simon Cancer Center and the Laboratory Animal Resource Center (LARC) of IU School of Medicine for their helps during completing these studies; and funding institutes and agencies which supported these studies, including the National Institute of Allergy and Infectious Diseases (NIAID) under contracts HHSN266200500043C and HHSN272201000046C and grants 1U01AI107340-01 and 2R44 AI088288-03A1, and National Institute on Aging (NIA) under grant R01AG046246-01, National Institutes of Health, Department of Health and Human Services, and the Department of Defense under grants PR140896, PR141527, and PR140433P1.

Tong Wu

# THE EXPLORATION OF AN EFFECTIVE MEDICAL COUNTERMEASURE ENHANCING SURVIVAL AND HEMATOPOIETIC RECOVERY AND PREVENTING IMMUNE INSUFFICIENCY IN LETHALLY-IRRADIATED MICE

There is an urgent demand for effective medical countermeasures (MCM) in the event of high-dose radiation exposure ranging from nuclear plant disasters to potential nuclear warfare. Victims of lethal-dose radiation exposure face multi-organ injuries including the hematopoietic acute radiation syndrome (H-ARS) and the delayed effects of acute radiation exposure (DEARE) years after irradiation. Defective lymphocyte reconstitution and its subsequent immune insufficiency are some of the most serious consequences of H-ARS and DEARE. In order to investigate potential MCMs to protect or mitigate these radiation injuries, the prolonged tissue-specific immunosuppression at all levels of lymphocyte development in established murine H-ARS and DEARE models was defined, along with unique sex-related and age-related changes present in some tissues but not others. The “double hits” of irradiation and age-related stress on lymphopoiesis led to significant myeloid skew and long-term immune involution. Different kinds and different combinations of hematopoietic growth factors, some in combination with angiotensin converting enzyme inhibitor, were administered to lethally irradiated mice. These radiomitigators were found to significantly increase survival and enhance hematopoiesis in H-ARS, but they did little to alleviate the severity of DEARE including immune insufficiency. 16,16 dimethyl-prostaglandin E2 (dmPGE2), a long-acting formulation of PGE2 with similar biological effects as PGE2, was found to enhance survival and hematopoiesis in lethal-irradiated mice when used as radiomitigator

or radioprotectant. The optimum time window for administration of radioprotectant and radiomitigator dmPGE2 was defined, which is -3hr to -15min prior to irradiation and +6hr to +30hr post irradiation. Significant survival efficacy of radioprotectant dmPGE2 was also demonstrated in pediatric and geriatric mice. Using specific PGE2 receptor (EP) agonists, the EP4 receptor was defined as the PGE2 receptor potentially responsible for dmPGE2 radioprotection. Radioprotectant dmPGE2 was also found to prevent radiation-induced thymic involution and to ameliorate the long-term immune suppression in radiation survivors in the DEARE phase via promoting hematopoietic stem cell differentiation towards to the lymphoid lineage. This is the first report of an effective MCM for H-ARS which also targets long-term thymic involution and lymphoid lineage reconstitution.

Christie M. Orschell Ph.D., Chair

TABLE OF CONTENTS

LIST OF TABLES

LIST OF FIGURES

LIST OF ABBREVIATIONS

| | |
|---|---|
| 13-PGR | 15- ketoprostaglandin D13-reductase |
| 15-PGDH | 15-hydroxyprostaglandin dehydrogenase |
| AA | Arachidonic acid |
| ACE | Angiotensin converting enzyme |
| ACEI | Angiotensin converting enzyme inhibitors |
| AcSDKP | N-acetyl-seryl-aspartyl-lysyl-proline |
| ADH | Antidiuretic hormone |
| AHS | Adult Health Study |
| Aire | Autoimmune regulator |
| AR | Animal Rule |
| ARB | Angiotensin II receptor blockers |
| ARS | Acute radiation syndromes |
| Ang I | Angiotensin I |
| Ang II | Angiotensin II |
| ATM | Ataxia-telangiectasia mutated kinase |
| BCS | Bovine calf serum |
| BFU-E | Burst-forming unit-erythroid |
| BM | Bone marrow |
| Bq | Becquerel |
| BSA | Bovine serum albumin |
| Cadm1 | Cell Adhesion Molecule 1 |
| cAMP | Cyclic adenosine monophosphate |

| | |
|---|---|
| CBC | Complete blood count |
| CCR5 | C-C chemokine receptor type 5 |
| CD62L | CD62 ligand |
| Cdk2 | Cyclin-dependent kinase 2 |
| Cdkn1c | Cyclin dependent kinase inhibitor 1C |
| CFC | Colony forming cell |
| CFU | Colony-forming unit |
| CFU-E | CFU-erythroid |
| CFU-GEMM | CFU-granulocyte/erythroid/macrophage/megakaryocyte |
| CFU-GM | CFU-granulocyte/macrophage |
| CFU-S | CFU-spleen |
| CFU-pre-B | Colony-forming unit-pre-B |
| Ci | Curie |
| c-kit | Stem cell factor receptor |
| CLP | Common lymphoid progenitor |
| CMJ | Cortico-medullary junction |
| CMP | Common myeloid progenitors |
| CNS | Central nerve system |
| COX | Cyclooxygenases |
| cTEC | Cortical thymic epithelial cell |
| CTZ | Chemoreceptor trigger zone |
| CXCR4 | C-X-C chemokine receptor type 4 |
| D | Day |

| | |
|---|---|
| DAG | Diglyceride |
| DAPI | 4’,6-diamidino-2-phenylindole |
| DDR | Dose response relationship |
| DEARE | Delayed effects of acute radiation exposure |
| DL | Delta-like |
| DmPGE2 | 16,16 dimethyl-prostaglandin E2 |
| DN | Double negative |
| DNA | Deoxyribonucleic acid |
| Dntt | DNA nucleotidylexotransferase |
| DP | Double positive |
| DRR | Dose response relationship |
| DSB | Double strand break |
| EDTA | Ethylenediaminetetraacetic acid |
| Efnb2 | Ephrin B2 |
| EMH | Extramedullary hematopoiesis |
| EoBP | Eosinophil/basophil progenitor |
| EP | PGE2 receptor |
| EPO | Erythropoietin |
| EpoR | EPO receptor |
| ETC | Electron transport chain |
| EtOH | Ethanol |
| ETP | Early thymic progenitor |
| Ets2 | ETS proto-oncogene 2, transcription factor |

| | |
|---|---|
| F | Female |
| FACS | Fluorescence-activated cell sorting |
| FBS | Fetal bovine serum |
| FDA | Food and Drug Administration |
| FDR | False discovery rate |
| Flt3 | FMS-like tyrosine kinase 3 |
| FLT3L | FMS-like tyrosine kinase 3 ligand |
| Furin | FES upstream region |
| G-CSF | Granulocyte colony-stimulating factor |
| GI | Gastrointestinal |
| GI-ARS | Gastrointestinal acute radiation syndrome |
| GM-CSF | Granulocyte macrophage colony-stimulating factor |
| GMP | granulocyte monocyte progenitor |
| GPCR | G-protein-coupled receptor |
| GSK-3 | Glycogen synthase kinase-3 |
| Gy | Gray |
| H-ARS | Hematopoietic-acute radiation syndromes |
| HBSS | Hank's balanced salt solution |
| H&E | Hematoxylin/eosin stain |
| HGF | Hematopoietic growth factor |
| HLA | Human leukocyte antigen |
| HPC | Hematopoietic progenitor cell |
| HPE | Homeostatic peripheral expansion |

| | |
|---|---|
| HSC | Hematopoietic stem cell |
| HSCT | Hematopoietic stem cell transplantation |
| HSPC | Hematopoietic stem and progenitor cell |
| Ifngr1 | Interferon gamma receptor 1 |
| IFN-γ | Interferon gamma |
| IHC | Immunohistochemistry |
| IL | Interleukin |
| Il6ra | Interleukin-6 receptor subunit alpha |
| IL-3 | Interleukin-3 |
| IL-7 | Interleukin-7 |
| IL7R | IL7 receptor |
| IP3 | Inositol trisphosphate |
| IP-10 | Interferon gamma-induced protein |
| IPA | Ingenuity pathway analysis |
| IR | Irradiated |
| IT-HSC | Intermediate-term HSC |
| K5/K14 | Cytokeratin 5/14 |
| K8/K18 | Cytokeratin 8/18 |
| KC | Keratinocyte chemoattractant |
| KGF | Keratinocyte growth factor |
| KM | Kaplan-Meier |
| LD | Lethal dose |
| LDR | Lymphocyte depletion rate |

| | |
|---|---|
| Lepr | Leptin receptor |
| LIF | Leukemia inhibitory factor |
| Lin | Lineage |
| Liso | Lisinopril |
| LIX | Lipopolysaccharide-induced CXC chemokine |
| Lmo1 | LIM domain only 1 |
| LMPP | Lymphoid-primed multipotent progenitors |
| LS | $Lin^{-}$ $Sca\text{-}1^{+}$ |
| LS $CD150^{+}$ | $Lin^{-}$ $Sca\text{-}1^{+}$ $CD150^{+}$ |
| LSK | $Lin^{-}$ $Sca\text{-}1^{hi}$ $c\text{-}Kit^{hi}$ |
| LSS | Life Span Study |
| LT-HSC | Long term-HSC |
| LY | Lymphocyte |
| M | Male |
| MCM | Medical countermeasure |
| MCSF | Macrophage colony-stimulating factor |
| MCSFR | MCSF receptor |
| MCP-1 | Monocyte chemoattractant protein-1 |
| MEP | Megakaryocyte erythrocyte progenitor |
| MFI | Median fluorescence intensity |
| MHC | Major histocompatibility complex |
| MIG | Monokine induced by gamma interferon |
| MIP-1α | Macrophage inflammatory protein 1 α |

| | |
|---|---|
| MIP-1β | Macrophage inflammatory protein 1 β |
| MIP-2 | Macrophage inflammatory protein 2 |
| m/o | Month-old |
| mo. | Months |
| MODS | Multiple organ dysfunction syndromes |
| MPP | Multipotent progenitor |
| MSC | Mesenchymal stromal cell |
| mTEC | Medullary thymic epithelial cell |
| mtDNA | Mitochondrial DNA |
| Myb | MYB proto-oncogene, transcription factor |
| NBF | Neutral buffered formalin |
| NE | Neutrophil |
| NI | Non-irradiated |
| NK | Natural killer |
| NOX | Nicotinamide adenine dinucleotide phosphate oxidase |
| NRC | Nuclear Regulatory Commission |
| NS | Not significant |
| NSAID | Nonsteroidal anti-inflammatory drug |
| PB | Peripheral blood |
| PBS | Phosphate buffered saline |
| Peg | Pegylated |
| PG | Prostaglandins |
| PGE2 | Prostaglandin E2 |

| | |
|---|---|
| PGI2 | Prostaglandin I2 |
| PI3K | Phosphoinositide 3-kinase |
| PIP2 | Phosphatidylinositol 4,5-bisphosphate |
| PKA | Protein kinase A |
| PKC | Protein kinase C |
| PLA2 | Phospholipase A2 |
| PLC | Phospholipase C |
| PLT | Platelet |
| PMA | Phorbol 12-myristate 13-acetate |
| Post-IR | Post-irradiation |
| Prkca | Protein kinase C alpha |
| R | Roentgen |
| Rad | Radiation absorbed dose |
| RANTES | Regulated upon activation normal T cell expressed and secreted |
| RAS | Renin-angiotensin system |
| RBC | Red blood cell |
| RBMD | Residual bone marrow damage |
| REM | Roentgen equivalent man |
| RGB | Red, green, and blue |
| rhSCF | Recombinant human stem cell factor |
| RNA | Ribonucleic acid |
| RNS | Reactive nitrogen species |
| Rora | RAR related orphan receptor A |

| | |
|---|---|
| ROS | Reactive oxygen species |
| RPKM | Reads Per Kilobase per Million |
| RTE | Recent thymic emigrant |
| Sca-1 | Stem cell antigen-1 |
| SCZ | Subcapsular zone |
| SDF1 | Stromal cell-derived factor 1 |
| SEM | Standard error of the mean |
| SLAM | Signaling lymphocyte activation molecule |
| Smad7 | Mothers against decapentaplegic homolog 7 |
| SP | Single positive |
| SQ | Subcutaneous |
| Stat3 | Signal transducer and activator of transcription 3 |
| ST-HSC | Short-term HSC |
| Sv | Sievert |
| TBI | Total body irradiation |
| TC | Triple combination |
| TC+L | TC + lisinopril |
| TCM | Central memory T |
| TCR | T cell receptor |
| TEC | Thymic epithelial cell |
| TEM | Effector memory T cell |
| Tgfbr1 | Transforming growth factor beta receptor 1 |
| Tk1 | Thymidine kinase 1 |

| | |
|---|---|
| TNF-α | Tumor necrosis factor alpha |
| TSP | Thymus-seeding progenitor |
| TXA2 | Thromboxane A2 |
| UD | Undetectable |
| UEA1 | Ulex europaeus agglutinin 1 |
| VEGF | Vascular endothelial growth factor |
| Veh | Vehicle |
| vWF | von Willebrand factor |
| WBC | White blood cell |
| w/o | Week-old |
| Zmiz1 | Zinc finger MIZ-type containing 1 |

# Chapter 1. Introduction

## 1.1. Rationale and Overview

There is an urgent demand for effective medical countermeasures (MCM) in the event of high-dose radiation exposure ranging from nuclear plant disasters to potential nuclear warfare. The first and only use of nuclear weapons to date occurred in Japan in 1945, when US forces dropped the atomic bombs “Little Boy” and “Fat Man” over Hiroshima and Nagasaki, respectively. While this act ended the Second World War, it resulted the deaths of over 200,000 people, over 80% of whom were civilians. This culminated in a loss of 28% of the population of Hiroshima, and 39% of the population of Nagasaki. Approximately 35,000 people in Nagasaki and 70,000 people in Hiroshima were killed instantly. The remaining victims died as a result of high-dose radiation exposure, typically within 20-30 days. At the time, the symptoms of high-dose radiation exposure were unknown, and were referred to as “atomic bomb disease” or “radiation poisoning”. Infection, hemorrhage, and multiple-organ failure were the main causes of death. Antibiotics and repeated blood transfusions were given, with limited success [1, 2]. Survivors suffered long-term effects of radiation exposure, including malignancies, birth defects in their offspring, cataracts, and cognitive decline [3, 4].

Nuclear reactors are another source of radiation threat. Explosions followed by core meltdown at Chernobyl (1986) and Fukushima (2011) nuclear power plants exposed employees and firefighters to high-dose radiation at the reactor site, and civilians to radiation from contaminated air, water, and soil. The Chernobyl accident released over four hundred times the amount of radioactive material in comparison with the atomic

bombs in Japan; however, due to the relative underpopulation of the surrounding area, mortality was significantly lower [5].Two hundred people in Chernobyl suffered acute complications similar to the atomic bombing victims, with 31 deaths within the first three months. Over 200,000 emergency workers, police, soldiers, firefighters, and volunteers responsible for clean-up after the Chernobyl accident experienced negative effects from radiation exposure at varying doses. The nearby city of Pripyat was evacuated the day after the accident, and an exclusion zone of 30 km radius around the site was instituted in the following years. The accident displaced over 300,000 people. However, people residing nearby were exposed to repeated low-dose radiation, and according to epidemiological studies, 4,000 cancer deaths occurred in the next 30 years among this population. This cancer rate is significantly higher than the global average [6, 7]. In the Fukushima accident, less radioactive material was released as the plant's radioactive cores remained largely intact. No immediate deaths occurred; however, it was confirmed that a worker died from radiation-related cancer in 2018. The impact of the release of radioactive material into the sea is still unknown, as are long-lasting health implications for people in the area surrounding the plant [4, 8].

During the Cold War years that followed World War II, the United States and the then Soviet Union stockpiled around 125,000 nuclear warheads between them. Most sovereign states participated in the 1970 Treaty on the Non-Proliferation of Nuclear Weapons, and the Soviet Union dissolved in 1991, resulting in a dramatic decrease of global nuclear warheads to under 15,000 among nine nations [9]. However, the threat from nuclear war to mankind is still a possibility. The use of nuclear energy presents the

most credible risk of radiation exposure through nuclear plant accidents. Over 100 serious nuclear accidents have been recorded since the first use of nuclear power. Two-thirds of these occurred in the USA [10]. Technological and safety advances have minimized risk; however, unpredictable factors such as the earthquake and tsunami responsible for the Fukushima accident pose a threat to these nuclear facilities. The development of interventions for people exposed to high-dose radiation is required to reduce mortality after nuclear accidents and warfare globally. This motivated me in Dr. Orschell's laboratory to study MCMs in response to high-dose radiation exposure.

### 1.2. Types of Ionizing Radiation

There are five types ionizing radiation: alpha, beta, gamma, x-ray, and neutron (Figure 1). Alpha, beta, and neutron radiation consists of small particles; gamma radiation and x-rays are high-energy photon waves. Alpha particles are ejected from unstable nuclei during alpha decay and are identical to the nucleus of helium, with the absence of surrounding electrons. These particles can travel only a few centimeters in air, thus their penetrating capacity is weak and can be blocked by clothing. Beta particles are high-energy electrons released during radioactive decay, with a smaller mass than alpha particles. They can travel approximately one meter in air, and have a higher penetrating capacity than alpha particles, though can be blocked by a thin aluminum plate. Beta particles are capable of penetrating the skin to the germinal layer, potentially resulting in injury. Alpha and beta radiation generally do not pose a serious risk to human health unless inhaled or ingested.

**Figure 1**

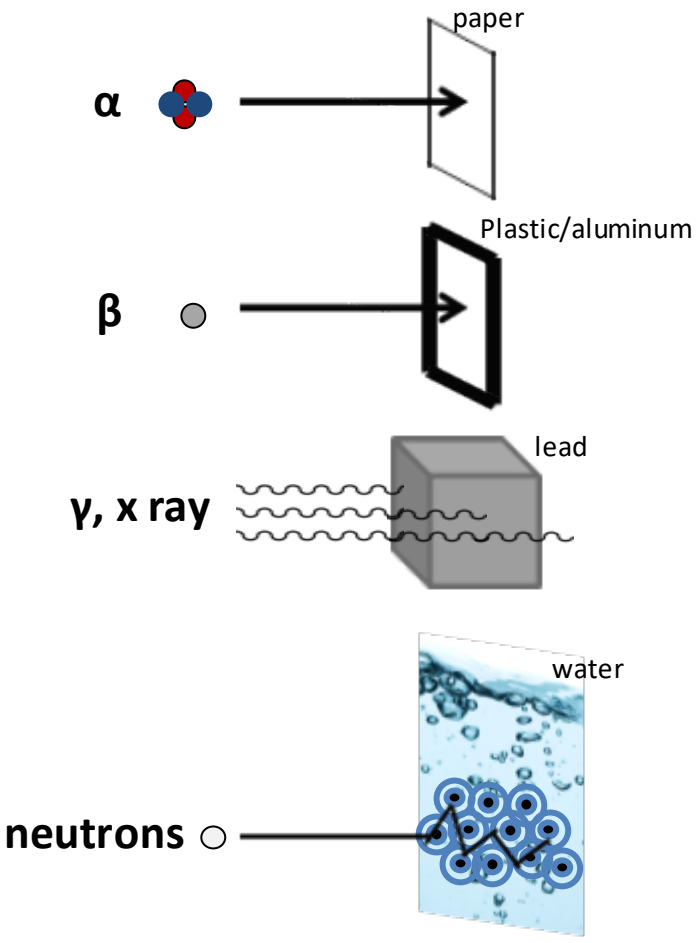

**Figure 1. Types of ionizing radiation.**

In the five types of ionizing radiation, alpha, beta and neutron radiation are small particles; gamma and x radiation are photon waves. Alpha radiation travels only a short distance with weak penetrating ability. Beta radiation travels longer and has higher penetrating ability than alpha radiation but still easily be blocked by a thin aluminum plate. Gamma and x radiation travels far in air and easily penetrate body tissue, which could be blocked by dense material such as lead. Neutron, which has excellent penetration ability, its effect is dependent on ionizing other atoms. Only hydrogen-rich material such as water can effectively block neutron radiation. The main radiation source in this thesis is gamma radiation. Figure adapted from Wikipedia contributors. (2020, June 21). Ionizing radiation. In Wikipedia, The Free Encyclopedia. Retrieved July 14, 2020, from https://en.wikipedia.org/wiki/Ionizing_radiation.

The fission of radioactive atoms results in the emission of numerous neutrons, which are uncharged. Neutron radiation is indirectly ionizing as a result of subsequent ionization of other atoms when the free neutrons react with other nuclei. Neutrons can travel hundreds or even thousands of meters in air and have high penetration ability -- only hydrogen-rich material can effectively block neutron radiation. Nuclear reactors are surrounded by meter-thick concrete or water outer layers for this reason [11, 12]. Alpha, beta, and neutron particles are either low-penetrating or hard to control, and thus are unlikely to be used in warfare, unlike gamma and x-rays, which pose a more significant threat (Figure 1).

Gamma and x-rays are electromagnetic radiation, with waves similar to visible light in form, but higher in energy. Both travel far in air and are high-penetrating, capable of reaching bodily tissue. This results in electron displacement and energy release sufficient to burn surrounding tissues. Gamma and x-rays are blocked only by extremely dense material such as lead. Common gamma radiation sources are $^{137}$Cs, $^{131}$I, $^{60}$Co, $^{226}$Ra, and $^{99m}$Tc. The $^{137}$Cs source was used in following studies. The difference between gamma and x-ray is controversial, though it is generally accepted that gamma radiation is emitted from the atom's nucleus, whereas x-rays are emitted from the electron cloud. Gamma radiation has a shorter wavelength and higher photon energy than x-rays [13, 14].

### 1.3. Radiation Quantities

The U.S. Nuclear Regulatory Commission (NRC) defines four radiation dose units: radioactivity, exposure, absorbed dose, and dose equivalent. The dose unit for radioactivity is the curie (Ci, British) or becquerel (Bq, international) and represents the number of decayed atoms in a material over a specific time. The does unit for exposure is roentgen (R), representing the amount of ionization in the air. The absorbed dose is the amount of energy absorbed by a defined mass of tissue, and its dose unit is gray (Gy) or radiation absorbed dose (Rad). The dose equivalent measures the clinical effect of radiation on the body as a product of the absorbed dose and tissue weighting factor, which varies depending on tissue sensitivity to radiation. It is expressed as roentgen equivalent man (REM) or Sievert (Sv) [11, 15]. The Gy or cGy (1 Gy = 100 cGy = 100 Rad) are used as the radiation unit in following studies.

The dose rate in the following studies refers to the rate of radiation dose exposure, measured in cGy per minute. Higher dose rates are associated with a more severe response to the radiation and increased carcinogenic risk [15]. Dose rate allows us to calculate the time necessary for whole-body irradiation. E.g. if the target dose for a mouse is 8.72 Gy, and the dose rate is 89.14 cGy/minute, the exposure time is 9 minutes and 47 seconds (8.72 Gy/89.14 cGy/minute = 9.78 minutes).

### 1.4. Biological Effects of Ionizing Radiation

The biological effects of ionizing radiation lead to the symptoms of radiation sickness. Absorbed radiation affects multiple cellular organelles. It disrupts atomic bonds

directly or indirectly via water radiolysis, which produces reactive oxygen species (ROS) and reactive nitrogen species (RNS). $^{137}Cs$ gamma radiation causes 60 nmol/L ROS per nanogram of tissue within one microsecond post- irradiation (post-IR) [16]. ROS metabolites produced via water radiolysis are predominantly $O_2^{\bullet -}$, $^{\bullet}OH$, and $H_2O_2$, causing deoxyribonucleic acid (DNA) damage via the induction of abasic sites and base oxidation, contributing to carcinogenic mutagenesis [17, 18]. These free radicals also oxidize accessory structures such as histone, which is critical for gene regulation and DNA packaging (Figure 2), and cause protein carbonylation and lipid peroxidation in non-nuclear organelles. The mitochondria are particularly affected as they produce most of the intracellular ROS. The mitochondria are responsible for energy production and oxidation-reduction balance [19-21], and persistent increased mitochondrial oxidative stress and heritable mitochondrial DNA (mtDNA) damage post-IR contributes to accelerated aging [17, 22].

Radiation-induced mitochondrial DNA damage occurs through several mechanisms. Firstly, radiation-induced lipid peroxidation disrupts the mitochondrial membrane, which is the location of the electron transport chain (ETC) [23]. Subsequent electron leakage from the ETC reduces $O_2$, producing more superoxide, leading to mitochondrial dysfunction, mitochondrial DNA mutation, and apoptosis [24]. Secondly, radiation damages protein translocation machinery, impairing the import of cytosolic proteins required for mitochondrial biogenesis into the mitochondria [25, 26]. Thirdly, radiation damages mtDNA in the same way as it does nuclear DNA, inducing abasic sites and base oxidation. This damage is heritable and transmitted to new mitochondria

**Figure 2**

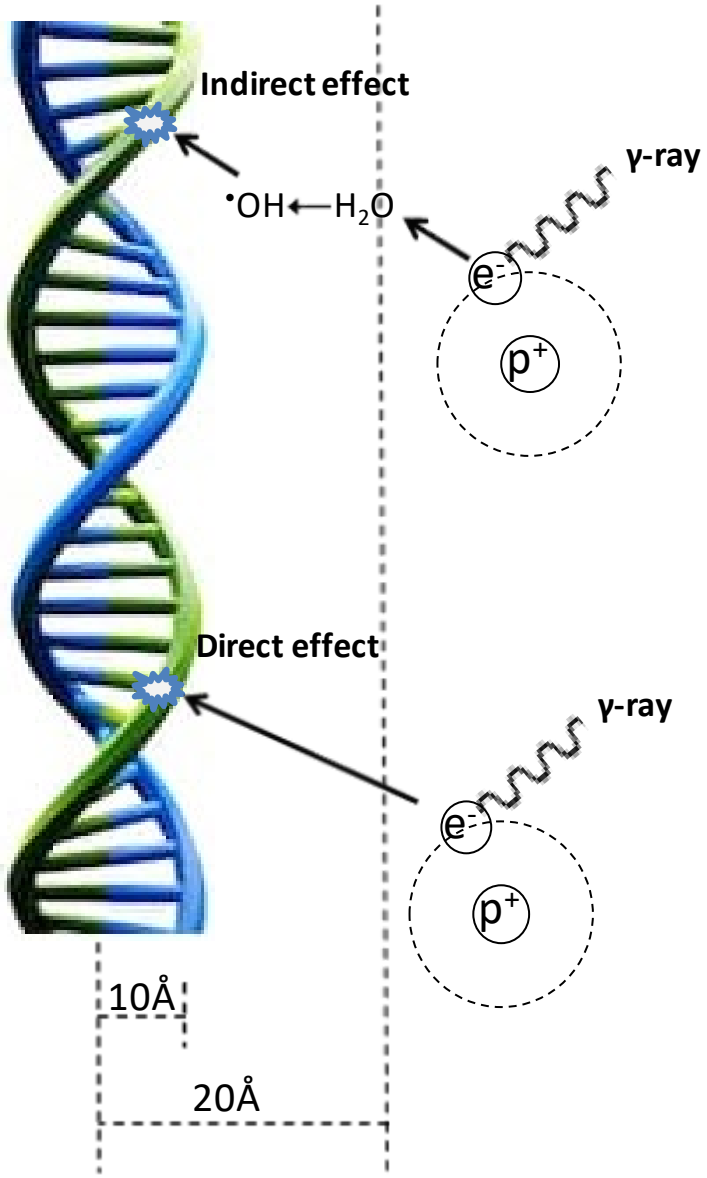

**Figure 2. Direct and indirect effects of ionizing radiation.**

There are two types of biological effects of ionizing radiation: the direct effect and the indirect effect. The disruption of DNA structure by indirect effect is mainly mediated by the production of ROS and RNS. The indirect damage is generally more severe than the direct damage since indirect effect also brings damage to other organelles as shown in Figure 3. Figure adapted from Hall, E. J. and Giaccia, A. J., Radiobiology for the Radiologist. 2012 [27].

generated post-IR [17, 28]. Finally, fragments of damaged mtDNA can migrate into the nucleus and insert into the nuclear genome during DNA double strand break (DSB) repair, which is induced by radiation. These insertions further increase radiation-induced genomic instability, heightening the potential for carcinogenesis [17] (Figure 3).

Another characteristic of radiation is the bystander effect, in which non-irradiated (NI) cells are affected by radiation through communication with irradiated cells. Several possible mechanisms have been proposed. Free radicals and cytokines produced by irradiated cells may impact non-irradiated cells via paracrine signaling [29]. Epigenetic alteration may also occur as a result of non-coding ribonucleic acid (RNA, such as miRNA or siRNA, which silence gene expression) detaching from irradiated cells and altering gene expression in non-irradiated cells [30]. mtDNA fragments also contribute to the bystander effect by migrating to non-irradiated cells [17]. Understanding of the biological effects of ionizing radiation helps delineate the short- and long-term effects of radiation, and the pharmacological mechanism of treatments.

### 1.5. Illnesses and Treatments Related to Radiation Exposure

#### 1.5.1. Acute radiation syndrome

Less than 24 hours after exposure to high doses of ionizing radiation, victims develop a continuum of multi-system symptoms referred to as acute radiation syndrome (ARS). Different tissues have different radio-sensitivity; less-differentiated and actively-proliferating cells are the most sensitive (Law of Bergonié and Tribondeau) [11, 31].

**Figure 3**

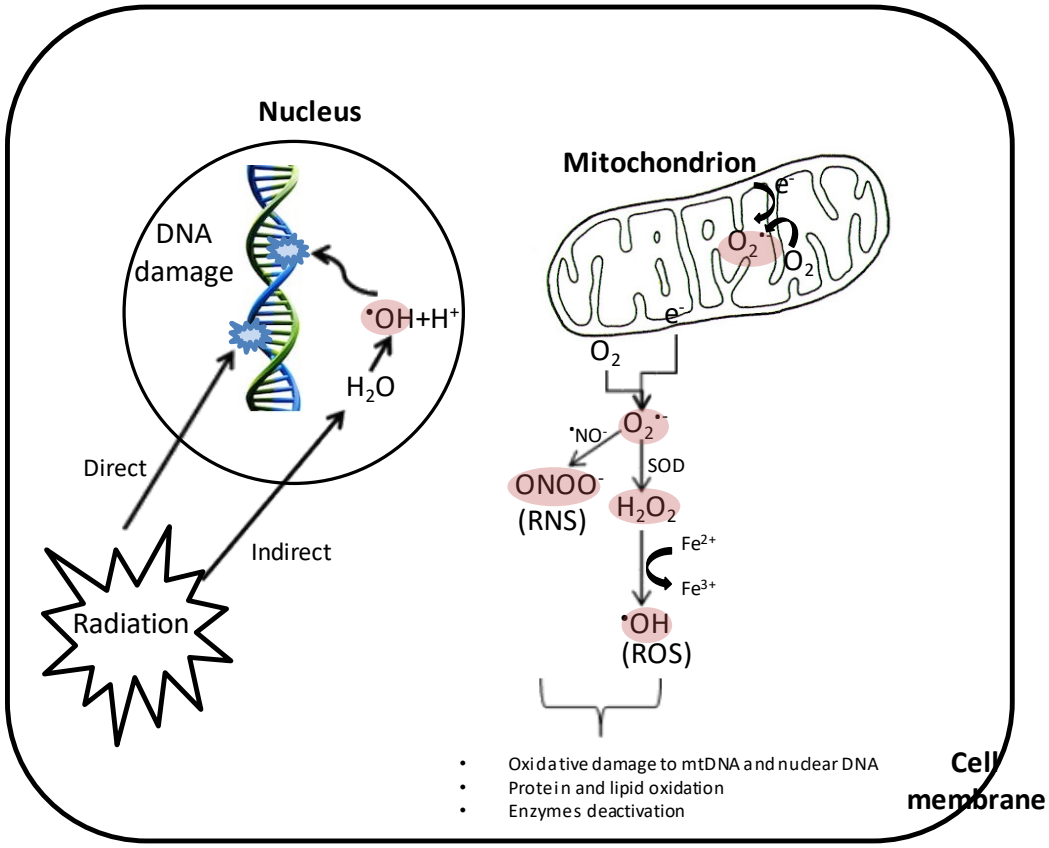
Nucleus
DNA damage
•OH+H+
H2O
Direct
Indirect
Radiation
Mitochondrion
e-
O2
O2•-
O2
e-
O2
•NO-
O2•-
SOD
ONOO-
(RNS)
H2O2
Fe2+
Fe3+
•OH
(ROS)
• Oxidative damage to mtDNA and nuclear DNA
• Protein and lipid oxidation
• Enzymes deactivation
Cell membrane

**Figure 3. Biological effects of ionizing radiation.**

Ionizing radiation causes direct damage to DNA structure, or indirect damage to DNA and mitochondrion by the free radicals produced from water radiolysis. The free radicals, mainly ROS and RNS, oxidize and permanently change the structure of lipids, proteins, nuclear DNA and mtDNA. Figure adapted from Azzam, E.I., Jay-Gerin, J.P. and Pain, D., Ionizing radiation-induced metabolic oxidative stress and prolonged cell injury. Cancer Lett, 2012 [17].

There are four stages of ARS: the prodromal phase, latent phase, manifestation phase and recovery/death phase (Figure 4). When the radiation dose is extremely high (>50 Gy), victims quickly progress into unconsciousness and hypotension, and death will occur within 48 hours as a result of neurologic and cardiovascular collapse (Figure 5) [32]. When the radiation does is less than 1 Gy, although there is sub-clinical damage to hematological system, the victim is generally asymptomatic. At a dose higher than 1 Gy but not at a level considered extremely high (e.g. 2-10 Gy), digestive tract symptoms appear first, including nausea, vomiting, and anorexia. This results from radiation-induced damage to the vomiting center of the chemoreceptor trigger zone (CTZ) in the medulla oblongata, as opposed to direct digestive tract damage. Typically, these symptoms persist no longer than 48 hours [15], and are followed by a short latent phase in which the victim appears to recover before live cell numbers decrease below the clinical threshold. The latent phase period varies and is inversely proportional to radiation dose. The subsequent manifestation phase results from cell depletion and dysfunction of the hematopoietic, gastrointestinal, and central nervous systems. This phase can last from days to months. If victims receive sub-lethal irradiation dose, the recovery phase will follow; without treatment, death is highly probably in victims exposed to a lethal dose (LD). LD××/×× days is used to define a lethal dose, representing number of deaths over time, i.e. LD70/30 means at this dose, 70% of the irradiated population will die within 30 days [11, 33].

**Figure 4**

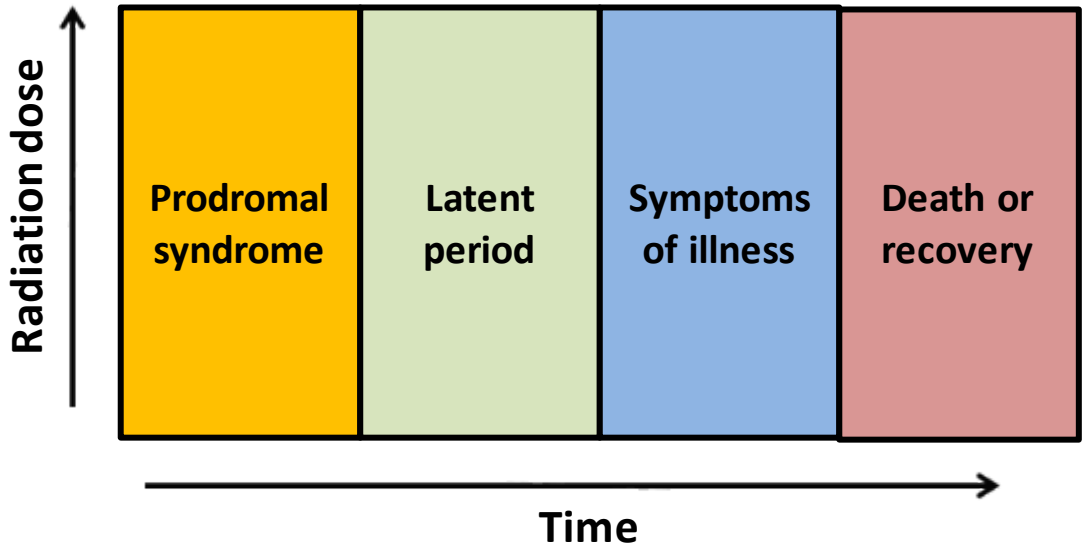
Radiation dose
Prodromal syndrome
Latent period
Symptoms of illness
Death or recovery
Time

**Figure 4. Stages of acute radiation syndrome.**

The prodromal syndrome develops first, followed by a latent period and then symptoms of illness shows up. The severity of symptoms at prodromal syndrome stage and symptoms of illness stage is directly proportional to radiation dose. The time of the latent period is inversely proportional to radiation dose. Figure adapted from Hall, E. J. and Giaccia, A. J., Radiobiology for the Radiologist. 2012 [27].

**Figure 5**

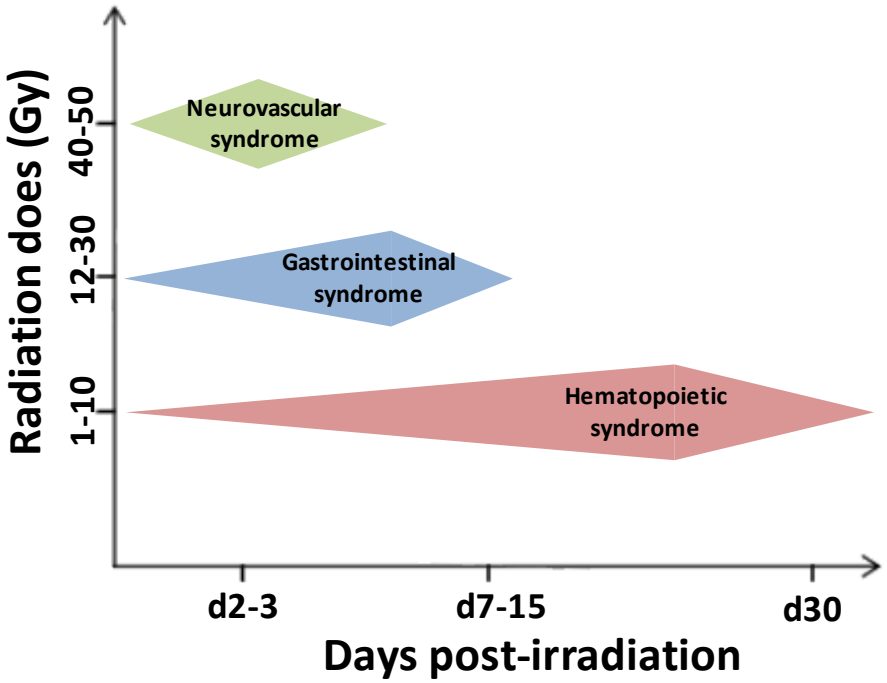
Radiation does (Gy)
40-50
12-30
1-10
Neurovascular syndrome
Gastrointestinal syndrome
Hematopoietic syndrome
d2-3
d7-15
d30
Days post-irradiation

**Figure 5. Acute radiation syndrome in different organs.**

Neurovascular system is one of the most radio-resistant system and victims will quickly progress death once the neurovascular symptoms develop. Hematological system is one of the most radio-sensitive system where the low radiation dose even as 1 Gy could induce sub-clinical damages and the recovery phase is late at around days 20-30 post-irradiation. If victims received lethal dose of radiation, there will be no recovery phase and will progress to death earlier. The radio-sensitivity of the gastrointestinal system is in the middle of neurovascular system and hematological system. Figure adapted from Seedhouse, E., Space Radiation and Astronaut Safety. 2018 [34].

#### 1.5.1.1. Gastrointestinal acute radiation syndrome

The epithelial cells lining the gastrointestinal (GI) tract are highly sensitive to radiation as they slough and replenish on a regular basis. In humans, Gastrointestinal acute radiation syndrome (GI-ARS) occurs following exposure to radiation >5 Gy. In addition to the nausea, vomiting, and anorexia observed in the prodromal phase, victims experience abdominal cramps, watery diarrhea, hematemesis, and melena. This results from compromise of the GI barrier, impairing the balance of absorption, secretion, and excretion. Associated dehydration and electrolyte imbalance can be lethal. The breakdown of GI integrity also increases the movement of normal or pathogenic bacteria from the GI into blood, leading to bacteremia and sepsis. Because the hematopoietic system is also inhibited, severe infection can lead to septic shock, multiple organ dysfunction syndromes (MODS), and death [32, 33, 35].

#### 1.5.1.2. Cerebrovascular acute radiation syndrome

Compared to the digestive and hematopoietic systems, the central nerve system (CNS) is relatively radioresistant. Although low-dose irradiation can disturb the vomiting center in the prodromal phase and induce some functional disorders, these effects are transient and no measurable damage occurs in the brain until the radiation dose reaches 10 Gy. The typical symptoms at total-body irradiation (TBI) doses >20 Gy include nausea, vomiting, dizziness, headache, disorientation, hypo- or hyper-reflexia, ataxia, seizure, delirium and dementia. The mechanism is believed to be due to direct nerve cell damage and indirect capillary circulation damage. The latter compromises blood-brain barrier integrity and leads to interstitial edema and intracerebral hemorrhage, contributing

to intracranial hypertension, brain herniation, and circulatory collapse. Most cerebrovascular damages are irreversible and severe symptoms generally represent poor prognosis [11, 15, 32].

#### 1.5.1.3. Hematopoietic acute radiation syndrome

Hematopoietic cells are the most proliferative cell type and the majority of bone marrow (BM) cells are immature progenitors. Thus, the hematopoietic system is one of the most radiosensitive, and a dose as low as 0.2 Gy can induce cell cycle arrest. Transient, mild cytopenia occurs at 0.2 - 2 Gy without significant clinical manifestations. Victims may experience prodromal symptoms such as nausea and fatigue. Clinical hematopoietic acute radiation syndrome (H-ARS) occurs when the absorbed dose is above 2 Gy [11, 33], and symptoms will not be apparent until circulating cell numbers have dropped significantly. The symptoms of H-ARS are due to leukopenia, which leads to susceptibility to infection and poor wound healing; erythropenia, leading to anemia, fatigue, and heart failure; and thrombocytopenia, leading to petechiae, purpura, and hemorrhage [15]. The radiosensitivity of blood cells varies by type. Lymphocytes (LY) are the most sensitive, despite being terminally-differentiated, and are the first population to be depleted in H-ARS [11]. LY depletion is positively proportional to the absorbed dose. The lymphocyte depletion rate (LDR) is used as a biodosimetry method. Biodosimetry is the measure of biological parameters to estimate the radiation dose a person has received (Figure 6). LDR is more accurate than observing clinical symptoms and less complicated than other biodosimetry, such as dicentric chromosome analysis or fluorescence in situ hybridization [11, 36]. LY depletion begins in the first 6-24 h after

**Figure 6**

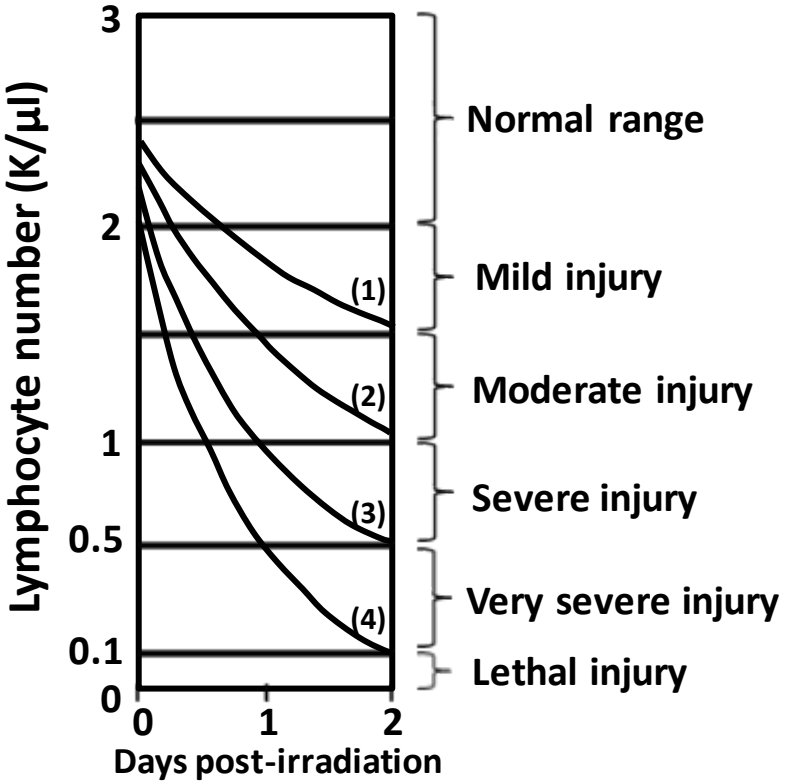
Lymphocyte number (K/µl)
3
2
1
0.5
0.1
0
0
1
2
Days post-irradiation
(1)
(2)
(3)
(4)
Normal range
Mild injury
Moderate injury
Severe injury
Very severe injury
Lethal injury

**Figure 6. Classical Andrews lymphocyte depletion kinetics and accompanying clinical severity ranges.**

Lymphocyte decreasing rate and degree of the decline is positively proportional to the absorbed radiation dose. The lymphocyte depletion rate is used as a biodosimetry method. Curves 1 to 4 roughly represent the following does of TBI: (1): 3.1 Gy; (2): 4.4 Gy; (3): 5.6 Gy; (4): 7.1 Gy. Figure adapted from Christensen, D.M., Iddins, C.J. and Sugarman, S.L., Ionizing radiation injuries and illnesses. Emerg Med Clin North Am, 2014 [11].

exposure and reaches nadir at 3-6 days, depending on the radiation dose. Neutrophils (NE) deplete to their lowest level 1- 2 weeks after TBI dosage greater than 2 Gy in human, which is later than LY [37, 38]. Neutropenia and lymphocytopenia render victims immunocompromised and highly susceptible to infection in the nadir phase. Red blood cells (RBC) and platelets (PLT) are considerably less radiosensitive than white blood cells (WBC). RBC typically renew every 120 days; PLT every 8-9 days; and they are non-nucleated end-product cells with terminal differentiation. Thus, RBC depletion is slow and nadir is not remarkable [11]. The decline pattern of PLT is similar to NE, reaching nadir 1- 2 weeks after exposure to a lethal dose. The time to nadir and the nadir level is inversely proportional to radiation dose, whereas nadir duration is positively proportional to the absorbed dose. The lower the nadir level and the longer its duration is, the risk of infection and hemorrhage risk increases, thus increasing the mortality risk [32].

#### 1.5.1.4. Other ARS sub-syndromes

Due to the limitations of this study, further ARS sub-syndromes are not discussed in detail. However, radiation also damages the eyes, skin, endocrine system, urogenital system, etc., some of which show specific ARS symptoms [11]. Additionally, inhalation or digestion of alpha and beta particles causes internal exposure and subsequent ARS in exposed organs, which may be more severe than ARS resulting from external exposure [15].

### 1.5.2. Deterministic and stochastic effects of ionizing radiation

Most of the discussed ARS are deterministic effects of ionizing radiation, meaning that the dose of radiation determines the severity of the effect. There are two characteristics of deterministic effect. Firstly, the severity of the effect is proportional to the absorbed dose. Secondly, there is a dose threshold and symptoms occur only when the dose is at or above this threshold. It is due to the damage of many cells by radiation. The shape of the curve is sigmoid (Figure 7). The effects on testis and bone marrow are the examples of the deterministic effect, which have the lowest thresholds of body tissue (0.15 Gy for testis and 0.5 Gy for bone marrow) [33].

In contrast, stochastic effects occur by chance. The probability of occurrence is proportional to the dose of radiation, but there is no obvious threshold, and the effect can occur even if only one cell is damaged. The shape of the curve is linear. Malignancy induced by irradiation an example of stochastic effect [15, 39] (Figure 7).

### 1.5.3. Delayed effects of acute radiation exposure

Delayed effects of acute radiation exposure (DEARE) is a spectrum of chronic illnesses involving multiple systems after years post-IR, which is the result of oxidative stress, inflammation, fibrosis, and loss of stem cell self-renewal in the ARS survivors [40, 41]. Little is known about DEARE in comparison with ARS, and most knowledge are gleaned from observing atomic bomb survivors and post-radiotherapy cancer survivors. There are three types of DEARE: somatic, genetic (hereditable), fetal (in utero). In following studies, somatic effect is the focus.

**Figure 7**

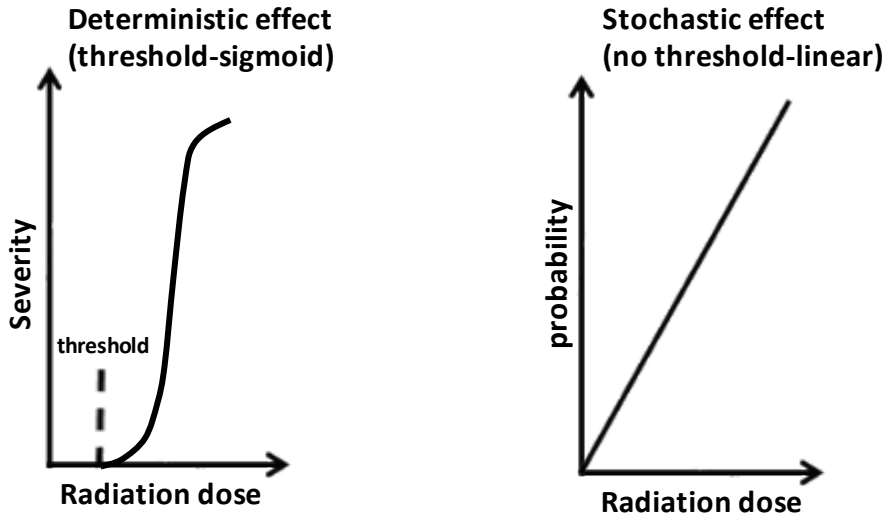
Deterministic effect
(threshold-sigmoid)
Severity
threshold
Radiation dose
Stochastic effect
(no threshold-linear)
probability
Radiation dose

**Figure 7. Deterministic effects and stochastic effect of radiation.**

Deterministic effect occurs when victim exposes to radiation exceeding a certain level (threshold). The higher the radiation dose, the more severe deterministic effect will be. The reason for deterministic effect is the cell killing/death. Stochastic effect does not have a threshold and does not happen at everyone exposed to radiation. The higher the radiation dose, the higher probability of certain stochastic effect (such as cancer) will be. It is due to accumulated damage to DNA and malignant proliferation. Figure adapted from Chouker, A., Stress Challenges and Immunity in Space. 2020 [42].

#### 1.5.3.1. Non-cancer diseases

According to the Life Span Study (LSS) and Adult Health Study (AHS) of the Hiroshima and Nagasaki atomic bomb survivors, cataract, thyroid disease, hyperparathyroidism, chronic liver disease and cirrhosis, uterine myoma, hypertension, myocardial infarction, stroke, chronic kidney diseases, pneumonia/influenza [3, 43] are significantly associated with radiation. Cancer survivors who received radiotherapy of the abdomen or pelvis have been reported to develop delayed radiation enteropathy, presenting as featured as malabsorption or dysmotility [44]. The risk for late-onset chronic kidney disease is increased significantly in patients receiving >16 Gy TBI before hematopoietic stem cell transplantation [45]. In patients receiving thoracic radiotherapy, around 5-15% develop symptomatic pneumonitis and 43% experience radiation-induced pneumonitis or pulmonary fibrosis 6-24 months after treatment [46, 47]. Neurocognitive deficits occur several months to years after treatment in 30-50% of patients who received radiotherapy for brain tumors [48, 49]. Some of the effects seen after radiotherapy were not reported in atomic bomb survivors as the TBI they received was much lower than targeted dose administered to specific organs during radiotherapy. According to the stochastic effect rule, the higher the dose, the higher possibility of a late effect occurs. The LD50 for humans is 4 Gy in TBI, but the dose required to eradicate an epithelial tumor is 60-80 Gy. This dose is achieved by providing multiple fractionated irradiations directed at the target organ.

#### 1.5.3.2. Solid tumors and hematopoietic malignancies

Unlike in radiotherapy, atomic bomb survivors received penetrating TBI, and their risk for developing malignancies increased in multiple organs and systems as a consequence. Over the years following radiation exposure, the risk for solid tumor development gradually increases at a greater extent than the age-related risk of tumors in non-irradiated humans (Figure 8). There is a significant linear dose-response relationship to tumor development in cancers of the oral cavity, esophagus, stomach, colon, liver, lung, etc. Other factors also increase risk, such as gender, age at exposure, time after exposure, and lifestyle. The relative risk for total solid tumors is 50% higher in females than males, and two-fold higher in survivors irradiated at a younger age than at an older age [3, 50, 51].

The latent period for hematopoietic malignancies is much shorter than for solid tumors. Leukemia is the predominant radiation-related cause of death in the early years post-exposure. The first instance of radiation-induced leukemia was reported 7 years after the atomic bombing of Japan[52]. In atomic bomb survivors, the risk for developing leukemia peaked 8-10 years after exposure and then rapidly decreased [53]. Risk for myelodysplastic syndromes (MDS) is also associated with radiation; unlike leukemias, these develop later in life [54]. There is little evidence to indicate that radiation exposure increases risk for lymphomas or multiple myeloma [55].

#### 1.5.3.3. Residual bone marrow damage

DEARE effects on the hematopoietic system are known as residual bone marrow

**Figure 8**

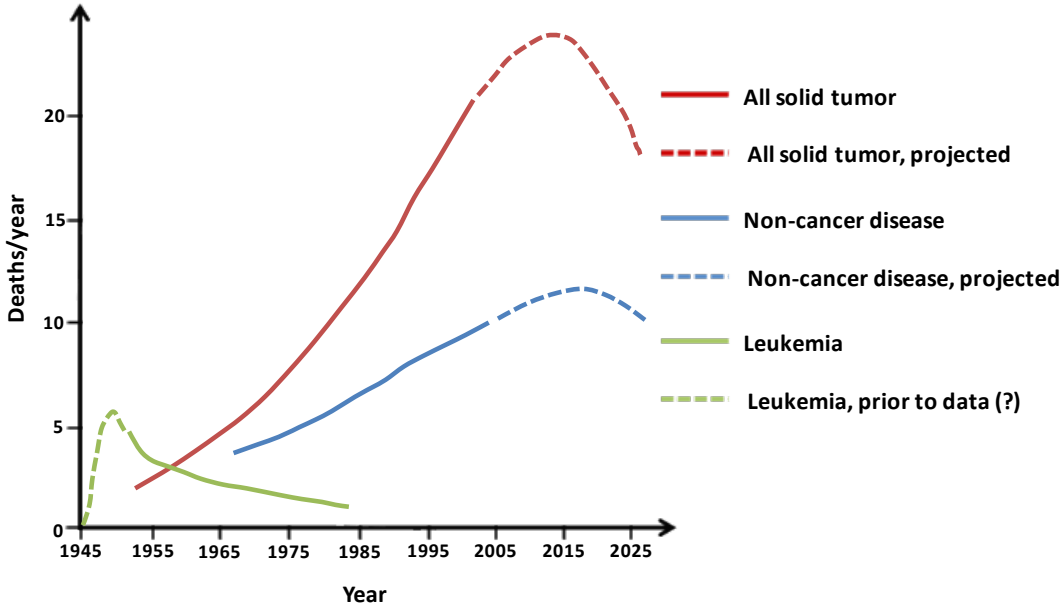
Deaths/year
20
15
10
5
0
1945
1955
1965
1975
1985
1995
2005
2015
2025
Year
All solid tumor
All solid tumor, projected
Non-cancer disease
Non-cancer disease, projected
Leukemia
Leukemia, prior to data (?)

**Figure 8. Life Span Study (LSS) radiation-associated deaths per year.**

Around 120,000 Hiroshima and Nagasaki atomic bomb survivors and control subjects were included in the LSS. Mortality data for solid tumor, leukemia and benign diseases were followed up through the year of 2002. Leukemia is the first radiation-associated long-term health effect observed in the LSS. Risk assessment of leukemia for the period 1945-1950 is not possible since victims had to be alive in 1950 to be in the cohort, the estimated leukemia deaths during this period are shown as green dotted line. Figure adapted from Douple, E.B., et al., Long-term radiation-related health effects in a unique human population: lessons learned from the atomic bomb survivors of Hiroshima and Nagasaki. Disaster medicine and public health preparedness, 2011 [50].

damage (RBMD), a latent condition characterized prolonged inhibition of hematopoiesis leading to immunosuppression and increased infection risk [4, 40, 56]. As previously described, radiation-induced apoptosis of hematopoietic stem cell (HSC) causes H-ARS. This damage to the hematopoietic system can persist long-term [40], though this phenomenon has been largely ignored due to seemingly-complete recovery of peripheral blood (PB) cell counts, BM cellularity, and number of colony-forming unit (CFU) early after exposure [57, 58].

There are three proposed mechanisms of RBMD: 1) exhaustion of the HSC pool; 2) HSC senescence; 3) HSC niche damage. First, radiation increases ROS level, which in turn induces DNA DSBs. Ataxia-telangiectasia mutated kinase (ATM) recognizes, and is activated by, DSBs and phosphorylates downstream p53 and PUMA, which inhibits the anti-apoptotic Bcl-2 and activates pro-apoptotic Bax and Bak [59, 60]. Bax and Bak open the voltage-dependent anion channel in mitochondria, leading to the release of cytochrome C, which activates caspase-9 and induces apoptosis. This is one possible mechanism of HSC pool depletion; however, quiescent, metabolically inactive HSC have few mitochondria and rely on glycolysis vs. aerobic metabolism [61], and the role of apoptosis in RBMD is still controversial.

The second proposed mechanism, HSC senescence, is based on ROS or p53-mediated activation of p38 and downstream p16. Activation of p16 results in irreversible cell cycle arrest and senescence [62, 63]. Increased ROS in HSC may occur through

endogenous oxygen consumption mediated by nicotinamide adenine dinucleotide phosphate oxidase (NOX) [64]. There are five isoforms of NOX (1-5), and NOX4 has been implicated in radiation-induced chronic oxidative stress in HSC [56, 65].

The third proposed mechanism is based on the role of the HSC niche in HSC self-renewal and differentiation. Radiation can induce senescence in bone marrow stromal cells via the p38/p16 pathway and this is at least partially responsible for RBMD [66]. Sinusoidal endothelial cells have also been known to be affected by radiation-induced senescence [67]. It is not clear if osteoblasts contribute to HSC senescence. Other niche cells may impact HSC self-renewal and differentiation via altered secretion of cytokines or cell-cell contact post-IR.

### 1.5.4. Medical management of radiation injury

In the event of unexpected atomic activity and radiation accidents, triage should be applied. Physicians must identify victims exposed to life-threatening doses and provide treatment prior to decontamination, such as removal of clothing. The priorities in triage of victims are based on their injuries, estimated radiation dose, and clinical symptoms [15, 68]. The following studies focused solely on the management of radiation injury to the hematopoietic system.

#### 1.5.4.1. Standard management of H-ARS

##### 1.5.4.1.1. Transfusion and supportive care

Blood transfusions are typically administered 10-30 days post-IR. These include blood component transfusion or irradiated whole blood transfusion. Antibiotics should be given to mitigate the effect of bacterial translocation from the GI system to the blood as GI tract barrier impairment and myelosuppression greatly increase infection risk in H-ARS patients. In the H-ARS mouse model, treatment with antibiotics and acidified water from day 4 to 30 post-TBI increases the survival rate and decreases infection risk [69]. In leukopenic patients, broad-spectrum antibiotics plus antiviral and antifungal agents should be provided prophylactically until the granulocyte number has recovered.

##### 1.5.4.1.2. Hematopoietic stem cell transplantation

Hematopoietic stem cell transplantation (HSCT) is an effective treatment for hematopoietic malignancies such as multiple myeloma or leukemia, and for benign hematopoietic diseases such as aplastic anemia. Aplastic anemia shares similarities with H-ARS, such as bone marrow failure. HSCT appears to be a promising option for H-ARS treatment; however, many obstacles prevent HSCT following a radiation event.

In the event of an atomic bomb detonation or large-scale radiation accident, the number of victims is likely to be disproportionately higher than the number of available HSC for transplantation. Human leukocyte antigen (HLA)-matched donors are required, and finding these in sufficient numbers is a significant complication. Additionally, the process of HLA typing takes 1-2 weeks, which is too long to wait for treatment [15]. It is

also difficult to determine radiation dose and whether the radiation dose a victim received was partial or whole-body. In mice, partial irradiation is associated with increased survival in comparison with mice receiving total-body irradiation (TBI) at the same dose [11]. Partially-irradiated victims and TBI victims exposed to a dose <3 Gy generally do not experience fatal hematological effects, so HSCT in these patients is unnecessary. The lethal TBI dose is 7-8 Gy, and victims exposed to >10 Gy die of CNS complications before H-ARS appears. The therapeutic window for HSCT, 7-10 Gy, is difficult to estimate immediately after exposure [15]. Finally, though available data are limited, HSCT has not produced favorable results. After the Chernobyl disaster, of 29 victims receiving HSCT, only three survived, and despite transient donor engraftment, autologous reconstitution eventually took over the bone marrow. The remaining 26 victims died with a median survival of 33 days [15, 68]. This evidence collectively indicates that HSCT is a suboptimal intervention following adverse radiation events.

#### 1.5.4.1.3. Growth factor therapy

Growth factor treatment is a more practical and economic therapy than HSCT. Currently, the Food and Drug Administration (FDA) has approved recombinant granulocyte colony-stimulating factor (G-CSF), recombinant granulocyte macrophage colony-stimulating factor (GM-CSF), and pegylated G-CSF to address neutropenia after radiation exposure. G-CSF binds to its receptors and subsequently activates the downstream signal pathways, Jak/Stat, Ras/MAPK, and phosphoinositide 3-kinase (PI3K) /Akt. This mediates the proliferation of myeloid progenitors and increases the number of circulating mature neutrophils [70, 71]. The mechanism of GM-CSF is similar,

but with a broader target, including monocyte-macrophages and eosinophils [72, 73]. LY, RBC, and PLT recovery is accelerated following growth factor treatment due to induction of HSC differentiation. However, this stimulating effect is short-lived and may expedite HSC pool exhaustion and exacerbate RBMD [65]. No MCM approved for treatment post-IR is effective in RBMD, highlighting a critical need to develop new strategies for RBMD/DEARE intervention.

#### 1.5.4.2. Potential new therapeutics of H-ARS and DEARE

Although current FDA-approved MCMs increase survival and complete blood count in H-ARS victims, survivors are plagued with long-term hematopoietic insufficiency; in particular, defective lymphocyte reconstitution [74]. These MCMs are myeloid lineage stimulators leading to early- and long-term myeloid reconstitution, but not long-term lymphoid reconstitution. No complete reconstitution of T-cells has been observed [75]. Long-term T-cell deficiencies include decreased T-cell number, imbalanced CD4/CD8 ratio, and compromised T-cell receptor diversity due to thymic involution [15]. Victims of radiation exposure often experience frequent infections and cancer in later life, which may be related to deficient T-cell surveillance [76, 77].

The application of growth factors and cytokines capable of enhancing T-cell reconstitution and thymic recovery are a promising new direction in therapeutic strategies for H-ARS. These include interleukin-7 (IL-7), keratinocyte growth factor (KGF), and fetal liver tyrosine kinase 3 (Flt3) ligand, which aid lymphocyte reconstitution in both H-

ARS and DEARE. Drugs such as lisinopril, which enhance the radio-mitigating effect of colony-stimulating factors, are another interesting therapeutic avenue.

#### 1.5.4.2.1. IL-7

While IL-7 efficacy in H-ARS has yet to be investigated, it has been reported that IL-7 accelerates thymopoiesis and increases CD4 and CD8 T-cell number following chemotherapy and bone marrow transplantation [78]. IL-7 induces cyclin-dependent kinase 2 (Cdk2) or Cdk4 activity, thus increasing cyclin E levels in lymphoid progenitors and promoting the proliferation of both T and B lymphocytes [79]. IL-7 administration also promotes homeostatic T-cell expansion in normal NI mice [15].

#### 1.5.4.2.2. KGF

KGF is known to protect epithelial cells from radiation damage [15, 80]. Its receptors are expressed on the surface of thymic epithelial cell (TEC), which produce IL-7 and promote thymopoiesis. KGF may protect TEC from radiation damage. Min et al. [81] demonstrated that administration of KGF for three consecutive days prior to allogeneic bone marrow transplant enhanced thymic cellularity for at least three months, and increased the number of donor-derived T-cells in recipient spleens.

#### 1.5.4.2.3. Flt3 ligand

Flt3 is an important surface marker for identifying lymphoid-primed multipotent progenitor (LMPP) and common lymphoid progenitor (CLP), which are the common progenitors of LY. Binding of FMS-like tyrosine kinase 3 ligand (FLT3L) to Flt3

dimerizes Flt3 and subsequently activates downstream PI3K and Ras pathways. This promotes the survival and growth of hematopoietic progenitors [82]. FLT3L has minimal biological effect when used alone; however, it exhibits synergy with other hematopoietic growth factors (HGF) including G-CSF, GM-CSF, interleukin-3 (IL-3), stem cell factor, or as an engineered protein containing both FLT3L and another colony-stimulating factor [83, 84]. Combination therapies and the engineered protein both accelerate granulocyte and immune recovery in mice whether administrated before or after irradiation [85, 86].

#### 1.5.4.2.4. Angiotensin converting enzyme inhibitor (ACEI)

The renin-angiotensin system (RAS) is known for its role in regulating blood pressure and hydro-electrolyte homeostasis [87]. Renin from the kidney cleaves and activates the angiotensinogen from the liver to form angiotensin I (Ang I). Angiotensin converting enzyme (ACE), abundant in the lung and blood vessel endothelium, converts Ang I into angiotensin II (Ang II). Ang II binds angiotensin receptors on arterial smooth muscle, inducing vasoconstriction and increasing blood pressure. Ang II also increases hypothalamic production of antidiuretic hormone (ADH) and aldosterone production in the zona glomerulosa of the adrenal cortex. Together, these hormones increase sodium and water retention in arteries and veins, further elevating blood pressure [88]. ACEI inhibits ACE activity and decreases the conversion of Ang I to Ang II, thus down-regulating blood pressure. Angiotensin II receptor blockers (ARB) is a competitive inhibitor of Ang II receptor, directly binding angiotensin receptors [87, 89]. ACEI and ARB are widely used for controlling hypertension and coronary artery disease. Angiotensin (1-7) is the metabolite of Ang I, catalyzed by neprilysin; or the metabolite of

Ang II, catalyzed by ACE2 [90]. Angiotensin (1-7) mediates vasodilation, and is also degraded by ACE. Therefore ACEI, as an inhibitor of ACE, increases angiotensin (1-7). This contributes to blood pressure control via mediation of vasodilation (Figure 9).

The RAS system may play a role in the regulation of hematopoiesis. Ang II receptors present on bone marrow $CD34^{+}CD38^{-}$ cells, stromal cells, erythroid progenitors, and mature lymphocytes [91, 92]. Mas is the receptor of angiotensin (1-7), which presents on BM hematopoietic stem and progenitor cells and its expression is enhanced during hematopoietic stress [93]. Ang II and angiotensin (1-7) may have direct effects on hematopoiesis. The Ang II receptor and Mas receptor also present on bone marrow endothelial cells, an important component of the bone marrow niche, indicating that Ang II and angiotensin (1-7) may regulate hematopoiesis indirectly through altering the bone marrow microenvironment [94]. Ang II and angiotensin (1-7) may also stimulate hematopoietic progenitors indirectly by modulating HGF such as erythropoietin (EPO) in kidney cells [95]. Both in vitro and in vivo experiments show that Ang II or angiotensin (1-7) enhances hematopoiesis only under hematopoietic stress, such as in myelosuppression following chemo- or radiotherapy. Ang II or angiotensin (1-7) are generally given along with other stimulating factors such as G-CSF or erythropoietin to facilitate the stimulating effect [93, 94, 96].

ACEI induces anemia and leukopenia when given at high dose [97, 98]. Paradoxically, however, ACE inhibition has been found to enhance hematopoiesis and mitigate hematopoietic injury after radiation in a time-dependent manner [95, 99-101].

**Figure 9**

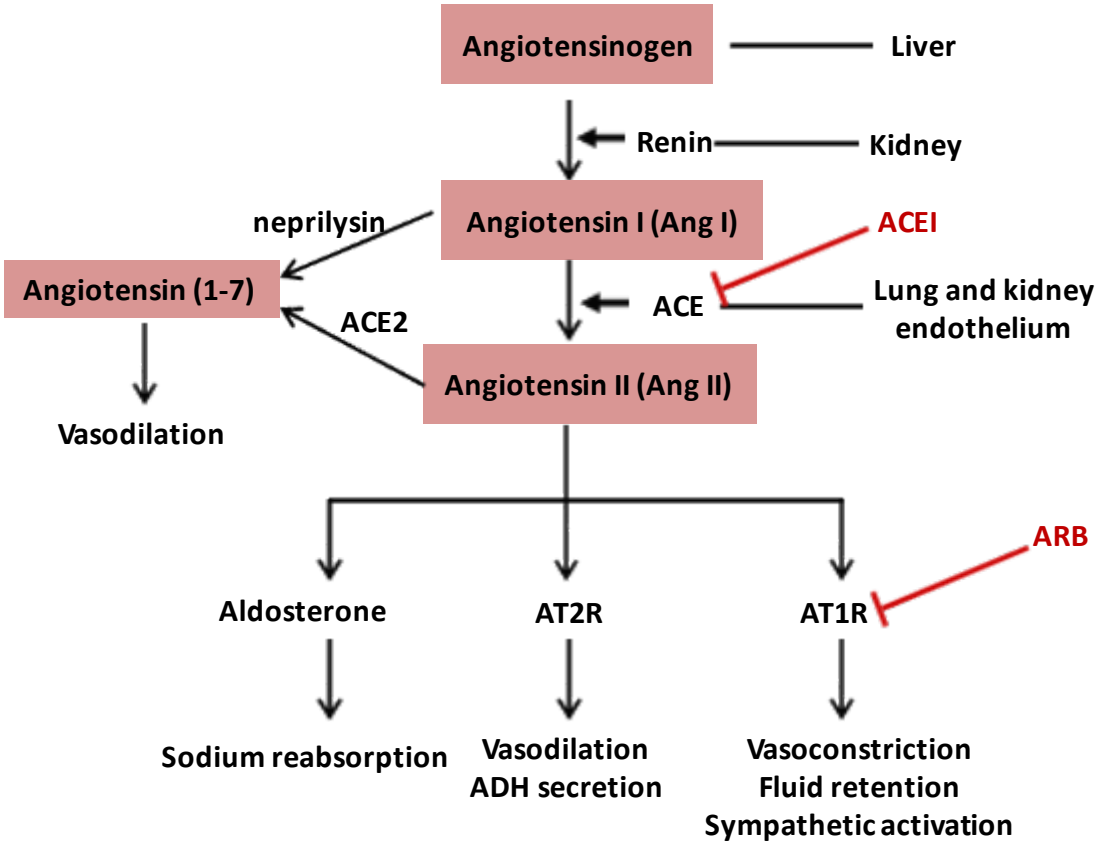
Angiotensinogen
Liver
Renin
Kidney
neprilysin
Angiotensin I (Ang I)
ACEI
Angiotensin (1-7)
ACE
Lung and kidney endothelium
ACE2
Angiotensin II (Ang II)
Vasodilation
ARB
Aldosterone
AT2R
AT1R
Sodium reabsorption
Vasodilation
ADH secretion
Vasoconstriction
Fluid retention
Sympathetic activation

**Figure 9. The renin-angiotensin system.**

Renin from kidney cleaves and activates the angiotensinogen from liver which turns into Ang I. ACE, which abounds in endothelium of lung and blood vessels, then converts Ang I into Ang II. Ang II regulates blood pressure by binding to angiotensin receptors and by regulating ADH production. ACEI inhibits ACE activity and ARB blocks the angiotensin receptors, which down-regulate blood pressure. The metabolite of Ang I and Ang II, angiotensin (1-7), has opposite effect on blood pressure, which down-regulates blood pressure by causing vasodilation. Figure adapted from Conti, S., Cassis, P. and Benigni, A., Aging and the renin-angiotensin system. Hypertension, 2012 [102].

When given for 7 consecutive days before irradiation, ACEI sensitizes the hematopoietic system to radiation damage by increasing the number of short-term HSC (ST-HSC) and hematopoietic progenitor cell (HPC) in the G2/M phase at the time of irradiation. This leads to severe pancytopenia and 100% lethality. When ACEI is given 1-48 hr after irradiation, and for 14 to 30 consecutive days, hematopoietic recovery is significantly increased, along with survival rate. There is no significant difference in survival between early (1 hr) and late (48 hr), short regimens (14 days) and longer regimens (30 days) of ACEI. This radiomitigating effect likely results from transient quiescence of ST-HSC and HPC, allowing for DNA damage repair and, thus, increased cellular survival [101, 103]. In NI mice, ACEI treatment induces quiescence after 2 days and proliferation after 7 days of administration. In NI humans, patients may experience one or multiple-lineage cytopenia. The tetrapeptide N-acetyl-seryl-aspartyl-lysyl-proline (AcSDKP) is the natural substrate of ACE and a negative regulator of hematopoiesis. ACE inhibition would decrease AcSDKP degradation and thus increase its plasma level [104]. Inhibition of Ang II formation and increase of AcSDKP explains the transient anemia and leukopenia resulting from ACE inhibition in non-irradiated scenario [99]. Administration of AcSDKP at peri-irradiation (both before and after TBI) does not decrease mortality, while Ang II-receptor antagonists does. Therefore, blocking the Ang II pathway, rather than increasing AcSDKP, and thus stopping the HSC from entering the cell cycle [105], is thought to be the mechanism of protection effect of ACEI and ARB, in which angiotensin (1-7)-Mas signal pathway might also involve [99].

Drugs targeting the Ang II receptor or Mas receptor also attenuate lung, cardiac and renal fibrosis in DEARE mice. Many reports of this phenomenon exist, but the mechanism remains unknown [103, 106, 107].

#### 1.5.4.2.5. Prostaglandin E2 (PGE2)

Arachidonic acid (AA) is a component of the inner cell lipid membrane. It is released by phospholipase A2 (PLA2) and converted to prostaglandins (PG) by cyclooxygenases (COX) and tissue-specific synthases. PGs have a short half-life and act as autocrine or paracrine factors on different systems with overlapping functions [108]. The rate of PG synthesis depends on local expression and activity of COX, which has two isozymes, COX-1 and COX-2. COX-1 is constitutively expressed in most tissues under physiological conditions. COX-2 expression is induced by inflammation, injury, or cytokines, and is the dominant source of PGs in pathological conditions. The products of COX-1 and COX-2 are different, but overlapping, as they are capable of interacting with different tissue-specific synthases, yet not mutually exclusive preferences. COX-1 primarily interacts with thromboxane synthase, prostaglandin F synthase, and the cytosolic prostaglandin E synthase. COX-2 prefers prostaglandin I synthase and microsomal prostaglandin E synthase [109, 110]. The main products of COX-1 are prostaglandin I2 (PGI2), thromboxane A2 (TXA2), and PGE2. PGI2 protects the gastric mucosa. TXA2 is a coagulant and a vasoconstrictor. PGE2 regulates renal blood flow and natriuresis [111, 112]. The main product of COX-2 is PGE2, which mediates many pathological processes, including pain, fever, and inflammation [113] (Figure 10). PGE2 is unstable with a half-life of 30 seconds and is rapidly catabolized by 15-

hydroxyprostaglandin dehydrogenase (15-PGDH) and 15- ketoprostaglandin D13-reductase (13-PGR) [114, 115].

The physiological and pathological effects of PGE2 are heterogeneous, including labor induction, bone resorption, vasodilation, anti-inflammation, and fever onset [108]. PGE2 interacts with four specific G-protein coupled receptor (GPCR) isoforms (EP1, EP2, EP3 and EP4) [115]. EP1 and EP2 are low-affinity receptors requiring high PGE2 levels for activation, whereas EP3 and EP4 are high-affinity receptors. EP2 and EP4 couple with $G_{\alpha s}$, EP3 couples with $G_{\alpha i}$, and EP1 couples with $G_{\alpha q}$ [116] (Figure 11). PGE2 binding to EP1 activates $G_{\alpha q}$ and phospholipase C (PLC), which hydrolyzes phosphatidylinositol 4,5-bisphosphate (PIP2) into diglyceride (DAG) and inositol trisphosphate (IP3). IP3 releases $Ca^{2+}$ from endoplasmic reticulum and increases intracellular $Ca^{2+}$ concentrations. DAG activates protein kinase C (PKC). PGE2 binding to EP2 or EP4 activates $G_{\alpha s}$ and adenylate cyclase, which stimulates cyclic adenosine monophosphate (cAMP) dependent protein kinase A (PKA), or directly stimulates the cAMP-independent PI3K signal pathway. Both PKA and PI3K activate Akt kinase, which inhibits glycogen synthase kinase-3 (GSK-3). GSK-3 inhibits the activation of β-catenin. The stimulation of EP2 or EP4 pathways therefore activates and translocates β-catenin into the nucleus [115, 117]. The nuclear translocation of β-catenin triggers transcription and translation of downstream proteins, including Survivin and Cyclin D, promoting cellular survival and proliferation. EP3 has multiple splice variants. Most couple with $G_{\alpha i}$, and a few with $G_{\alpha s}$. The $G_{\alpha i}$ subunit inhibits adenylate cyclase and decreases cAMP [118] (Figure 12). Susceptibility to desensitization also regulates PGE2

**Figure 10**

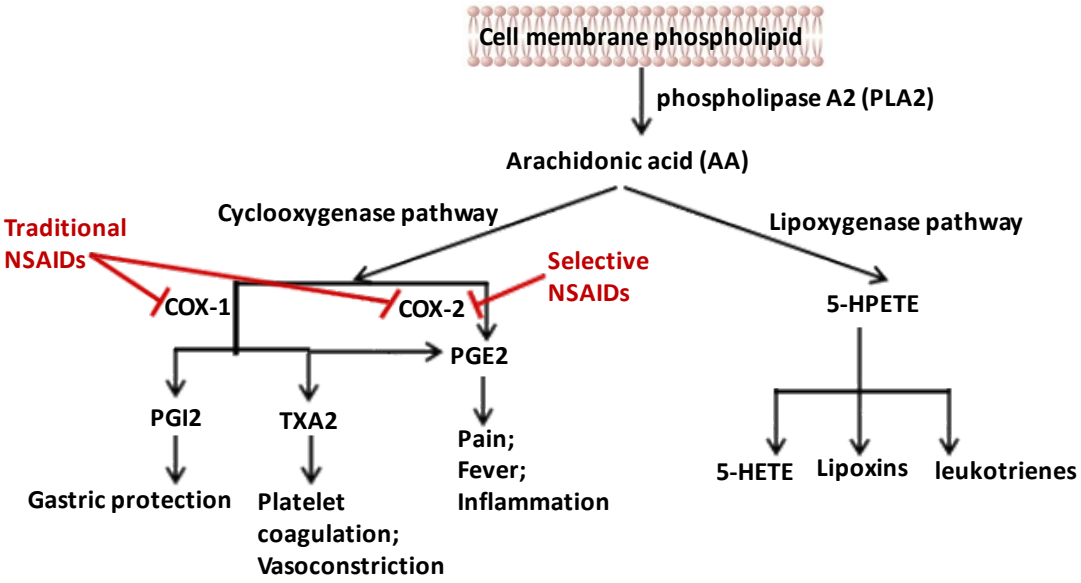
Cell membrane phospholipid
phospholipase A2 (PLA2)
Arachidonic acid (AA)
Cyclooxygenase pathway
Lipoxygenase pathway
Traditional NSAIDs
Selective NSAIDs
COX-1
COX-2
PGE2
PGI2
TXA2
Pain; Fever; Inflammation
Gastric protection
Platelet coagulation; Vasoconstriction
5-HPETE
5-HETE
Lipoxins
leukotrienes

**Figure 10. Eicosanoid biosynthesis from arachidonic acid.**

Arachidonic acid is released from cell membrane by PLA2 and is converted to prostaglandins by COX, or to leukotrienes and lipoxins by lipoxygenase. COX-1 constitutively express in most tissues under physiological condition, and COX-2 is induced by pathological conditions such as inflammation and injury. The main products of COX-1 are PGI2, TXA2 and PGE2. The main product of COX-2 is PGE2, which mediates many pathological processes such as pain, fever and inflammation. Figure adapted from Harizi, H., Corcuff, J.B. and Gualde, N., Arachidonic-acid-derived eicosanoids: roles in biology and immunopathology. Trends Mol Med, 2008 [108].

**Figure 11**

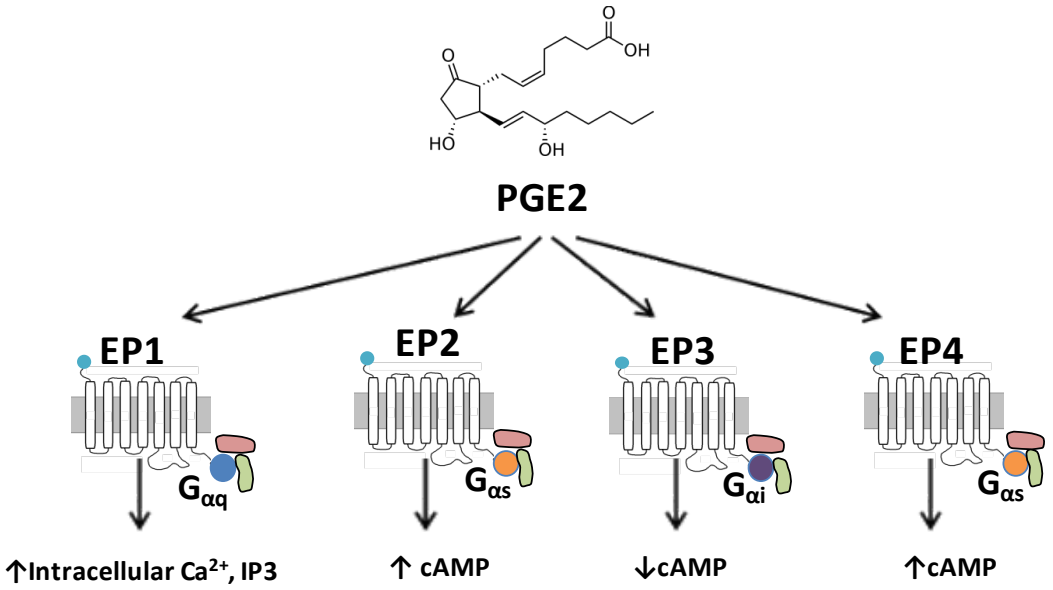
O
OH
O
HO
OH
PGE2
EP1
EP2
EP3
EP4
$G_{\alpha q}$
$G_{\alpha s}$
$G_{\alpha i}$
$G_{\alpha s}$
↑Intracellular $Ca^{2+}$, IP3
↑ cAMP
↓cAMP
↑cAMP

**Figure 11. Prostaglandin E2 receptors.**

PGE2 receptors are G-protein-coupled receptors, which have four isoforms (EP1, EP2, EP3 and EP4). EP1 couples to $G_{\alpha q}$ in which the activation results in the increase of intracellular $Ca^{2+}$. EP2 and EP4 couple to $G_{\alpha s}$ in which the activation results in the increase of intracellular cAMP. EP3 couples to $G_{\alpha i}$ in which the activation results in the decrease of intracellular cAMP. Figure adapted from Dey, I., Lejeune, M., and Chadee, K., Prostaglandin E2 receptor distribution and function in the gastrointestinal tract. Br J Pharmacol, 2006 [117].

**Figure 12**

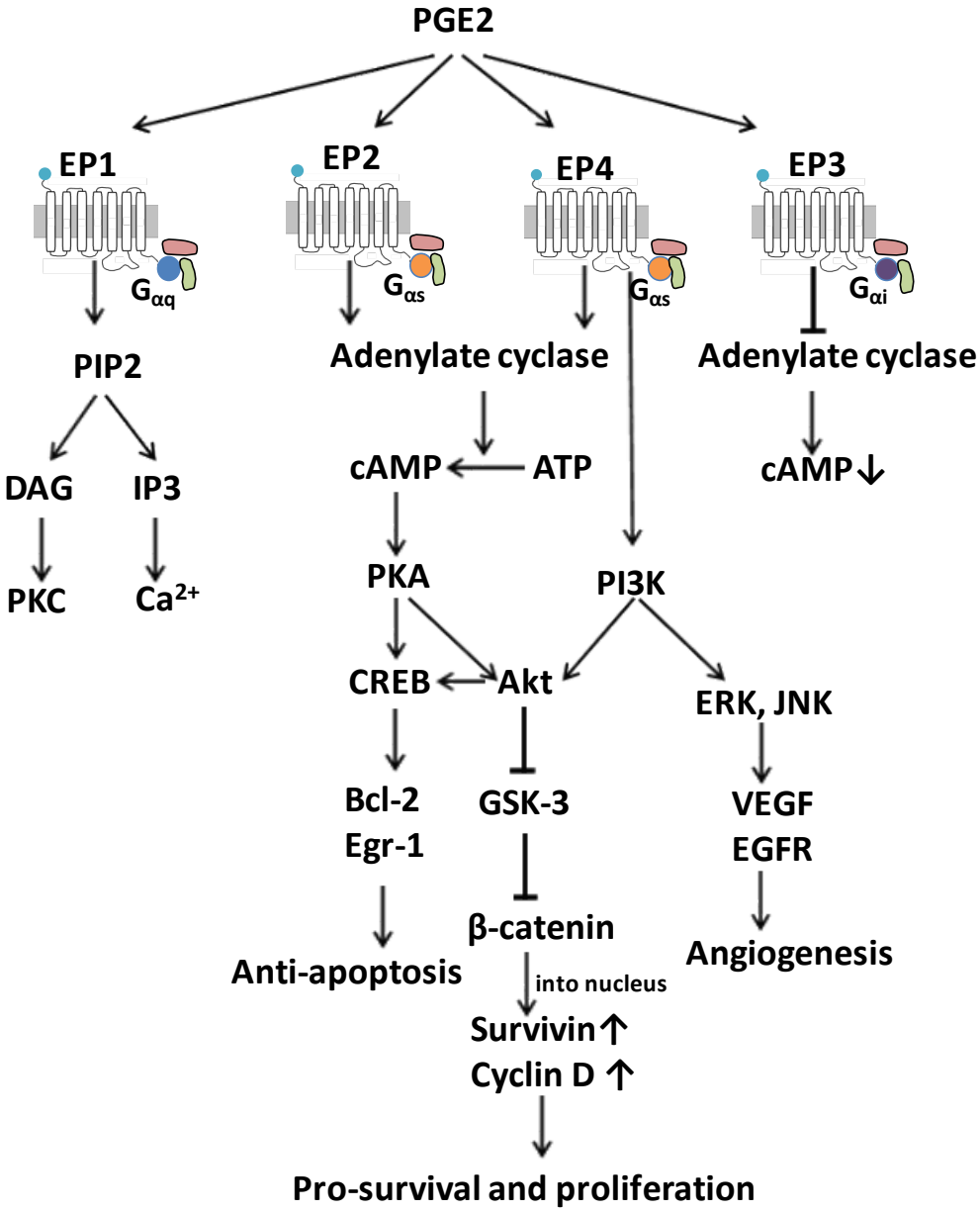
PGE2
EP1
EP2
EP4
EP3
$G_{\alpha q}$
$G_{\alpha s}$
$G_{\alpha s}$
$G_{\alpha i}$
PIP2
Adenylate cyclase
Adenylate cyclase
DAG
IP3
cAMP
ATP
cAMP↓
PKC
$Ca^{2+}$
PKA
PI3K
CREB
Akt
ERK, JNK
Bcl-2
Egr-1
GSK-3
VEGF
EGFR
β-catenin
Anti-apoptosis
into nucleus
Angiogenesis
Survivin↑
Cyclin D ↑
Pro-survival and proliferation

**Figure 12. Prostaglandin E2 signaling.**

Binding of PGE2 with EP2 or EP4 activates $G_{\alpha s}$ and adenylate cyclase, which stimulates cAMP dependent PKA through the increase of cAMP; or directly stimulates cAMP independent PI3K pathway. Both PKA and PI3K activate Akt kinase which inhibits GSK-3. GSK-3 inhibits the activation of β-catenin. So, the stimulation of EP2 or EP4 pathways eventually activates and translocates β-catenin into nucleus. The nuclear translocation β-catenin triggers the transcription and translation of downstream proteins such as Survivin and Cyclin D, which correspond to the final results of EP2/EP4 activation, such as pro-survival and proliferation. Most of EP3 variants couple to $G_{\alpha i}$ which decrease the intracellular cAMP and thus have opposite effects to EP2/EP4. Activation of EP1 increases intracellular $Ca^{2+}$ concentrations and activates PKC. The effects of PGE2 are pleiotropic. Figure adapted from Dey, I., Lejeune, M. and Chadee, K., Prostaglandin E2 receptor distribution and function in the gastrointestinal tract. Br J Pharmacol, 2006 [117].

responsiveness. After agonist stimulation, GPCRs can become desensitized and internalized, and signal intensity decreases. EP4 is more rapidly desensitized after PGE2 binding compared with EP2, which is resistant to PGE2-induced desensitization [115, 117, 119]. EP4 and EP3 isoform-I are more rapidly internalized than EP2, EP3 isoform-III, and EP3 isoform-IV [117, 120]. To summarize, the different EP receptor pathways are both alternative and overlapping; therefore, PGE2 effects are diverse and depend on tissue-specific receptor expression and G protein coupling [118].

The effects of PGE2 on hematopoiesis are pleiotropic. Different timing, concentration, and formulation of PGE2 may lead to different results. Nanomolar levels of PGE2 exposure in vitro inhibits granulocyte-macrophage progenitor cell (colony-forming unit - granulocyte/macrophage, CFU-GM) growth, indicating myeloid progenitor inhibition [121, 122]. In vivo, injected PGE2 inhibited CFU-GM growth [123]. PGE2 also enhanced erythroid progenitor cell (burst-forming unit-erythroid, BFU-E) and multipotential progenitor cell (colony-forming unit granulocyte/erythrocyte/macrophage/megakaryocyte, CFU-GEMM) growth. This may result from direct stimulation or indirect mediation via increased renal EPO production [124-126].

PGE2 synthesis is indispensable for HSC formation and hematopoietic development in zebra fish embryogenesis [127]. For adult human HSC, two-hour ex vivo exposure to 16,16 dimethyl-prostaglandin E2 (dmPGE2) (1 μM) increases Survivin and decreases caspase-3, inhibiting HSC apoptosis. Short-term exposure to dmPGE2 also initiates cell cycle activation in long term-HSC (LT-HSC) but not in progenitor cells

[128]. In a competitive transplantation study, short-term dmPGE2 exposure increased chimerism in the peripheral blood 20 weeks post-transplantation and increased homing to bone marrow within 16 hr due to increased self-renewal and proliferation of LT-HSC [128]. Conversely, in another study, bone marrow cells from mice treated with 6 mg/kg dmPGE2 twice daily for 16 days were used for competitive transplantation and demonstrated superior lymphomyeloid reconstitution that was lost at 16 weeks post-transplantation, indicating that ST-HSCs were predominantly stimulated [129]. These discrepancies may be due to different concentration of dmPGE2 treatment, different treatment duration, and different stimulatory effect on HSC between ex vivo and in vivo dmPGE2 exposure. The effects of dmPGE2 on both HSC and HSC niche in vivo vs. the effect of dmPGE2 on HSC alone ex vivo may also contribute to the discrepancies.

Short term ex vivo exposure to dmPGE2 increases HSC homing to the bone marrow via increased expression of C-X-C chemokine receptor type 4 (CXCR4), which promotes chemotactic migration to stromal cell-derived factor 1 α (SDF1α) in the stem cell niche. This effect is blocked by the CXCR4 antagonist AMD3100 [128]. This supports the finding that HSC engraftment is enhanced following short-term ex vivo dmPGE2 exposure [130]. In contrast, endogenous PGE2 enforces HSC marrow retention through the activation of EP4 receptor and independent of the SDF-1-CXCR4 axis, highlighting the difference in mechanisms on HSC between in vivo and ex vivo experiment [131]. Recently, another CXCR4/SDF1-independent, osteopontin-dependent axis was found to mediate nonsteroidal anti-inflammatory drug (NSAID)-induced HSC trafficking through inhibiting PGE2-EP4 signaling pathway [131].

As dmPGE2 appears to promote HSC survival and self-renewal, it was considered to be a potential MCM, either as a radioprotectant or radiomitigator. Since nuclear attacks and accidents cannot be predicted in advance, first responders and military personnel facing radiation threats need radioprotectant MCM, whereas civilian victims need radiomitigator MCM. Hanson et al. [132, 133] demonstrated that dmPGE2 protected intestinal clonogenic cells from radiation damage in B6D2F1 mice when used as a radioprotectant one hour prior to radiation exposure. Walden TL et al. [134] found that dmPGE2 increased the LD50/30 survival rate of CD2F1 mice when administrated 30 min prior to radiation. Recently, Hoggatt J et al. [135] demonstrated that dmPGE2 significantly increases the day 30 survival rate of C57Bl/6 mice in a radiomitigating manner when administered 6 or 24 hr post-IR, potentially by enhancing HSC survival and self-renewal. These studies were performed in adult mice with different genetic backgrounds, encouraging researchers to evaluate the efficacy and optimal time window of dmPGE2, either as radioprotectant or radiomitigator, in a well-defined animal model [69]. Since there is no effective MCM against DEARE, the potential for dmPGE2 to alleviate DEARE in H-ARS survivors was investigated.

## 1.6. Hematopoiesis

### 1.6.1. Colony assays and competitive transplantation assays

The adverse impacts on hematopoietic stem and progenitor cell (HSPC) and hematopoiesis from radiation exposure are the main causes of H-ARS and RBMD. Investigation into the extent of damage and which cell compartment is targeted by a

specific treatment are crucial to develop and evaluate MCM. Thus, in this section, the concept of hematopoiesis and methods to evaluate hematopoiesis will be introduced. HSC is at the top of the hematopoietic hierarchy and continuously gives rise to all mature blood cells, including neutrophils, eosinophils, basophils, monocytes, macrophages, lymphocytes, red blood cells, and platelets. The two key characteristics of HSC are self-renewal, either symmetric or asymmetric; and differentiation, which gives rise to mature progenies (Figure 13). The idea of HSC originated in the 1950s when it was discovered that shielding the spleen or injecting bone marrow cells prevented the death in mice with radiation-induced bone marrow failure mice [136]. In the 1960s, Till & McCulloch further hypothesized that there existed common progenitors in the bone marrow, and that a single cell may be capable of reconstituting hematopoiesis after radiation - the colony forming unit-spleen (CFU-S) [137]. They later confirmed that CFU-S is clonal after identifying the same unique chromosomal aberrations between the irradiated donor cells and CFU-S cells [138]. With the advent of in vitro hematopoietic cell culture system, the colony forming cell (CFC) assay was developed as a method for quantifying multi-potent or committed HPC. HPC is lineage-restricted, meaning that it can only differentiate into certain types of mature blood cells [139]. CFC assays in solid methylcellulose-based medium can be used to quantify HPC of myeloid, erythroid and megakaryoid lineages. Terminology for colony forming units are: BFU-E, colony-forming unit-erythroid (CFU-E), CFU-GM and CFU-GEMM [139-142]. Lymphoid lineage progenitor culture methodology was developed much later. B-lymphoid progenitor cells (colony-forming unit-pre-B, CFU-pre-B) can be detected by adding IL-7 into the medium or on special medium such as Whitlock-Witte culture [143].

**Figure 13**

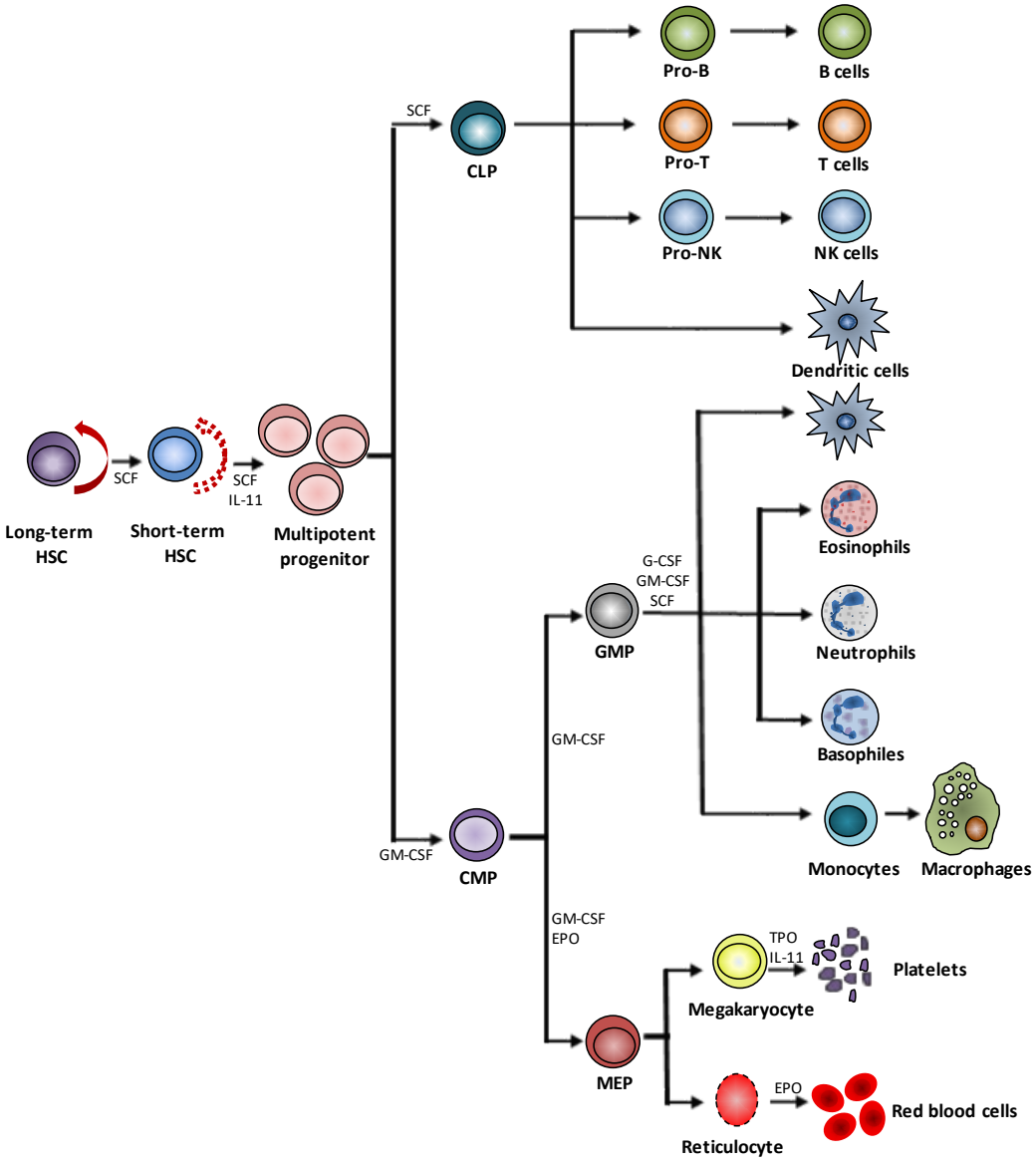
Pro-B
B cells
SCF
CLP
Pro-T
T cells
Pro-NK
NK cells
Dendritic cells
SCF
SCF
IL-11
Long-term HSC
Short-term HSC
Multipotent progenitor
Eosinophils
G-CSF
GM-CSF
SCF
GMP
Neutrophils
Basophiles
GM-CSF
GM-CSF
CMP
Monocytes
Macrophages
GM-CSF
EPO
TPO
IL-11
Platelets
Megakaryocyte
MEP
EPO
Red blood cells
Reticulocyte

**Figure 13. Hierarchy of hematopoietic tree.**

The classic view of hematopoietic tree uses phenotypical markers to identify multipotent HSC and bi-/oligopotent and unipotent progenitors where HSC is at the top of the hematopoietic tree with self-renewal ability. The HSCs give rise to CLP and CMP, which then give rise to all lymphoid and myeloid cells. The hematopoietic growth factors which are used as MCMs to radiation damage mimic the endogenous cytokine pathways. Figure adapted from Reya, T., et al., Stem cells, cancer, and cancer stem cells. Nature, 2001 [144].

The aforementioned CFC assay was initially thought to measure HSC; however, it actually measures multi-potent progenitors with limited self-renewal. The true measurement of HSC is the ability to recapitulate hematopoiesis in a transplant recipient where endogenous hematopoiesis has be ablated. Competitive bone marrow transplantations is a commonly used variant [145, 146], in which a mixture of donor and competitor bone marrow cells are transplanted into lethally irradiated mice. Cell surface markers for donor cells, competitor cells and host cells are all different, which allows these markers to be used to determine the source of mature blood cells. Donor cell ability to produce multi-lineage reconstitution relative to the standard competitor is evaluated. In following studies, donor mice are C57Bl/6 ($CD45.2^+$), and the recipient and competitor mice are B6.SJL-PtrcAPep3B/BoyJ mice (B6.BoyJ; $CD45.1^+$) or the F1 hybrid mice of C57Bl/6 and BoyJ mice ($CD45.1^+CD45.2^+$) [147]. CD45 expression on the white blood cells of these congenic mice differs and can be distinguished by flow cytometry. Chimerism is estimated from the percentage of $CD45.2^+CD45.1^-$ cells in recipient mice and is evaluated monthly post-transplantation.

HSC is a heterogeneous group of cells with various levels of "stemness". There are 3 subgroups of HSC with different self-renewal capacities and multipotent differentiation: ST-HSC, intermediate-term HSC (IT-HSC) and LT-HSC with capability to reconstitute <16 weeks, 16-32 weeks, and >32 weeks, respectively [148, 149]. To demonstrate LT-HSC potential, serial transplantations are required in which primary donor cells are transplanted from the primary recipient into secondary recipients. This

may be repeated in tertiary and quaternary recipients and beyond. Secondary transplantation is typically carried out 4-6 months after the primary transplantation [150].

### 1.6.2. HSPC phenotype

Fluorescence-activated cell sorting (FACS) is used to quantify, separate, or sort subpopulations of blood cells, including HSPCs and mature peripheral blood cells. The immunophenotypic assay determines the percentage or frequency of a specific subpopulation of blood cells by using the fluorophore-conjugated antibodies to probe antigens expressed on the cell surface or inside the cell. Lineage-specific antigens present on the surface of mature cells. Different mouse blood cells express different lineage markers, for example, Ter119 for erythroid cells, Gr1 for myeloid cells, CD3 for T lymphocytes, B220 for B lymphocytes, and CD11b for monocytes/macrophages and natural killer (NK) cells. Using a combination of these antibodies allows for negative selection of cells that do not express these lineage markers. The lineage negative ($Lin^-$, $Ter119^-$ $CD3^-$ $Gr1^-B220^-$ $CD11b^-$) population is enriched for immature hematopoietic cells. The stem cell antigen-1 (Sca-1) and stem cell factor receptor (c-kit, CD117) further define the HSPC population in the $Lin^-$ population. $Lin^-$ c-kit $^{hi}$ $Sca\text{-}1^{hi}$ (LSK) cells are enriched for HSC, whereas the $Lin^-$ c-kit $^{hi}$ $Sca\text{-}1^{lo}$ cells are enriched for myeloid-erythroid HPC and $Lin^-$ c-kit $^{intermediate}$ $Sca\text{-}1^{intermediate}$ cells ($Lin^-$ c-kit $^{int}$ $Sca\text{-}1^{int}$) are enriched with lymphoid HPC. CD16/32 and CD34 further divide the myeloid-erythroid HPCs in $Lin^-$ $c^-kit^{hi}$ $Sca\text{-}1^{lo}$ population into common myeloid progenitor (CMP, $CD34^+CD16/32^-$), granulocyte monocyte progenitor (GMP, $CD34^+CD16/32^+$) and megakaryocyte erythrocyte progenitor (MEP, $CD34^-CD16/32^-$) [151, 152]. Flt3 and IL-7

receptor (IL7R, CD127) further define lymphoid HPC (CLP) in the $Lin^-$ c-kit $^{int}$ Sca-$1^{int}$ population as $Lin^-$ c-kit $^{int}$ Sca-$1^{int}$ Flt3 $^{hi}$ $IL7R^+$ [153, 154].

LSK cells are heterogeneous, including both HSC and HPC. There are two gating strategies to sub-divide LSK cells, one is based on the introduction of two signaling lymphocyte activation molecule (SLAM) family markers (CD150 and CD48) with or without CD34; and another one is based on the introduction of CD34 and Flt3. The first method subdivides the LSK cells into HSC (SLAM LSK, $CD150^+CD48^-$), multipotent progenitor (MPP, $CD150^-CD48^-$), HPC-1 ($CD150^-CD48^+$) and HPC-2 ($CD150^+CD48^+$) [155, 156]. By adding the CD34, the HSC can be further subdivided into LT-HSC ($CD34^-$) and ST-HSC ($CD34^+$) [149]. The second method subdivides the LSK cells into LMPP ($Flt3^{hi}CD34^+$), MPP ($Flt3^{int}CD34^+$), LT-HSC ($Flt3^-CD34^-$) and ST-HSC ($Flt3^-CD34^+$) [82, 157, 158]. There is no standard criterion on the phenotype of HSPC and there are many overlaps between these two methods.

Flt3 is a type III receptor tyrosine. Binding of FLT3L with Flt3 plays an important role in B and T cell lymphopoiesis. Flt3 expression on different HSPC compartments is variable. LT-HSC and ST-HSC express low levels of Flt3 (5%-8%), whereas 60% of MPP are Flt3 positive. Thirty percent of CMP express Flt3 on their surface and have the potential to differentiate into granulocytes/erythrocytes/megakaryocytes but with limited potential to lymphocytes. HPC-1 and LMPP express the highest level of Flt3 (60%-100%) and preferentially differentiate to lymphocytes/granulocytes. LMPP/HPC-1 give rise to the lymphoid lineage-restricted CLP and the myeloid lineage-restricted GMP.

More than 80% of CLP and only 15% of GMP express Flt3 on their surface. Rare HPC-2 (<10%) and MEP (<1%) express Flt3 and HPC-2 and almost exclusively differentiate into erythrocytes and megakaryocytes [159-162]. Other growth factor receptors such as receptors for MCSF (MCSFR) and EPO (EpoR) are involved in myeloid lineage differentiation, but are not widely accepted as markers [82]. In summary, Flt3 expression is confined to myeloid-lymphoid progenitors as opposed to megakaryoid-erythroid progenitors.

Hematopoiesis is not deficient in $Flt3^{-/-}$ mice [159]; however, $Flt3L^{-/-}$ mice demonstrate a severe deficiency in myeloid and B-lymphoid progenitors [161]. MPP, LMPP, CLP, and early thymic progenitor (ETP) are affected in this knockout model, either due to decrease in number or decrease in differentiation potential [163]. This suggests that the Flt3 signal promotes lymphoid development, possibly at the expense of myelopoiesis [164]. There are controversies regarding whether Flt3 is the sole deciding factor in the fate choice between myeloid and lymphoid lineages, but there is no doubt that lymphoid development is dependent on Flt3 expression [82, 163, 164]. Myelopoiesis may depend on the combined action of Flt3 and MCSFR or EpoR [82, 158].

### 1.6.3. Hematopoietic differentiation tree

HSC are at the top of the hematopoietic differentiation tree and have the capacity to divide into all mature peripheral blood cells. The microscope-dependent and morphology-based classification of HSPC is limited in its ability to differentiate between HSC and early HPC, which lack of distinguishable morphological characteristics.

Initially, the more advanced colony-forming assay and single cell bone marrow transplantation assays identified the first branch point at MPP, followed by the separation of myeloid and lymphoid potential identified by CMP and CLP [144]. MPP do not have self-renewal ability and their differentiation ability is increased in comparison with HSC. CLP give rise to B-, T- and NK cells. CMP give rise to MEP and GMP, which give rise to red blood cells and platelets, and neutrophils, monocytes/macrophages, and eosinophils respectively (Figure 14 A). This model of hematopoiesis was later revised with the identification of LMPP which expresses high level of Flt3 and preferentially generates lymphoid lineages, while retains myeloid potential [158, 165]. This challenged the classic model as the separation between the myeloid and lymphoid potential is not defined as previously thought. Later, it was proposed that GMP are heterogeneous, containing eosinophil/basophil progenitors (EoBP) associated with erythrocyte and megakaryocyte fate (erythro-myeloid progenitor) but not with granulocytes precursors [166-169]. It has also been reported that HSC is functionally and molecularly heterogeneous, containing myeloid-biased (MPP2), balanced (MPP3) and lymphoid-biased (MPP4) HSC [170-172]. These progenitors are downstream of "true" HSC and have self-renewal ability and are referred to collectively as the "HSC pool" (Figure 14 B).

Recently, a group of von Willebrand factor (vWF)-positive, platelet-primed HSCs was identified, which differentiates into megakaryocytes independently from any other lineages. This suggests that the separation of megakaryoid-erythroid potential may be the earliest lineage commitment [171, 173] (Figure 15). Additionally, recent single-cell

**Figure 14**

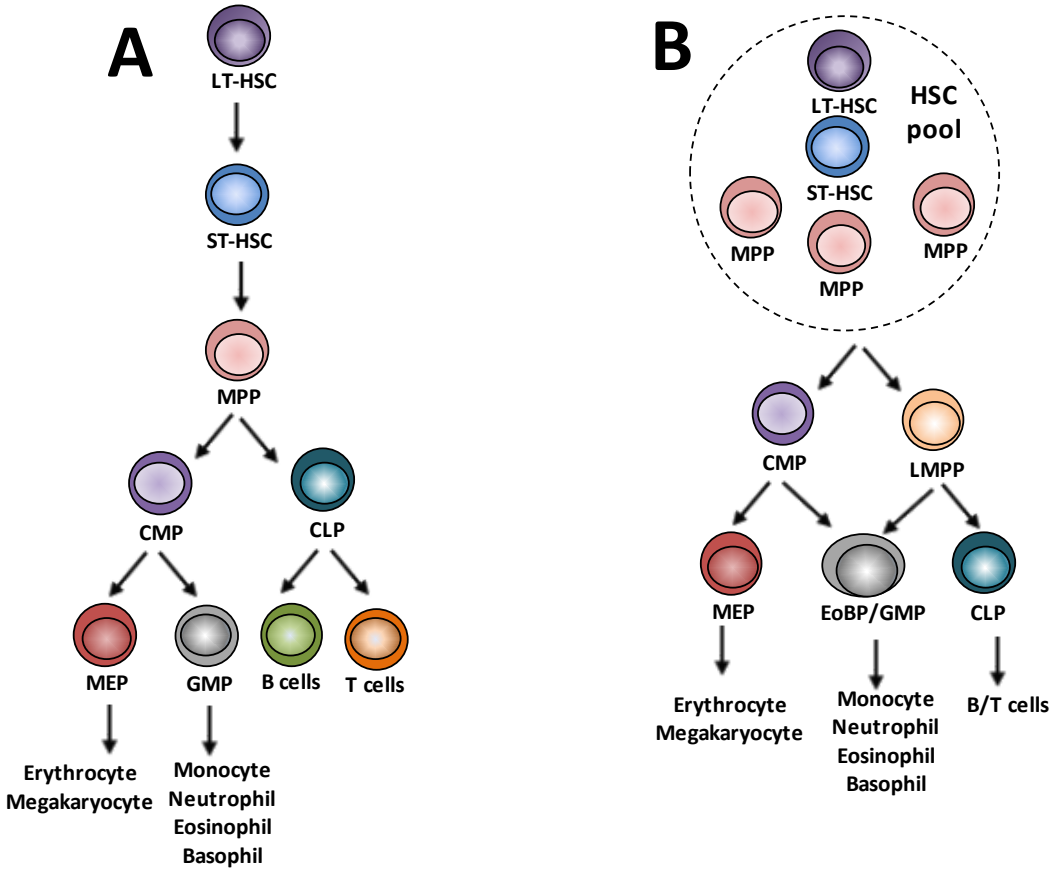
A
LT-HSC
ST-HSC
MPP
CMP
CLP
MEP
GMP
B cells
T cells
Erythrocyte
Megakaryocyte
Monocyte
Neutrophil
Eosinophil
Basophil
B
LT-HSC
HSC
pool
ST-HSC
MPP
MPP
MPP
CMP
LMPP
MEP
EoBP/GMP
CLP
Erythrocyte
Megakaryocyte
Monocyte
Neutrophil
Eosinophil
Basophil
B/T cells

**Figure 14. Classic hematopoietic differentiation tree.**

At earlier era, it is generally accepted that the first branch point separating the myeloid and lymphoid lineages in differentiation tree is via the separation of CMP and CLP populations. The primitive cells differentiate from multipotent to bipotent and then to unipotent progenitor cells. HSCs are homogeneous, which consist of LT-HSC and ST-HSC (panel A). But later on, HSCs were found functionally and molecularly heterogeneous which contain at least myeloid-biased (MPP2), balanced (MPP3) and lymphoid-biased (MPP4) groups. Myeloid and lymphoid separation is not as strict as researchers previously thought and the myeloid and lymphoid potentials remain coupled in the LMPP. GMPs are phenotypically homogenous but are functionally heterogeneous which contain the eosinophil/basophil progenitor (panel B). Figure adapted from Laurenti, E. and Gottgens B., From haematopoietic stem cells to complex differentiation landscapes. Nature, 2018 [165].

**Figure 15**

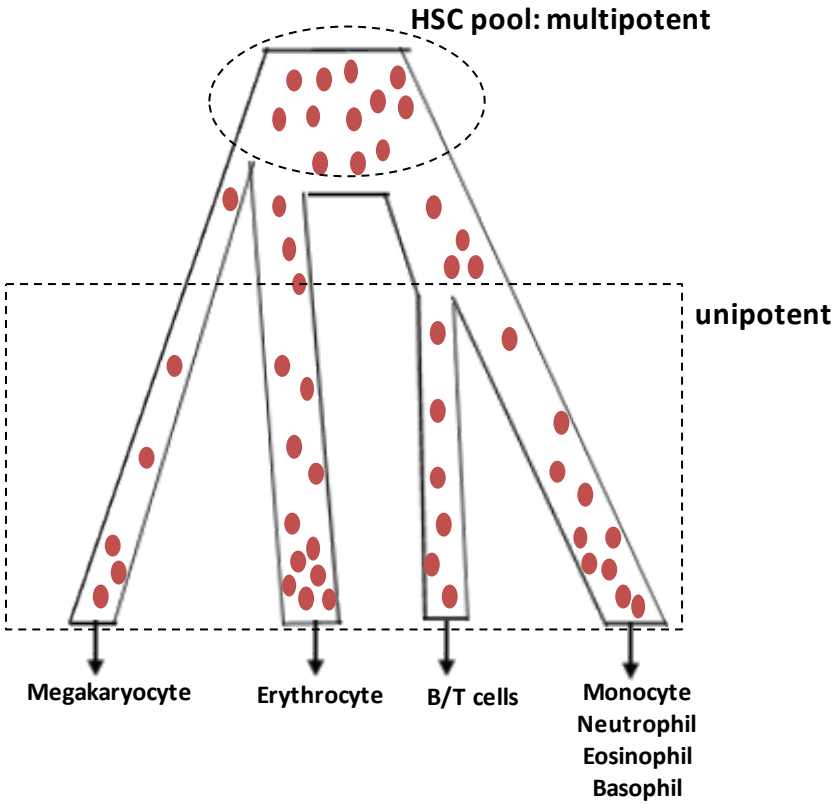
HSC pool: multipotent
unipotent
Megakaryocyte
Erythrocyte
B/T cells
Monocyte
Neutrophil
Eosinophil
Basophil

**Figure 15. Revised hematopoietic differentiation tree.**

Platelet-biased stem cells were found at the apex of the hematopoietic stem-cell hierarchy which suggest that the first branch point in the differentiation tree is much more complicated than a simple segregation of myeloid and lymphoid lineages. Lineage choice occurs earlier than previously thought. Multipotent and unipotent progenitors dominate adult BM, whereas the oligopotent progenitors are rare or absent, or transient exist. Lineage fate choice is a continuous process where the low-primed undifferentiated hematopoietic stem and progenitor cells gradually differentiate to unilineage-restricted cells. A consensus on the revised model of hematopoiesis has not been reached. Figure adapted from Laurenti, E. and Gottgens B., From haematopoietic stem cells to complex differentiation landscapes. Nature, 2018 [165].

transcriptome analysis revealed that lineage fate choice may be a continuous process, where low-primed undifferentiated HSPC gradually differentiates to unilineage-restricted cell without a multipotent or bipotent progenitor (Figure 15) [174-176]. The hematopoietic differentiation model is therefore not yet fully understood, and is continuously evolving as new findings reveal that hematopoietic differentiation is more sophisticated than previously thought.

### 1.6.4. T cell hematopoiesis

T cell hematopoiesis is relatively unique compared with other lineages as T cells mature in the thymus, a specialized primary lymphoid organ critical to the adaptive immune system. Other hematopoietic cells mature in the bone marrow. In the bone marrow, after MPP differentiates into LMPP and CLP, a portion of LMPP and CLP cells termed thymus-seeding progenitors (TSP) enter the thymus via postcapillary venules at the cortico-medullary junction (CMJ) [177]. In the thymus, BM TSP differentiate into ETP, then differentiate into double negative (DN) cells, which gives rise to double positive (DP) cells and further differentiate into either CD4 or CD8 single positive (SP) T cells. DN thymocytes can be further divided into DN1, DN2, DN3 and DN4 cells based on the expression of CD44 and CD25 (DN1: $CD44^{+}CD25^{-}$; DN2: $CD44^{+}CD25^{+}$; DN3: $CD44^{-}CD25^{+}$; DN4: $CD44^{-}CD25^{-}$). As thymocytes differentiate from DN1 to DN4, they progressively migrate from the CMJ toward the subcapsular zone (SCZ) [178, 179].

The T cell receptor (TCR) consists of an alpha (α) and a beta (β) chain [180]. The major histocompatibility complex (MHC) is a group of cell surface molecules that

present foreign epitopes to TCR and thus trigger T-cell activation [181, 182]. In order to recognize the foreign epitope presented by MHC, TCR must go through α and β rearrangement. The TCRβ chain is rearranged at the DN3 stage and then paired with the pre-Tα to form the pre-TCR. This step is called β-selection [183]. Cells that do not produce functional pre-TCR are eliminated by apoptosis. Cells that successfully traverse through β-selection undergo TCRα rearrangement, resulting in complete TCR and transition into the DP stage [184]. DP thymocytes undergo positive selection, which means that they will be eliminated if their complete TCRs are unable to bind MHCs [179]. CD8 is a coreceptor that binds MHC class I molecule and CD4 is a coreceptor for MHC class II molecule. Cell receiving signal from TCR/MHC I binding develops into SP $CD8^+$ T cell and likewise, cell receiving signal from TCR/MHC II binding develops into SP $CD4^+$ T cell. SP thymocytes then migrate from thymic cortex to medulla [185]. In the medulla, SP thymocytes go through negative selection in order to eliminate autoreactive thymocytes. The SP thymocytes which have high affinity for self-peptides presented on MHC molecules are driven to apoptosis through upregulating the pro-apoptotic molecules [186]. Non-autoreactive thymocytes that have appropriate affinity for MHC molecules enter into the peripheral blood and become mature T cells. These recent thymic emigrants (RTEs) are naïve cells expressing CD62 ligand (CD62L) [187]. After encountering novel foreign antigens, naïve T cells proliferate and produce inflammation to eliminate the pathogens [188, 189]. A protective memory effect mediated by memory T cells will forms during the latter phase of inflammation. There are two types of memory T cells circulating in the peripheral blood and lymphoid organs: effector memory T cell (TEM) which can be identified as $CD44^+CD62L^-$, and central memory T (TCM) cell as

$CD44^{+}CD62L^{+}$ [190, 191]. The T cell developmental pathway from bone marrow to peripheral blood is summarized in Figure 16.

TEC cells are the main component of thymic niche, which support T-cell development and maturation as “nursing cells”. TECs reside in specialized anatomical regions, and are defined as cortical TEC (cTEC) or medullary TEC (mTEC) [192]. Markers commonly associated with cTEC include cytokeratin 8/18 (K8/K18), Ly51, CD205, and the proteasomal subunit β5t and delta-like (DL) 4. Markers commonly associated with mTEC include cytokeratin 5/14 (K5/K14), the lectin ulex europaeus agglutinin 1 (UEA1), CD80, autoimmune regulator (Aire), MTS10, ERTR5, and the tight junction components claudin-3/claudin-4 [192, 193]. The ratio of cTEC/mTEC quantified by K8/K5 by fluorescent immunohistochemistry (IHC) is 1.78 in the neonatal mouse thymus and 0.56 in adults [12]. LMPP and CLP express CCR7 and CCR9, and interact with their ligands, CCL21/CCL19 and CCL25, which mainly express on endothelial cell and TEC in thymus [194-196]. Progenitors settling in the thymus are exposed to the cytokines IL-7 and Notch ligand DL4, which are highly expressed by cTEC [197]. mTEC is indispensable in establishing central tolerance with the expression of Aire gene and in promoting the development of $CD4^{+}CD25^{+}Foxp3^{+}$ T regulatory and NK cells [192, 198]. The T cell development from bone marrow to thymus then to peripheral blood is summarized in Figure 16 [178].

In this chapter, I introduce the concept and biological effects of ionizing radiation; describe the clinical syndromes of radiation damages and potential treatments

**Figure 16**

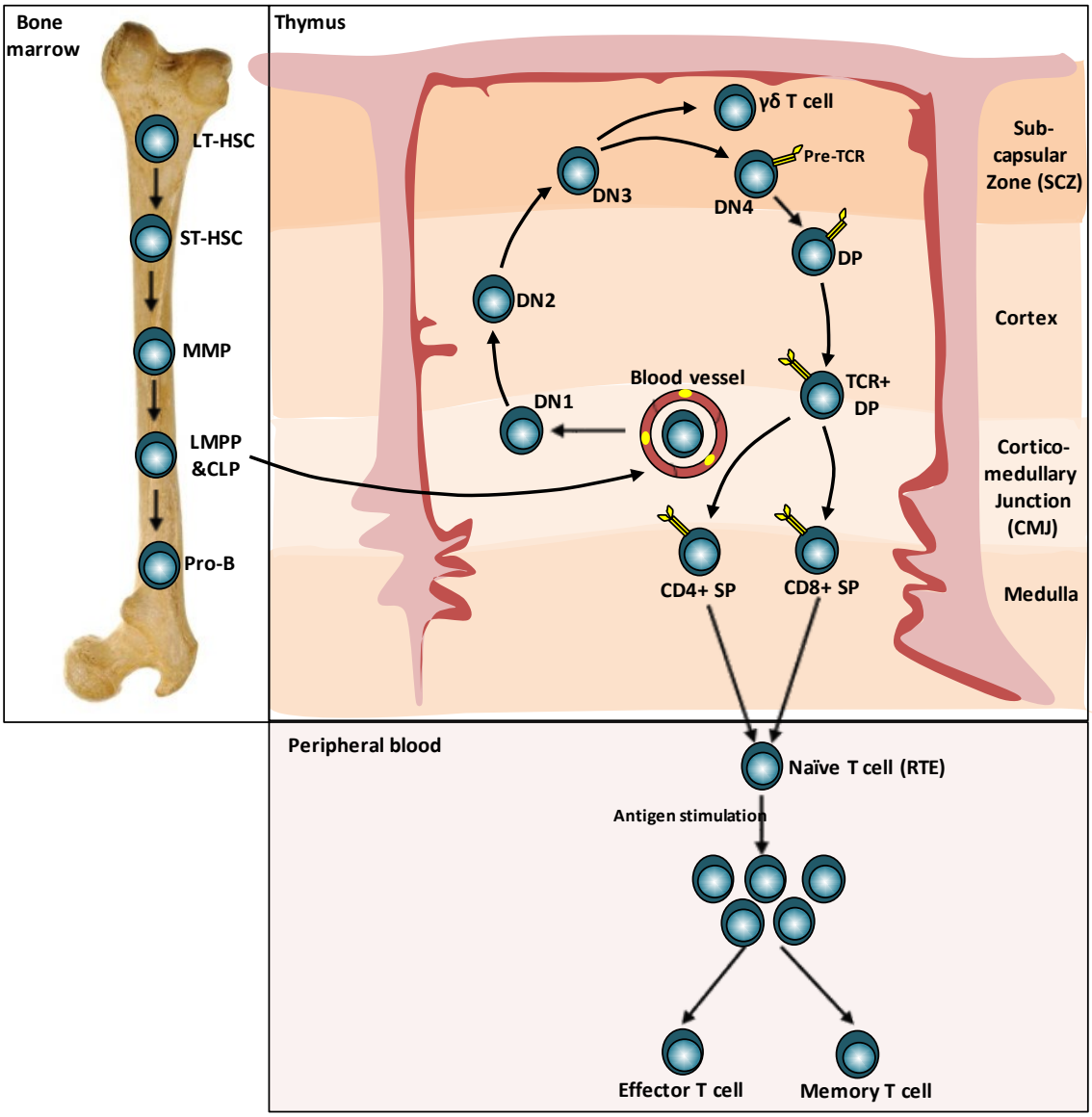
Bone marrow
LT-HSC
ST-HSC
MMP
LMPP &CLP
Pro-B
Thymus
γδ T cell
Pre-TCR
DN3
DN4
DP
DN2
Cortex
Blood vessel
TCR+ DP
DN1
Cortico-medullary Junction (CMJ)
CD4+ SP
CD8+ SP
Medulla
Sub-capsular Zone (SCZ)
Peripheral blood
Naïve T cell (RTE)
Antigen stimulation
Effector T cell
Memory T cell

**Figure 16. T cell development from bone marrow to thymus.**

A portion of LMPPs and CLPs enters the thymus via postcapillary venules at CMJ and differentiates into DN cells and then to DP cells and follow with CD4 and CD8 SP cells. DN cells can be further divided into DN1, DN2, DN3 and DN4 cells based on their expression of CD44 and CD25. As thymocytes differentiate from DN1 to DN4, they progressively migrate from the CMJ toward SCZ. Mature thymocytes, which have appropriate affinity for MHC molecules, enter into the peripheral blood and become naïve T cells (RTE, recent thymic emigrant). After encountering novel foreign antigens, naïve T cells proliferate and produce effector T cells to eliminate the pathogens. A protective memory effect mediated by memory T cells forms during the latter phase of inflammation. Figure adapted from Aifantis, I., Raetz, E. and Buonamici, S., Molecular pathogenesis of T-cell leukaemia and lymphoma. Nat Rev Immunol, 2008 [199].

currently available for these damages, especially focusing on the damage of hematopoietic system; and characterize the hematopoietic development and research methods in hematopoiesis. In chapter two to chapter five, the hematopoietic irradiation damages by a well-established mouse model, both in short-term and long-term, will be defined; and the radioprotective and radiomitigative effects of several promising MCMs will be presented. The hypothesis will be proposed as the hematopoietic recovery, including the immune recovery, would be severely impaired in survivors of H-ARS through interference on HSPC differentiation; and this defect can be corrected or prevented by the optimized administration of MCM. The following specific aims were planned in order to test the hypothesis: Aim 1. Characterize the hematopoietic and immune suppression during the H-ARS phase and the recovery of different lymphoid compartments in H-ARS survivors. Aim 2. Evaluate the impact of different MCMs on the hematopoietic and immune systems during H-ARS and DEARE phases; and investigate the potential intrinsic and extrinsic mechanisms responsible for the effectiveness of these MCMs. The research is expected to pave the road for more extensive and efficient MCM screening to combat the threat of radiation damage in the future.

# Chapter 2. Immune Reconstitution and Thymic Involution in the Acute and Delayed Hematopoietic Radiation Syndromes

## 2.1. Introduction

H-ARS and DEARE are serious and potentially lethal outcomes of exposure to high-dose radiation. Treatments for H-ARS include the recently approved MCM including Neupogen (G-CSF), Neulasta (pegylated G-CSF) and Leukine (GM-CSF) [200], which stimulate primitive hematopoietic progenitor cells to produce life-saving blood elements, primarily of the myeloid lineage [69, 201-204]. Although these MCM significantly increase survival from H-ARS, they do little to alleviate the morbidity of DEARE and its devastating multi-organ dysfunction, including long-term hematopoietic insufficiency.

One of the most serious consequences of hematopoietic DEARE is defective lymphocyte reconstitution and its subsequent immune insufficiency. Survivors of H-ARS often suffer from long-term T-cell deficiencies that dampen robust protective immune responses, including decreased T cell number, imbalanced CD4/CD8 ratio, and compromised naive T cell receptor diversity [15]. Long-term survivors, as well victims of the atomic bombings of Hiroshima and Nagasaki [4, 205] and cancer patients that have received radiotherapy [206], also experience increased incidence of infections and cancer, likely due to deficient T cell surveillance [76]. Many of these immune perturbances also occur to a lesser degree during normal aging in association with thymic involution. Thymic involution, the age-related loss of thymic mass and reduction of naïve T cell output, correlates with reduced immune surveillance and onset of cancers, autoimmunity,

and infectious diseases in aging [186]. Age-related thymic involution and its associated immune dysfunction are exacerbated by previous radiation exposure, further compounding the immune deficiencies in hematopoietic DEARE.

While immune dysfunction has been well characterized in normal aging [207], as well as in the acute phase of radiation exposures, little is known regarding the immune suppression that occurs during DEARE. Generation of functional immunity is a complex process. Briefly, BM LT-HSC differentiate into MPP, followed by LMPP, and then CLP. LMPP and CLP emigrate from the BM to the thymus where they differentiate into $CD4^-$ $CD8^-$ DN cells, followed by $CD4^+CD8^+$ DP cells, and finally single positive $CD4^+$ or $CD8^+$ T cells, remaining CLP in the BM develop into mature B cells [178, 179], as described in Chapter 1. Mature $CD4^+$ and $CD8^+$ T cells migrate from the thymus into peripheral blood and secondary lymphoid organs, where they initiate immunosurveillance. Due to the rapid proliferation and turnover of thymocytes, the thymus is highly radiosensitive.

Dr. Orschell's laboratory has previously developed a well characterized murine model of H-ARS and DEARE in young adult C57BL/6 mice, and have used this model to study mechanisms and efficacy of MCM against radiation for licensure and treatment strategies [41, 69, 107, 135, 147, 201, 208-215]. Herein, the prolonged immunosuppression is characterized, at all levels of lymphocyte development in these acute and chronic radiation models. Data presented here aims to increase understanding of the severe immune dysfunction that occurs in radiation survivors, with the ultimate goal of generating a mouse model suitable for assessing the efficacy of potential MCM and therapeutic strategies.

## 2.2. Materials and Methods

### 2.2.1. Mice and husbandry

Specific pathogen-free C57BL/6 mice (50:50 male:female; Jackson Laboratory, Bar Harbor, ME) were received at 10-week-old (w/o) and acclimatized for 2-week prior to irradiation. Husbandry and health status monitoring were carried out as previously described [147, 210]. All studies were approved by the Indiana University School of Medicine Institutional Animal Care and Use Committee.

### 2.2.2. Irradiation, dosimetry and monitoring

Irradiation and dosimetry were performed as previously described [147, 210]. In sum, mice were placed in single chambers of a Plexiglas irradiation apparatus and rotated horizontally (thus irradiated posterior-anteriorly) with a single uniform TBI doses of 8.72 (estimated LD70/30) or 9.04 Gy (estimated LD90/30) gamma radiation from a $^{137}$Cs radiation source (Mark 1 Irradiator, JL Shepherd, San Fernando, CA) at an exposure rate of 0.93-1.03 Gy/min. Inflight OSL nanodosimeters (Landauer Inc, Glenwood, IL) were used to verify homogeneity of exposure. Between day (d) 1-30 post-TBI, mice were provided with autoclaved acidified water and wet feed *ad libitum*. In H-ARS phase, irradiated mice were observed twice daily and scored for signs meeting the criteria for early euthanasia as Dr. Orschell's laboratory described [69]. Surviving mice at day 30 post-TBI were allowed to age for the study of DEARE and fed with regular extruded chow. Since there were no differences in the experimental outcomes assessed in these

studies between the LD70/30 and LD90/30, data from mice exposed to either dose were combined.

### 2.2.3. Complete blood cell count (CBC)

Around 2-3 mm was snipped from the tail of randomly selected male and female mice and 40 µl of peripheral blood was collected into an ethylenediaminetetraacetic acid (EDTA)-coated capillary tube. Stiptic stick containing silver nitrate was applied to the tail to stop the bleeding. Complete blood cell counts with differentials were performed at baseline and on various days after irradiation, using a validated HEMAVET® 950FS Hematology System (Drew Scientific, Waterbury, CT), as previously described [69, 147, 211]. To minimize stress effects, mice were bled no less than 14 days apart during H-ARS phase.

### 2.2.4. Tissue harvest and single cell suspension

All tissues were harvested following euthanasia by $CO_2$ inhalation. Thymi were carefully cleared of fat and connective tissue under a dissecting microscope to eliminate contamination with non-thymic tissue. Thymus and spleen weights were obtained using a Mettler Toledo Balance XS204 (Mettler-Toledo LLC, Columbus, OH). Single cell suspensions of thymocytes and splenocytes were generated by macerating tissues between the frosted ends of two microscope slides or with the blunt end of a syringe plunger, respectively. PB was collected from tail snips and BM cells were flushed from femurs, tibias, pelvis, and humeri. Single cells were suspended in Hank's balanced salt solution (HBSS, Lonza, Walkersville, MD) with 20U/ml heparin (Hospira Inc., Lake

Forest, IL). Erythrocytes were removed from samples by ammonium chloride lysis (0.16M $NH_4Cl$, 0.01M $KHCO_3$) [40].

### 2.2.5. Tissue fixation, histological staining, and imaging

Thymi and spleens were fixed in neutral buffered formalin (NBF) overnight. Formalin-fixed tissues were paraffin embedded and sectioned, then stained with hematoxylin/eosin (H&E) and Picrosirius red. For H&E sections, digital images were acquired using an Aperio Scan Scope CS system (Aperio, Inc., Vista, CA). For Picrosirius red sections, digital images were acquired using a Leica DM 5000B microscope (Leica Microsystems, Inc., Buffalo Grove, IL) with a Diagnostic Instruments Spot RTKE camera (SPOT Imaging Solutions, Sterling Heights, MI) [41, 216]. For quantifying the Picrosirius red stained thymus tissue, 4-6 images were obtained randomly per slide at 5× magnification. All images were analyzed using ImageJ (version 1.50v; National Institutes of Health). Red, green, and blue (RGB) images were converted to grayscale then percentage of red-stained collagen in the background of pale-stained medullar area was measured. The measurement follows the guidance at https://imagej.nih.gov/ij/docs/examples/stained-sections/index.html.

### 2.2.6. Antibody staining and flow cytometric analyses

$B220^+$ B cells were identified using B220-PE-Texas Red or APC, $CD4^+$ T cells by CD4-APC or PECY5, and $CD8^+$ T cells by CD8a-PE or Pacific Blue. Naïve $CD4^+$ and $CD8^+$ T cells ($CD44^{lo}$ $CD62L^{hi}$) were detected using the additional antibodies CD44-APCCY7 and CD62L- PerCPCY5-5. DN thymocytes were defined as $CD4^-$ $CD8^-$ cells

and subdivided into DN1, DN2, DN3, and DN4 cells based on expression of CD44 and CD25 as follows: DN1: $CD44^{+}$ $CD25^{-}$; DN2: $CD44^{+}$ $CD25^{+}$; DN3: $CD44^{-}CD25^{+}$; DN4: $CD44^{-}CD25^{-}$ using CD4-PerCPCY5-5, CD8-PE or Pacific Blue, CD44-APC or APCCY7 and CD25-PECY7 antibodies. BM LMPP ($Lin^{-}$ c-$Kit^{hi}$ Sca-$1^{hi}$ $Flt3^{hi}$ $CD34^{+}$) and CLP ($Lin^{-}$ c-$Kit^{int}$ Sca-$1^{int}$ $IL7R^{+}$ $Flt3^{hi}$) were identified using CD11b-FITC, Ter119-FITC, CD3-FITC, Gr1-FITC, B220-FITC, Sca-1-PECY7 or BV650, c-Kit-APC, CD34-Pacific Blue or BV421, IL7R-APCCY7 and FLT3-PE or PECY5 antibodies. All antibodies were purchased from BD Biosciences (San Jose, CA), Biolegend (San Diego, CA), eBiosciences (San Diego, CA) or R&D Systems (Minneapolis, MN). The staining processes were carried out for 20 min at 4°C in the dark, followed by washing with 1% bovine calf serum (BCS)/phosphate buffered saline (PBS). Samplers were acquired using BD LSRII system (Becton Dickinson Immunocytometry Systems, San Jose, CA) and analyzed using FlowJo Software (FlowJo LLC, Ashland, OR).

### 2.2.7. Statistical analysis

Unpaired Student's t-tests were performed to compare the following parameters: CBC, thymus and spleen weight and cellularity, thymic collagen deposition, and lymphoid cell types. If no sex differences were observed, data from males and females were combined. While many parameters measured over time were also significantly different at individual time-points, a single asterisk denoting significance comparing all mice over a specific time range was used rather than multiple asterisks at individual time-points, for the ease of the reader. Data are expressed as mean ± standard error of the mean (SEM). $P<0.05$ was considered significant.

## 2.3. Results

### 2.3.1. Reconstitution and involution of peripheral blood cells

Dr. Orschell's laboratory has previously documented significantly decreased numbers of all blood elements in the PB of aged H-ARS survivors compared to NI age-matched controls [147]. To investigate male / female differences in the decreased blood production in H-ARS survivors, as well as in normal aging in NI age-matched controls, PB CBC from males and females were examined separately. The fluctuation in animal number during the course of the study is due to the fact that these are retrospective analyses that combined data from several studies, and also because mortality increases with age, especially in radiation survivors, leaving fewer aged mice available for analyses at later time-points. When CBC from NI male or NI female mice of multiple ages between 3- and 24-month-old (m/o) were compared, WBC, NE, LY, and PLT were all found to be significantly higher in NI males compared to females. In IR mice, all blood parameters were significantly reduced during the H-ARS phase, as Dr. Orschell's laboratory and others have reported [69, 211, 217], and did not differ between males and females. However, sex differences in CBC became again apparent as H-ARS survivors aged. When data from IR males or IR females between 6 and 21 months post-TBI were compared, all blood elements were found to be significantly decreased in IR females compared to IR males (Figure 17 A-E). NE gradually increased in the DEARE phase in both IR males and IR females (Figure 17 B), whereas LY declined over time, most dramatically in IR females (Figure 17 C). A similar trend was observed in NI mice during aging, in which NE increased and LY decreased, indicative of myeloid skew. The

enhanced radiosensitivity of LY compared to other blood elements is evidenced by the sustained lymphopenia at the end of the H-ARS phase (day 30 post-TBI) compared to the nearly complete recovery of most other blood elements (Figure 17 A-E).

### 2.3.2. Reconstitution and involution of thymus and spleen

Lymphocytes originate in the BM from the LT-HSC and migrate as LMPP and CLP to the thymus, where they continue maturation to become mature $CD4^+$ and $CD8^+$ T lymphocytes. Given the high degree of radiosensitivity of the thymus [218, 219], and potential impact of radiation-induced thymic damage on long-term T cell maturation, thymus weight and cellularity in IR mice were examined during the H-ARS and DEARE phases in comparison to NI age-matched controls.

Thymus weight and cellularity were found to be significantly greater in young 12 w/o NI female mice compared to young males (Figure 17 F & G), in agreement with others [220, 221]. However, as NI mice aged, thymus weight and cellularity gradually decreased in both sexes, and sex differences in geriatric mice lessened with age, similar to other reports [220, 222].

During the H-ARS phase, thymic weight and cellularity changed in a biphasic pattern, with nadirs at day 3 and day 20 post-IR and a transient peak at day 10 which reached 60% and ~32% of the NI baseline value, respectively (Figure 17 F & G). Due to the higher baseline values in NI females, radiation-induced thymic suppression was proportionally greater in females than males. Similar to CBC shown in Figure 17 A-E,

there were no sex differences in thymic weight or cellularity during H-ARS. By day 30, thymus weight in IR males and females combined was 40% of that in NI mice ($p<0.01$, Figure 17 F). Thymus weights in both NI and IR mice continued to decrease as mice aged, with values from IR mice remaining significantly less than those in NI mice throughout the DEARE phase ($p<0.01$). Parallel trends were observed for thymic cellularity (Figure 17 G).

Naïve T cells migrate from the thymus to the spleen where they encounter foreign antigens and undergo activation. Spleen weight and cellularity reached their nadirs by day 3 post-IR, followed by a partial recovery by day 20 (Figure 17 H & I). Similar to peripheral blood, the reconstitution of spleen in the H-ARS phase was monophasic. Spleen weight and cellularity from both NI and IR survivors did not change drastically as mice aged, unlike the age-related involution observed in thymus (Figure 17 F-I).

### 2.3.3. Histological analyses of thymus and spleen

Thymi and spleens from NI and IR mice at different ages were stained by H&E to evaluate histological changes throughout the H-ARS and DEARE phases. Young (3 m/o) NI thymi were characterized by a large cortex:medulla ratio of 3:1-4:1 with a distinct cortico-medullary junction (CMJ) (Figure 18 A). The cortex thinned significantly after irradiation, such that by day 20 post-IR (second nadir) the cortex:medulla ratio dropped to 1:1-2:1 and the CMJ became blurry. Thymi from aged NI mice (15 m/o) also displayed a thin cortex but with a clear CMJ, as well as focal fibrous proliferation. Aged thymi

from H-ARS survivors [12 months (mo.) post-IR] demonstrated a large mass of adipose tissue and reticular connective tissue surrounding a small, hypocellular thymus with

**Figure 17**

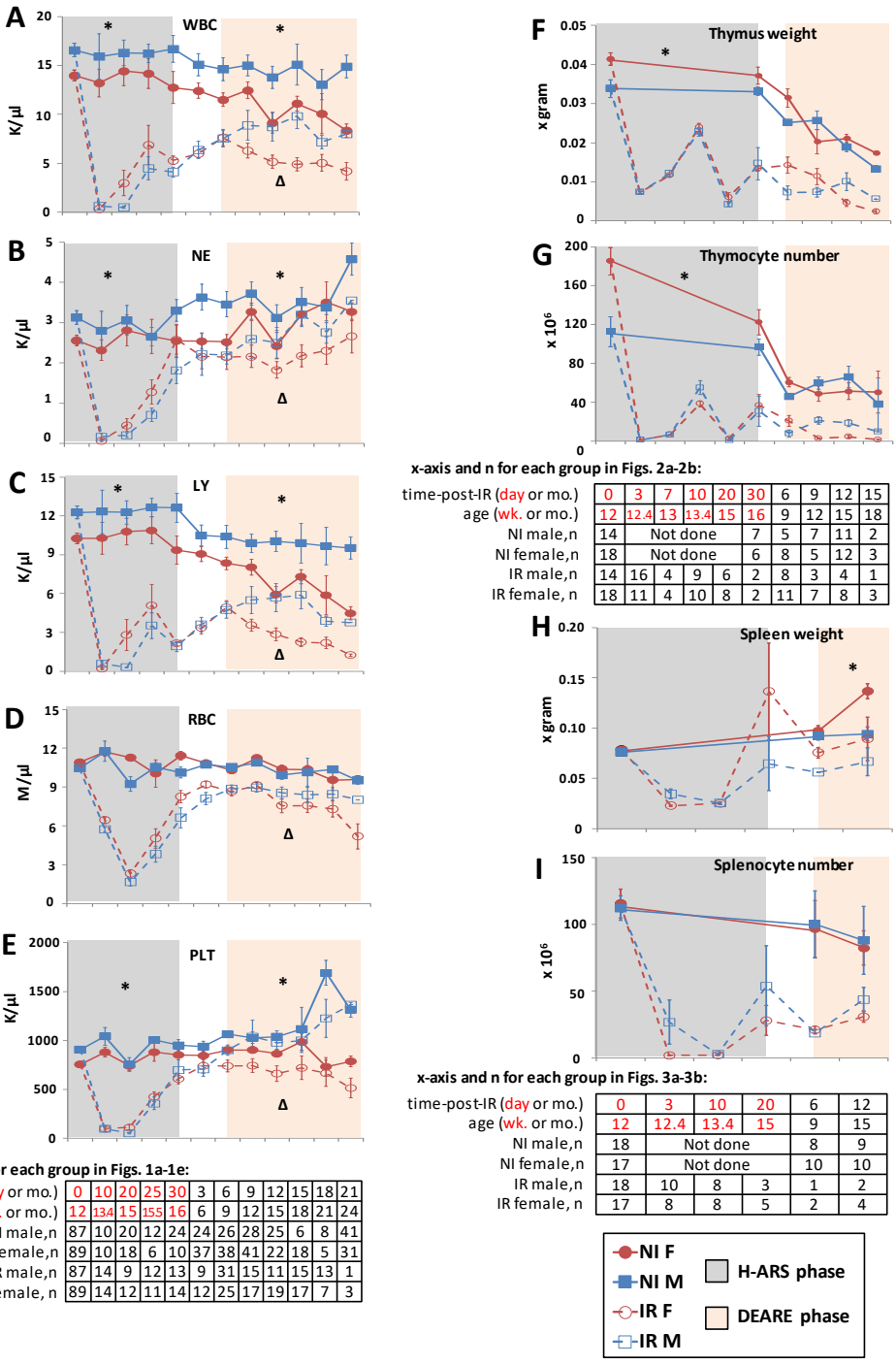


**x-axis and n for each group in Figs. 1a-1e:**

| time-post-IR (day or mo.) | 0 | 10 | 20 | 25 | 30 | 3 | 6 | 9 | 12 | 15 | 18 | 21 |
|---|---|---|---|---|---|---|---|---|---|---|---|---|
| age (wk. or mo.) | 12 | 13.4 | 15 | 15.5 | 16 | 6 | 9 | 12 | 15 | 18 | 21 | 24 |
| NI male,n | 87 | 10 | 20 | 12 | 24 | 24 | 26 | 28 | 25 | 6 | 8 | 41 |
| NI female,n | 89 | 10 | 18 | 6 | 10 | 37 | 38 | 41 | 22 | 18 | 5 | 31 |
| IR male,n | 87 | 14 | 9 | 12 | 13 | 9 | 31 | 15 | 11 | 15 | 13 | 1 |
| IR female, n | 89 | 14 | 12 | 11 | 14 | 12 | 25 | 17 | 19 | 17 | 7 | 3 |

**x-axis and n for each group in Figs. 2a-2b:**

| time-post-IR (day or mo.) | 0 | 3 | 7 | 10 | 20 | 30 | 6 | 9 | 12 | 15 |
|---|---|---|---|---|---|---|---|---|---|---|
| age (wk. or mo.) | 12 | 12.4 | 13 | 13.4 | 15 | 16 | 9 | 12 | 15 | 18 |
| NI male,n | 14 | Not done | | | | | 7 | 5 | 7 | 11 | 2 |
| NI female,n | 18 | Not done | | | | | 6 | 8 | 5 | 12 | 3 |
| IR male,n | 14 | 16 | 4 | 9 | 6 | 2 | 8 | 3 | 4 | 1 |
| IR female, n | 18 | 11 | 4 | 10 | 8 | 2 | 11 | 7 | 8 | 3 |

**x-axis and n for each group in Figs. 3a-3b:**

| time-post-IR (day or mo.) | 0 | 3 | 10 | 20 | 6 | 12 |
|---|---|---|---|---|---|---|
| age (wk. or mo.) | 12 | 12.4 | 13.4 | 15 | 9 | 15 |
| NI male,n | 18 | Not done | | | 8 | 9 |
| NI female,n | 17 | Not done | | | 10 | 10 |
| IR male,n | 18 | 10 | 8 | 3 | 1 | 2 |
| IR female, n | 17 | 8 | 8 | 5 | 2 | 4 |

**Figure 17. Reconstitution and involution in peripheral blood, thymus and spleen post-IR.**

Peripheral blood, thymi, and spleens were harvested from C57Bl/6 mice that had received a single TBI dose of 8.72 or 9.04 Gy gamma radiation at 12 w/o (IR) and from age-matched NI controls at various time-points. NI and IR mice were evaluated for WBC (panel A), NE (panel B), LY (panel C), RBC (panel D), PLT (panel E), thymus weight (panel F), thymus cellularity (panel G), spleen weight (panel H) and spleen cellularity (panel I) and analyzed separately by gender. Data are mean ± SEM. Asterisk (*) indicates $p<0.05$ comparing female (F) with male (M) in NI group. Triangle (Δ) indicates $p<0.05$ comparing F with M in IR group. All data are significantly different between NI and IR mice and thus not indicated on each graph. Time post-IR, age, and number of mice analyzed for CBC, thymus and spleen at each time-point are given below panels E, G and I, respectively.

undistinguishable CMJ. The cortex:medulla ratio of aged thymus ranged between 1.1-2.1. Photographs of thymi from NI and IR mice at different ages in Figure 18 A illustrate the vast differences in size.

To further confirm that radiation induces fibrous proliferation in the thymus early post-IR, thymi at 30 days post-IR were stained with Picrosirius red to identify collagen deposition, which was found to be localized to the medulla (Figure 18 B). Quantification with ImageJ revealed 20-30% more collagen deposition in the medulla of IR mice in comparison with NI mice as early as day 30 post-IR (Figure 18 B).

### 2.3.4. Phenotypic analyses of lymphoid compartments

Dr. Orschell's laboratory has previously documented significantly decreased PB lymphocytes in H-ARS survivors, which correlated with significant myeloid skew [147] and decreased number of functional BM-derived lymphoid progenitors [40]. To better understand the effects of lethal radiation exposure on specific lymphoid subpopulations, lymphocyte populations were phenotypically defined and enumerated in PB, thymus, spleen, and BM of aged H-ARS survivors in comparison to age-matched NI controls and young NI mice. Aged H-ARS survivors exhibited significantly decreased numbers of PB $B220^+$ B cells, $CD4^+$ T cells, $CD4^+$ naïve cells, and CD8+ naïve T cells compared to age-matched NI controls (Figure 19 A, B, D & E). PB CD8+ cells of aged H-ARS survivors also had similar trend but not significantly different comparing to aged NI controls (Figure 19 C), as were $CD4^+$ memory and $CD8^+$ memory cells (non-significantly; data not shown). Normal aging in NI mice resulted in non-significant reductions in all PB T

**Figure 18**

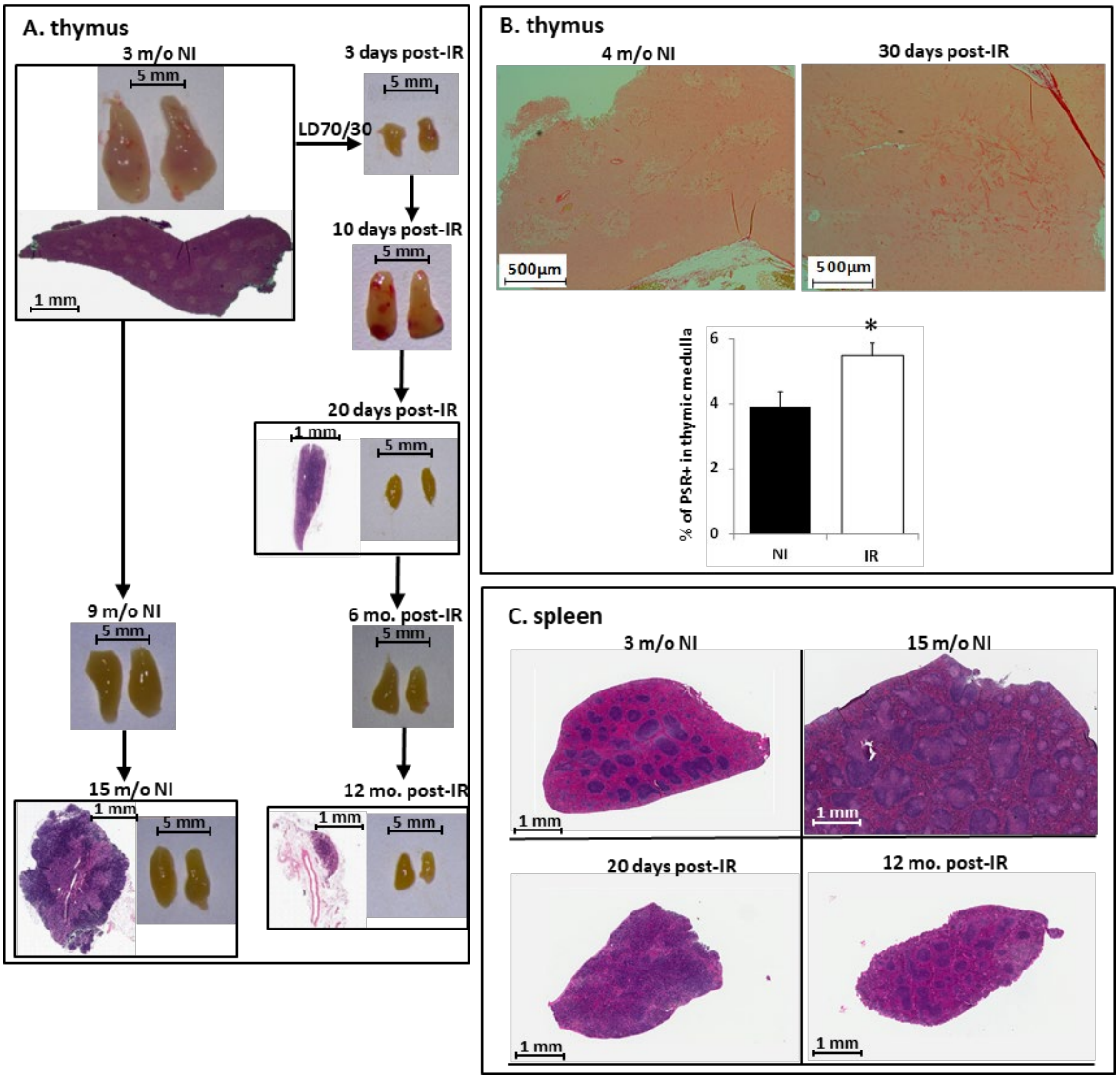
A. thymus
3 m/o NI
5 mm
1 mm
LD70/30
3 days post-IR
5 mm
10 days post-IR
5 mm
20 days post-IR
1 mm
5 mm
9 m/o NI
5 mm
15 m/o NI
1 mm
5 mm
6 mo. post-IR
5 mm
12 mo. post-IR
1 mm
5 mm
B. thymus
4 m/o NI
30 days post-IR
500µm
500µm
% of PSR+ in thymic medulla
6
4
2
0
*
NI
IR
C. spleen
3 m/o NI
15 m/o NI
1 mm
1 mm
20 days post-IR
12 mo. post-IR
1 mm
1 mm

**Figure 18. Images and histology of thymi and spleens in NI and IR mice.**

Panel A shows representative photographs of thymi from NI and IR mice at various time-points, and thymi that were fixed in formalin, embedded in paraffin and stained for hematoxylin and eosin. Panel B shows representative micrographs of thymic sections from 4 m/o NI mice and IR mice 30 days post-IR stained with Picrosirius red. Collagen deposition is presented as the percentage of Picrosirius red positive area in the medullary area using ImageJ software. Data are mean ± SEM. n=6 mice per group (2 females and 4 males per group), with one tissue section stained per mouse. *$p<0.05$ comparing IR and NI mice. Panel C shows spleens from 3 and 15 m/o NI mice and IR mice 20 days and 12 mo. post-IR. Tissues were fixed in formalin, embedded in paraffin and stained for hematoxylin and eosin. Dr. George E. Sandusky and Jennifer Stashevsky provided the histological staining.

**Figure 19**

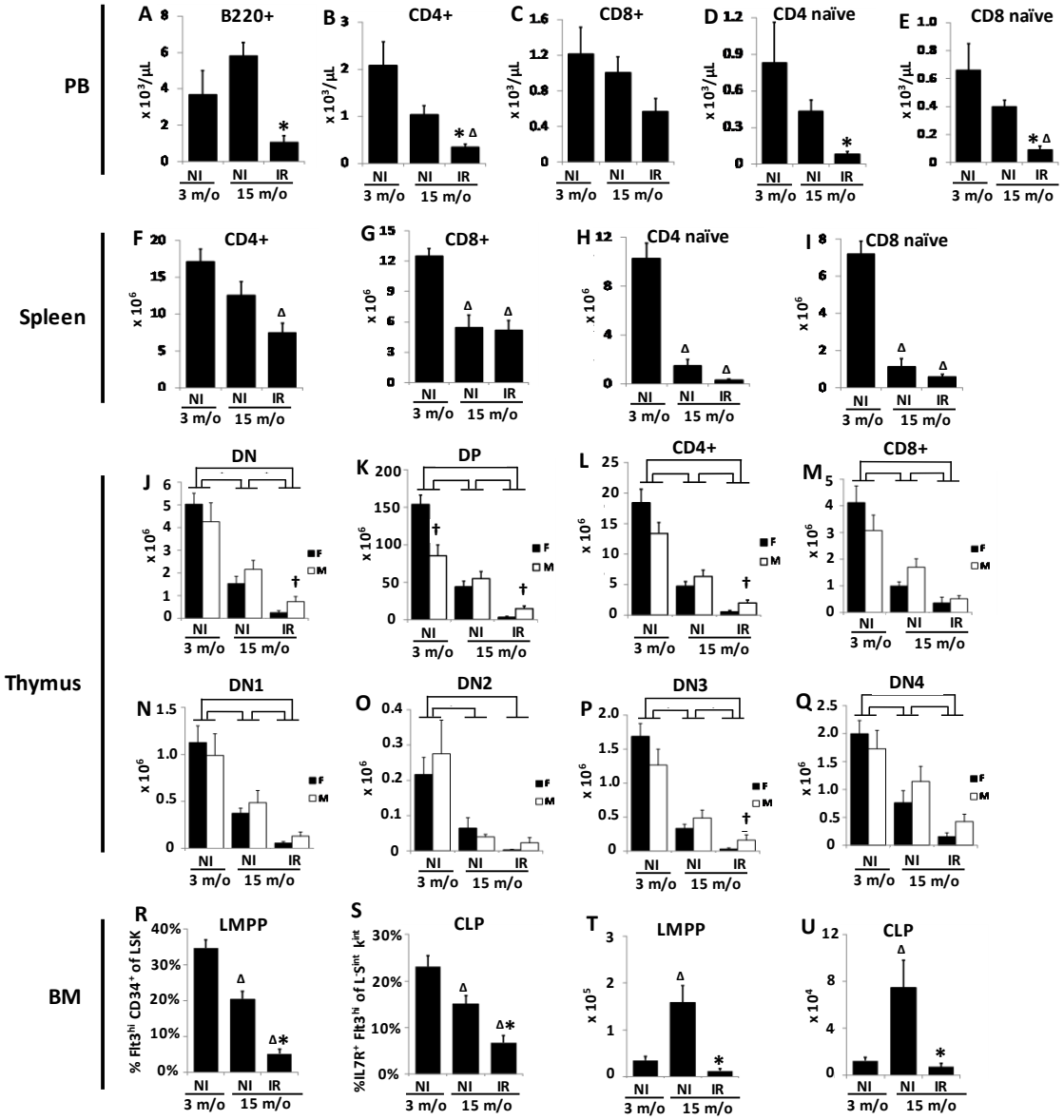
PB
Spleen
Thymus
BM
A B220+
B CD4+
C CD8+
D CD4 naïve
E CD8 naïve
F CD4+
G CD8+
H CD4 naïve
I CD8 naïve
J DN
K DP
L CD4+
M CD8+
N DN1
O DN2
P DN3
Q DN4
R LMPP
S CLP
T LMPP
U CLP
NI
IR
3 m/o
15 m/o
F
M

**Figure 19. Lymphocyte subsets in young and aged NI mice and aged H-ARS survivors.**

C57Bl/6 mice were exposed to a single TBI dose of 8.72 or 9.04Gy gamma radiation at 12 w/o and euthanized at 15 m/o, along with 3 m/o and 15 m/o NI mice. Peripheral blood, splenocytes, thymocytes and bone marrow cells were processed and stained with antibodies as described in Materials and Methods. Flow cytometric analyses identifies peripheral blood $B220^+$ cells (panel A), $CD4^+$ T cells (panel B), $CD8^+$ T cells (panel C), CD4 naïve T cells (panel D) and CD8 naïve T cells (panel E); splenic $CD4^+$ T cells (panel F), $CD8^+$ T cells (panel G), CD4 naïve T cells (panel H), and CD8 naïve T cells (panel I); thymic DN (panel J), DP (panel K), $CD4^+$ (panel L), $CD8^+$ (panel M), DN1 (panel N), DN2 (panel O), DN3 (panel P) and DN4 (panel Q) cells; and percentages of BM LMPP (panel R) and CLP cells (panel S), and absolute number of LMPP (panel T) and CLP cells (panel U). Data from male and female PB, spleen, and BM were not significantly different and thus combined. Data are mean ± SEM. n=4-6 mice per group. * $p<0.05$ compared to 15-month-old NI; Δ $p<0.05$ compared to 3-month-old NI group in panels A-I and R-U. Brackets (⊓) in panels J-Q indicate $p<0.05$ comparing F and M combined data to other groups, and dagger (†) indicates $p<0.05$ comparing F to M within each NI or IR group.

lymphocyte populations examined in comparison to 3 m/o NI mice (Figure 19 B-E), with an apparent increase in B cells (Figure 19 A). There were no sex differences in numbers of PB lymphocyte subpopulations in any group, so male and female data were combined.

In the spleen, a similar pattern of decreased numbers of $CD4^+$, $CD4^+$ naïve, and $CD8^+$ naïve cells was observed in H-ARS survivors versus NI age-matched controls as in PB, but differences did not reach significance (Figure 19 F, H & J). More prominent was a significant age-related decrease in $CD8^+$, $CD4^+$ naïve, and $CD8^+$ naïve splenocytes in aged NI mice compared to young NI mice (Figure 19 G-I). There was no difference in the number of $CD8^+$ lymphocytes between aged NI and IR mice, similar to PB (Figure 19 G), and there were no sex differences in splenocyte T cell subgroups.

The age-related and radiation-related decrease in total thymocytes presented in Figure 19 G was also found to exist when thymic subpopulations were examined: DN, DP, $CD4^+$, $CD8^+$, DN1, DN2, DN3, and DN4 were all significantly decreased in H-ARS survivors compared to NI age-matched controls. Likewise, all these populations were significantly decreased in aged NI mice compared to young NI mice, illustrating the normal age-related thymic involution (Figure 19 J-Q, male and female data combined). Of interest, sex differences in thymic subpopulations were found to exist. In agreement with others [223], 3 m/o females had more DP cells than males (Figure 19 K). In addition, all thymic subpopulations trended higher in male H-ARS survivors compared to females, similar to the increased PB CBC in males versus females, and these differences reached significance for DN, DP, CD4+, and DN3 cells (Figure 19 J-L & P).

Peripheral lymphocytes originate from primitive BM progenitors termed LMPP and CLP, which originate from multi-potent HSC. To better understand BM involvement in immune deficiencies, BM LMPP and CLP were enumerated in H-ARS survivors in comparison to age-matched NI mice and young NI controls. Both frequency (as a percentage of LSK cells or $Lin^{-}$ $Sca\text{-}1^{int}$ $c\text{-}Kit^{int}$ cells) and absolute number of LMPP and CLP were significantly decreased in H-ARS survivors compared to age-matched controls (Figure 19 R-U). In NI mice, LMPP and CLP frequencies were also found to decrease significantly with age (Figure 19 R & S), as previously reported [224, 225]. However, when calculated as a percentage of whole BM, the percentages of both LMPP and CLP were found to be two-fold higher in aged NI mice compared to young NI (LMPP of old vs. young: 0.04 ± 0.009% vs. 0.02 ± 0.005%, p=0.02; CLP of old vs. young: 0.013 ± 0.0029 vs. 0.007 ± 0.0015%, p=0.06). Similarly, absolute numbers of LMPP and CLP were 5-fold and 6-fold increase in old vs. young NI mice, respectively (Figure 19 T & U). This apparent dichotomy between decreased frequency and increased number can be explained by the significant phenotypic expansion of LT-HSC with age, as Dr. Orschell's laboratory [147] and others [226] have reported, despite declining functional potential [40, 147, 227-234]. No sex differences were observed in the frequency or number of BM lymphoid progenitors.

## 2.4. Discussion

Lymphoid organs and lymphocytes are highly radiosensitive [235] due in part to their propensity toward rapid apoptosis when exposed to radiation. The acute effects of

radiation exposure on the lymphoid system are well known, but the late effects and long-term immune suppression in survivors of H-ARS are less well characterized [147, 236, 237]. In this report, radiation damage was investigated at all levels of lymphopoiesis in both male and female long-term H-ARS survivors, and was found to be characterized by significant tissue-specific reconstitution and involution patterns, age-related differences, and noteworthy male/female differences, especially in the thymus.

Dr. Orschell's laboratory previously reported persistent long-term dysfunction in competitive transplantation assays of phenotypically defined BM LT-HSC isolated from H-ARS survivors. Of note, lymphoid reconstitution in recipients of these BM LT-HSC transplants was severely diminished [40, 147], illustrating the loss of multi-lineage reconstitution potential of LT-HSC from DEARE mice. Herein, the primitive BM progenitors LMPP and CLP, progenies of LT-HSC, were enumerated and found to be significantly decreased in frequency and absolute number in DEARE mice, strongly implicating LT-HSC dysfunction as a significant contributor to the diminished lymphoid reconstitution in DEARE mice.

Peripheral blood reconstitution in long-term H-ARS survivors was marked by significant myeloid skew, as previously reported [147, 237], and found herein to be present in both males and females. Of interest, myeloid skew was found to be more severe in IR females compared to males, and was characterized by a steady decline in lymphocyte number beginning around 9 months of age. Declining PB LY numbers in IR females paralleled observations in the thymus, which also showed worse recovery of

most classes of thymocytes (DN, DP, $CD4^+$, $CD8^+$ cells) in females, illustrating curious sex differences in immune reconstitution in the DEARE phase. Phenotypic analyses of PB LY subpopulations of DEARE mice revealed that the loss of LY was primarily due to significant loss of B cells, $CD4^+$ T cells, and both $CD4^+$ and $CD8^+$ naïve T cells compared to NI age-matched controls. The LY subpopulation least affected by radiation exposure was $CD8^+$ T cells, which are known to undergo homeostatic peripheral expansion (HPE) in lymphopenic environments [238, 239]. Similar trends in these LY subpopulations were also present in spleen.

A biphasic recovery pattern of thymocytes was documented during the H-ARS phase with recovery to only ~40% of baseline values, similar to other reports [218, 219]. The first spike of cellularity in the biphasic recovery pattern is thought to be due to proliferation of remaining thymocytes [240, 241], which eventually deplete [242, 243]. This depletion, along with lack of BM support [244], leads to the second nadir. Thymic precursors migrating from the bone marrow to the thymus are responsible for eventual reconstitution [241, 245]. However, in H-ARS mouse model with high dose radiation, BM insufficiency is evident [40, 147], leading to long-term thymic insufficiency. The observed increase in medullary fibrosis in the thymus also likely contributes to thymic dysfunction in long-term H-ARS survivors. Thymic fibrosis early post-IR has also been reported in non-human primate radiation models [246].

Interesting male/female differences were also documented in normal NI C57BL/6 mice. First, males possessed significantly increased numbers of most PB CBC parameters

compared to females (WBC, NE, LY, and PLT), and these sex differences persisted into old age. For LY, these differences intensified as mice aged, leading to more severe myeloid skew in NI geriatric females than in males. The presence of myeloid skew in both NI aged mice and H-ARS survivors illustrates similarities between normal aging and radiation damage on hematopoiesis [147, 247]. The decrease in LY in aged NI mice was primarily due to a decline in all classes of T cells, while B cells increased, as previously shown [248, 249]. Evidence of homeostatic peripheral expansion of PB $CD8^+$ T cells was also present in aged NI mice. While most thymus parameters (mass, cellularity and T cell subpopulations) were increased in young NI females compared to males (in agreement with others [223, 250] and consistent with human data [251]), these differences diminished as mice aged. Spleen also showed decreased numbers of T cell subpopulations with age in both genders, but significantly increased spleen mass in NI aged females. Sex differences in PB and thymus parameters were both abolished after radiation exposure.

Sex differences in lymphoid organs [250] and age-related thymic involution [252] have been postulated to be due to sex hormones, which may be further exacerbated by radiation damage to sex organs. Other factors independent of sex hormones, such as sex chromosomes, may also contribute to the observed sex differences. Many genes implicated in immune function are located on the X chromosome, including theinterleukin-2 receptor gamma chain gene [253] which participates in signal transduction of a number of cytokines, and *FOXP3* gene which is involved in regulatory T cell development [254]. The X chromosome in general imparts an immunological

advantage to females in the face of various immune challenges, but can also lead to increased autoimmune diseases [255]. In addition, radiation-induced epigenetic changes in the murine thymus have been shown to differ between males and females [256], which may also contribute to sex-related differences in the radiation response and immune reconstitution.

Taken together, this study has defined the prolonged immunosuppression at all levels of lymphocyte development in established murine H-ARS and DEARE models. These data build upon previous work by others and add to the understanding of the severe immune dysfunction that occurs in radiation survivors, with the hope that they will be useful for development of potential MCM and therapeutic strategies for radiation-induced long-term immune deficiency.

In conclusion, immune suppression is a serious health risk in individuals exposed to myelosuppressive or ablative radiation, and has not been well-defined in long term survivors of H-ARS. Herein radiation-induced changes in primitive and mature lymphoid cells at all levels of lymphopoiesis were delineated in mice exposed to potentially lethal doses of radiation. Tissue-specific reconstitution and involution patterns were documented in PB, thymus, spleen, and BM tissues, along with unique sex-related and age-related changes present in some tissues but not others. The “double hits” of irradiation and age-related stress on lymphopoiesis lead to significant myeloid skew and long-term immune involution. These H-ARS and DEARE mouse model provide useful

tools for developing and evaluating medical countermeasures against the immune-suppressing effects of irradiation.

# Chapter 3. Optimizing and Profiling Prostaglandin E2 as a Medical Countermeasure for the Hematopoietic Acute Radiation Syndrome

## 3.1. Introduction

Terrorist activities, nuclear warfare, and radiation accidents have the potential to expose humans to dangerous levels of radiation. Victims of exposure to a lethal dose of radiation face acute and chronic organ injuries, including H-ARS and DEARE. H-ARS and DEARE have been characterized by Dr. Orschell's laboratory in Chapter 2.

MCM can be radioprotectant, when used pre-exposure for protection, or radiomitigator, when used post-exposure for mitigation [257]. Current FDA-approved radiomitigators including Neupogen (G-CSF), Leukine (GM-CSF), and Neulasta (pegylated G-CSF) are effective in increasing the survival rate and ameliorating H-ARS in victims of civilian radiation accident [200]. However, for first responders and military personnel who work in the radioactive-material contaminated environment, no radioprotectant has been approved [258]. Amifostine is approved for tissue protection in patients undergoing with chemotherapy and/or radiotherapy, but has not been approved as radioprotectant for H-ARS [259]. An effective radioprotectant for H-ARS is a significant, unmet medical need.

PGE2 is one of the most abundant eicosanoids and mediates diverse physiological and pathological processes, including hematopoiesis [130, 260], bone metabolism [261],

blood pressure regulation [262], and pain and inflammation [263, 264]. The radioprotective and radiomitigating properties of dmPGE2, a long-acting analogue of PGE2 with similar biological effects as PGE2 but with a longer half-life, have been investigated. Hanson et al. [132, 265] indicated that dmPGE2 protected intestinal clonogenic cells from radiation damage in B6D2F1 mice when used as radioprotectant 1 hr prior to radiation exposure. Walden et al. [134] demonstrated that dmPGE2 increased the LD50/30 survival rate of CD2F1 mice when administrated -30 min prior to radiation. Hoggatt J et al. [135] investigated dmPGE2 as a radiomitigator at +6 and +24 post-IR, demonstrating significantly enhanced day 30 survival rate and accelerated hematopoietic recovery in C57Bl/6 mice, possibly due to enhanced HSC survival and self-renewal (Figure 20). These early studies were performed on adult mice with different genetic backgrounds.

The FDA Animal Rule (AR) is a set of FDA guidance about drug development when human studies are unethical, such as studies on lethal radiation exposure. Besides expecting the drug response in animal model could predict the response in human, FDA AR also encourages researchers to investigate the efficacy of MCMs in special populations, including pediatric and geriatric populations. In order to develop dmPGE2 as an effective MCM, the efficacy of dmPGE2 was evaluated in the well-defined animal model [69] to investigate the optimal time window of dmPGE2 treatment and age-related effects on its radioprotective and radiomitigative properties. Additionally, the potential PGE2 receptor that might play a role in mediating dmPGE2 protection was identified, and the hematopoietic recovery and bone marrow environment changes post-IR were

evaluated. These findings may contribute to the possibility of stockpiling and widely distributing dmPGE2 as an MCM for H-ARS in the future.

**Figure 20**

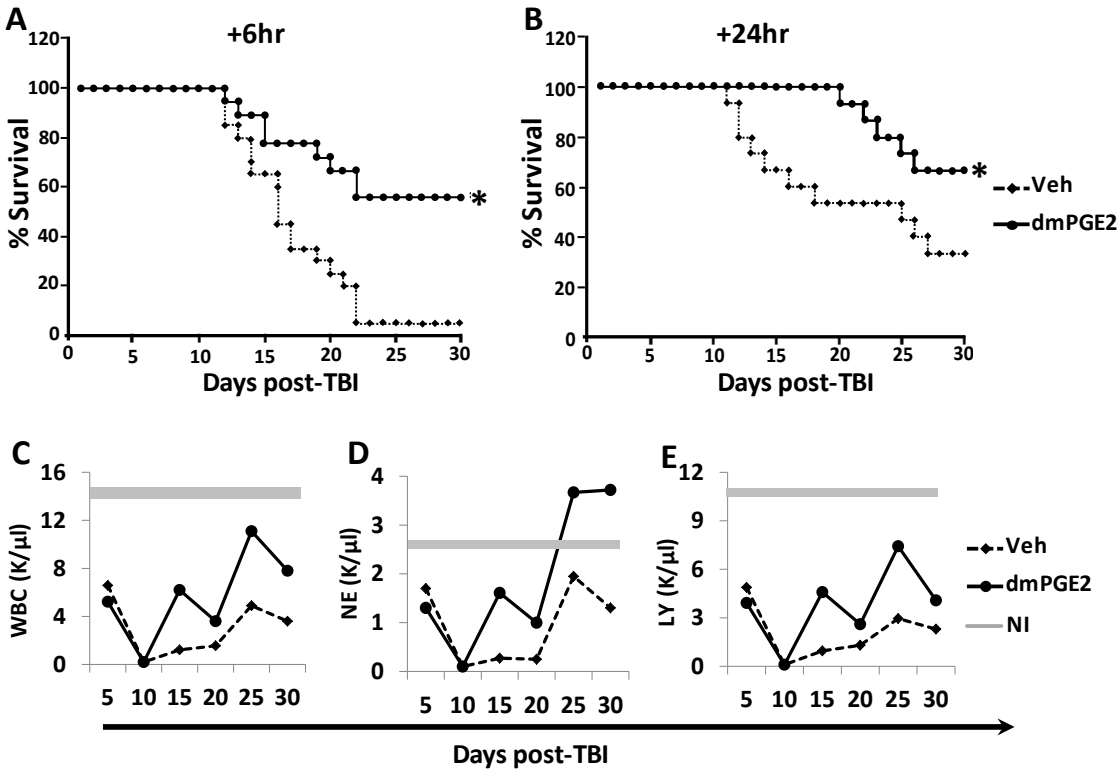

**Figure 20. Effect of dmPGE2 as radiomitigator given at +6 hr or +24 hr post-TBI on day 30 survival and hematopoietic recovery of lethal-irradiated mice.**

Mice were exposed to 7.96 Gy (LD70/30) TBI at 12 w/o. DmPGE2 was injected subcutaneously single dose of 40 μg per mouse at +6 hr (panel A) or +24 hr (panel B) post-TBI. The survival in each group was monitored daily for consecutive 30 days after TBI. Thirty-day survival rates between the dmPGE2 and Veh group were compared using the Kaplan-Meier method and log-rank test. n=20-40 per group. * $p<0.05$ comparing to Veh group. For the +6 hr group, WBC, NE and LY were analyzed at various days post-TBI (panel C-E). n=3 per group per time-point. Reproduced from Hoggatt J, Singh P, Stilger KN, et al. Recovery from hematopoietic injury by modulating prostaglandin E (2) signaling post-irradiation. Blood Cells Mol Dis. 2013 Mar;50(3):147-53.

## 3.2. Materials and Methods

### 3.2.1. Mice, husbandry, monitoring and irradiation

Male and female young adult C57BL/6 mice were purchased from Jackson laboratory (Bar Harbor, ME) at 10 w/o and acclimated with acidified water for 2-week prior to irradiation. In accordance with pilot studies, the adult mice were irradiated at 12 w/o, an age analogous to a "young adult" human at 20 years old [266], with an unfractionated TBI dosage of 8.53 Gy (LD50/30), 8.72 Gy (LD70/30), or 9.04 Gy (LD90/30). Geriatric mice were aged in-house to 23.5 months and then provided acidified water for 2-week prior to irradiation. The geriatric mice were irradiated at 24 m/o (analogous to human at 70 years old [266]) with 10.08 Gy for male mice and 9.47 Gy for female mice. The pediatric mice were received from in-house breeding colony at the Indiana University Melvin and Bren Simon Cancer Center In Vivo Therapeutics Core (Indianapolis, IN), and were not provided acidified water until after TBI. The pediatric mice were irradiated at 6 w/o (analogous to human at 11.5 years old [266]) with 7.41 Gy for male mice and 8.01 Gy for female mice. Husbandry, health status monitoring, irradiation, and dosimetry were carried out as previously described in Chapter 2 and in earlier paper [69, 267]. The irradiation dosages for pediatric and geriatric mice were chosen based on previous dose response relationship (DRR) probit plots to reach lethality around LD70/30 in Veh group (data not shown). Males and females were exposed separately since the sex-specific LD70/30 at this pediatric or geriatric age differs by 0.6 Gy, much greater than the difference in young adult (12 w/o) mice which is only 0.1 Gy (unpublished data). All studies were approved by the Indiana University School of Medicine Institutional Animal Care and Use Committee.

### 3.2.2. Compounds

DmPGE2 in methyl acetate was purchased from Cayman Chemicals (Cayman Chemicals, Ann Arbor, MI), and evaporated on ice under N2 then reconstituted in 100% ethanol (EtOH) at a final concentration of 0.1 M. DmPGE2 was injected subcutaneously at one dose of 35 μg or two doses of 20 μg as indicated in Figures and Legends. Vehicle (Veh; 1.75% EtOH/PBS solution) was injected at the same time as dmPGE2, respectively. In PGE2 receptor activation study, the EP agonists are EP1+3 dual agonist (17-phenyl trinor PGE2, Cayman Chemical, Ann Arbor, MI), EP2 selective agonist (butaprost free-acid, Cayman Chemical, Ann Arbor, MI) and EP4 selective agonist (L902-688, Cayman Chemical, Ann Arbor, MI). EP receptor agonists (10 μg or 35 μg per mouse) were injected subcutaneously -30 min prior to TBI [131, 268]. The volume of all compounds to deliver per mouse per injection was 200 μl.

### 3.2.3. CBC

Complete blood count was performed on peripheral blood of mouse on a validated HEMAVET 950FS Hematology System (Drew Scientific, Waterbury, CT). The procedures of blood collection and HEMAVET validation were carried out as previously described [69].

### 3.2.4. Antibody staining and flow cytometry analysis

For HSC analysis, whole BM cells were acquired from femurs crushed with a mortar and pestle in PBS with 2% fetal bovine serum (FBS) and 2 mM EDTA. Filtered

cells then were stained with FcR blocking antibody followed by anti-Lin, anti-c-Kit, anti-Sca-1, anti-CD48, and anti-CD150 antibodies (Biolegend, San Diego, CA) in PBS containing 0.5% bovine serum albumin (BSA) and 2 mM EDTA. HSC was identified by the LSK and SLAM markers ($CD48^-$ $CD150^+$) as previously described [128].

For mesenchymal stromal cells (MSC) analysis, crushed femurs were digested with 0.25% collagenase IV (Invitrogen, Waltham, MA) in PBS and 10% FBS, 30 min at 37°C. Cells were stained with FcR blocking antibody followed by anti-CD45, anti-ter119, anti-CD31, anti-CD51 and anti-PDGFR antibodies (Biolegend, San Diego, CA). MSCs were identified as $CD45^-$ $Ter119^-$ $CD31^-$ $CD51^+$ $PDGFR^+$ as previously described [131, 269]. Flow cytometry analyses were performed on LSR-II flow cytometer (Becton Dickinson Immunocytometry Systems, San Jose, CA) (Andrea Patterson and Pratibha Singh in Dr. Pelus' laboratory provided the bone marrow phenotype analyses).

### 3.2.5. Colony assay

The surviving mice of the "young adult" group at day 35 post-TBI were sacrificed and $5\times10^4$ BM cells acquired from femurs were plated in ColonyGEL Mouse Complete Medium (Reach Bio, Seattle, WA) as previously described [131, 135]. After 7 days of incubation in a 37°C 5% CO2 incubator, CFC, CFU-GM, BFU-E and CFU-GEMM were counted by microscopy. CFC was the total number of all colonies. Colony assay for each mouse were done in triplicate.

### 3.2.6. BM cellularity and BM cytokine quantification

BM supernatants were collected by flushing 2 femurs and 2 tibiae twice with a single volume of 500 µl cold PBS, stored at -80°C and thawed on ice before analysis. Samples were centrifuged at 16,300 g for 10 min to remove debris and measured in duplicate for 32 cytokines/chemokines by Milliplex Map Kit (EMD Millipore, Billerica, MA) using a Bio-Plex 200 system with High Throughput Fluidics Multiplex Array System (Bio-Rad Laboratories, Hercules, CA) according to the manufacturer's instructions. Data were analyzed with Bio-PlexTM 6.0 Manager software (Bio-Rad Laboratories, Hercules, CA). The 32-plex cytokine panel contained the following cytokines: MCSF, GM-CSF, G-CSF, IL-3, IL-7, leukemia inhibitory factor (LIF), IL-15, vascular endothelial growth factor (VEGF), IL-1α, IL-1β, tumor necrosis factor alpha (TNF-α), IL-2, IL-12 (p40), IL-12 (p70), interferon gamma (IFN-γ), IL-6, IL-17, IL-4, IL-5, IL-9, IL-10, IL-13, keratinocyte chemoattractant (KC, CXCL1), macrophage inflammatory protein 2 (MIP-2, CXCL2), lipopolysaccharide-induced CXC chemokine (LIX, CXCL5) , monokine induced by gamma interferon (MIG, CXCL9), interferon gamma-induced protein 10 (IP-10, CXCL10), monocyte chemoattractant protein-1 (MCP-1, CCL2), macrophage inflammatory protein 1 α (MIP-1α, CCL3), macrophage inflammatory protein 1 β (MIP-1β,CCL4), regulated upon activation normal T cell expressed and secreted (RANTES, CCL5) and Eotaxin (CCL11). Since the results of Bio-Plex analysis represent the concentration of BM cytokines diluted in 500 µl PBS, and the mean BM cavity volume of 2 femurs + 2 tibiae for each mice are 53.1178 µl for males and 39.1072 µl for females (personal communication with Dr. Laura Wright who did the microcomputed tomography on the BM cavity of young adult mice), the

following dilution factor was applied to values from the BioPlex to obtain the actual concentration of cytokines as they exist in the BM space: for males, 500 µl /53.1178 µl = 9.413; for females, 500 µl /39.1072 µl = 12.7854. For example, the concentration of cytokine A in Bio-Plex analysis of female mice is 1 pg/ml, so the weight of cytokine A in 500 µl BM flush is 0.5 pg, and the concentration of cytokine A in BM milieu is 0.5 pg/ 39.1072 µl = 12.7854 pg/ml. Total BM cells concentration in BM flush was performed on HEMAVET 950FS Hematology System (Drew Scientific, Waterbury, CT) as previously described in CBC analysis. Similar dilution factor was applied to the BM cellularity.

### 3.2.7. Statistical analysis

All data are expressed as mean ± SEM. Binary comparisons between dmPGE2-treated group and Veh-treated group, or Veh-treated group and NI group were subjected to a two-sample unpaired t test using Microsoft Excel 2010 (Microsoft Corp, Redmond, WA). The day 30 survival Kaplan-Meier (KM) analyses and log-rank tests were performed with SPSS Statistics Version 24 (IBM, Armonk, NY). A p value less than 0.05 was considered significant. All data shown with error bars represent mean ± SEM.

## 3.3. Results

### 3.3.1. DmPGE2 increases day 30 survival post-IR

Hoggatt J et al. [135] previously found that a single dose of dmPGE2 acts as a radiomitigator when administered +6 hr post-TBI, increasing the day 30 survival rate from 5% to 55%. When administered +24 hr post-TBI, the day 30 survival rate was increased from 35% to 70% (Figure 20). To test the hypothesis that dmPGE2 may be as

effective as a radioprotectant as it is as a radiomitigator and explore the optimal time window of dmPGE2 administration, the previously described well-established H-ARS mouse model was used [69]. Day 30 survival efficacies of 1 dose of 35 μg dmPGE2 when given at -24 hr, -3 hr, -1 hr, -30 min, -15 min, +3 hr, +24 hr, or +30 hr relative to time of irradiation; or 2 doses of 20 μg at -15 min and -45 min prior to TBI, were tested. Survival efficacies were verified by two different irradiation doses, i.e., LD70/30 and LD90/30. The results demonstrated that dmPGE2 administration in the -3 hr to -15 min time window prior to TBI has the best survival efficacy, which reaches 100% survival in LD70/30 and 90-100% in LD90/30. No statistically significant difference was observed between the survival rate of one dose of 35 μg dmPGE2 injected at -30 min and two doses of 20 μg injected at -15 and -45 min prior to TBI, respectively. Administration of dmPGE2 at +24 hr post 8.72 Gy TBI significantly increased day 30 survival, supporting previous observation [135]. Now the time frame of radiomitigating dmPGE2 was extended to +30 hr. Interestingly, when dmPGE2 was used as radioprotectant at -24 hr prior to TBI or as radiomitigator at +3 hr post TBI, the day 30 survival rates in dmPGE2 group were the same as Veh group (Figure 21). These results indicated that there exists a specific time window pre- and post-TBI at which dmPGE2 is effective.

**Figure 21**

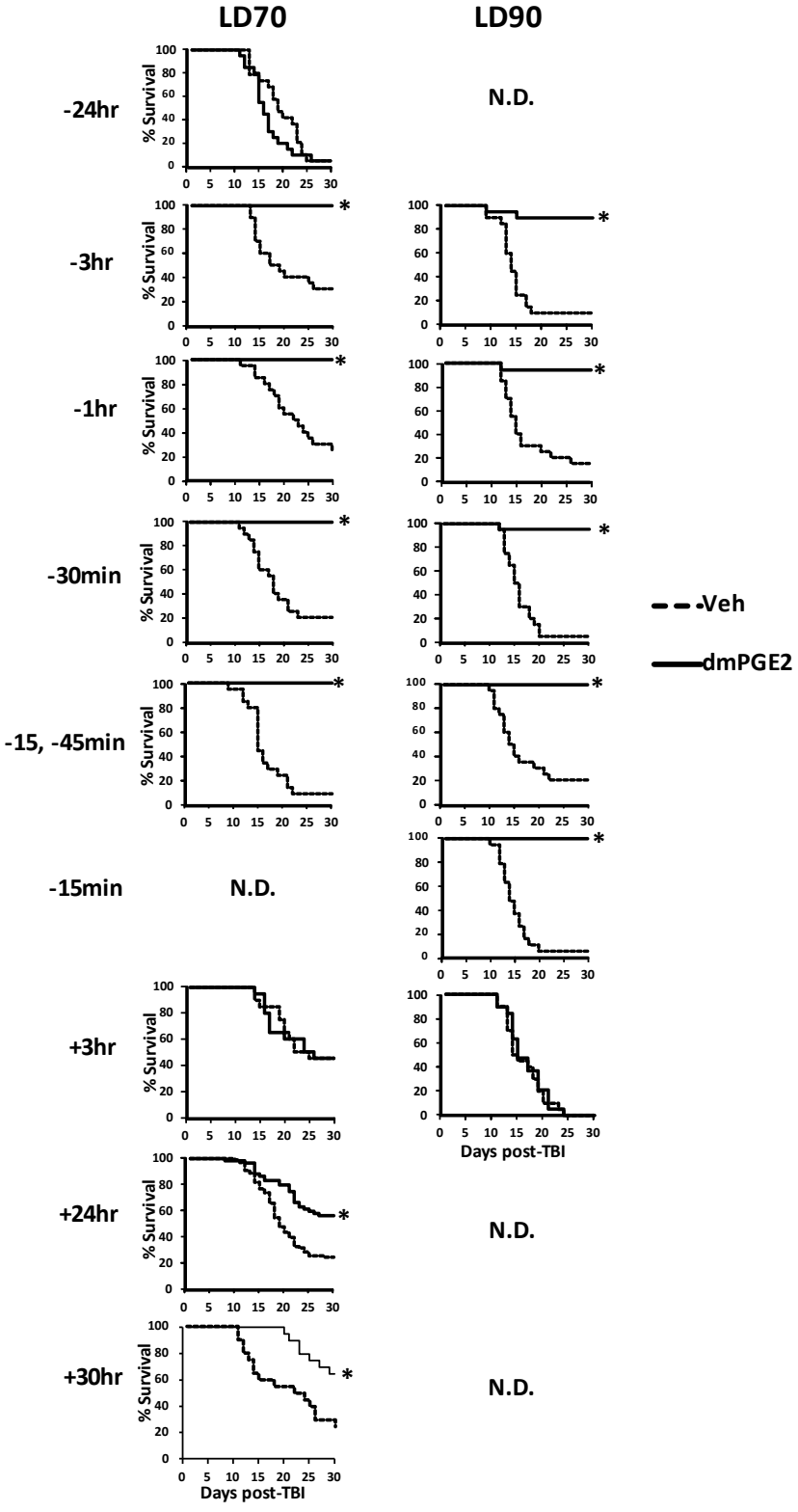
LD70
LD90
-24hr
N.D.
-3hr
-1hr
-30min
-15, -45min
-15min
N.D.
+3hr
+24hr
N.D.
+30hr
N.D.
% Survival
Days post-TBI
Veh
dmPGE2

**Figure 21. Thirty-day survival of lethal-irradiated mice treated with radioprotectant or radiomitigator dmPGE2.**

Mice were exposed to 8.72 Gy (LD70/30) or 9.04 Gy (LD90/30) TBI at 12 w/o. Single dose of 35 μg dmPGE2 per mouse was injected subcutaneously at -24 hr, -3 hr, -1 hr, -30 min, -15 min, +3 hr, +24 hr, or +30 hr relative to time of irradiation; or 2 doses of 20 μg at -15 min and -45 min prior to TBI. Veh control of same dose was given at same time-points as dmPGE2. Male and female mice were equally distributed in each group. The survival in each group was monitored twice daily for consecutive 30 days after TBI. Thirty-day survival rates between the dmPGE2 and Veh group were compared using the Kaplan-Meier method and log-rank test. n=19-20 mice per group except LD70/30 +24hr where n=60 per group. *$p<0.05$ comparing to Veh group.

### 3.3.2. DmPGE2 effects are different in pediatric and geriatric mice

Radiation victims represent a heterogenous population; therefore, age effects of treatments need to be taken into consideration to ensure MCMs are suitable and/or optimized to use in children and the elderly. Pre-clinical animal studies in young and aging mice can be used to determine the impact of age on efficacy when human irradiation studies are not ethical. To date, there has been no research on the efficacy of dmPGE2 as a radioprotectant or radiomitigator in pediatric or geriatric animals. Therefore the efficacy of dmPGE2 was investigated in 6 w/o and 2-year-old mice which represent the juvenile and senior human populations, respectively. The 35 µg dose of dmPGE2 was tested previously and tolerated well by pediatric and geriatric mice with no mortality 24 hr after administration (data not shown). The -30 min and +24 hr Veh-injected mice were combined into one Veh group in the pediatric or geriatric analysis, respectively. In pediatric mice, dmPGE2 given -30 min before TBI (7.41-8.01 Gy) protected 95% ($p<0.001$) of mice compared to 33% survival in vehicle treated mice. However, dosing at +24 hr was not radiomitigative in pediatric mice (Figure 22 A). In geriatric mice, dmPGE2 given -30 min before TBI (9.47-10.08 Gy) protected 80% ($p=0.005$) of mice compared to 36% survival in vehicle treated mice, and it is an effective radiomitigator given at +24 hr, which increased the survival rate to 67% ($p=0.008$) in comparison with 36% survival in vehicle treated mice (Figure 22 B).

### 3.3.3. EP4 Receptor is the potential target receptor in dmPGE2 radioprotection

PGE2 interacts with four conserved G-protein receptors: EP1, EP2, EP3 and EP4. In order to identify the responsible receptor involved in the survival efficacy of dmPGE2

**Figure 22**

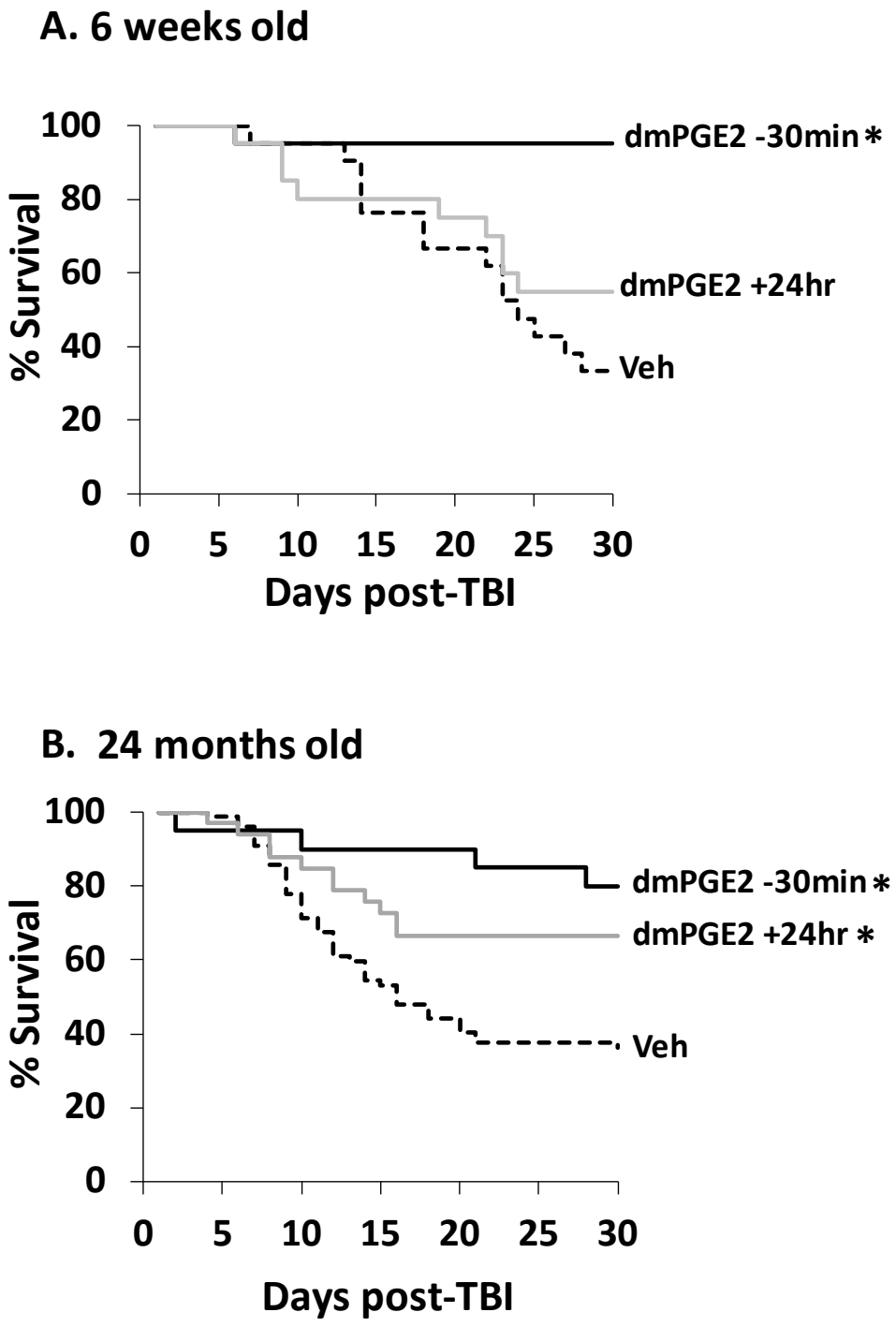
A. 6 weeks old
100
80
60
40
20
0
% Survival
0
5
10
15
20
25
30
Days post-TBI
dmPGE2 -30min *
dmPGE2 +24hr
Veh
B. 24 months old
100
80
60
40
20
0
% Survival
0
5
10
15
20
25
30
Days post-TBI
dmPGE2 -30min *
dmPGE2 +24hr *
Veh

**Figure 22. Thirty-day survival of lethal-irradiated pediatric or geriatric mice treated with radioprotectant or radiomitigator dmPGE2.**

Pediatric mice were exposed to 7.41 Gy for males or 8.01 Gy for females at 6 w/o (panel A). Geriatric mice were exposed to 10.08 Gy for males and 9.47 Gy for females at 24 m/o (panel B). Radioprotectant dmPGE2 was injected subcutaneously single dose of 35 μg per mouse at -30 min prior to TBI, and radiomitigator dmPGE2 was injected with the same dose at +24 hr post TBI. Thirty-day survival rates of radioprotectant dmPGE2, radiomitigator dmPGE2 and Veh groups were compared using the Kaplan-Meier method and log-rank test. In panel A, n=20-21 mice per group. In panel B, dmPGE2 -30 min, n=20 mice; dmPGE2 +24 hr, n=33 mice; Veh -30 min and +24 hr groups were combined, n=77 mice. *$p<0.05$ comparing to Veh group; † $p<0.05$ comparing dmPGE2 +24 hr group to dmPGE2 -30 min group.

administered as a radioprotectant, agonists highly specific for EP1&3 (17-phenyl trinor PGE2; Ki=14/3.7 nM), EP2 (Butaprost-free acid; Ki=11 nM), or EP4 (L-902,688; Ki=0.38 nM) were tested for survival efficacies in comparison with dmPGE2 (Table 1). Only the EP4 agonist, used as radioprotectant, significantly increased the day 30 survival compared with the Veh control (45% in EP4 group vs. 13% in Veh group), although this rate was still significantly lower than the day 30 survival with radioprotectant dmPGE2, which provided nearly 100% protection. Neither EP1&3 nor EP2 agonist increased the day 30 survival rate (Figure 23). Radioprotection appears to be the result of activating the signal pathway via the EP4 receptor.

### 3.3.4. DmPGE2 accelerates hematopoietic recovery post-IR

Hoggatt, J et al. [135] previously found that dmPGE2 administered +24 hr post-TBI effectively enhanced the recovery of peripheral blood cells and HPC potential. Here, the effects of radioprotectant dmPGE2 (-30 min) on the hematopoietic recovery were investigated. The nadir of hematopoietic inhibition post-TBI is around day 7-10, and under the protection of dmPGE2, WBC, NE, RBC and PLT started to recover as early as day 10 post-TBI, and continuously accelerated the hematopoietic recovery to 38 days post-TBI. DmPGE2 treatment had little effect on LY nadir where LY started to recover after day 20 post-TBI (Figure 24 A). Analyses of SLAM LSK and MSC phenotypes in BM at day 50 post-TBI showed a significant increase in HSCs and niche cells (mainly MSC) in dmPGE2-radioprotectant-treated mice compared with mice treated with the Veh control (Figure 24 B & C, Andrea Patterson and Pratibha Singh in Dr. Pelus' laboratory

**Table 1. Selectivity and sensitivity of EP receptor agonists.**

| Compound | Receptor Utilization | Selectivity ($K_i$) at Receptor (nM) | | | |
|---|---|---|---|---|---|
| | | EP1 | EP2 | EP3 | EP4 |
| $PGE_2$ | EP1,2,3,4 | 20 | 12 | 0.85 | 1.9 |
| $dmPGE_2$ | EP2,3,4 | x | 17 | 1.9 | 43 |
| 17-phenyl trinor $PGE_2$ | EP1,3 | 14 | x | 3.7 | x |
| Butaprost-free acid | EP2 | x | 11 | x | x |
| L-902,688 | EP4 | x | x | x | 0.38 |

All compounds are commercially available from Cayman Chemical, Ann Arbor, MI and data are from Cayman Chemical product sheets.

**Figure 23**

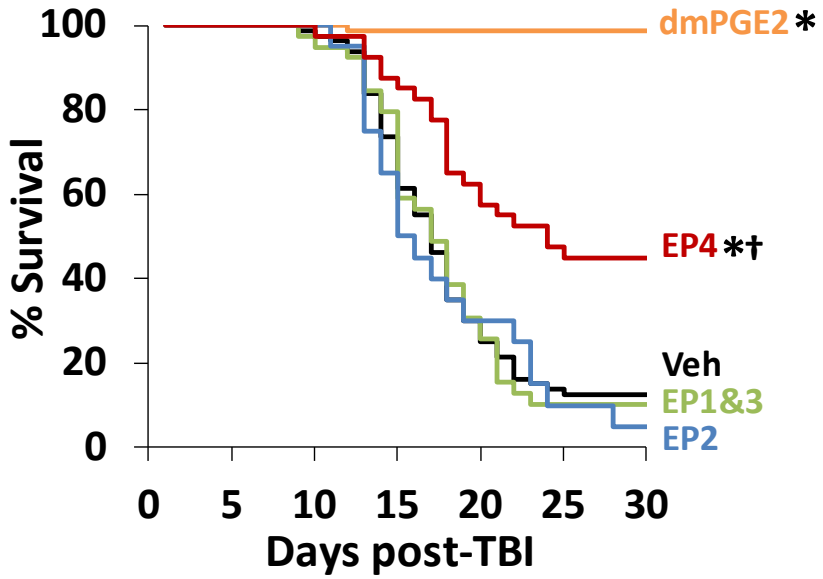
100
80
60
40
20
0
% Survival
0
5
10
15
20
25
30
Days post-TBI
dmPGE2 *
EP4 *†
Veh
EP1&3
EP2

**Figure 23. Thirty-day survival of lethal-irradiated mice treated with dmPGE2 or PGE2 receptor agonists at -30 min prior to TBI.**

Mice were exposed to 8.72 Gy TBI at 12 w/o. 17-phenyl trinor PGE2 (EP1+3 agonist), Butaprost free-acid (EP2 agonist), L-902,688 (EP4 agonist) or dmPGE2, were injected at 35 μg per mouse subcutaneously -30 min prior to TBI, respectively. Thirty-day survival rates of each group were compared using the Kaplan-Meier method and log-rank test. n=20-40 mice per agonist group and n=79-80 mice per dmPGE2 and Veh group. *$p<0.05$ comparing to Veh group; † $p<0.05$ comparing to dmPGE2 group.

provided the bone marrow phenotype analyses). The HPC potential analysis (presented as CFU-GM, BFU-E, CFU-GEMM, and CFC frequency per femur) at day 35 post-TBI demonstrated that dmPGE2 enhanced expansion of myeloid, erythroid, and megakaryoid progenitors in the bone marrow when used as a radioprotectant (Figure 24 D, Liqiong Liu in Dr. Pelus' laboratory provided the CFC analysis).

### 3.3.5. DmPGE2 affects BM cytokines and BM cellularity post-IR

Irradiation induces cytokine storm where cytokines could play positive or negative roles in hematopoiesis post-TBI. Some of them have been proved to be as radioprotectant when given before radiation [270]. Considering the key role of BM cytokine in hematopoietic regulation [271, 272], cytokine levels in BM milieu post-TBI with radioprotectant dmPGE2 treatment were investigated. In order to accurately evaluate the cytokine concentration in BM, Dr. Laura Wright used micro computed tomography to calculate the volume of femur and tibia marrow cavity in male and female mice respectively, in which male had significantly 1.4 times more BM volume than female, emphasizing the importance of cytokine analyses in BM milieu in a gender-specific manner. The values in the Y-axes of Figure 25 represent the cytokine levels in the BM milieu after conversion of the Bio-Plex reads by dilution factor as described in the Materials and Methods section. The cytokine levels in mice sacrificed 30 min after 35 μg dmPGE2 or Veh injection without sham-irradiation represent the cytokine levels at the time of irradiation, in which the hematopoiesis-supporting cytokine KC was significantly increased by dmPGE2. KC was equally increased in both dmPGE2 and Veh groups at 6 hr post-TBI and equally reduced in the two groups at 24 hr post-TBI (Figure 25 A).

**Figure 24**

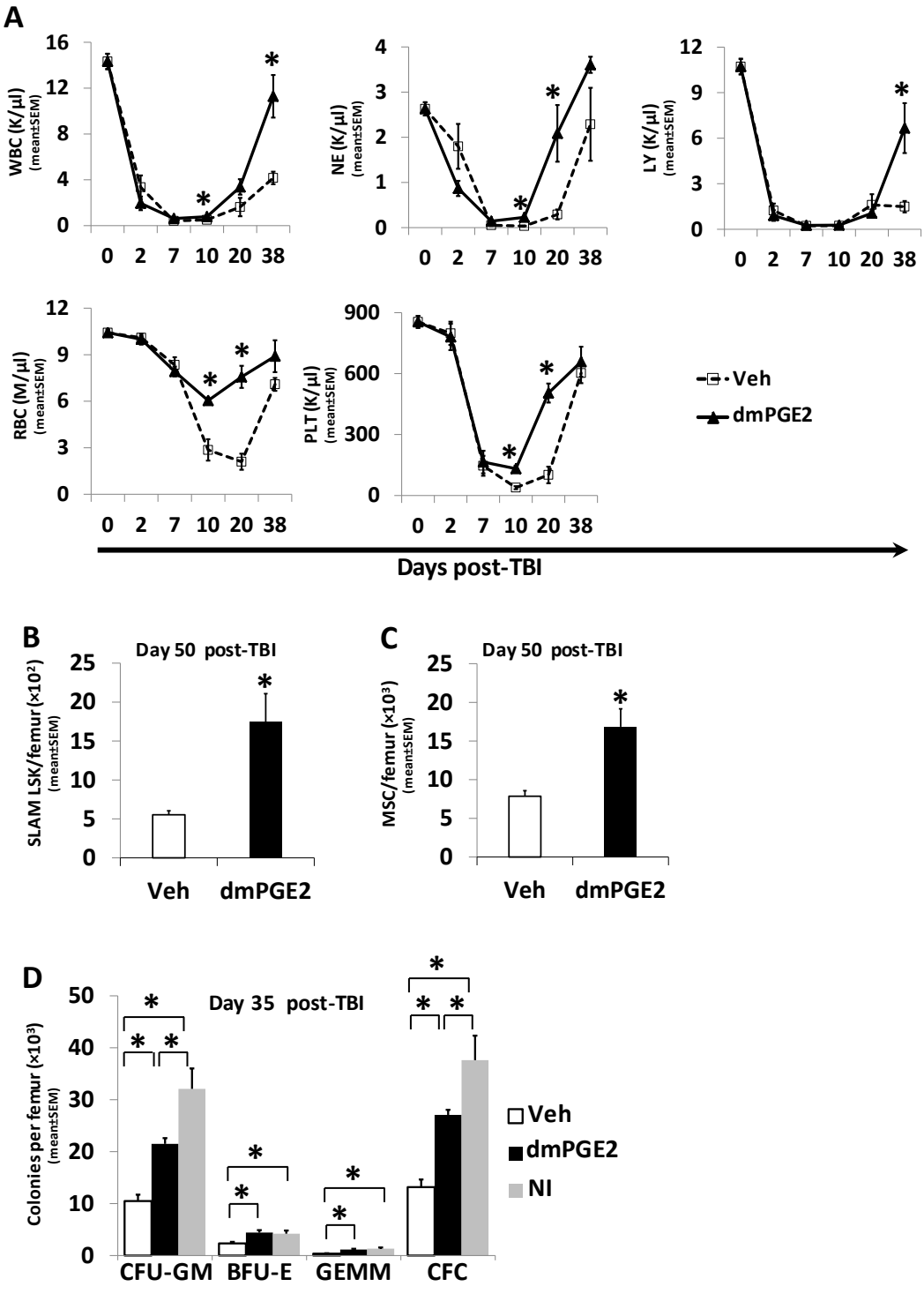
A
WBC (K/µl) (mean±SEM)
NE (K/µl) (mean±SEM)
LY (K/µl) (mean±SEM)
RBC (M/µl) (mean±SEM)
PLT (K/µl) (mean±SEM)
0 2 7 10 20 38
Veh
dmPGE2
Days post-TBI
B
Day 50 post-TBI
SLAM LSK/femur (×10²) (mean±SEM)
Veh
dmPGE2
C
Day 50 post-TBI
MSC/femur (×10³) (mean±SEM)
Veh
dmPGE2
D
Day 35 post-TBI
Colonies per femur (×10³) (mean±SEM)
CFU-GM
BFU-E
GEMM
CFC
Veh
dmPGE2
NI

**Figure 24. Hematopoietic recovery of lethal-irradiated mice treated with radioprotectant dmPGE2.**

Mice were exposed to 8.72 Gy or 9.04 Gy TBI at 12 w/o and treated with single dose of 35 μg dmPGE2 or Veh at -30 min prior to TBI. WBC, RBC and PLT were enumerated at steady-state before irradiation and at day 2, 7, 10, 20 and 38 post-TBI. n=3-6 mice per group per time-point (panel A). In another similar experiment, mice were exposed to 8.72 Gy TBI at 12 w/o and treated with radioprotectant dmPGE2 or Veh as described above. At day 50 post-TBI, the numbers of SLAM LSK and MSC per femur were determined by flow cytometry as described in Materials and Methods (panel B & C). At day 35 post-TBI, $5\times10^4$ bone marrow cells were suspended in ColonyGEL Mouse Complete Medium for CFC assay. After 7 days of incubation, the frequencies of CFU-GM, BFU-E and CFU-GEMM per femur were counted separately and total number of colonies was combined as CFC (panel D). n=4 mice per group. Lines and bars represent mean ± SEM. *$p<0.05$ comparing to Veh group. Andrea Patterson and Pratibha Singh in Dr. Pelus' laboratory provided the bone marrow phenotype analyses. Liqiong Liu in Dr. Pelus' laboratory provided the CFC data.

# Figure 25

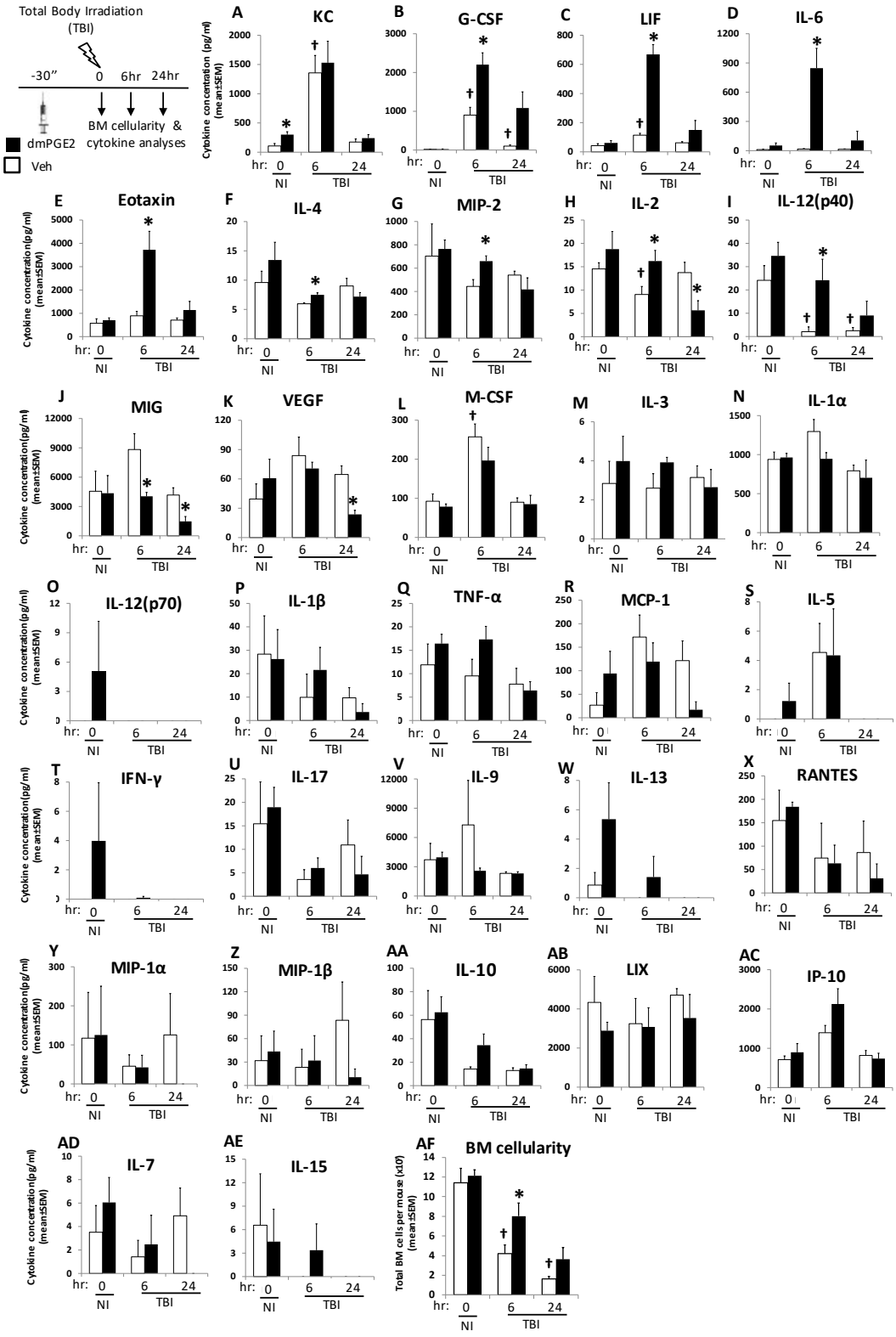
Total Body Irradiation (TBI)
-30"
0
6hr
24hr
BM cellularity & cytokine analyses
dmPGE2
Veh
A KC
B G-CSF
C LIF
D IL-6
E Eotaxin
F IL-4
G MIP-2
H IL-2
I IL-12(p40)
J MIG
K VEGF
L M-CSF
M IL-3
N IL-1α
O IL-12(p70)
P IL-1β
Q TNF-α
R MCP-1
S IL-5
T IFN-γ
U IL-17
V IL-9
W IL-13
X RANTES
Y MIP-1α
Z MIP-1β
AA IL-10
AB LIX
AC IP-10
AD IL-7
AE IL-15
AF BM cellularity
Cytokine concentration (pg/ml) (mean±SEM)
Total BM cells per mouse (x10) (mean±SEM)
hr: 0 6 24
NI
TBI

**Figure 25. BM cytokines and BM cellularity at 6 and 24 hr post-TBI treated with radioprotectant dmPGE2.**

Twelve w/o NI mice were treated with single dose of 35 μg dmPGE2 or Veh subcutaneously at -30 min prior to sacrifice. Irradiated mice (8.53 Gy TBI) were treated with single dose of 35 μg dmPGE2 or Veh per mouse subcutaneously at -30 min prior to TBI and sacrificed at 6 and 24 hr post-TBI. Femurs and tibias were flushed by cold PBS, BM cellularity was enumerated and cytokine levels in BM supernatant were measured by bead-based multiplex technology as described in Materials and Methods. Bars represent mean ± SEM. n=4-5 mice per group per time-point. *$p<0.05$ comparing dmPGE2 group to Veh group at each indicated time-point; † $p<0.05$ comparing TBI Veh group to NI Veh group (0 hr time-point). Huilin Chua and Hailin Feng did the Bio-Plex study; Tong Wu did the analyses.

By 6 hr post-TBI, irradiation exposure increased G-CSF and LIF in BM and dmPGE2 further increased their concentrations (Figure 25 B & C). IL-6, Eotaxin, IL-4 and MIP-2 were not influenced by irradiation but increased in dmPGE2 group at 6 hr post-TBI (Figure 25 D-G). Radioprotectant dmPGE2 attenuated the irradiation-induced decreases of IL-2 and IL-12(p40) (Figure 25 H & I); or attenuated the irradiation-induced increase of MIG (Figure 25 H & I). There were also cytokines which only impacted by irradiation but not by dmPGE2, such as M-CSF (Figure 25 L); or neither impacted by irradiation nor by dmPGE2 (Figure 25). The BM cell loss induced by irradiation was attenuated by dmPGE2 prior to TBI (Figure 25 AF).

By 24 hr post-TBI, most irradiation-induced or dmPGE2-induced cytokine production subsided. IL-2 was decreased at 24 hr in dmPGE2 group although it was increased at 6 hr (Figure 25 H). MIG and VGEF were lower in dmPGE2 group comparing to Veh group at 6 hr and further suppressed at 24 hr (Figure 25 J & K).

### 3.4. Discussion

PGE2 could be an inhibitor and a stimulator of hematopoiesis depending on regimen and dose [123, 127, 260, 273]. Early studies demonstrated that short-term in vitro culture of BM cells with PGE2 stimulated quiescent cells to enter the cell cycle and increased colony-forming unit-spleen (CFU-S) following transplantation [273]. However, in vivo treatment with PGE2 had little or no impact on hematopoiesis [130, 274]. Recently, ex vivo embryonic exposure to dmPGE2 was shown to increase HSC numbers in a Zebrafish embryo model, while blocking PGE2 production by indomethacin

decreased the HSC number [127]. On the contrary, Gentile P et al. and Hoggatt J et al. [123, 260] showed that in vivo repeated treatments (3 or 7 consecutive days) with native PGE2 or dmPGE2 decreased bone marrow and splenic cellularity, and CFU-GM frequency. Considering that these different studies used different timing and duration of exposure, it is reasonable to hypothesize that the administration schedule of dmPGE2 (or PGE2) plays a critical role in deciding its stimulatory or inhibitory effect on hematopoiesis under the radiation scenario, and certain schedules might be ineffective or even deleterious to survival, which makes the optimization of dmPGE2 dosing windows important.

Survival analysis indicates that administration of dmPGE2 as radioprotectant during -3 hr to -15 min prior to TBI confers almost complete survival but -24 hr schedule was not radioprotective (Figure 21). Data from Dr. Pelus' laboratory show that the PGE2's inhibition on proliferation of HSPC lasts longer than 24 hr after injection [123, 275]. The potential mechanism that dmPGE2 inhibits cell cycling and thus decrease DNA damage brought by irradiation, cannot explain the phenomenon that -24hr schedule is not radioprotective. The attenuation of irradiation-induced increase in HSPC cycling by dmPGE2 administration at -30 min or earlier prior to TBI is more likely a direct dmPGE2 signaling response at the time of irradiation.

The dmPGE2 +3 hr administration schedule fails to increase day 30 survival rate. Hoggatt J et al. [135] showed that radiomitigator dmPGE2 administrated at +6 hr and +24 hr post-TBI increases survival, and now the efficacy of +24 hr time-point in another

cohort of mice is confirmed and the time window is extended to +30 hr post-TBI. So, the time-window for dmPGE2 radiomitigator is +6 to +30 hr post-TBI. This information is important for maximizing survival in civilian victims of unexpected lethal radiation when radioprotection is impossible. Although Porter RL et al. [276] reported that dmPGE2 given immediately after sub-lethal irradiation decreased the loss of functional HSPC, another survival study reported by Walden TL et al. [134] demonstrated that dmPGE2 given at either +5, +15, +30, or +60 min after lethal irradiation was not radiomitigative. This discrepancy might relate to different mouse stain, different irradiation dose and different dmPGE2 dose. These studies indicate that irradiation transient induces unknown mechanisms to prevent dmPGE2 to take effect in at least 3 hr post-TBI.

The obtained dmPGE2 survival data in pediatric and geriatric populations are important considerations for real-life radiation scenarios. Although there were detailed studies about using prostaglandin analogues, most focused on the use of PGE1 in maintaining the patency of the ductus arteriosus in neonates [277]. The information from these studies could not apply to the radiation scenario because of the different disease status and differences between neonates and juveniles. This study, for the first time, indicates that radioprotectant dmPGE2 is effective both in pediatric and geriatric population, although the survival in geriatric population (80%) is slightly lower than in pediatric and adult population (95-100%), which might relate to the underlying impairment in aging mice. Radiomitigator PGE2 injected at +24 hr post-irradiation is effective in geriatric population but not in pediatric population (Figure 22). Sex difference in adolescence where male and female have significantly different sex

hormones profile might interfere the dmPGE2 radiomitigation. These results provide evidence that the stockpiling of dmPGE2 for use as a radioprotectant for H-ARS might benefit more widely diverse populations.

By using specific EP agonists, the potential EP receptor responsible for dmPGE2 radioprotection was investigated. Survival efficacy was only observed in mice receiving an EP4 agonist. However, while strongly suggestive of an EP4 binding effect, the level of protection provided by EP4 agonist was less than that by dmPGE2 (Figure 23). Binding of PGE2 to EP4 activates the cAMP dependent PKA/GSK3β/β-catenin pathway or cAMP independent GPCR kinase/PI3K/GSK3β/β-catenin pathway and then enhances the Wnt signaling pathway by stabilizing β-catenin. The nuclear translocation β-catenin activates the transcription and translation of CXCR4, Survivin and Cyclin D, thus promotes the homing, survival, and proliferation of HSCs [278-280]. When EP agonists given as radiomitigators, none of them show survival efficacy (unpublished data from Dr. Pelus' laboratory), which indicates that the mechanisms of radioprotection and as a radiomitigation is different. The possible reasons for EP4 agonist not achieving the same level of protection as dmPGE2 might be the low agonist potency or dosing regimen, or more than one EP receptors activation needed for full survival efficacy. Experiments on combination of EP receptor agonists, intensive agonist regimens, EP receptor antagonists and genetic knockouts of EP receptors are ongoing to further confirm the responsible EP receptors.

Enhanced day 30 survival of dmPGE2-treated mice coincided with more robust recovery of all CBC parameters (Figure 24 A), indicative of enhanced hematopoietic recovery. Enhanced recovery of CBC correlated with increased HPC potential (Figure 24 D). The result of the colony assay seems be contradictory to an early study that in vivo PGE2 administration inhibits the production of CFU-GM [123]. One probable reason is that inhibition might not last as late as the time-point of colony assay was taken; another reason is that the increased HPC potential came from HSC protection, where SLAM-LSK levels were increased in dmPGE2-treated mice (Figure 24 B). The increased number of MSCs in dmPGE2 treated mice (Figure 24 C), a critical component of the HSC-supportive BM microenvironment, indicates the possibility that dmPGE2 influences HSC indirectly by protecting the BM microenvironment. It was previously demonstrated that PGE2 regulates dendritic cell generation through EP1 and EP3 receptors and the downstream STAT3/Survivin pathway [268]. Ikushima et al. found that PGE2 indirectly induced hematopoiesis through the activation of mesenchymal progenitor cells, which is consistent with finding of increased MSC in dmPGE2-treated mice [281].

BM supernatant is the extracellular fluid component of the BM microenvironment, which is rich in cytokines and growth factors. As the BM supernatant "bathes" HSCs and HPCs in their specialized niches, the BM cytokine milieu is more informative than the peripheral blood cytokine level in determining the effect of treatment on hematopoiesis [282]. Cytokines induced by dmPGE2 at the time of irradiation may enhance survival and hematopoietic recovery post-TBI. Since straining mouse in a limited space during irradiation is a huge pressure on mouse and this

procedure itself will impact the cytokine level, the NI mice in this study were not sham-irradiated, which the levels of BM cytokines at 30 min post-injection represent the cytokine levels at the time of irradiation. In NI group, although most cytokines between dmPGE2-injected and Veh-injected NI mice were not statistically different, KC significantly increased in dmPGE2 group (Figure 25), which play roles in neutrophil recruitment [283] and has potent hematopoietic activities in truncated form [284]. Future study would need to verify the radioprotective effect of KC. Some other cytokines, which have been proven to be effective radioprotectants in vivo or in vitro, such as TNF-α [285], LIF [286], VEGF [287], IL-12 [288, 289] and IL-6 [290, 291], had trends of increasing in the dmPGE2 group at the time-point of 0 hr although not statistically different from the Veh-injected NI group (Figure 25). All these results indicate that radioprotectant dmPGE2 enhances survival through up-regulating BM cytokines or activating a network of cytokines interaction.

In mice sacrificed at 6 hr and 24 hr post-TBI, the BM cytokine levels reflect how dmPGE2 injected before irradiation impacts cytokines post-TBI and hence promotes hematopoietic recovery. In cytokines that up-regulated in the dmPGE2 group, some have potent effect in stimulating the proliferation of hematopoietic progenitor cells, such as G-CSF and IL-12(p40) [272]; some others need synergistic actions from other cytokines to promote hematopoiesis, such as LIF, IL-6 and IL-4 [292, 293]; and some chemokines which do not have directly stimulating effect but can help with the transmigration and diapedesis of HSCs or attract inflammatory cells to bone marrow niche to regulate the HSCs, such as Eotaxin [294] and MIP-2 [295] (Figure 25). In cytokine down-regulated in

the dmPGE2 group, MIG has pleotropic effects, which acts as mediators of chemotaxis and as myelosuppressor [296]. The attenuation of HPC inhibition from the down-regulation of suppressive factors, together with the up-regulation of stimulatory factors, might be one of the mechanisms for quick recovery of CBC parameters (Figure 24 A) and enhances survival (Figure 21) in dmPGE2 group. DmPGE2 also promotes hematopoiesis through regulating the pro-inflammatory vs. anti-inflammatory status of BM microenvironment by cytokine such as IL-2. The transient increase and rapid decrease of IL-2 in dmPGE2-treated mice indicated that in less than 24 hr post-TBI, the stresses and free-radical attacks on HSC from the inflammatory microenvironment were attenuated by dmPGE2, which might relate to the immunosuppressive effect of dmPGE2 [297]. In addition to angiogenesis, VEGF inhibits the maturation of dendritic cells and differentiation of lymphocytes through inhibiting the activation of NF-κB in HPC. The lower expression of VEGF at 24 hr post-TBI in dmPGE2-treated group indicates that NF-κB signal pathway was activated by inhibiting VEGF, thus indirectly enhancing hematopoiesis [298, 299]. The study on RNA-sequencing and Ingenuity pathway analysis (IPA) of these cytokines related gene expression changes in HSC are ongoing and will provide more insight on how these cytokines regulate hematopoiesis post-TBI (data unpublished).

In summary, these studies characterized the optimum time window for administering dmPGE2 as radioprotectant and radiomitigator, showed the survival efficacy in pediatric and geriatric populations, investigated the potential receptor for dmPGE2's radioprotective effect, revealed hematopoietic recovery in peripheral blood

and bone marrow, and further demonstrated the bone marrow cytokine milieu changes in mice received dmPGE2 as a radioprotectant. These studies provide supports for developing dmPGE2 as a MCM for H-ARS with FDA approval.

# Chapter 4. Prostaglandin E2 and Lymphoid Lineage Reconstitution

## 4.1. Introduction

Exposure to a lethal dose of irradiation results in H-ARS and DEARE, as previously discussed. Immune involution is an important component of DEARE, mainly resulting from defective de novo lymphopoiesis and partially compensated by lymphocyte HPE. Thymic and peripheral lymphocytes are highly radiosensitive. The "double hit" from radiation and aging accelerates long-term thymic involution and immune deficiency. Immune deficiency is linked to the increased incidence of infection, cancer, and defective immune surveillance functions in H-ARS survivors [4, 205, 206]. Thymic involution in H-ARS survivors can result from: 1) decreased number and/or function of bone marrow-derived thymic precursors, 2) inability of these precursors to settle in the thymic niches, or 3) disruption of the thymic nurturing niches [4, 40, 56]. Currently, there are no effective treatments or preventions for radiation-induced thymic involution.

DmPGE2 has demonstrated remarkable radioprotection effect in the H-ARS model (discussed in Chapter 3). DmPGE2 is a long-acting analog of PGE2, which has similar biological effects to PGE2. PGE2 inhibits T cell activation and proliferation by up-regulating cAMP and down-regulating IL-2 [300-302], and thus is considered detrimental to T cells. The potential for dmPGE2 to play a positive role in lymphoid lineage reconstitution post-IR had not been previously investigated.

Dr. Orschell's laboratory has developed robust murine models of H-ARS in adult mice [69], which were used to evaluate thymic involution and immune reconstitution in survivors of lethal irradiation and to elucidate potential protective effects of dmPGE2. In this chapter, the radioprotection effect of dmPGE2 on radiation-induced thymic involution and long-term immune suppression in irradiation survivors is investigated. This is the first report of an effective radioprotectant MCM targeting thymic involution and lymphoid lineage reconstitution post-IR.

## 4.2. Materials and Methods

### 4.2.1. Mice, radiation, dosimetry, husbandry, and tissue harvest

Specific pathogen-free C57BL/6 mice ($CD45.2^+$), B6.SJL-PtrcaPep3b/BoyJ mice (B6.BoyJ, $CD45.1^+$) and Fgd5-ZsGreen mice were purchased from Jackson laboratory (Bar Harbor, ME). F1 hybrids of C57Bl/6 and B6.BoyJ mice ($CD45.2^+/CD45.1^+$) were bred in-house. Mice were received at 10 w/o and allowed to acclimate for 2-week prior to irradiation. Husbandry, irradiation, dosimetry, tissue harvest and process are described as in Chapter 2. The TBI dose is either 8.53 (LD50/30), 8.72 (LD70/30) or 9.04 Gy (LD90/30) as specified. All studies were approved by the Indiana University School of Medicine Institutional Animal Care and Use Committee.

### 4.2.2. Compounds

DmPGE2 and EP1-EP4 were purchased from Cayman Chemicals (Ann Arbor, MI). The reconstitution, dosage, administration of dmPGE2 and EP agonists were the same as in Chapter 3 and were indicated in Figures and Legends.

### 4.2.3. CBC

Peripheral blood CBC was performed as previously described in Chapter 2. For CBC from cardiac puncture, mice were euthanized by $CO_2$ inhalation and laid in dorsal position. A 25-G 5/8inch needle was inserted toward the mouse's left ventricle, under the sternum, and into the heart. The plunger of the syringe was slowly pulled and 100-150 µl blood was collected. Complete blood count was analyzed by HEMAVET 950FS Hematology System (Drew Scientific, Waterbury, CT).

### 4.2.4. Antibody staining, flow cytometry analysis and flow cytometric cell sorting

Antibodies used for identifying HSC, HPC, thymocyte subsets, and peripheral lymphocyte subsets were described in Chapter 2. In the in vitro lymphoid lineage differentiation assay, lysed bone marrow cells were stained with CD11b-FITC, Ter119-FITC, CD3-FITC, Gr1-FITC, B220-FITC, Sca-1-PECY7 or BV650, c-Kit-APC antibodies and sorted for LSK cells to seed on the monolayer stromal cells. The live cells harvested from the culture system at different time-points were stained with CD11b-APCCY7, B220-PE-TEXAS RED, CD4-PECY5, CD8α-PE, CD44-APC, CD25-PECY7, CD62L-PerCPCY5-5 antibodies. In bone marrow competitive transplantation study, thymi of recipients were processed into single cell suspension and stained with CD45.1-PE, CD45.2-FITC, CD4-PerCPCy5.5, CD8α-PECy5, CD44-APC and CD25-PECy7 antibodies to evaluate thymic donor chimerism and thymocyte subgroups reconstitution. In short-term thymus homing study, recipient thymocytes were stained with CD45.1-PE and CD45.2-FITC antibodies to evaluate the homing efficiency. In TEC analysis study,

the single thymocyte suspensions after enzyme digestion were stained with CD45-PE, EpCAM-APCCy7, UEA-1-FITC and Ly51-APC antibodies. All antibodies were purchased from BD Biosciences (San Jose, CA), Biolegend (San Diego, CA), eBiosciences (San Diego, CA) and Vector Laboratories (Burlingame, CA). Analytical data were collected on an LSR-II flow cytometer (Becton Dickinson Immunocytometry Systems, San Jose, CA).

### 4.2.5. T and B cell development in vitro and PMA stimulation assay

To test the ability of progenitor cells to differentiate into B and T lymphoid lineages in vitro, I used the OP9 or OP9-DL4 co-culture system, respectively. The co-culture system and the staining protocol are described by Zuniga-Pflucker et al. [303-305]. OP9 and OP9-DL4 cell lines were obtained from Zúñiga-Pflücker JC (University of Toronto, Canada). The culture medium for OP9 and OP9-DL4 was minimal essential medium (HyClone Laboratories Inc., Logan, UT) with 20% FBS and 1% penicillin streptomycin (Lonza, Walkersville, MD). OP9 and OP9-DL4 cells were thawed and passaged 2-3 times and grown to 80% confluence in a T25 flask, and $4\times10^4$ OP9 or OP9-DL4 cells were plated per well in a 24-well plate 24 hours prior to co-culture at 80-90% confluence. Co-culture was carried out with OP9 medium plus 1 ng/ml IL-7 and 5 ng/ml FLT3L (both from PeproTech, Rocky Hill, NJ). One thousand sorted LSK cells were resuspended with 1 ml co-culture medium and were applied to the stromal monolayer at the first day of co-culture. Half of the medium was changed every 3-4 days. The cultured cells were demi-depopulated and transferred to new monolayers every 5-7 days after the appearance of the first colony (~day 9). Half of the acquired cells were transferred to new

monolayer stromal cells and the rest of the cells were used for phenotyping until the end of the co-culture [304].

At day 16 or day 32 of co-culture, $5\times10^5$ cultured cells from OP9-DL4 co-culture system were stimulated with 20 ng/ml phorbol 12-myristate 13-acetate (PMA) (Santa Cruz Biotechnology Inc., Santa Cruz, CA) plus 500 ng/ml Ionomycin (Santa Cruz Biotechnology Inc., Santa Cruz, CA) for 5 hr at 37°C with 5% atmospheric $CO_2$. Brefeldin A (1 μg/ml; GolgiPlug, BD Biosciences, NJ) was added to inhibit intracellular protein transport. After 5 hr of activation, cells were fixed and permeabilized with Cytofix and Cytopermb buffers (BD Biosciences, NJ), and stained with intracellular IFN-γ APC.

### 4.2.6. Long-term competitive transplantation and short-term thymus homing study

Donor whole bone marrow cells were flushed from long bones of NI or IR mice (C57BL/6, CD45.2$^+$), and $3\times10^5$ of these cells were transplanted intravenously along with $2\times 10^5$ congenic competitor bone marrow cells into congenic recipients. The competitors and recipients were B6.BoyJ (CD45.1$^+$) or the F1 hybrid of C57Bl/6 and B6.BoyJ mice (CD45.1$^+$ and CD45.2$^+$). Recipients had been irradiated with 11 Gy which consisted with a split-dose of 5.5 Gy followed by 5.5 Gy four hours later. The use of congenic mice in competitive bone marrow transplantation has been previously described [40, 306, 307]. Recipient mice were sacrificed at 6 months post-transplantation and thymi were used for chimerism analysis. For short-term thymus homing study, $2\times10^7$ whole BM cells from donor mice (C57Bl/6, CD45.2$^+$) were transplanted intravenously into lethally-irradiated

recipient mice (B6.BoyJ, CD45.1$^{+}$). After 16 hr, recipient thymocytes were analyzed by flow cytometry for homing efficiency.

### 4.2.7. Thymus epithelial cells identification

Thymi were cut into small pieces with fine scissors and incubated with 0.5 ml thymic enzyme solution [RPMI1640 medium with 0.05% (w/v) Liberase TH (Roche Diagnostics, Indianapolis, IN) and 100 U/ml DNase I (New England Biolabs, Ipswich, MA)] at 37 °C for 20 min. Supernatant was discarded and fresh enzyme solution was added to remaining debris until digestion was complete [308]. The cTEC was defined as CD45$^{-}$EpCAM$^{+}$UEA-1$^{-}$Ly51$^{+}$ and mTEC was defined as CD45$^{-}$EpCAM$^{+}$UEA-1$^{+}$Ly51$^{-}$ by flow cytometry analysis.

### 4.2.8. RNA sequencing and IPA analysis of HSC

Fgd5 mice received one 35 μg dose of dmPGE2 or equivalent Veh injection -30 min prior to TBI (8.53 Gy, LD50/30) and were sacrificed 24 hr post-TBI. Fgd5 ZsGreen was used to enhance the purity of HSCs due to the loss of c-kit expression after radiation [309]. HSCs were identified as CD45$^{+}$SLAM-LSK$^{wide}$ZsGreen$^{+}$ and sorted by FACSAria. RNA was extracted with a RNeasy Plus Micro kit (Qiagen, Hilden, Germany). To obtain adequate amounts of high-quality cDNA, due to the low cell number (1,000-6,000 HSCs per sample), SMART-Seq v4 Ultra Low Input RNA Kit (Takara Bio, Mountain View, CA) was used for cDNA synthesis. RNA sequencing was performed by the Genomics Core at Indiana University School of Medicine. To compare gene expression between different groups, results were converted to Reads Per Kilobase per Million (RPKM).

Significant differences were defined as false discovery rate (FDR) <0.05 and fold change >2. IPA analysis was used to evaluate differentially expressed genes. Lymphopoiesis and its related genes were identified by IPA cellular function predictions. The RPKM values were transformed to Z-scores for visualization purposes. The Z-score was defined as the difference of individual and average RPKM value divided by standard deviation. Blue represented lower scores and red for higher scores (Andrea Patterson in Dr. Pelus' laboratory provided the RNA sequencing and IPA analysis).

### 4.2.9. Bone marrow cytokine analysis

C57BL/6 mice were treated with one dose of 35 μg dmPGE2 at -30 min or equivalent Veh prior to 8.53 (LD50/30) and were sacrificed 9 days post-TBI. The BM cytokine detection and analyses were the same as described in Chapter 3. The Z-score of each cytokine was calculated as the difference of individual and average cytokine level divided by standard deviation. The Z-scores were transferred to color scale with blue for low and red for the high expression levels.

### 4.2.10. Statistical analysis

Lifespan in DEARE mice were analyzed by Kaplan-Meier analyses and log-rank tests using SPSS Statistics Version 24 (IBM, Armonk, NY). Blood parameters comparisons between dmPGE2-injected NI and baseline were subjected to unpaired two-tailed t-tests using Microsoft Excel 2010 (Microsoft Corp, Redmond, WA). Comparisons of more than two groups were performed by one-way analysis of variance (ANOVA) with post-hoc Tukey-Kramer HSD or Welch ANOVA for unequal variances using JMP

14 (SAS Institute, Cary, NC). Fisher's exact test was used to assess the incidence of thymic mass post-TBI and was performed using online Fisher exact test calculator from www.socscistatistics.com/tests. The day 30 survival difference between vehicle-treated and dmPGE2-treated groups were compared with the Kaplan-Meier (log-rank) test using SPSS Statistics Version 24 (IBM, Armonk, NY). $P<0.05$ was considered significant. All data are expressed as mean ± SEM.

### 4.3. Results

#### 4.3.1. DmPGE2 extends lifespan and prevents the myeloid skew of DEARE mice

When used as a radioprotectant, dmPGE2 greatly increased the day 30 survival rate of lethally irradiated mice. There was no statistical difference in day 30 survival rates between mice received one dose of 35 μg or two doses of 20 μg dmPGE2 at -15 min to -3 hr time-window prior to TBI (Chapter 3, Figure 21). And there was no statistical difference in long-term survival rates between mice exposed to LD50/30, LD70/30 or LD90/30 (unpublished data). Data from theses dmPGE2 schedules with different lethal-irradiation exposure were therefore combined and referred to as radioprotectant dmPGE2 group in all the following studies unless specifically stated otherwise. Consistent with earlier reports [310, 311], lifespan was significantly shortened in Veh mice comparing with age-matched NI controls. Radioprotectant dmPGE2 greatly extended the long-term survival rate comparing with Veh but still lower than the NI control (Figure 26). Complete blood counts in Veh and dmPGE2-treated survivors and NI controls were followed up to 12 months post-TBI. At 6 months post-TBI, NE count in the Veh and dmPGE2 group were lower than the NI group. No statistical difference among these

**Figure 26**

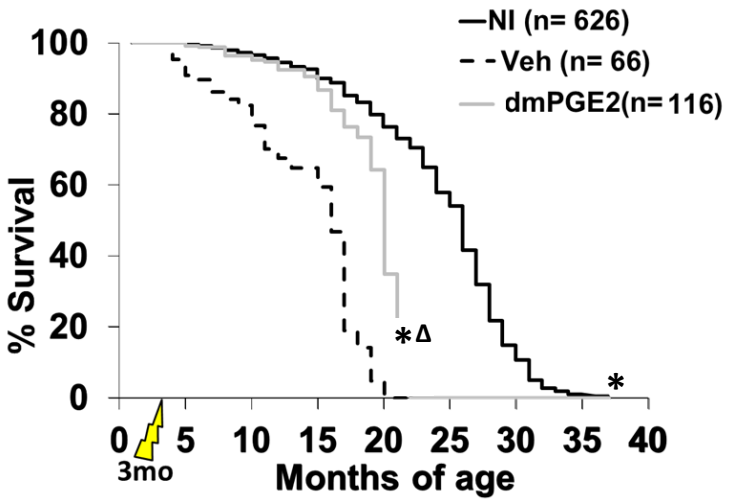
—NI (n= 626)
- - Veh (n= 66)
dmPGE2(n= 116)
100
80
60
40
20
0
% Survival
*Δ
*
0
5
10
15
20
25
30
35
40
3mo
Months of age

**Figure 26. Long-term survival of lethal-irradiated mice treated with radioprotectant dmPGE2.**

Twelve w/o C57BL/6 mice were treated with one dose of 35 μg dmPGE2 at -15 min, -30 min, -1 hr or -3 hr, or 2 doses of 20 μg dmPGE2 at -15 and -45 min prior to 8.53 Gy, 8.72 Gy, or 9.04 Gy TBI as previously described. Mice survived over day 30 post-TBI were transferred to RBMD study for long-term survival monitor until the end of study (24 months post-TBI). The survival mice were recorded when found dead, or were euthanized when severely moribund or scheduled time-point sacrifices. All the mice received radioprotectant dmPGE2 were combined in radioprotectant dmPGE2 group and all Veh-treated mice were combined into Veh group. NI mice from multiple studies were used as control. Survival is shown as Kaplan-Meier curve. * $p<0.05$ comparing to Veh group; Δ $p<0.05$ comparing to NI group.

groups remained at 12 months post-TBI. At 6 and 12 months post-TBI, LY count in the Veh group was significantly lower than in the NI and dmPGE2 groups, with no difference between the NI and dmPGE2 groups (Figure 27 A-C). Myeloid skewing was also obvious when expressed as percentages (Figure 27, D & E), where the percentage of NE was significantly higher in the Veh group than the NI group, and the percentage of LY was significantly lower in the Veh group than the NI group. These differences increased as mice aged. DmPGE2 effectively prevented myeloid skew in DEARE mice, where the dmPGE2 group had higher LY percentage and lower NE percentage than Veh group. NI mice had higher RBC and PLT counts than Veh, and dmPGE2 group had higher RBC and PLT than Veh group (Figure 27 F & G).

### 4.3.2. DmPGE2 transiently decreases lymphocyte level in normal mice

Lymphocyte recovery post-TBI is relatively later than neutrophil recovery in dmPGE2 group, which has been discussed in previous Chapter and in Figure 24), whether dmPGE2 itself, in NI scenario, could regulate lymphocyte number, has not been tested. Complete blood count was evaluated in non-irradiated mice receiving one shot of dmPGE2 or Veh and followed up to 10 days post injection (Figure 28 A-C). The basal levels of WBC, NE, LY, RBC and PLT from cardiac puncture were lower than the corresponding values from the tail-bled CBC, corresponding with earlier study from Hoggatt J et al. [312]. Compared with untreated controls (day 0, Figure 28 A-G), dmPGE2-treated mice had rapidly decreasing LY numbers and a relatively higher percentage of NE day 1 post-injection, demonstrating the early toxicity of dmPGE2 in

**Figure 27**

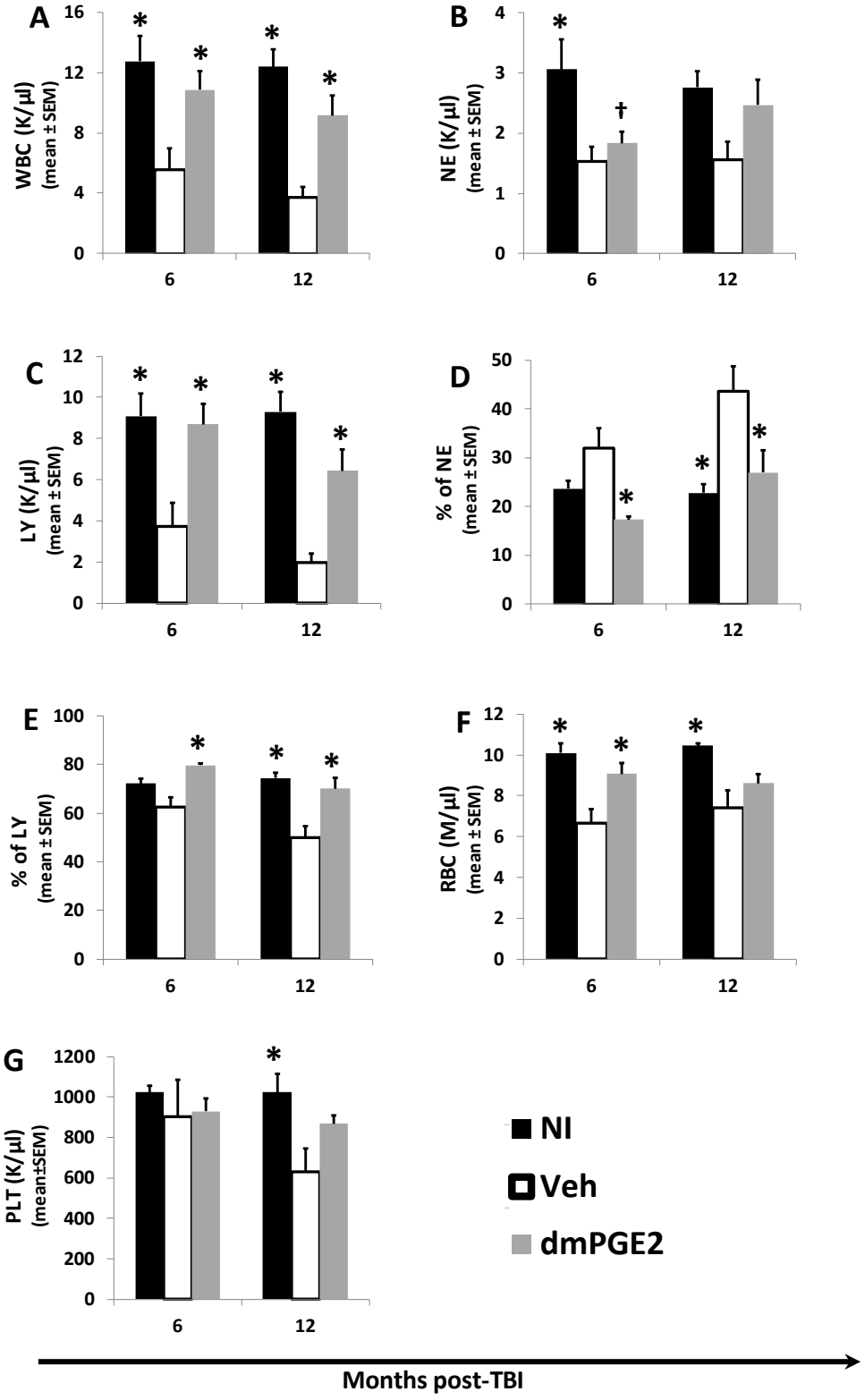
A
WBC (K/µl)
(mean ± SEM)
16
12
8
4
0
6
12
B
NE (K/µl)
(mean ± SEM)
4
3
2
1
0
†
C
LY (K/µl)
(mean ± SEM)
12
10
8
6
4
2
0
D
% of NE
(mean ± SEM)
50
40
30
20
10
0
E
% of LY
(mean ± SEM)
100
80
60
40
20
0
F
RBC (M/µl)
(mean ± SEM)
12
10
8
6
4
2
0
G
PLT (K/µl)
(mean±SEM)
1200
1000
800
600
400
200
0
NI
Veh
dmPGE2
Months post-TBI

**Figure 27. CBC profiles in DEARE phase of lethal-irradiated mice treated with radioprotectant dmPGE2.**

C57BL/6 mice were treated with radioprotectant dmPGE2 or Veh prior to lethal TBI. Complete blood count analyses of WBC (panel A), NE (panel B), LY (panel C), %NE (panel D), %LY (panel E), RBC (panel F) and PLT (panel G) were followed up at 6 and 12 months post-TBI. Lines represent mean ± SEM. n=6-12 mice per group (panel A-G). *$p<0.05$ comparing to Veh; † $p<0.05$ comparing to NI.

**Figure 28**

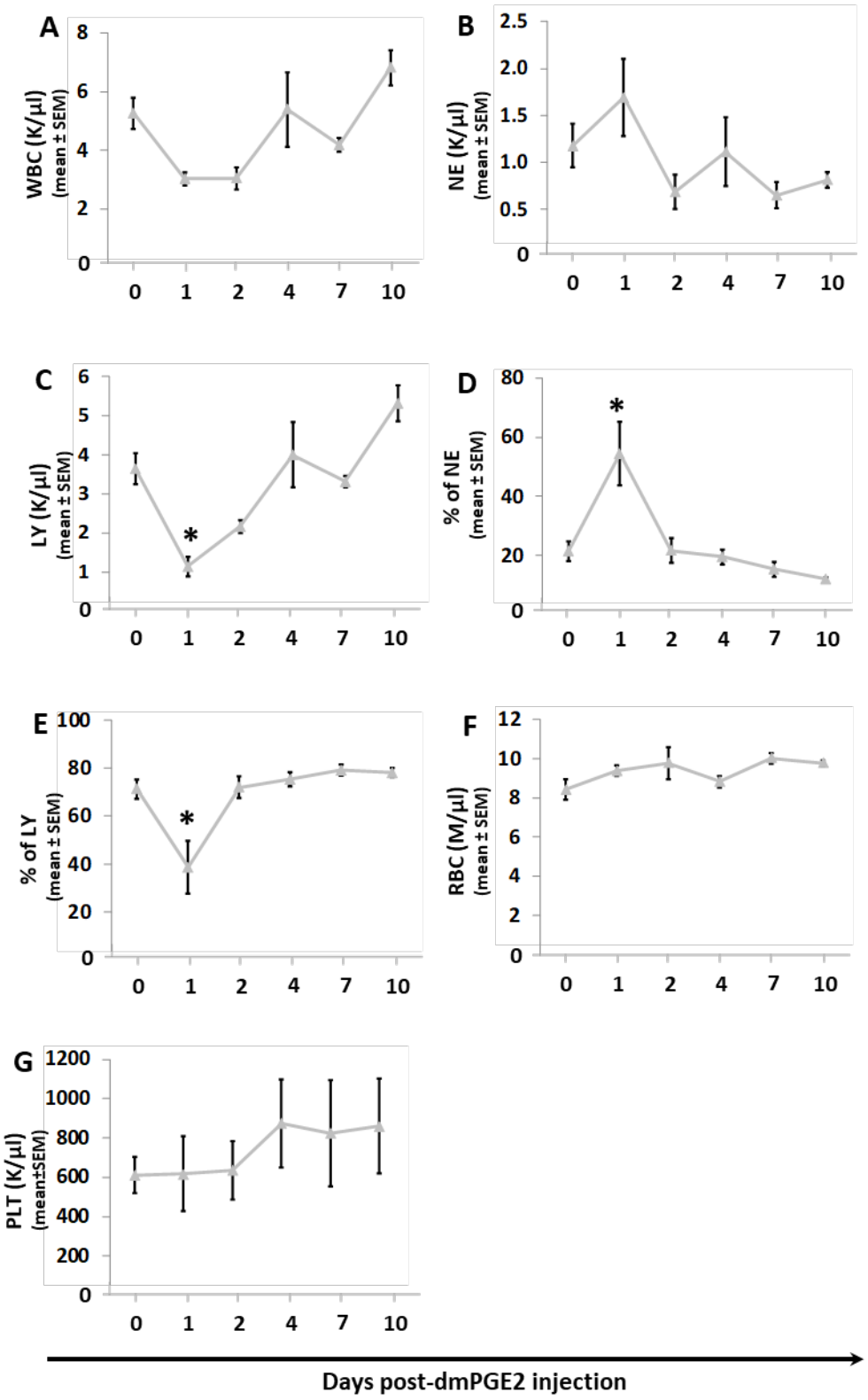
A
WBC (K/µl) (mean ± SEM)
8
6
4
2
0
0 1 2 4 7 10
B
NE (K/µl) (mean ± SEM)
2.5
2.0
1.5
1.0
0.5
0
0 1 2 4 7 10
C
LY (K/µl) (mean ± SEM)
6
5
4
3
2
1
0
*
0 1 2 4 7 10
D
% of NE (mean ± SEM)
80
60
40
20
0
*
0 1 2 4 7 10
E
% of LY (mean ± SEM)
100
80
60
40
20
0
*
0 1 2 4 7 10
F
RBC (M/µl) (mean ± SEM)
12
10
8
6
4
2
0
0 1 2 4 7 10
G
PLT (K/µl) (mean±SEM)
1200
1000
800
600
400
200
0
0 1 2 4 7 10
Days post-dmPGE2 injection

**Figure 28. CBC profiles in NI mice injected with dmPGE2.**

NI C57BL/6 mice were injected with one dose of 35 μg dmPGE2 and CBC analyses of WBC (panel A), NE (panel B), LY (panel C), %NE (panel D), %LY (panel E), RBC (panel F) and PLT (panel G) were followed up to 10 days post-injection. Lines represent mean ± SEM. n=3 mice per group per time-point. *$p<0.05$ comparing to baseline parameters before the injection (day 0 points). Andrea Patterson provided the data; Tong Wu did the analyses.

lymphocytes. The LY number started to recover at day 2 and had returned to normal at day 4 (Figure 28 C and E). There was no significant difference in the absolute values of other types of blood cell (NE, RBC and PLT) between dmPGE2-treated and Veh-treated mice (Figure 28 B, F & G). The CBC data indicate that the negative effect of dmPGE2 on peripheral lymphocytes is transient.

### 4.3.3. Both B and T cells are increased in the spleen of dmPGE2-treated mice

Since splenic lymphocytes are representative of circulating lymphocytes [248, 313] and naïve T cell in secondary lymphoid organ is an estimation of RTE [314, 315], the lymphocyte subsets in the spleen were analyzed. At 12 months post-TBI, spleens were processed into a single cell suspension and phenotyped by flow cytometry. Veh group had less $CD4^+$ T cells and naïve $CD4^+$ T cells and $B220^+$ B cells than NI group, and radioprotectant dmPGE2 prevented the loss. The differences in $CD8^+$ T and $CD8^+$ naïve T cells between NI and Veh group, Veh and dmPGE2 group followed the similar trend as $CD4^+$ T cell but were not significant (Figure 29 A-E). Treatment with radioprotectant dmPGE2 not only alleviates T lymphocyte involution by increasing thymic output, but also increases B lymphocytes, which indicates that dmPGE2 may protect the common lymphoid progenitor cells.

### 4.3.4. DmPGE2 protects thymus from irradiation-induced involution

Hoggatt J et al. [128] have previously shown that PGE2 protects stem cells from apoptosis in vitro and dmPGE2, when used as radioprotectant, accelerates hematopoiesis, including lymphopoiesis in H-ARS phase (Figure 24). In DEARE mice model,

**Figure 29**

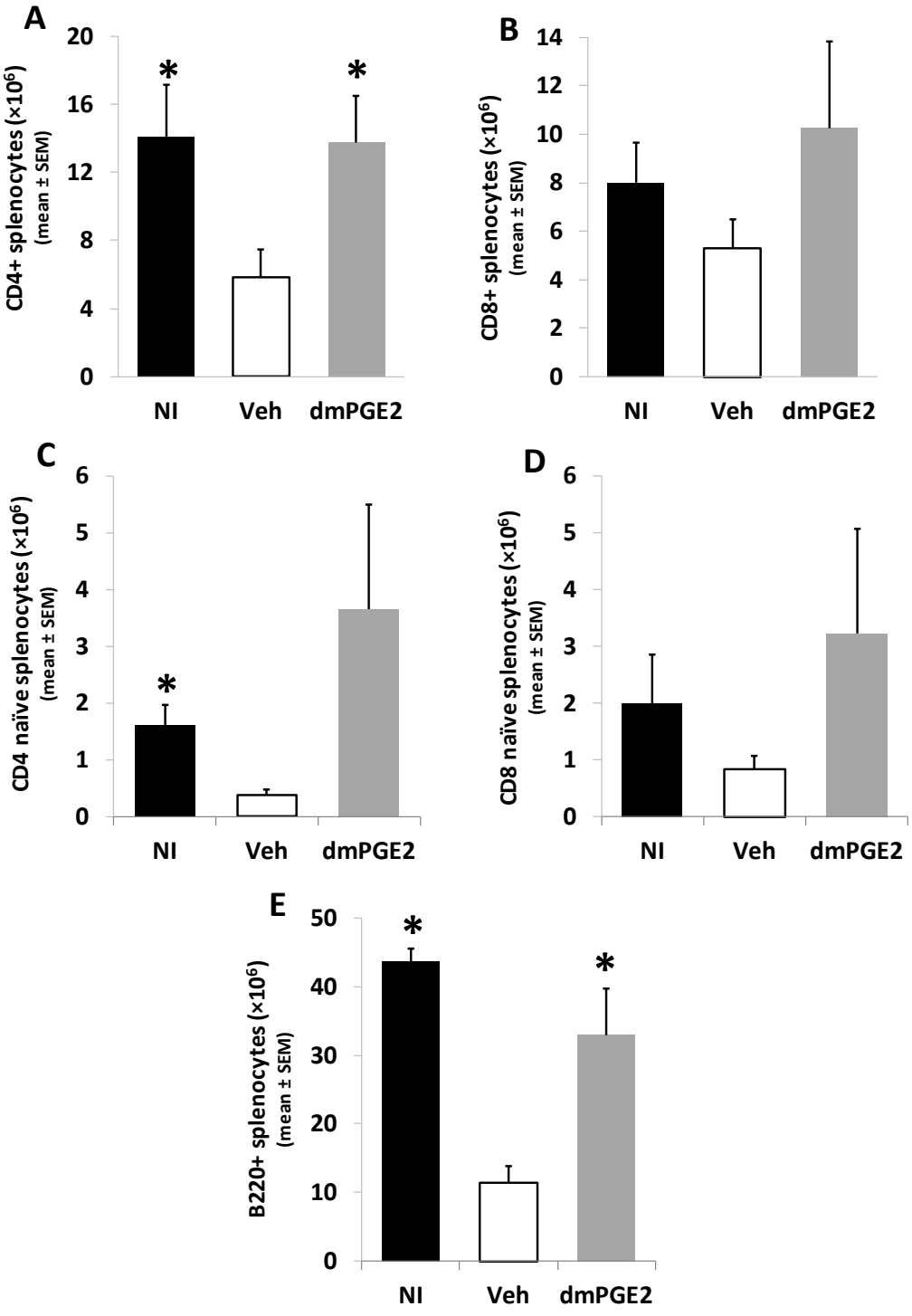
A
CD4+ splenocytes (×10⁶)
(mean ± SEM)
20
16
12
8
4
0
*
*
NI
Veh
dmPGE2
B
CD8+ splenocytes (×10⁶)
(mean ± SEM)
14
12
10
8
6
4
2
0
NI
Veh
dmPGE2
C
CD4 naïve splenocytes (×10⁶)
(mean ± SEM)
6
5
4
3
2
1
0
*
NI
Veh
dmPGE2
D
CD8 naïve splenocytes (×10⁶)
(mean ± SEM)
6
5
4
3
2
1
0
NI
Veh
dmPGE2
E
B220+ splenocytes (×10⁶)
(mean ± SEM)
50
40
30
20
10
0
*
*
NI
Veh
dmPGE2

**Figure 29. Spleen T and B cells in DEARE phase of lethal-irradiated mice treated with radioprotectant dmPGE2.**

C57BL/6 mice were treated with radioprotectant dmPGE2 or Veh prior to lethal TBI and were sacrificed at 12 months post-TBI. Splenocytes from age-matched NI, Veh and dmPGE2 group were stained with CD4, CD8, CD44, CD62L and B220 antibodies and analyzed by flow cytometry for the absolute number of $CD4^+$ splenocytes (panel A), $CD8^+$ splenocytes (panel B), CD4 naïve (CD44-CD62L+) spleen T cells (panel C), CD8 naïve ($CD44^-CD62L^+$) spleen T cells (panel D), $B220^+$ splenocytes (panel E) as described in Materials and Methods. Bars represent mean ± SEM. n=3 mice per group. *$p<0.05$ comparing to Veh group.

radioprotectant dmPGE2 also prevents the decline of lymphocytes and myeloid skew (Figure 27). Since the thymus is where T cells are educated and the site of de novo T lymphopoiesis, I tracked thymic weight and cellularity post-TBI in NI, Veh-treated, and dmPGE2-treated group, from H-ARS to DEARE phase. No difference in thymic weight or cellularity was observed between the dmPGE2 and Veh groups at the early time-point of H-ARS (day 3 and day 10 post-TBI). The protective effect became apparent at day 20 post-TBI and extended to the 6 and 12 months post-TBI (Figure 30 A & B). As dmPGE2 has a minimal effect on body weight change post-TBI, the difference in thymic weight between groups was not related to body weight change (the trend of thymic index, which is represented by thymus weight/body weight is similar to Figure 30 A & B, data not shown).

### 4.3.5. DmPGE2 protects thymocytes from delay in DN to DP transition induced by irradiation

Differences in thymocyte subpopulation distribution between dmPGE2- and Veh-treated mice at DEARE phase were analyzed. Thymocytes were measured at 12 months post-TBI from the earliest thymic settling cells [$CD4^-CD8^-CD44^+CD25^-$ DN1 cells, and $CD44^+CD25^+$ DN2 cells, $CD44^-CD25^+$ DN3 cells, and $CD44^-CD25^-$ DN4 cells]; to the intermediate $CD4^+CD8^+$ DP cells and then to the mature CD4 or CD8 single positive cells, which are ready to immigrate into peripheral blood. At 12 months post-TBI, the percentages of DN2, DN3 and DP in the dmPGE2-treated mice were 5.2, 4.4 and 1.1 times more than the Veh-treated mice, respectively ($p<0.05$) (Table 2). Fewer thymocytes in the dmPGE2-treated mice were trapped in DN1 stage than Veh-treated mice. The

**Figure 30**

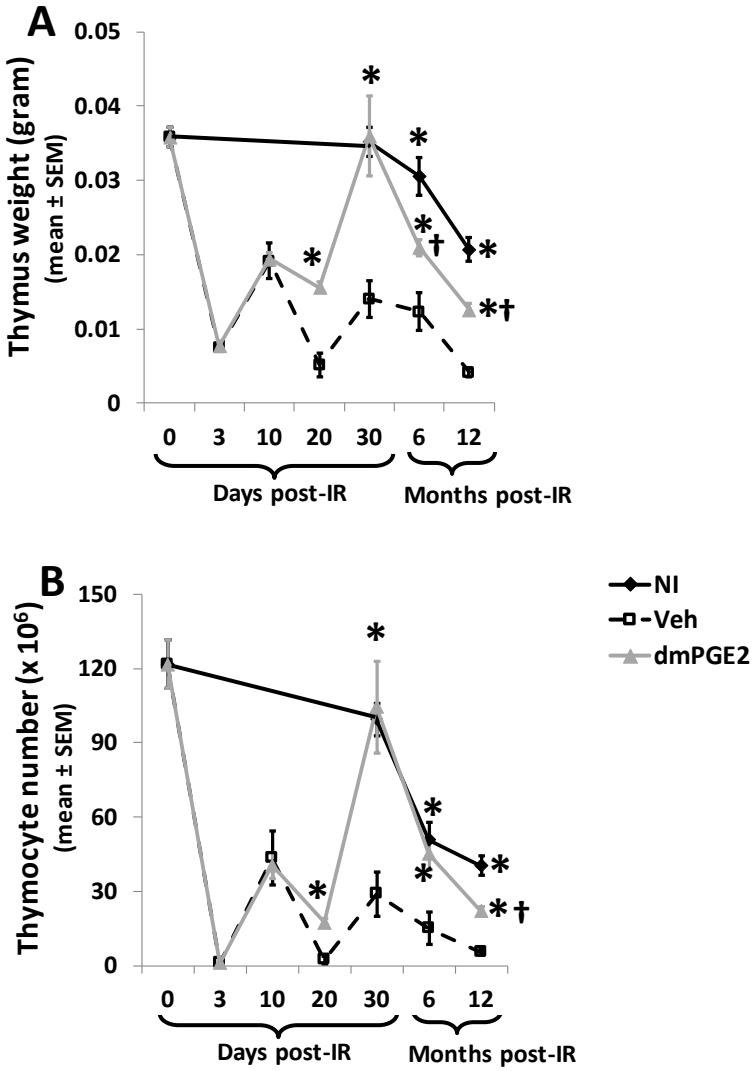
A
Thymus weight (gram)
(mean ± SEM)
0.05
0.04
0.03
0.02
0.01
0
0 3 10 20 30 6 12
Days post-IR
Months post-IR
B
Thymocyte number (x 10⁶)
(mean ± SEM)
150
120
90
60
30
0
0 3 10 20 30 6 12
Days post-IR
Months post-IR
NI
Veh
dmPGE2

**Figure 30. Thymus weight and cellularity in H-ARS and DEARE phases of lethal-irradiated mice treated with radioprotectant dmPGE2.**

C57BL/6 mice were treated with radioprotectant dmPGE2 prior to lethal TBI. The thymus weight (panel A) and cellularity (panel B) were calculated and analyzed up to 1-year post-TBI. Lines represent mean ± SEM. n=3-10 mice per group per time-point. *$p<0.05$ comparing to Veh; † $p<0.05$ comparing to NI.

**Table 2. Comparisons of thymocyte subpopulations at 12 months post-TBI of lethal-irradiated mice treated with radioprotectant dmPGE2.**

| | %CD4 | %CD8 | %DP | %DN | %DN1 | %DN2 | %DN3 | %DN4 |
|---|---|---|---|---|---|---|---|---|
| NI vs. Veh | 0.96 | 3.25* | 1.10* | 1.53 | 0.64* | 7.97* | 5.21* | 1.05 |
| dmPGE2 vs. Veh | 1.08 | 1.38 | 1.11* | 1.25 | 0.79 | 5.24* | 4.39* | 0.95 |
| | **#CD4** | **#CD8** | **#DP** | **#DN** | **#DN1** | **#DN2** | **#DN3** | **#DN4** |
| NI vs. Veh | 3.51* | 12.81* | 5.04* | 7.35* | 4.04* | 24.86* | 28.67* | 9.09* |
| dmPGE2 vs. Veh | 2.74* | 3.69* | 3.36* | 3.75* | 2.97* | 9.39* | 13.20* | 3.64* |

Numbers in the table are the ratio of NI/Veh or dmPGE2/Veh. *$p<0.05$ comparing to Veh group.

absolute values of most subpopulations were higher in the NI and dmPGE2-treated mice than in the Veh-treated mice due to the increase in the total thymocyte number. The distribution of thymocyte subpopulations in dmPGE2-treated mice was similar to NI mice. These results suggest that more thymocytes accumulate in the earlier undifferentiated stage with fewer differentiating into mature cells in the Veh-treated mice than in the dmPGE2-treated mice and dmPGE2 prior to TBI prevents the delay in DN to DP transition observed in Veh mice as a consequence of irradiation.

### 4.3.6. Lymphoid progenitors increase in bone marrow of dmPGE2-treated mice

T cells in thymus, and B cells in the secondary lymphoid organs, are the progenies of committed bone marrow progenitors. The LMPP and CLP are the committed progenitors of lymphoid lineage; whereas the CMP, GMP and MEP are the committed progenitors of myeloid and erythroid lineages [316]. In order to back-track the influence of dmPGE2 on HSPC, HSPC compartments in BM at day 20 post-TBI in H-ARS phase and 12 months post-TBI in DEARE phase were analyzed. LT-HSC were identified as $Lin^{-}$ c-$Kit^{hi}$ Sca-$1^{hi}$ $Flt3^{lo}$ $CD34^{-}$, ST-HSC were identified as $Lin^{-}$ c-$Kit^{hi}$ Sca-$1^{hi}$ $Flt3^{lo}$ $CD34^{+}$, LMPP were identified as $Lin^{-}$ c-$Kit^{hi}$ Sca-$1^{hi}$ $Flt3^{hi}$ $CD34^{+}$, CLP were identified as $Lin^{-}$ c-$Kit^{int}$ Sca-$1^{int}$ $IL7R^{+}$ $Flt3^{hi}$, CMP were identified as $Lin^{-}$ c-$kit^{hi}$ Sca-$1^{lo}$ $CD34^{+}CD16/32^{-}$, GMP were identified as $Lin^{-}$ c-$kit^{hi}$ Sca-$1^{lo}$ $CD34^{+}CD16/32^{+}$, and MEP were identified as $Lin^{-}$ c-$kit^{hi}$ Sca-$1^{lo}$ $CD34^{-}CD16/32^{-}$. At day 20 post-TBI, dmPGE2 prevented the decrease of total BM cells and all types of HSPC (Figure 31 A-H). At 12 months post-TBI, the total BM cells, HSC, CMP, GMP and MEP were completely or partially recovered in the Veh mice whereas the lymphoid progenitors, LMPP and CLP,

were still severely inhibited (Figure 31 I-P). But the number of LMPP and CLP in the dmPGE2-treated group was 5.8 times and 7.9 times higher than Veh group, respectively. DmPGE2 effectively prevented the decrease of LMPP and CLP for at least 12 months post-TBI (Figure 31 J & K).

### 4.3.7. Bone marrow cells from dmPGE2-treated mice have higher engraftment and lineage reconstitution potential than Veh mice

Post-TBI HSPCs do not regain full multi-lineage repopulating potential during the lifetime of the irradiated survivors [40]. Since T cell development in thymus is dependent on the proliferation and differentiation of HSPCs entering into thymus, the ability of BM HSPCs to repopulate the thymus was investigated. Whole BM cells isolated from Veh-treated mice at 6 months post-TBI were found to have <1% of the repopulating potential in recipient thymus in comparison with NI mice. BM cells from mice treated with radioprotectant dmPGE2 had significantly higher chimerism rate than Veh-treated mice, although still significantly lower than in NI mice, indicates that dmPGE2 treatment partially protected the thymic repopulating potential of BM HSPCs (Figure 32 A). Donor cells from Veh-treated mice showed lower level of DP reconstitution, and higher level of DN reconstitution than the NI mice (Figure 32 B). Within the donor-derived DN cells, the Veh group showed a significantly higher percentage of DN cells arrested in the DN1 stage than the NI group (Figure 32 C). Interestingly, the donor cells from mice that received radioprotectant dmPGE2 partially corrected the deficiencies, which with more cells developed into DP stage and fewer cells stuck in the DN and DN1 stages than Veh-treated mice (Figure 32 B-D and Table 3).

**Figure 31**

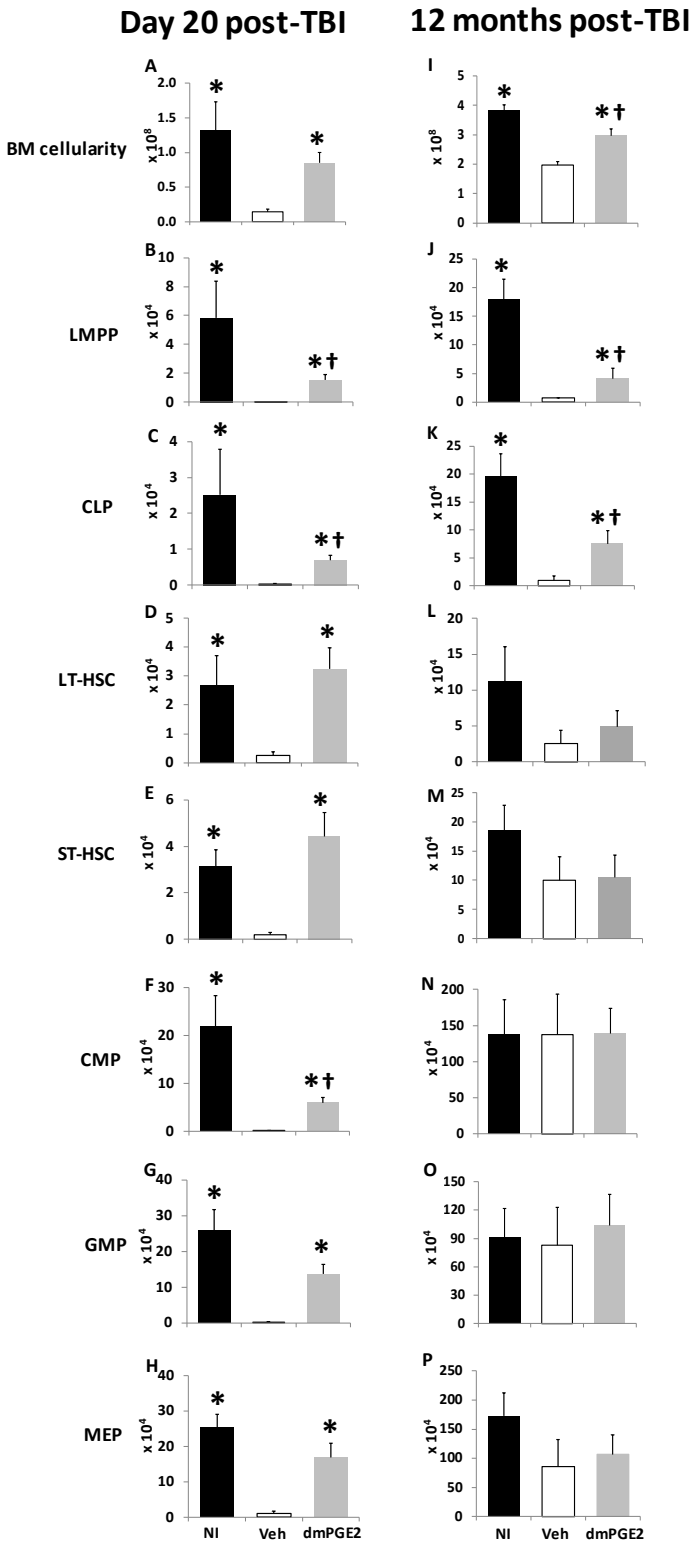
Day 20 post-TBI
12 months post-TBI
BM cellularity
LMPP
CLP
LT-HSC
ST-HSC
CMP
GMP
MEP
NI
Veh
dmPGE2

**Figure 31. BM cellularity and HSPC phenotypes in H-ARS and DEARE phases of lethal-irradiated mice treated with radioprotectant dmPGE2.**

C57BL/6 mice were treated with radioprotectant dmPGE2 prior to lethal TBI and were sacrificed at 20 days and 12 months post-TBI. BM cells were enumerated and stained with antibodies as described in Materials and Methods. Flow cytometric analyses identifies LMPP (panel B & I), CLP (panel C & J), LT-HSC (panel D & K), ST-HSC (panel E & L), CMP (panel F & M), GMP (panel G & N) and MEP (panel H & O). Bars represent mean ± SEM. n=3-6 mice per group. *$p<0.05$ comparing to Veh group; † $p<0.05$ comparing to NI group.

**Figure 32**

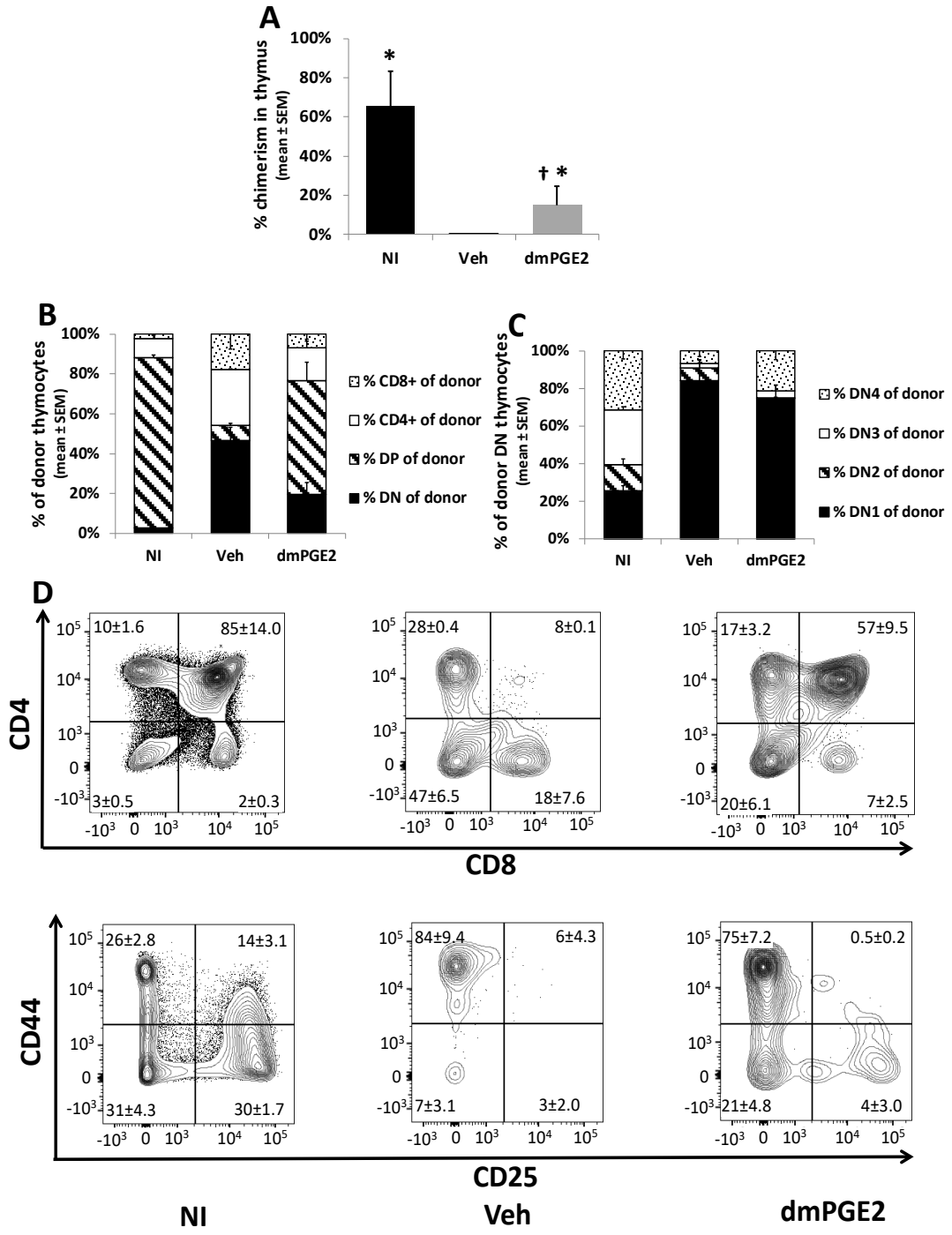
A
% chimerism in thymus (mean ± SEM)
100%
80%
60%
40%
20%
0%
*
† *
NI
Veh
dmPGE2
B
% of donor thymocytes (mean ± SEM)
% CD8+ of donor
% CD4+ of donor
% DP of donor
% DN of donor
C
% of donor DN thymocytes (mean ± SEM)
% DN4 of donor
% DN3 of donor
% DN2 of donor
% DN1 of donor
D
CD4
CD8
CD44
CD25
10±1.6
85±14.0
3±0.5
2±0.3
28±0.4
8±0.1
47±6.5
18±7.6
17±3.2
57±9.5
20±6.1
7±2.5
26±2.8
14±3.1
31±4.3
30±1.7
84±9.4
6±4.3
7±3.1
3±2.0
75±7.2
0.5±0.2
21±4.8
4±3.0
NI
Veh
dmPGE2

**Figure 32. Thymic engraftment and thymocyte subpopulation reconstitution of BM cells from mice treated with radioprotectant dmPGE2 in competitive transplantation assays.**

C57BL/6 mice were treated with radioprotectant dmPGE2 prior to lethal TBI. Survivors were sacrificed at 6 months post-TBI, and $3\times10^5$ whole bone marrow cells isolated from age-matched NI, Veh or dmPGE2 mice, along with $2\times10^5$ competitor cells of congenic origin were transplanted into congenic recipients conditioned with lethal radiation as described in Materials and Methods. Thymocytes from recipients at 6 months post-transplantation were stained by CD45.1, CD45.2, CD4, CD8, CD44 and CD25 antibodies and analyzed by flow cytometry to determine donor chimerism (panel A) and thymocyte subgroups reconstitution (panel B and C). Panel D is representing flow plots of recipient's thymocytes in each group. Bars represent mean ± SEM. n=3-13 per group. *$p<0.05$ comparing to Veh group; † $p<0.05$ comparing to NI group.

**Table 3. Comparisons of thymocyte subpopulation reconstitution in competitive transplantation assay of lethal-irradiated mice treated with radioprotectant dmPGE2.**

| % of donor / Donor treatments | DN | DP | CD4 | CD8 | DN1 | DN2 | DN3 | DN4 |
|---|---|---|---|---|---|---|---|---|
| NI vs. Veh | 0.0002 | <.0001 | 0.0023 | 0.0102 | 0.0001 | NS | <.0001 | 0.0192 |
| NI vs. dmPGE2 | 0.0423 | 0.0172 | NS | NS | <.0001 | 0.0031 | <.0001 | NS |
| dmPGE2 vs. Veh | 0.0105 | 0.0019 | NS | NS | NS | NS | NS | NS |

Numbers in the table are p values of comparisons. Donor bone marrow cells were from NI, Veh and dmPGE2 treated mice at 6 months post-TBI and recipient mice were sacrificed at 6 months post-transplantation. NS: Not significant.

### 4.3.8. BM progenitor cells from dmPGE2-treated mice have better lymphoid differentiation in vitro than Veh mice

The HSPC count and competitive transplantation suggest dmPGE2 protects against TBI-related defects in primitive cell proliferation and/or differentiation. To test this hypothesis, LSK cells were co-cultured with OP9 or OP9-DL4 cells to mimic B cells and thymic T cells development in vitro, respectively. The function of the delta-like (DL) signal (Notch ligand) and the features of this co-culture system were described by Zuniga-Pflucker et al. [303-305].

Cell proliferation in the Veh group was much slower than in the NI and dmPGE2-treated groups in both OP9 or OP9-DL4 co-culture systems (Figure 33 A & B). In the OP9-DL4 co-culture system, the phenotype analysis showed that at early days of co-culture, the Veh-treated group had higher percentage of T cells arrested at the DN1 stage and fewer cells developed to the DN2 and DN3 stage compared with NI and dmPGE2-treated groups (Figure 33 C-F). As co-culture progressed, the Veh-treated group had a lower percentage of T cells in the DP, $CD4^+$ and $CD8^+$ mature stages, and a higher percentage in DN the stage than NI and dmPGE2-treated groups (Figure 33 G- J). Mature CD8 naïve T cells group grew more slowly in the Veh group than the NI and dmPGE2-treated groups (Figure 33 K). T cell development in mice treated with dmPGE2 prior to TBI was almost indistinguishable from NI mice but apparently better than Veh mice.

In the OP9 co-culture system, B cell progenitors showed a mature phenotype (B220) much earlier than T cell progenitors. At day 8, NI and dmPGE2-treated groups

had higher B220 expression level than the Veh-treated group, and B220 expression quickly increased in all groups and there was no difference between groups in the following days (Figure 33 L). These results indicate that HSPCs from DEARE mice are deficient in both T and B lineage differentiation, and that treating with dmPGE2 prior to TBI partially prevents this deficiency.

### 4.3.9. Mature T cells generated from OP9-DL4 co-culture system are functional

In order to further prove that the T cells under dmPGE2 protection are functionally intact, IFN-γ production stimulated by PMA and Ionomycin in mature CD4 and CD8 from OP9-DL4 co-culture system was used to evaluate T cell function. Since the difference of IFN-γ positive percentages between day 16 and day 32 was minimal, data of these two time-points were combined for analysis. Mature CD4 and CD8 T cells in the OP9-DL4 co-culture system from NI and dmPGE2-treated group produced 1.5 to 2 times more IFN-γ than cells from Veh group (Figure 34). This result indicates that mature cells developed from primitive cells that protected by dmPGE2 are functional, rather than only increased in number.

### 4.3.10. DmPGE2 increases chemokine receptors expression on lymphoid progenitors but does not increase homing to thymus

DmPGE2 enhances HSC homing by increasing CXCR4 expression [128, 317]. Both CXCR4 and C-C chemokine receptor type 5 (CCR5) mediate the homing of primitive BM cells to thymus [318]. Radioprotectant dmPGE2 treated mice were sacrificed at 12 months post-TBI and CXCR4 and CCR5 expressions were evaluated

**Figure 33**

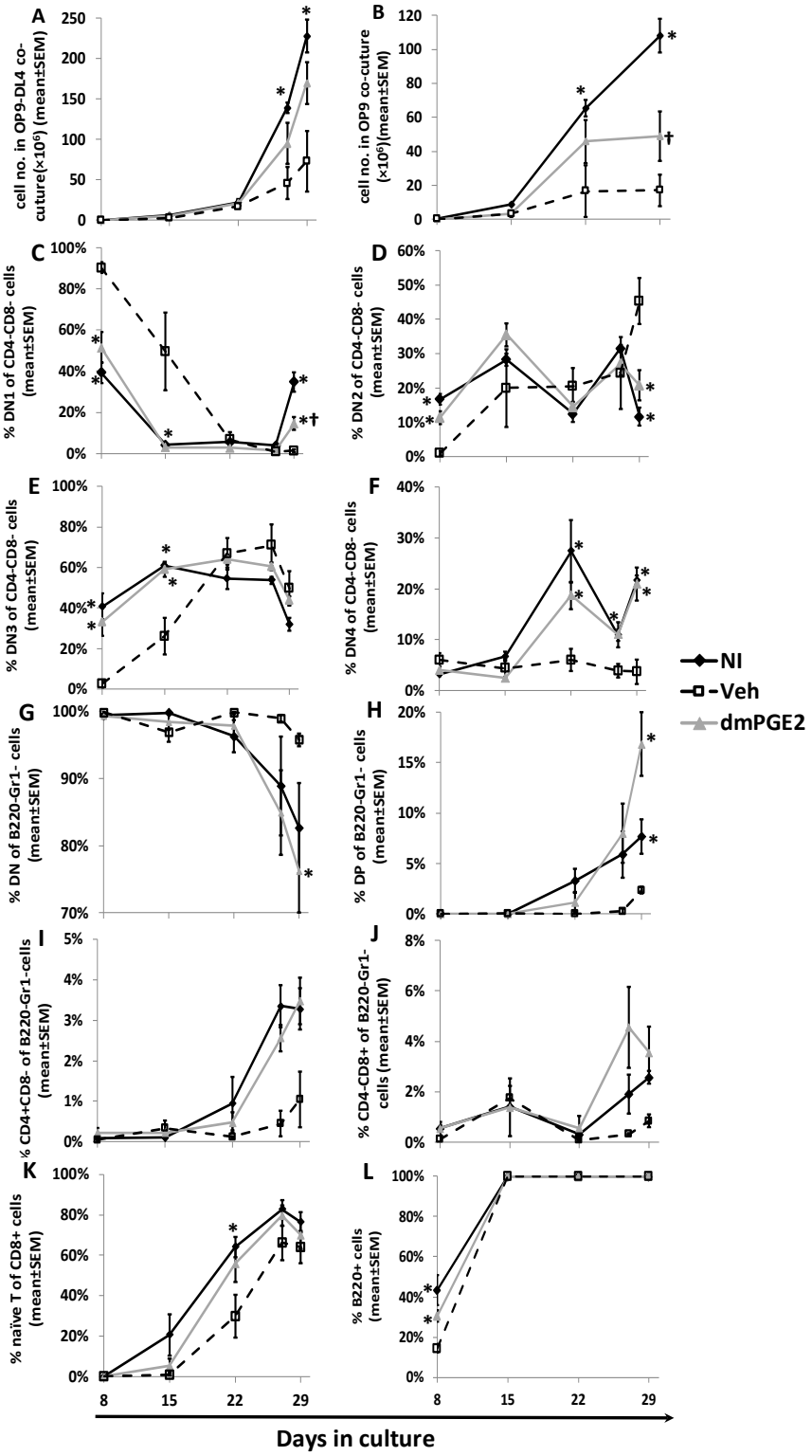
A
cell no. in OP9-DL4 co-cuture(×10⁶) (mean±SEM)
B
cell no. in OP9 co-cuture (×10⁶)(mean±SEM)
C
% DN1 of CD4-CD8- cells (mean±SEM)
D
% DN2 of CD4-CD8- cells (mean±SEM)
E
% DN3 of CD4-CD8- cells (mean±SEM)
F
% DN4 of CD4-CD8- cells (mean±SEM)
G
% DN of B220-Gr1- cells (mean±SEM)
H
% DP of B220-Gr1- cells (mean±SEM)
I
% CD4+CD8- of B220-Gr1-cells (mean±SEM)
J
% CD4-CD8+ of B220-Gr1- cells (mean±SEM)
K
% naïve T of CD8+ cells (mean±SEM)
L
% B220+ cells (mean±SEM)
NI
Veh
dmPGE2
8
15
22
29
Days in culture

**Figure 33. In vitro T and B cell lineage differentiation in lethal-irradiated mice treated with radioprotectant dmPGE2.**

C57BL/6 mice were treated with radioprotectant dmPGE2 prior to lethal TBI and were sacrificed at 12 months post-TBI. BM cells from age-matched NI, Veh and dmPGE2 group were flushed and $1\times10^3$ flow cytometry sorted LSK cells per mouse were co-cultured with 80-90% confluent OP9 or OP9-DL4 monolayer. Cultured cells were demi-depopulated and transferred to new monolayers every 5-7 days. Half of the depopulated cells were used for phenotyping at the time-points indicated in the plots till to the end of the co-culture. Cells were stained with CD11b, B220, CD4, CD8, CD44, CD25 and CD62L antibodies and analyzed by flow cytometry. Panel A and B depict the total number of T cell progenies in OP9-DL4 (panel A) and B cell progenies in OP9 (panel B) co-culture at different time-points. Panel C-F show the percentages of DN1-4 cells in the OP9-DL4 co-culture. Panel G-J show the percentages of DN, DP, $CD4^+$ and $CD8^+$ cells in the OP9-DL4 co-culture. Panel K shows the percentages of naïve T cells in the $CD8^+$ T cells of OP9-DL4 co-culture system. Panel L shows the percentages of $B220^+$ cells in the OP9 co-culture. Lines represent mean ± SEM. n=3-7 per group per time-point. *$p<0.05$ comparing to Veh group; † $p<0.05$ comparing to NI group at different time-points.

**Figure 34**

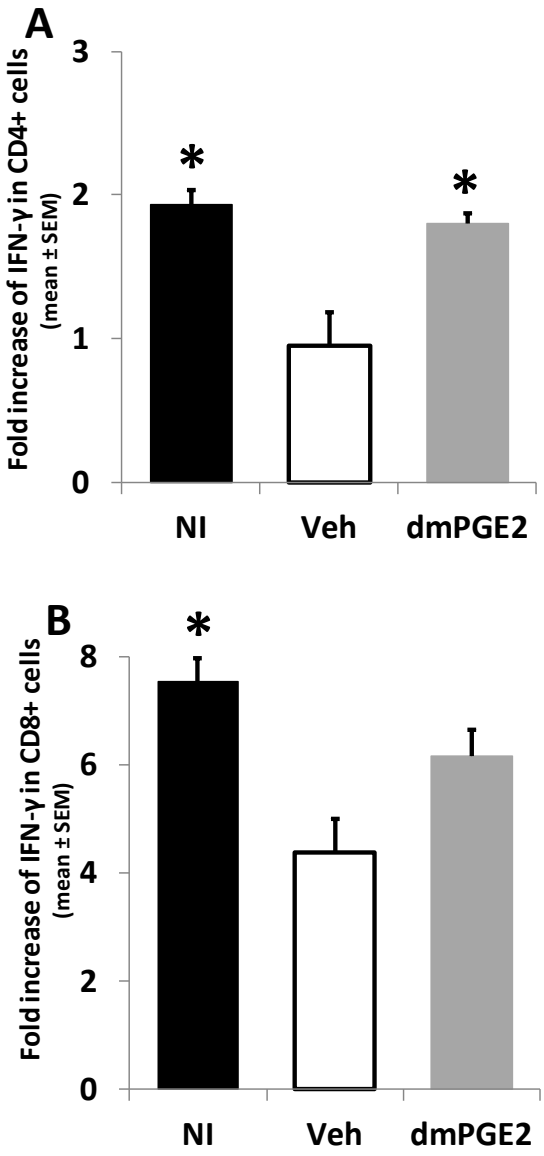
A
Fold increase of IFN-γ in CD4+ cells
(mean ± SEM)
3
2
1
0
*
*
NI
Veh
dmPGE2
B
Fold increase of IFN-γ in CD8+ cells
(mean ± SEM)
8
6
4
2
0
*
NI
Veh
dmPGE2

**Figure 34. IFN-γ production in CD4 and CD8 T cells from OP9-DL4 co-culture.** $5\times10^5$ cultured cells from OP9-DL4 co-culture system were stimulated by PMA and Ionomycin for 5 hr and then stained with intracellular IFN-γ antibodies as described in Materials and Methods. Percentage of IFN-γ positive cells after PMA/Ionomycin stimulation divided by the percentage before stimulation is the fold increase of IFN-γ in Y-axis. Bars represent mean ± SEM. n=4-13 per group. *$p<0.05$ comparing to Veh group.

based on the staining of LMPP and CLP. Results showed that CXCR4 and CCR5 expressions were lower in the Veh-treated group than NI group and radioprotectant dmPGE2 increased their expression, albeit still lower than NI group (Figure 35 A & B). As the input of KSL or LMPP/CLP cells provided too few homed cells to analyze, unfractionated BM cells ($CD45.2^{+}$) were transplanted into lethally-irradiated congenic recipient mice ($CD45.1^{+}$) in another similar study in which donor mice were sacrificed at 6 months post-TBI. There was no significant difference in the percentage of homed cells at 16 hr post-transplantation among NI, Veh, and dmPGE2-treated groups (Figure 35 C). The result indicates that the long-term protective effect of dmPGE2 probably is not mediated by increasing the thymic homing in the early stages post-TBI.

### 4.3.11. DmPGE2 does not increase incidence of thymic mass

The protective effect of dmPGE2 on HSC raises concerns that it may increase the prevalence of malignancies in DEARE. Thymic lymphoma is the most common radiation-induced malignancy in C57/BL6 mice, presenting as increased thymic mass, variable splenomegaly, and lymphadenopathy [319, 320]. Thymic mass was evaluated in mice from previous radioprotectant and radiomitigator dmPGE2 studies at 6 and 12 months post-TBI with an irradiation dose range of 8.53-9.04 Gy at 12 w/o. There was no thymic mass in the NI group. The incidences of thymic mass in both dmPGE2 and Veh-treated mice increased as aging, consistent with previous reports on thymic mass post-TBI [321, 322]. The dmPGE2 group had lower thymic mass incidence than Veh group at 6 months post-TBI (1.8% vs. 14.8%) and 12 months post-TBI (6.6% vs. 20%) (Figure 36),

**Figure 35**

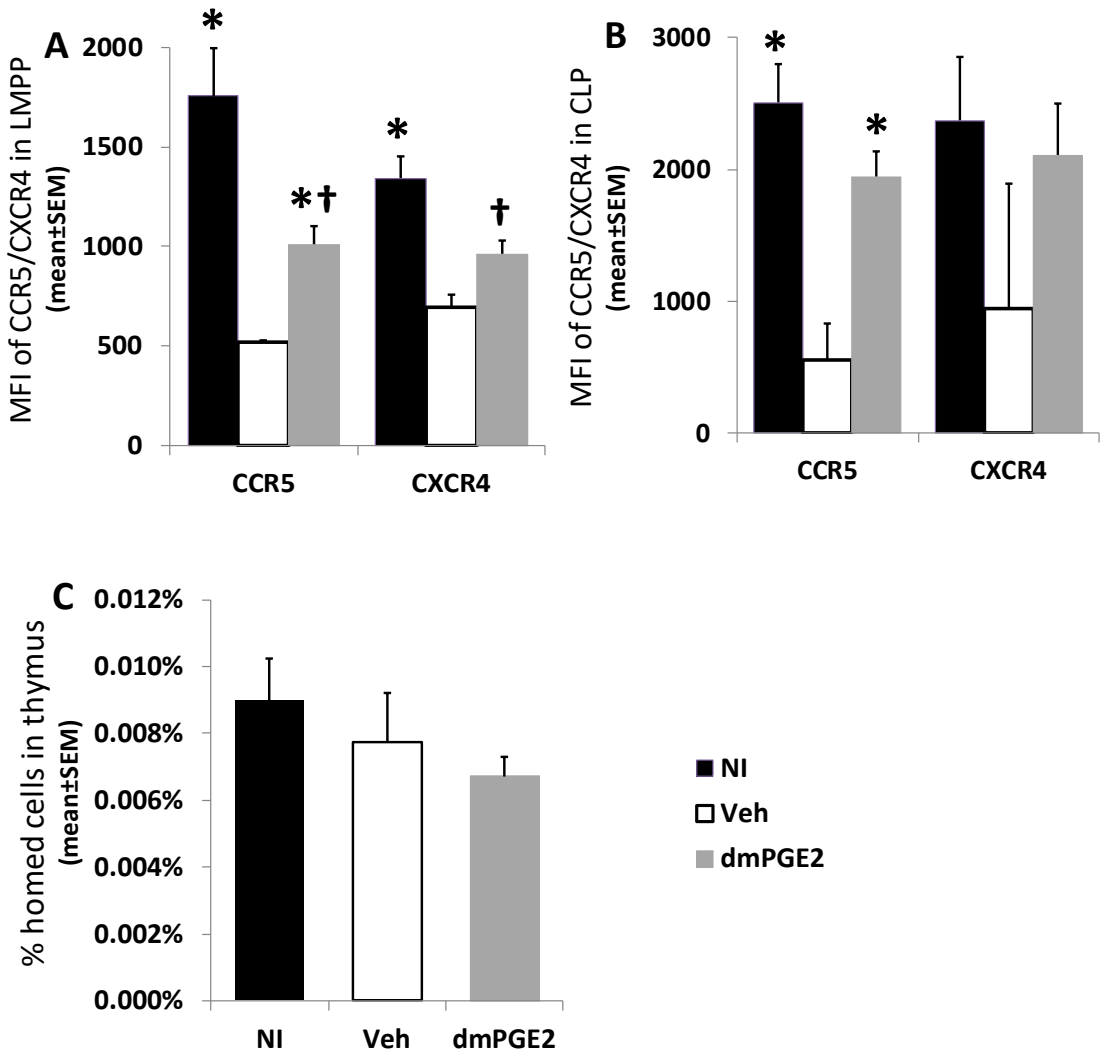
A
MFI of CCR5/CXCR4 in LMPP (mean±SEM)
2000
1500
1000
500
0
*
*†
*
†
CCR5
CXCR4
B
MFI of CCR5/CXCR4 in CLP (mean±SEM)
3000
2000
1000
0
*
*
CCR5
CXCR4
C
% homed cells in thymus (mean±SEM)
0.012%
0.010%
0.008%
0.006%
0.004%
0.002%
0.000%
NI
Veh
dmPGE2
NI
Veh
dmPGE2

**Figure 35. CXCR4 and CCR5 expression on DEARE lymphoid progenitors and homing of DEARE BM cells to thymus.**

C57BL/6 mice were treated with radioprotectant dmPGE2 prior to lethal TBI and were sacrificed at 12 months post-TBI. BM cells from age-matched NI, Veh and dmPGE2 group were stained with LMPP/CLP markers and CXCR4/CCR5 antibodies as described in Materials and Methods, and analyzed by flow cytometry for MFI of CXCR4 and CCR5 in the LMPP (panel A) and CLP population (panel B). For short-term thymus homing study (panel C), donor mice were treated with radioprotectant dmPGE2 prior to lethal TBI and were sacrificed at 12 months post-TBI, $2\times10^7$ whole bone marrow cells from donor mice (C57Bl/6, CD45.2+) were transplanted intravenously into lethally irradiated recipient mice (B6.BoyJ, CD45.1$^+$). After 16 hr, recipient thymocytes were stained with CD45.1 and CD45.2 antibodies and analyzed by flow cytometry. The thymus homing efficiency was calculated as percentage of CD45.2$^+$ donor cells within recipient's thymocytes. Bars represent mean ± SEM. n=2-7 per group. *$p<0.05$ comparing to Veh; † $p<0.05$ comparing to NI group.

**Figure 36**

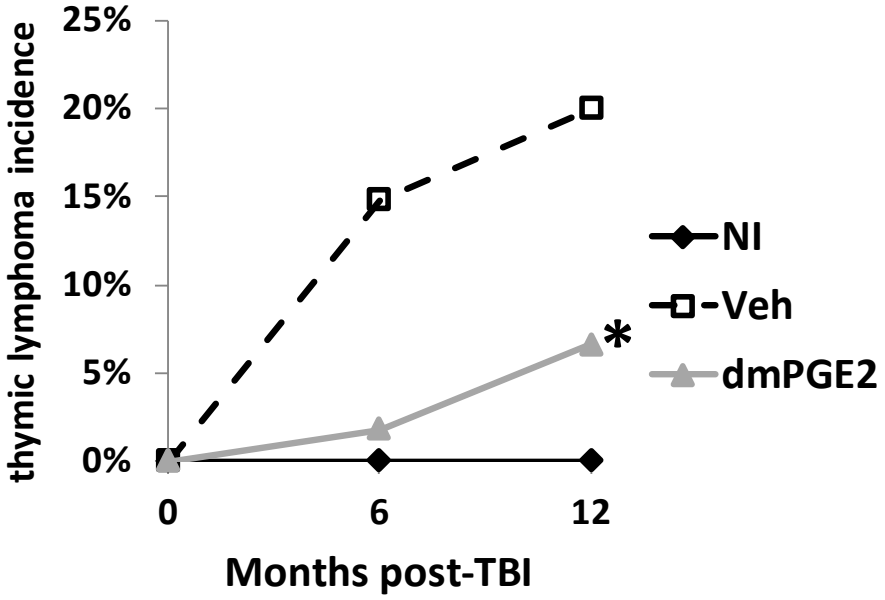
thymic lymphoma incidence
25%
20%
15%
10%
5%
0%
0
6
12
Months post-TBI
NI
Veh
dmPGE2
*

**Figure 36. Thymic mass incidence in aged irradiation survivors.**

C57BL/6 mice were exposed to 8.53-9.04 Gy irradiation at 12 weeks old and treated with radioprotectant or radiomitigative dmPGE2 as described in Chapter 3. Any mice that received dmPGE2 treatment were pooled in dmPGE2 group, no matter it is as radioprotectant or radiomitigator. The Veh group was the pooled mice received equivalent volume of Veh at the same study at the same time. The thymic masses were identified at necropsy of 6 and 12 months post-TBI. Thymic mass (lymphoma) incidence was calculated as a percentage of thymic mass positive mice over all evaluable mice. n=34-89 per group. *$p<0.05$ comparing to Veh in total number of thymic masses at 6 and 12 months post-TBI.

and there was statistical difference in total thymic mass incidence rate between dmPGE2 and Veh group (3.7% vs. 17.3%, $p<0.05$).

### 4.3.12. DmPGE2 thymic protection effect is time-sensitive and intensive treatment is not necessary

Because the time-point of dmPGE2 injection impacts the day 30 survival rate of H-ARS mice (Chapter 3, Figure 21), the impact of different treatment time-points on day 30 thymic recovery were investigated. Mice received 8.72 Gy TBI (LD70/30) with 1 dose of 35 μg dmPGE2 injection at different time [24 hr prior to TBI (-24 hr), 30 min prior to TBI (-30 min), 3 hr post-TBI (+3 hr) and 24 hr post-TBI (+d1)]. The result shows that the -30 min and +d1 groups had better thymic recovery compared to the Veh group, and there was no difference among -24 hr, +3 hr and Veh groups (Figure 37 A), which is consistent with the survival efficacies for -30 min and +d1 schedule. Whether intensive treatment could further increase the protection effect of dmPGE2 in DEARE mice was also investigated. The multiple injection schedule included: dmPGE2 injected at both prior to and after TBI (one dose of 35 μg dmPGE2 injected at -30 min, +d1, d2 and d3) , dmPGE2 injected at prior to TBI and consolidated by monthly injection post-TBI (one dose of 35 μg dmPGE2 injected at -30 min and one dose of 35 μg dmPGE2 injected every 28 days beginning on days 92-93 post-TBI), and one dose of 35 μg dmPGE2 injected at days 1, 2 and 3 post-TBI (Figure 37 B). Thymi were collected at 6 months post-TBI. The results showed that one dose of 35 μg dmPGE2, -30 min prior to TBI, is sufficient to achieve the thymic protection. Injection of dmPGE2 +d1 post-TBI is not as effective as injection at -30 min prior to TBI in maintaining thymus in DEARE phase,

**Figure 37**

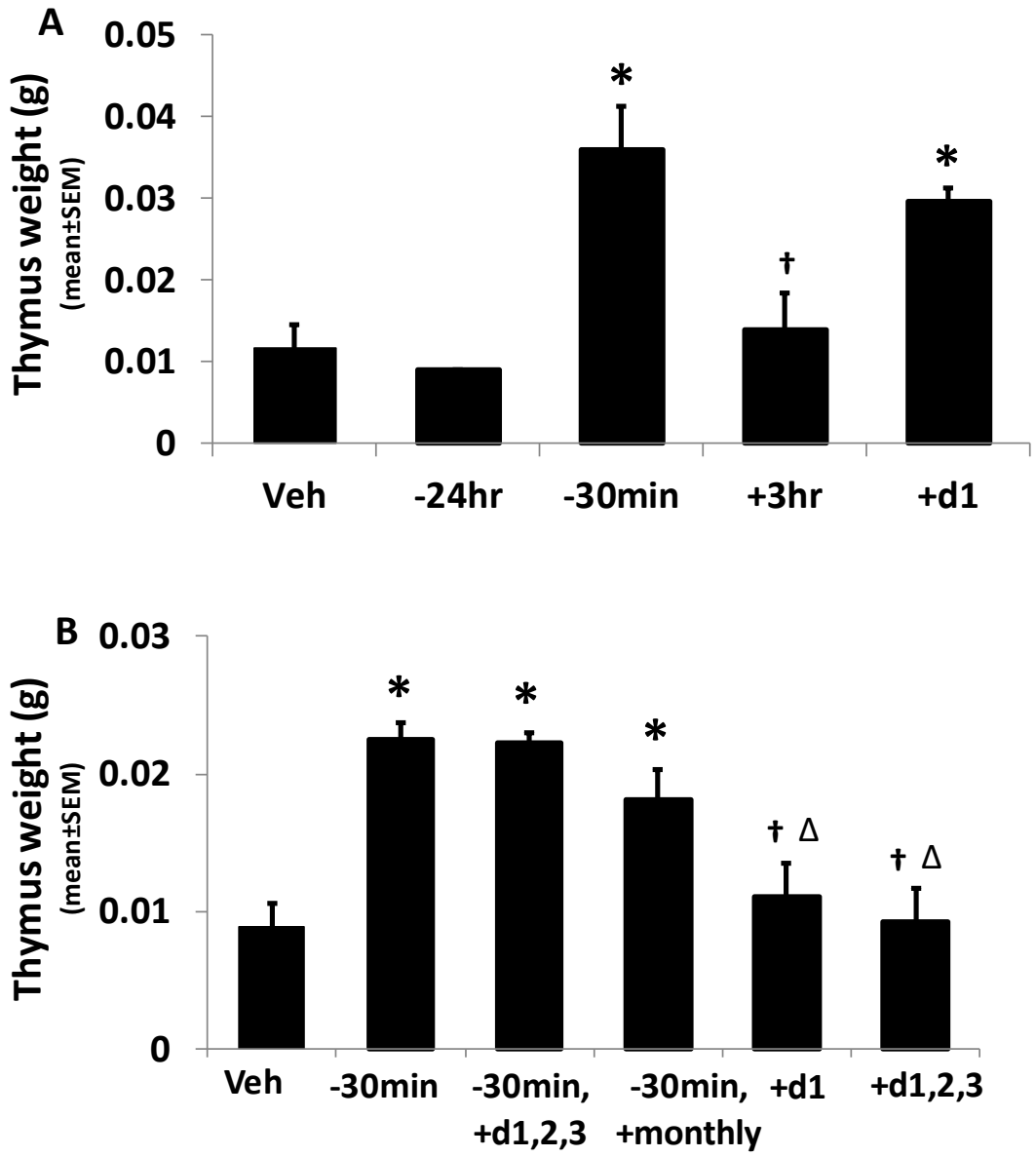
A
Thymus weight (g)
(mean±SEM)
0.05
0.04
0.03
0.02
0.01
0
*
†
*
Veh
-24hr
-30min
+3hr
+d1
B
Thymus weight (g)
(mean±SEM)
0.03
0.02
0.01
0
*
*
*
† Δ
† Δ
Veh
-30min
-30min, +d1,2,3
-30min, +monthly
+d1
+d1,2,3

**Figure 37. Impact of different times and dosing schedule of dmPGE2 injections on thymic recovery.**

All mice received one-time TBI dose of 8.72 Gy. Panel A: Mice received 1 dose of 35 μg dmPGE2 injection at 24 hr prior to TBI (-24 hr), 30 min prior to TBI (-30 min), 3 hr post-TBI (+3 hr) or 24 hr post-TBI (+d1). Veh mice in each group were pooled into Veh group since no difference in thymus weight between different time-points of Veh injection. Thymi were collected at day 30 post-TBI. *$p<0.05$ comparing to Veh group; † $p<0.05$ comparing to -30 min group. In -24 hr group, there was only one mouse survived at day 30 post-TBI; n=4 mice in other groups. Panel B: Mice received 1 dose of 35 μg dmPGE2 injection at -30 min prior to TBI (-30 min), 1 dose 30 min prior to TBI and 1 dose on days 1, 2 or 3 post TBI (-30 min, +d1,2,3), 1 dose 30 min prior to TBI and monthly 35 μg injections beginning on day 92-93 post-TBI(-30 min, +monthly), 1 dose on 24 hr post-TBI (+d1) or 1 dose on days 1, 2 and 3 post-TBI (+d1,2,3). Thymi were collected at 6 months post-TBI. Bars represent mean ± SEM. n=6-10 mice per group. *$p<0.05$ comparing to Veh group; † $p<0.05$ comparing to -30 min; Δ $p<0.05$ comparing to -30 min, +d1,2,3 group.

and multiple injections after the -30 min or +24 hr injection neither enhance thymic recovery nor further increase the protective effect.

### 4.3.13. DmPGE2 receptors partially involve in the thymic protection

DmPGE2 has four receptor subtypes, designated EP1, EP2, EP3, and EP4 [323]. Hoggatt J et al. demonstrated that regulatory effects of NSAID on HSPC retention through the reduction of EP4 receptor signaling [131]. The role of the EP receptors in the thymic protection effect of dmPGE2 has not been investigated. Mice were injected with one dose of 35 μg dmPGE2 or same dose of EP1+3 agonist (17-phenyl trinor dmPGE2), EP2 agonist (butaprost free-acid), or EP4 agonist (L902-688) -30 min prior to 8.72 Gy TBI. The thymi analysis at day 30 post-TBI showed that none of the EP agonists were as effective as dmPGE2 in protecting the thymus, and that thymocyte subpopulation distributions were aberrant in agonist groups compared with the dmPGE2 group (Figure 38 A & B). Because only one mouse survived to day 30 in the EP1+3 and EP2 groups, statistical comparison was not available for these two groups. This result indicates that activation of EP1-4 receptors may only be partially responsible for dmPGE2's thymic protection effect; or that simultaneous activation of all or some combination of EP receptors is required for the full protection effect; or the currently used agonists are not potent enough.

**Figure 38**

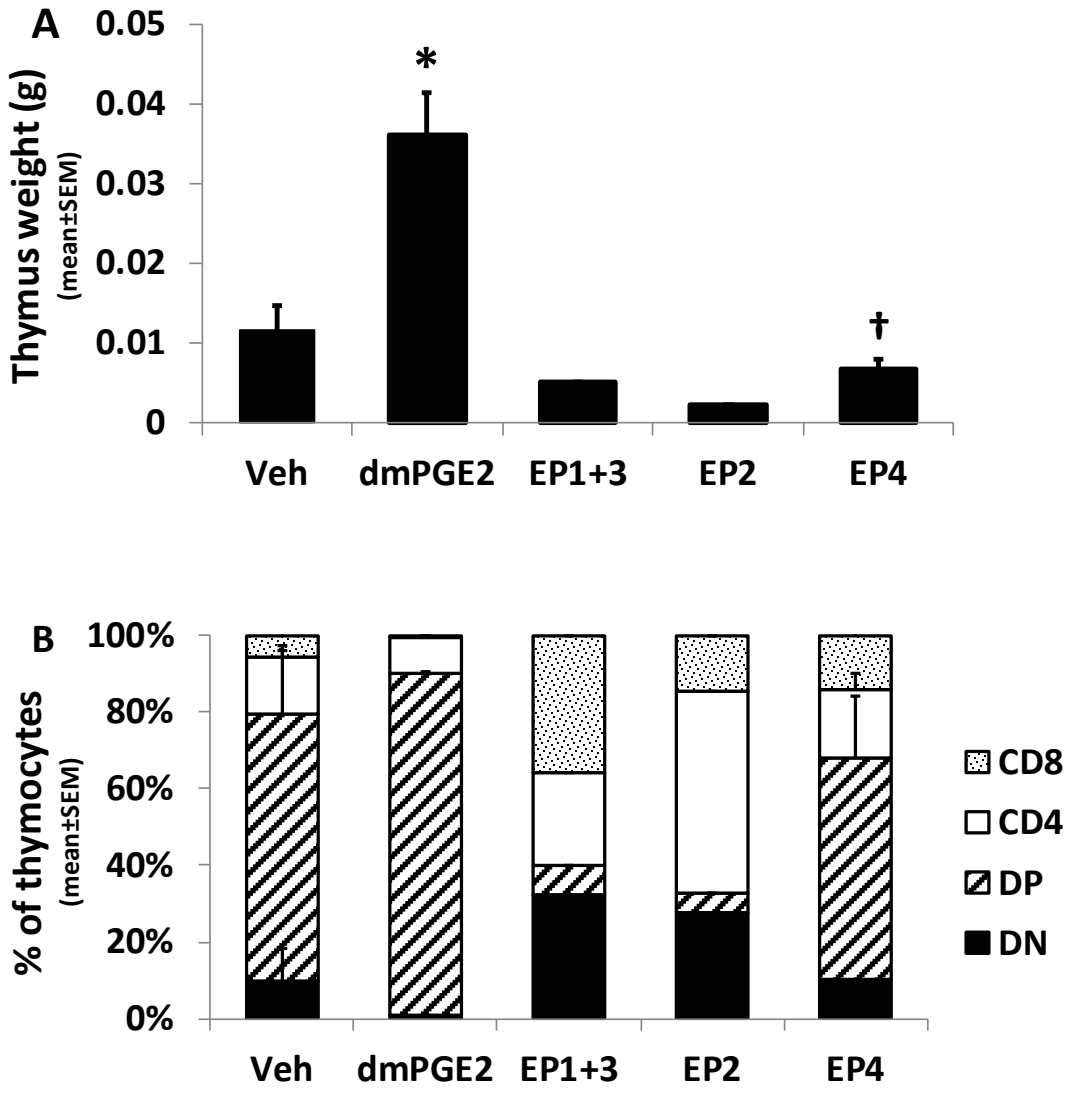
A
Thymus weight (g)
(mean±SEM)
0.05
0.04
0.03
0.02
0.01
0
*
†
Veh
dmPGE2
EP1+3
EP2
EP4
B
% of thymocytes
(mean±SEM)
100%
80%
60%
40%
20%
0%
CD8
CD4
DP
DN
Veh
dmPGE2
EP1+3
EP2
EP4

**Figure 38. Impact of different dmPGE2 receptors activation on thymic recovery.** C57BL/6 mice received one dose of 35 μg dmPGE2 or same dose of EP1+3 agonist (17-phenyl trinor dmPGE2) or EP2 agonist (butaprost free-acid) or EP4 agonist (L902-688) - 30 min prior to 8.72 Gy TBI. Thymi were weighed (panel A) and thymocytes were phenotyped for CD4, CD8 single positive, DP and DN subpopulations by flow cytometry at day 30 post-TBI (panel B) as previously described. Bars represent mean ± SEM. In EP1+3 and EP2 group, there was only one mouse survived at day 30 post-TBI in each group; n=4 mice in other groups. *$p<0.05$ comparing to Veh group; † $p<0.05$ comparing to dmPGE2 group.

### 4.3.14. DmPGE2 does not change the number of thymic stromal cells in DEARE mice

Thymic stromal cells, mainly TECs, support the development of T cell progenitors and direct positive and negative selection [324, 325]. DmPGE2 might provide thymic protection by indirectly influencing thymic stromal cells. The number of cTECs and mTECs at 12 months post-TBI were investigated. The flow cytometry analysis showed that there was no significant difference in the numbers of cTECs and mTECs between the dmPGE2 and Veh groups (Figure 39 A & B).

### 4.3.15. Lymphopoiesis related genes are impacted by radioprotectant dmPGE2

To investigate whether the benefit of radioprotectant dmPGE2 treatment on long-term immune reconstitution results from its early impact on HSC differentiation, RNA sequencing was carried out on highly-purified HSCs from mice that received one dose of 35 μg dmPGE2 -30 min prior to TBI. Mice were sacrificed 24 hr post-TBI. IPA predicted that lymphopoiesis was increased at 24 hr post-TBI in dmPGE2 group with a high activation z-score of 4.34 when compared with Veh group, and 115 associated genes were identified. Meanwhile, IPA also predicted that lymphopoiesis was decreased in Veh group at 24 hr post-TBI with a z-score of 2.01 when comparing with NI group, with 186 associated genes were identified. Nineteen genes either decreased in Veh but increased in dmPGE2 group; or increased in Veh but decreased in dmPGE2 group. The following lymphopoiesis-associated genes were up-regulated by radioprotectant dmPGE2: Lepr (Leptin receptor), Dntt (DNA nucleotidylexotransferase), Flt3, Smad7 (Mothers against decapentaplegic homolog 7), Il6ra (Interleukin-6 receptor Subunit Alpha), Efnb2 (Ephrin

**Figure 39**

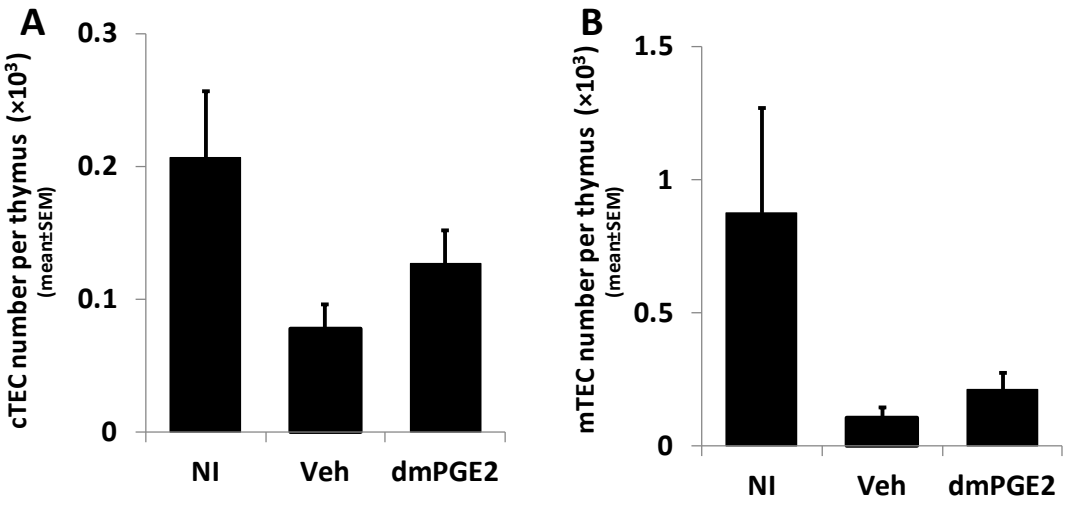
A
cTEC number per thymus (×10³)
(mean±SEM)
0.3
0.2
0.1
0
NI
Veh
dmPGE2
B
mTEC number per thymus (×10³)
(mean±SEM)
1.5
1
0.5
0
NI
Veh
dmPGE2

**Figure 39. Thymic stromal cells in DEARE phase of lethal-irradiated mice.**

C57BL/6 mice were treated with radioprotectant dmPGE2 and were sacrificed at 12 months post-TBI. Thymi were enzyme-digested and stained with CD45, EpCAM, UEA-1 and Ly51 antibodies and analyzed by flow cytometry as described in Materials and Methods. The absolute cell numbers of cTEC (Panel A) and mTEC (Panel B) were the total thymocyte numbers multiplied by the percentage of cTEC and mTEC. Bars represent mean ± SEM. n=3-6 mice per group.

B2), Cadm1(Cell adhesion molecule 1), Ifngr1 (Interferon gamma receptor 1), Rora (RAR related orphan receptor A), Furin (FES upstream region), Stat3 (Signal transducer and activator of transcription 3), Cdkn1c (Cyclin dependent kinase inhibitor 1C), Tgfbr1 (Transforming growth factor beta receptor 1), Myb (MYB proto-oncogene, transcription factor), Ets2 (ETS proto-oncogene 2, transcription factor) and Zmiz1(Zinc finger MIZ-type containing 1). And the following genes which inhibit the lymphopoiesis were down-regulated by radioprotectant dmPGE2: Prkca (Protein kinase C alpha), Lmo1 (LIM domain only 1) and Tk1 (Thymidine kinase 1) (Figure 40). Radioprotectant dmPGE2 may impact HSC differentiation through these genes as early as 24 hr post-TBI. (Andrea Patterson in Dr. Pelus' laboratory provided the RNA sequencing and IPA analysis).

### 4.3.16. Cytokines that support lymphopoiesis were prevented from decreasing by dmPGE2

To investigate whether the bone marrow environment helps immune reconstitution at early time-points, BM supernatant was collected from NI, Veh, and dmPGE2-treated mice at day 9 post-TBI, and 32 cytokines were detected by Millipore mouse cytokine/chemokine panel. DmPGE2-treated mice had increase in the average levels of growth factor, both anti- and pro-inflammatory cytokines than Veh-treated mice, although most differences were not statistically significant. In the growth factor category, growth factors that support lymphopoiesis (IL-2 and IL-7) were increased in dmPGE2-treaed mice compared with the Veh at day 9 (green box labeled at Figure 41). On the contrary, growth factors that support myelopoiesis (MGSF, G-CSF, IL-3) were increased

**Figure 40**

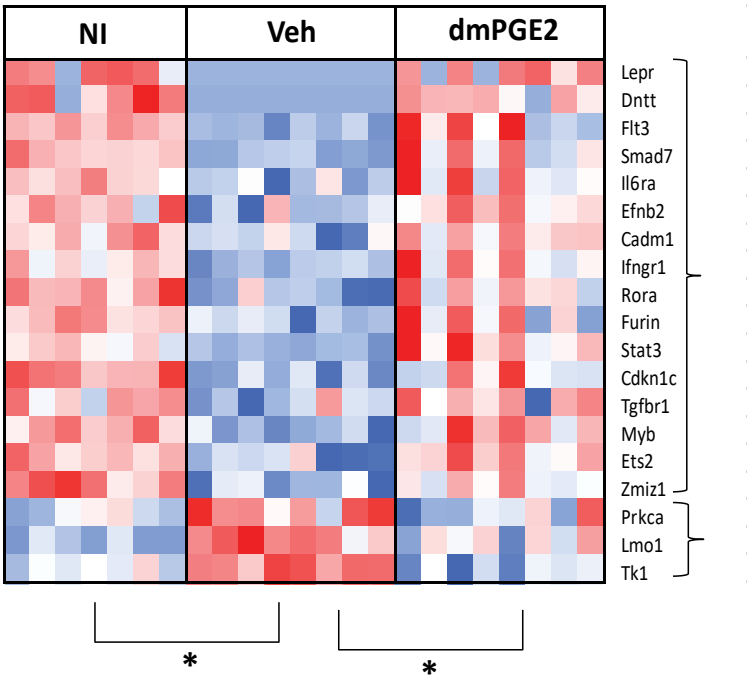
NI
Veh
dmPGE2
Lepr
Dntt
Flt3
Smad7
Il6ra
Efnb2
Cadm1
Ifngr1
Rora
Furin
Stat3
Cdkn1c
Tgfbr1
Myb
Ets2
Zmiz1
Prkca
Lmo1
Tk1
*
*

**Figure 40. Heat map of genes associated with enriched GOTERM_BP: lymphopoiesis.**

Fgd5 mice were treated with one dose of 35 μg dmPGE2 or equivalent Veh at -30 min prior to 8.53 Gy TBI and were sacrificed at 24 hr post-TBI. 1,000-6,000 HSCs ($CD45^{+}$SLAM-$LSK^{wide}ZsGreen^{+}$) per mouse were sorted from BM by FACSAria and were subjected to RNA sequencing. Genes were identified by IPA with FDR <0.05 and fold change >2. Lymphopoiesis and its related genes were identified by IPA cellular function predictions. Genes up-regulated in HSC are presented in red and genes down-regulated are in blue. n=7-8 mice per group. *FDR <0.05 in all genes between indicated groups. Andrea Patterson provided the RNA sequencing and IPA analysis.

**Figure 41**

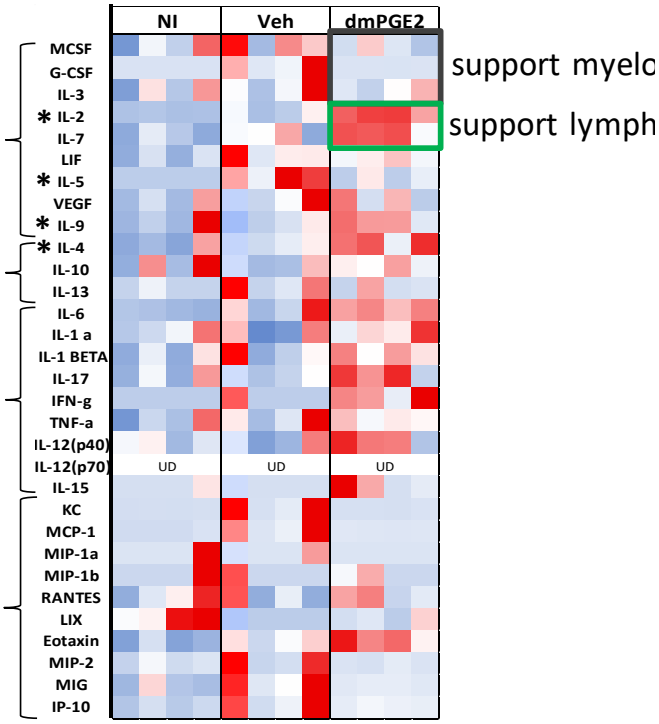
NI
Veh
dmPGE2
MCSF
G-CSF
IL-3
* IL-2
IL-7
LIF
* IL-5
VEGF
* IL-9
* IL-4
IL-10
IL-13
IL-6
IL-1 a
IL-1 BETA
IL-17
IFN-g
TNF-a
IL-12(p40)
IL-12(p70)
IL-15
KC
MCP-1
MIP-1a
MIP-1b
RANTES
LIX
Eotaxin
MIP-2
MIG
IP-10
UD
UD
UD
support myelo
support lymph

**Figure 41. BM cytokines in NI mice and irradiated mice at day 9 post-TBI.**

C57BL/6 mice were treated with one dose of 35 μg dmPGE2 or equivalent Veh at -30 min prior to 8.53 Gy and mice were sacrificed at day 9 post-TBI. Cytokines in BM supernatant were analyzed by Bio-Plex multiplex system. Expression level of individual cytokine is represented by shades of blue (low value) to red (high value) as described in Materials and Methods. n=4 mice per group. *$p<0.05$ comparing dmPGE2 to Veh group. UD: undetectable, values out of range. Huilin Chua and Hailin Feng did the Bio-Plex study; Tong Wu did the analyses.

in Veh-treated mice at day 9 post-TBI but attenuated by radioprotectant dmPGE2 (black box labeled at Figure 41).

### 4.4. Discussion

The thymus is the central lymphoid organ for T cell maturation and education. Although there are controversies regarding the extent of thymic recovery post-TBI, it is generally accepted that an irradiated thymus would be inevitably more involuted than the non-irradiated one, and that there is no effective method to prevent or delay this involution [186, 218, 219]. Ventevogel MS et al.[75] and Majumdar S et al. [326] reported that leuprolide, IL-7, IL-22, keratinocyte growth factor, growth hormone, and Ghrelin have thymic-regeneration potential in aged mice. However, none of these has been shown to prevent the effect of irradiation. Developing a treatment to protect against radiation-induced thymic involution is of significant importance to victims of radiation disasters, and to radiotherapy patients.

PGE2, a lipid arachidonic acid derivative, induces lymphocyte apoptosis through DNA fragmentation by up-regulating c-Myc expression [327], and suppresses T cell activation by down-regulating IL-2 production [300-302]. Since PGE2 has been considered a “foe” to lymphoid cells, previous studies about MCMs targeting immune recovery post-IR had not considered PGE2 or dmPGE2 as candidate. However, many recent studies indicate that PGE2 has both pro- and anti-inflammatory effects [301, 328] and its derivative dmPGE2 plays a positive role in hematopoiesis post-TBI [130, 135,

276]. To date, no study has evaluated the effect of PGE2/dmPGE2 on the lymphoid lineage in the context of irradiation.

Drs. Orschell and Pelus have recently discovered that one dose of dmPGE2 -30 min prior to TBI greatly increased the day 30 survival rate (Figure 21). Here, I observed that radioprotectant dmPGE2 also prevents irradiation-induced thymic involution as early as 20 days post-TBI, and that this effect is maintained for at least one-year post-TBI. The thymic protection effect is time-sensitive and works best when dmPGE2 is administered as a radioprotectant, -30 min prior to TBI. The exact reason for this time sensitivity is unclear.

Treatment with radioprotectant dmPGE2 does not demonstrate the thymic protection effect until day 20. At day 3 and day 10, there is no difference in thymic weight between dmPGE2- and Veh-treated groups. Takada et al. [218] reported that the first recovery peak of the thymus, at day 10 post-IR, is due to the proliferation of surviving residual thymocytes, and the second recovery peak at day 30 is due to the enter and proliferation of progenitor cells from the bone marrow. Here, the hypothesis is that the thymic protection from dmPGE2 occurs as a result of protection of early bone marrow progenitors as opposed to directly protecting mature T cells. Under protection from dmPGE2, lymphoid progenitors with less irradiation damage enter thymus and proliferate post-IR. Increases in CXCR4 and CCR5 expression were observed in LMPP and CLP of dmPGE2-treated mice group compared with the Veh control, although an increase in thymic homing was not observed (Figure 35). This is inconsistent with other

studies on chemokine receptors and HSC homing to the bone marrow [22] and may relate to a difference in the time at which the "gate" opens post-IR between the bone marrow niche and thymic niche. Post-IR and until the second recovery peak, the thymic "gate" is not open which does not allow bone marrow progenitors anchor in the thymus.

In in vivo competitive transplantation studies, a better thymic reconstitution is achieved by donor cells from dmPGE2 group than Veh group (Figure 32). The Veh mice were deficient in thymus repopulation, supporting result from previous report of reduced T cell lineage reconstitution in peripheral blood by donor cells from Veh mice [40]. These results also supported previous data (Table 2) showing an increased percentage of DP thymocytes and decreased percentage of DN1 thymocytes in dmPGE2-treated mice. These data indicate that dmPGE2 as a radioprotectant likely protects the thymus through the protection of bone marrow HSPCs.

In further support of the hypothesis that dmPGE2 protects the thymus via the "intrinsic mechanism" (HSPC protection) rather than the "extrinsic mechanism" (thymic stromal cell protection), I demonstrated that the lymphoid progenitors, LMPP and CLP, were decreased in Veh group and attenuated by radioprotectant dmPGE2 at 12 months post-TBI, whereas myeloid progenitors were not (Figure 31). Additionally, co-culture studies revealed that HSPCs from dmPGE2-treaetd mice had increased proliferation and differentiation capabilities compared with cells from Veh-treated mice (Figure 33), and the dmPGE2-treated mice did not have significantly higher cTEC and mTEC numbers compared with Veh group (Figure 39). These data indicate that HSPCs are protected by

radioprotectant dmPGE2, and that these cells have better lymphoid lineage development than HSPCs in the Veh-treated mice, although the impact of radioprotectant dmPGE2 on bone marrow niche prior to LMPP/CLP entering the thymus cannot be ruled out.

In mice treated with radioprotectant dmPGE2, lymphoid progenies (T and B cells) in thymus (Table 2) and spleen (Figure 29) were increased in comparison with the Veh control group. In the mature peripheral T cell subsets, naïve T cells were trended higher in dmPGE2 group than Veh group although not significant, which is probably because of the limited number of mice in each group. There are two mechanisms for T cell regeneration: one is thymus-dependent de novo regeneration originated from the proliferation of BM-derived progenitors; another is thymus-independent HPE. In normal mice, naïve T cells in the spleen are predominantly RTE, which represents the thymus-dependent de novo regeneration, as opposed to homeostatic proliferation of naïve T cells [314, 315]; in lymphopenic situation, such as post-TBI or post-transplantation, how thymic output involves in T cell reconstitution and whether peripheral naïve T cells still represent RTE are not clear, but from the consistency of increased thymocytes and peripheral naïve T cells in dmPGE2 group, it is highly possible that the increased thymic output by dmPGE2 protection comprises, at least involve in, the peripheral T cell reconstitution. Further measurement of the ratio of thymic output and HPE in Veh and dmPGE2 group would further verify the effect of dmPGE2 on T cell reconstitution post-TBI.

B cells were increased in the spleens of DEARE mice treated with radioprotectant dmPGE2 (Figure 29), and HSPCs from dmPGE2-treated mice have enhanced mature B cell development in comparison with the Veh mice in OP9 co-culture (Figure 33 L). The protective effect of dmPGE2 treatment prior to TBI on B and T lymphocytes ameliorates myeloid skewing, which is a sign of immune suppression (Figure 27). Myeloid skewing is also seen in geriatric mice with HSPCs that have accumulated DNA damage [329]. The prevention of myeloid skewing by radioprotectant dmPGE2 indicates that dmPGE2 may successfully prevent radiation-induced DNA damage and that its target stage of hematopoietic differentiation is likely before the LMPP and CMP stage, whether it is the earlier HSC or the latter MPP stage is not clear.

Although all current evidence indicates that dmPGE2 plays a positive role in lymphocyte recovery post-IR. Interestingly, dmPGE2 is also a “foe” to lymphocytes in an unirradiated scenario (Figure 28 C). The CBC analysis in unirradiated mice received dmPGE2 injection demonstrates that dmPGE2 has quick, transient, toxicity to peripheral lymphocytes, which is similar to the reports from Mastino et al. [327, 330] showing that PGE2 induces apoptosis of lymphocytes both in vivo and in vitro; and the report from Chouaib et al. [331] showing that PGE2 inhibits T lymphocyte proliferation. This effect is probably mediated through the activation of EP2 and EP4 since murine mature T cells do not express EP1 and EP3 [301, 328]. Other components of the peripheral blood are not significantly affected by dmPGE2. The “double hit” from irradiation and dmPGE2 exposure delays lymphocyte recovery in comparison with neutrophil recovery until the cells are replenished by RTEs; however, during the lymphocyte-low period (until day 20

post-TBI), the death rate of the dmPGE2-treated group does not increase (Figure 21). Considering that infection is the main cause of death during this period [15, 69], the main anti-infection effect arises from neutrophils, which are higher in the dmPGE2-treated group than Veh-treated group (Figure 24 A).

DmPGE2 represents a simple and effective radioprotectant with the potential to provide immense benefits to emergency personnel responding to radiation emergency and/or patient receiving radiotherapy. It is known that radiation increases the risk of secondary cancers [4, 205], and whether dmPGE2 would exacerbate this situation is unknown. In C57BL/6 mice, the most common secondary cancer post-TBI is thymic lymphoma [319], which correlates with radiation dosage. In thymic mass study, the thymic mass incidence in the dmPGE2-treated group was only 1/5 of that observed in the Veh-treated group (Figure 36), indicating that pmPGE2 may protect against secondary tumors. The prevention of DNA damage and enhanced immune surveillance in dmPGE2-treaetd group are potential mechanisms for this finding. This result, however, should be interpreted with caution as this study is not designed for estimating thymic mass incidence post-TBI, and the total mouse number was relatively low to make a definitive conclusion.

Lineage commitment occurs early in the HSC differentiation pathway. As myeloid skewing was prevented by dmPGE2 treatment prior to TBI, in order to elucidate whether lymphopoietic potential is protected by dmPGE2, RNA sequencing was carried out on HSCs +24 hr post-TBI. The IPA analysis indicates that a group of genes that

support lymphopoiesis were up-regulated in dmPGE2-treated group and another group of genes inhibiting lymphopoiesis were up-regulated in Veh group and attenuated by radioprotectant dmPGE2 (Figure 40). Those genes promote lymphopoiesis through different mechanisms. Flt3 is a cytokine tyrosine kinase receptor and is one of surface markers of LMPP. $Flt3^{-/-}$ and $Flt3L^{-/-}$ mice are deficient in B cell development and earliest thymic progenitors [332]. By synergizing with other cytokine defects, such as in $Flt3L^{-/-}$ $Il\text{-}7r^{-/-}$ mice, the thymopoiesis and subsequent T lymphopoiesis are more exacerbated [333]. The RNA sequencing shows that Flt3 was significantly up-regulated in dmPGE2 group comparing to Veh group. IL-7R is the receptor for IL-7 and is an important surface mark for CLP. IL-7R gene follows a similar trend as Flt3 with eight times higher expression level in dmPGE2 group than Veh group, although this difference was not statistically significant ($p<0.05$ but $FDR>0.05$), which might be attributed to the limited number in this study. The changes in Flt3 and IL-7R gene expression in dmPGE2 group accelerate T cell reconstitution post-TBI. Other cytokine receptors in which the ligand-receptor signal pathways are important for either B cell or T cell development (Lepr, Il6ra, Ifngr1 and Tgfbr1) display elevated gene expression in the HSCs from dmPGE2-treated mice. Additionally, several downstream genes regulating the cell cycle (Stat3, Cdkn1c), and genes involving in V(D)J recombination (Dntt) and Notch ligand cleavage (Furin) were higher in HSCs from dmPGE2-treated mice than Veh-treated mice. Some genes reportedly take action in later lymphopoiesis, such as Zmiz1 coordinates with Notch1 to promote thymocyte proliferation [334] and Ets2 promotes thymocyte proliferation via inhibition of dexamethasone-induced apoptosis [335].

The following BM cytokine analysis represents the bone marrow microenvironment difference between dmPGE2 and Veh mice. At day 9 post-TBI, the dmPGE2-treated group had a higher average cytokine level than the Veh-treated group in growth factor and anti- and pro-inflammatory categories, in which IL-2, IL-4, IL-9 and Eotaxin levels were significantly elevated (Figure 41). IL-4 and IL-9 are both produced by activated mature T cells, mast cells, and basophils. These cytokines regulate the mature T cell response, B cell class switching, and promote B and T cell proliferation. A group of growth factors (MCSF, G-CSF and IL-3) that support myelopoiesis (black box labeled in Figure 41) were decreased in the dmPGE2-treated group, although not significantly. In contrast, the cytokines IL-2 and IL-7, supporting lymphopoiesis (green box labeled in Figure 41), increased in dmPGE2-treated group in comparison with Veh control group. IL-$7^{-/-}$ or IL-$2^{-/-}$ mice have severe reduction in T and B cells, an involuted thymus, and a high incidence of autoimmune disease [336, 337]. Compared with IL-7, IL-2 has a broader biological function since the γ chain of the IL-2R is the common gamma chain for multiple cytokines such as IL-4, IL-7, IL-9, IL-15 and IL-21 [338]. IL-$2^{-/-}$ mice, therefore, have several additional hematopoietic defects in addition to dysfunctional lymphopoiesis. It has been reported that PGE2 inhibits mature T cell function and proliferation by decreasing IL-2 production [10-12]. The cytokine analysis indicates that radioprotectant dmPGE2 increases IL-2 shortly after the injection (Figure 25) and still increases as late as day 9 post-TBI (Figure 41), which further supports the "friend or foe" nature of dmPGE2. The change in IL-7 expression also indicates that, as early as day 9 post-TBI, the mice under dmPGE2 protection have pro-lymphopoietic environment despite peripheral lymphocyte recovery starts to show in CBC analysis

around day 20 (Figure 24). This can be explained by the slow process of development from LMPP to mature peripheral T cells. The decrease in IL-7 in BM microenvironment post-IR and the prevention of this decrease by dmPGE2 corresponds to the RNA sequencing findings in which the decrease of IL-7R gene expression in HSC post-IR is also prevented by dmPGE2. Determining whether BM cytokines act either in permissive (only promote the proliferation and survival of HSC) or instructive (activate a lineage differentiation direction) pattern will be helpful to illustrate the mechanism of dmPGE2 protection [332]. Other cytokine levels, such as FLT3L and CXCL12 which are not included in the Millipore mouse 32 cytokines panel, also need to be evaluated in H-ARS mouse model in order to investigate other important signal pathways in lymphopoiesis under the protection of dmPGE2.

In conclusion, these studies, for the first time, show that radioprotectant dmPGE2 results in long-lasting protection to the immune system including increased thymic-settling progenitors in BM, prevention of irradiation-induced thymic involution, enhanced differentiation of T and B cells, increased peripheral lymphocyte number, and blunted myeloid skewing. DmPGE2 is detrimental to peripheral lymphocytes immediately on administration; however, this toxicity is transient, and its pro-development and pro-differentiation effects rapidly counteract the toxicity, leading to lymphoid lineage reconstitution in the long-term post-IR. Further safety test to evaluate the effect of dmPGE2 on primary tumor in patients undergoing radiotherapy scenario and studies to determine the mechanism of dmPGE2 including the targeted cells and receptors and downstream signal pathways are necessary before applying dmPGE2 as a

radioprotectant to first responders and military personnel facing radiation disasters and/or patients undergoing radiotherapy.

# Chapter 5. Other stories: Pegylated Hematopoietic Growth Factors and Lisinopril as Radiomitigators

## 5.1. Introduction

The majority of clinical symptoms and radiation-related deaths occur early post-IR in the ARS phase. Treatment development has therefore largely focused on early intervention. Irradiation doses higher than two Gy and five Gy induce clinical H-ARS and GI-ARS, respectively [2, 35, 339]. H-ARS and GI-ARS are the most common causes of radiation-related death. Blood transfusions, supportive care, and administration of HGF-based regimens are used to rescue pancytopenia in H-ARS.

G-CSF and GM-CSF have similar signaling pathway and mechanism in hematopoiesis, as discussed in Chapter 1. IL-11 belongs to the IL-6 family and has a heterodimer receptor composed of IL-11Rα and gp130. IL-11 activates the downstream Jak/Stat, RAS/MAPK and PI3K/AKT signaling pathways to promote thrombopoiesis and erythropoiesis. It is also an anti-inflammatory cytokine and is cytoprotective for intestinal crypt cells [340, 341]. Recombinant human IL-11 (Oprelvekin, Neumega®) is FDA-approved for the treatment of chemotherapy-induced thrombocytopenia. The most common adverse effects of IL-11 are tolerable, including edema and fluid retention. More severe adverse effects such as atrial fibrillation occur less frequently [342]. Recombinant IL-11 has a longer half-life than natural IL-11, but still requires daily injection [343, 344]. Dr. Orschell's laboratory and others have shown that long-acting pegylated (peg) IL-11 analogs with a 10-fold higher half-life result in a sustained platelet increase for 7-10 days [74, 345]. Dr. Orschell's laboratory has shown that multiple injections or higher

doses of peg-IL-11 did not further increase survival compared to single, lower dose schedule (1.0 mg/kg vs. 0.3 mg/kg; three doses at day 1, 3, 5 vs. 1 dose at day 1 post-TBI) [74]. Similar trends were observed with peg-G-CSF and peg-GM-CSF in the same study. This efficacy of a single-dose treatment is of particular significance in treatment of victims of nuclear accidents, where daily dosing is complicated by the chaotic aftermath.

Since G-CSF, GM-CSF, and IL-11 interact with different receptors, work through different mechanisms, and target different HPCs (as discussed in Chapter 1), the combined treatment (double and triple combination of different peg-HGFs) were hypothesized to be able to further enhance survival rate and hematopoietic recovery.

Many other potential interventions have been investigated for H-ARS, as discussed in Chapter 1. In this study, the efficacy and mechanism of action of lisinopril, an ACE inhibitor, were investigated in the well-established H-ARS mouse model. Lisinopril decreases Ang II plasma levels by inhibiting ACE and has been approved for the treatment of hypertension, congestive heart failure, coronary artery disease, and diabetic nephropathy. Ang II receptors express on HSCs, BM stromal cells, erythroid progenitors, and mature LY [91, 92]. It has minimal positive effect on hematopoiesis when administered alone in the non-irradiated scenario [93, 94, 96], with adverse effects including anemia and leukopenia at high dose or when used long-term. This adverse effect results from an increase in plasma AcSDKP, an ACE substrate which negatively regulates hematopoiesis [99, 104]. The negative regulation of hematopoiesis does not, however, rule out the potential of ACEI used as a MCM to radiation. There are many

evidences showing that ACE inhibition post-IR is radiomitigating and the increased DNA damage repair in HSC due to ACEI-induced quiescence is thought to be a possible mechanism [101, 103]. Lisinopril is safe with tolerable adverse effects, and it is economical and easily accessible. It neither needs to be injected, nor to be refrigerated during the logistics chain. All these advantages make lisinopril an ideal MCM to stockpile in case of significant radiation event. Because only using lisinopril alone has minimal effect on hematopoiesis, and previous study indicates that there is a synergistic response on the hematopoietic recovery when angiotensin (1-7) and G-CSF combined [93], the effect of triple HGFs combination therapy in conjunction with lisinopril was evaluated in the H-ARS mouse model.

## 5.2. Materials and Methods

### 5.2.1. Mouse husbandry and irradiation

C57BL/6 mice were purchased from Jackson Laboratory (Bar Harbor, ME) at 10 w/o and housed in microisolators with up to five mice per cage. Extruded chow (Harlan 2018SXC) and acidified water were provided ad libitum. Mice were irradiated at 12 w/o after 2 weeks of acclimatization. At day 0, mice were exposed to single uniform TBI doses of gamma radiation a $^{137}$Cs radiation source (Mark 1 Irradiator, JL Shepherd, San Fernando, CA) at 8.72 Gy (LD70/30), 9.04 Gy (LD90/30) or 9.27 Gy (LD95/30). Autoclaved acidified water and wet feed were provided from day 4 to day 30 post-TBI. In the competitive transplantation study, recipients and competitors were congenic PtrcaPep3b/BoyJ (B6.BoyJ; CD45.1$^{+}$) or the F1 hybrid of C57Bl/6 and B6.BoyJ mice (CD45.2$^{+}$/CD45.1$^{+}$). B6.BoyJ and F1 hybrid mice were bred in-house and used between

8-12 w/o. Morbidity and mortality of irradiated mice was monitored twice daily for the duration of the H-ARS study (day 30). Mice were evaluated daily using a scale system incorporating body posture, activity level, and eye appearance to determine when euthanasia was required as previously described [69]. Day 30 post-TBI, surviving mice were transferred to the RBMD study. All studies were approved by the Indiana University School of Medicine Institutional Animal Care and Use Committee (IACUC protocol 10689).

### 5.2.2. Compounds

The manufacturing process of pegylated-HGFs have been described [74]. All pegylated-HGFs (subsequently referred to as "peg-HGFs" or "HGFs"**)** were administered by subcutaneous injection (SQ) 24±4 hr post-TBI at the following doses: peg-huG-CSF (BBT-015, subsequently referred to as "G"), 1.0 mg/kg; peg-muGM-CSF (BBT-007, subsequently referred to as "GM"), 1.0 mg/kg; peg-huIL-11 (BBT-059, subsequently referred to as "IL-11"), 0.3 mg/kg) were obtained from Bolder Biotech and formulated in 10 mM sodium phosphate, 4% mannitol, 1% sucrose pH 6.2 before use. The final volume of HGFs (~100 µl) was adjusted by mouse weight resulting in a dose of 6 µg of peg-IL-11, 20 µg of peg-G-CSF or 20 µg of peg-GM-CSF per mouse. An equivalent volume of vehicle (10 mM sodium phosphate, 4% mannitol, 1% sucrose, subsequently referred to as Veh) was delivered to the control group. The doses were chosen based on the previous efficacy study [74]. The different regimens of HGFs are summarized in Table 4. Lisinopril was supplied by Dr. Medhora at Medical College of Wisconsin and

**Table 4. Dose and combination regimens of pegylated HGFs.**

| Group ID | Treatment |
|---|---|
| 1 | Vehicle (Veh) |
| 2 | peg-G-CSF (1.0 mg/kg) (G) |
| 3 | peg-GM-CSF (1.0 mg/kg) (GM) |
| 4 | peg-IL-11 (0.3 mg/kg) (IL-11) |
| 5 | peg-G + peg-IL-11 (G+IL-11) |
| 6 | peg-GM + peg-IL-11 (GM+IL-11) |
| 7 | peg-G + peg-GM (G+GM) |
| 8 | peg-G + peg-GM + peg-IL-11 (triple combo, TC) |
| 9 | Non-irradiated controls (NI) |

dissolved into 60 mg/L in autoclaved acidified water for dosing on days 7-30 post-TBI. Lisinopril was delivered at a dose of 9 mg/kg (180 μg/20 g mouse) based on a previous finding that mice consume ~3 ml water per day in the absence of wet chow [69].

### 5.2.3. CBC and tissue harvest

Mice were tail-bled for CBC, which was performed at baseline and repeated throughout the study. NI, Veh-treated, and MCM-treated mice were assessed at various time-points at H-ARS and DEARE stage for CBC, bone marrow cellularity, and thymus weight/cellularity as previously described in Chapter 2. For the brain hemorrhage study, mice were sacrificed immediately at day 10 post-TBI. The scalp was cut in a sagittal direction with a scalpel from the forehead to the neck and the skull was broken between the eyes with scissors. A scoop was used to extract the cerebrum and cerebellum from the brain stem for counting macroscopic petechiae on the brain surface.

### 5.2.4. Antibody staining and flow cytometry analysis

Twelve w/o C57BL/6 mice were injected with different HGF regimens 24 hr post-TBI as described above. At day 2 post-TBI, peripheral blood cells were harvested by tail snip. Erythrocytes were lysed, and leukocytes ("total cells" in figures) were stained with antibodies for T cells (CD3-PE), B cells (B220-FITC), and myeloid cells (Gr-1-PerCPCy5.5). Annexin-V-APC was used as an apoptosis marker and 7-AAD as a viability stain. Apoptotic rate in each white blood cell subpopulation was evaluated by flow cytometry. Expression of c-Kit was rapidly down-regulated post-IR at cell numbers were very low at myelosuppressive nadir. Therefore, for bone marrow stem cell

population analysis, lineage-, Sca-$1^+$ and $CD150^+$ ($SLCD150^+$ cells) markers were used to identify the enriched population in HSCs at day 2, 7, 10 post-TBI in the H-ARS study to gain sufficient cells for flow cytometry analysis. The gating strategy used in DEARE stage was different from in the H-ARS stage since hematopoiesis had almost or partially recovered at the DEARE time-points. Therefore, in the DEARE study, $lineage^-$, c-$Kit^+$, Sca-$1^+$, $CD150^+$ and CD48- ($KSLCD150^+CD48^-$) markers were used to identify the enriched population in HSCs at 6 and 12 months post-TBI. Thymocyte subgroup staining and analysis was as described in Chapter 2. For cell cycle analysis in the lisinopril study, bone marrow cells were stained at day 10 post-TBI for the $SLCD150^+$ marker, or 6 months post-TBI for KSL $CD150^+CD48^-$, as described above. Cells were fixed overnight in 1% (v/v) formaldehyde and stained with 4',6-diamidino-2-phenylindole (DAPI, Invitrogen, Eugene, OR). All antibodies were purchased from BD Biosciences (San Jose, CA), Biolegend (San Diego, CA), eBiosciences (San Diego, CA), or R&D Systems (Minneapolis, MN). Staining procedures and flow cytometric analyses were as previously described [40].

### 5.2.5. CFC assays and competitive transplantation

Twelve w/o C57BL/6 mice were exposed to 9.27 Gy (LD95/30) and treated with different HGF regimens at 24 hr post-TBI as previously described. In H-ARS phase, four mice per treatment group were euthanized at day 5, 7, 14, and 30. BM cells were flushed from eight bones (humeri, pelvis, femurs, and tibias) and pooled together because cell number was very low at days 5, 7, and 14. Three quarters of the total cells were transplanted into three recipient mice (one aliquot number of cells per recipient, total of

three recipients per group); remaining cells were used for the colony assay. In H-ARS CFC assays, one aliquot of BM cells was suspended in 1 ml semi-solid methylcellulose media supplemented with murine SCF, murine IL-3, recombinant human IL-6, and recombinant human EPO (Methocult M3434, Stem Cell Technologies, Vancouver, BC, Canada) and incubated for 7 days (37°C, 5% $CO_2$) prior to quantification of CFU-GM, BFU-E and CFU-GEMM. In H-ARS transplantation studies, one aliquot of BM cells was transplanted into one recipient along with $2\times10^5$ competitor cells. Peripheral blood was analyzed monthly for donor-derived chimerism for 1-5 months post-transplantation. In DEARE CFC assays, $2.5\times10^4$ whole BM cells were cultured in duplicate in similar procedures as in H-ARS CFC studies. In DEARE transplantation studies, donor mice were sacrificed at 12 months post-TBI, and BM cells were flushed from pelvis, femurs, and tibias, and $3\times10^5$ whole BM donor cells were transplanted intravenously with $2\times10^5$ competitor cells into congenic recipient. Peripheral white blood cells were stained with CD45.1, CD45.2, Gr-1, B220, CD4 and CD8 antibodies for chimerism and lineage reconstitution at 6 months post-transplantation. Similar studies were also carried out on TC ± lisinopril study.

### 5.2.6. Plasma and bone marrow cytokine analysis

Plasma samples were obtained by cardiac puncture. BM supernatants were obtained from 2 femurs and 2 tibiae flushed twice with 500 µl cold PBS. Plasma samples were acquired after centrifuging EDTA-anticoagulant whole blood from cardiac puncture at 956 g for 4 min. BM supernatants and plasma samples were stored at -80°C and

thawed on ice before analysis. The cytokine detection and analysis were described in Chapter 3.

### 5.2.7. Statistical analysis

Thirty-day survival in H-ARS studies and lifespan in DEARE studies were analyzed by KM analyses and log-rank tests using SPSS Statistics Version 24 (IBM, Armonk, NY). Unpaired two-tailed t-tests were performed on Microsoft Excel 2010 (Microsoft Corp, Redmond, WA) to compare the parameters between "with xx" and "no xx" as the combined analysis strategy, or between female and male in lisinopril studies, where at least three mice of either gender were analyzed. In rest studies, when comparing more than two groups, one-way ANOVA with post-hoc Tukey-Kramer HSD or Welch ANOVA for unequal variances were performed by JMP 14 (SAS Institute, Cary, NC). Data were expressed as mean ± SEM. $P<0.05$ was considered significant.

## 5.3. Results

### 5.3.1. Peg-HGFs increase post-TBI day 30 survival rate

Dr. Orschell's laboratory recently reported a significantly increased day 30 survival rate in mice treated with SQ injections of single-dose individual peg-HGFs +24 hr post-TBI [74]. In the current study, the efficacy of combined HGFs strategy on day 30 survival was investigated. The difference between LD90/30 and LD95/30 is minimal so mice were combined. The day 30 survival rate in mice receiving the Veh injection was 7.5%, consistent with the expected LD. The day 30 survival rate significantly increased in mice receiving a single individual dose of G, GM, or IL-11 (50%, 32.5%, and 62.5%,

respectively), consistent with previous report [74] (Figure 42 A and Table 5). Mice receiving combinations of two or three HGFs had higher day 30 survival rates than mice treated with individual HGFs. Treating with G+IL-11, GM+ IL-11, G+GM, and G+GM+IL-11 (triple combination, TC) increases day 30 survival to levels of 65%, 72.5%, 55%, and 80%, respectively. TC-treated mice had a significantly higher survival than G, GM, and G+GM groups; however, no statistical difference was found in comparison with IL-11-containing regimens (IL-11, G+IL-11, GM+IL-11) (Figure 42 A and Table 5). Comparable results were obtained in a subsequent study with a lower dose of irradiation (8.72 Gy, LD70/30; data not shown).

To further understand how combining HGFs contributes to increased survival, different HGF-treated mice were pooled together for analysis. Mice treated with G, G + GM, G + IL-11, or TC were pooled as G-CSF regimens ("with G" in figures) and compared with a pooled group of mice treated with GM, IL-11, or GM + IL-11 ("no G" in figures). The pooling criteria were applied to mice treated with GM-CSF regimens and IL-11 regimens. To compare the use of multiple HGFs vs. a single HGF, the G+IL-11, GM+IL-11, G+GM, and TC groups were combined into one group ("combined" in Figures and Legends) and the G, GM and IL-11 groups into one group ("single" in Figures and Legends). To compare HGFs vs. Veh, all HGF-treated groups were combined ("HGFs" in figures) and compared with the Veh group. The analyses showed that the "with IL-11" and "combined" groups had a higher day 30 survival rate than the "no IL-11" and "single" groups, respectively (Figure 42 D & E). However, there were no differences in the day 30 survival rates between "with G" and "with GM" groups in

comparison with the “no G” and “no GM” groups, respectively (Figure 42 B & C). All HGF-treated groups had significant higher day 30 survival rates than the Veh group (Figure 42 A & F).

### 5.3.2. Peg-HGFs accelerate recovery of peripheral blood cells

To examine the relationship of hematopoietic recovery to survival, CBC with differential counts were performed at baseline as well as at day 2, 4, 7, 10, 21, and 30 post-TBI. The fluctuation in animal number during the course of the study is due to the fact that these are retrospective analyses that combined data from several MCM screening studies. At day 2 post-TBI, LY level was at a low level approaching their nadir at day 7-10, whereas NE level only decreased to 33-50% of normal (Figure 43 B & C, Table 7 & 8, for comparisons of other CBC parameters, please see Table 6-10). As expected, the declines of RBC and PLT were delayed in comparison with NE and LY. RBC and PLT decreased at day 10 and at day 7 post-TBI, respectively, in comparison with NI mice. The nadirs of WBC, LY and NE occurred at day 7-10, whereas RBC and PLT reached nadir around day 21. At the time-points around the nadirs (day 4, 7, and 10), almost all HGF-treated groups had no significant differences in WBC, NE, and LY compared with Veh-treated mice. All irradiated mice (both HGF-treated and Veh-treated mice) had significant differences in these parameters in comparison with NI mice. At day 30, NE levels had recovered to normal in all irradiated mice with no difference to NI mice; in contrast, WBC and LY numbers remained significantly lower in IRR mice than in NI mice. No HGF treatment rescued this low LY count at day 30. At day 21, the nadir time-point of RBC and PLT, mice receiving HGF treatments had higher numbers of these cells than

**Figure 42**

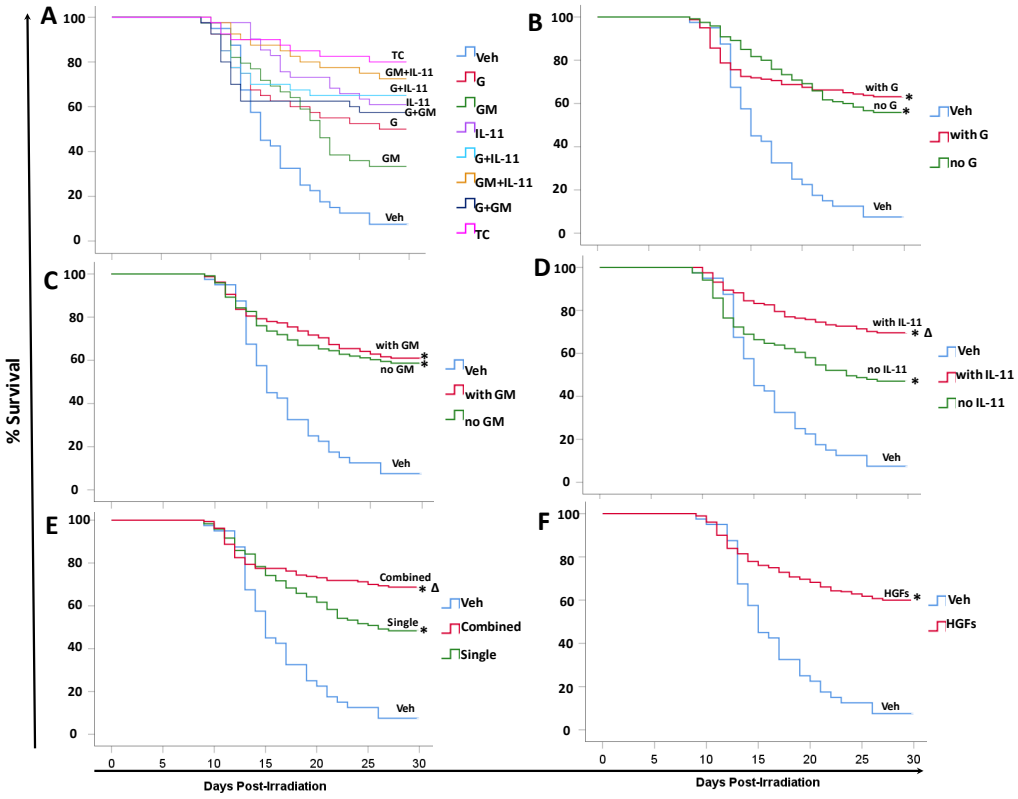
A
B
C
D
E
F
% Survival
Days Post-Irradiation
Days Post-Irradiation
TC
GM+IL-11
G+IL-11
IL-11
G+GM
G
GM
Veh
Veh
G
GM
IL-11
G+IL-11
GM+IL-11
G+GM
TC
with G
no G
Veh
with G
no G
with GM
no GM
Veh
Veh
with GM
no GM
with IL-11
no IL-11
Veh
Veh
with IL-11
no IL-11
Combined
Single
Veh
Veh
Combined
Single
HGFs
Veh
Veh
HGFs

**Figure 42. Thirty-day survival of lethal-irradiated mice treated with pegylated HGFs.**

Mice were exposed to 9.04 Gy or 9.27 Gy TBI and treated with pegylated HGFs in single, double, or triple combination (TC) 24 hr later. Survival on day 30 is shown as Kaplan-Meier survival curve. n=39-41 mice in each group (panel A). P values of comparisons in panel A were summarized in Table 5. The day 30 survival data were also analyzed in the method of combining different HGF groups into "with G" vs. "no G" (panel B), "with GM" vs. "no GM" (panel C), "with IL-11" vs. "no IL-11" (panel D), "single" vs. "combined" (panel E), or combining all HGF groups into one "HGFs" group and compared with Veh group (panel F). *$p<0.05$ comparing to Veh group. $\Delta$ $p<0.05$ comparing to "no IL-11" group (panel D) or comparing to "single" group (panel E). Sasidhar Vemula acquired the data; Tong Wu did the analyses.

**Table 5. Comparisons of day 30 survival rates of lethal-irradiated mice treated with pegylated HGFs.**

| Treatment | Veh | G | GM | IL-11 | G+IL-11 | GM+IL-11 | G+GM | TC |
|---|---|---|---|---|---|---|---|---|
| Veh | | <.0001 | 0.002 | <.0001 | <.0001 | <.0001 | <.0001 | <.0001 |
| G | <.0001 | | NS | NS | NS | 0.027 | NS | 0.005 |
| GM | 0.002 | NS | | 0.011 | 0.027 | 0.001 | NS | <.0001 |
| IL-11 | <.0001 | NS | 0.011 | | NS | NS | NS | NS |
| G+IL-11 | <.0001 | NS | 0.027 | NS | | NS | NS | NS |
| GM+IL-11 | <.0001 | 0.027 | 0.001 | NS | NS | | NS | NS |
| G+GM | <.0001 | NS | NS | NS | NS | NS | | 0.025 |
| TC | <.0001 | 0.005 | <.0001 | NS | NS | NS | 0.025 | |

Numbers in the table are p values of comparisons. NS: Not significant

Veh-treated mice. This difference no longer existed by day 30, though RBC and PLT in mice treated with most HGF regimens were lower than NI control mice (Figure 43 D & E, Table 9 & 10).

To reduce the number of comparisons and identify which HGF or which combination regimen promoted hematopoietic recovery, data were analyzed as "with IL-11" vs. "no IL-11", "with G" vs. "no G", "with GM" vs. "no GM", "single" vs. "combined", and "HGFs" vs. "Veh"(Figure 44-48). The "with IL-11" group had higher NE numbers than "no IL-11" group at day 2 post-TBI (Figure 44). The "with G" group had higher NE, RBC and PLT numbers, but not LY number, than "no G" group at day 21 post-TBI (Figure 45). The "with GM" group had lower WBC and LY numbers at day 21 post-TBI than "no GM" group (Figure 46). These analyses indicate that the three different HGFs took effect at different time-points and affect different cell types. Regimens containing G-CSF increase NE, RBC and PLT levels at day 21 post-TBI, which is when most Veh-treated mice die from infection and hemorrhage. This was not observed in mice treated with GM-CSF or IL-11-containing regimens. The "single" vs. "combined" analysis indicated that combining HGFs increased WBC and NE at day 2 post-TBI; RBC and PLT at day 21 post-TBI. However, LY at day 21 post-TBI was lower with combined treatment than treatment with single HGF (Figure 47). Analyzing all HGF-treated groups together in comparison with the Veh group (Figure 48) revealed that the most significant increases in CBC parameters were at day 21, where WBC, NE, LY, RBC, and PLT counts were higher in HGF-treated mice than in Veh-treated mice.

**Figure 43**

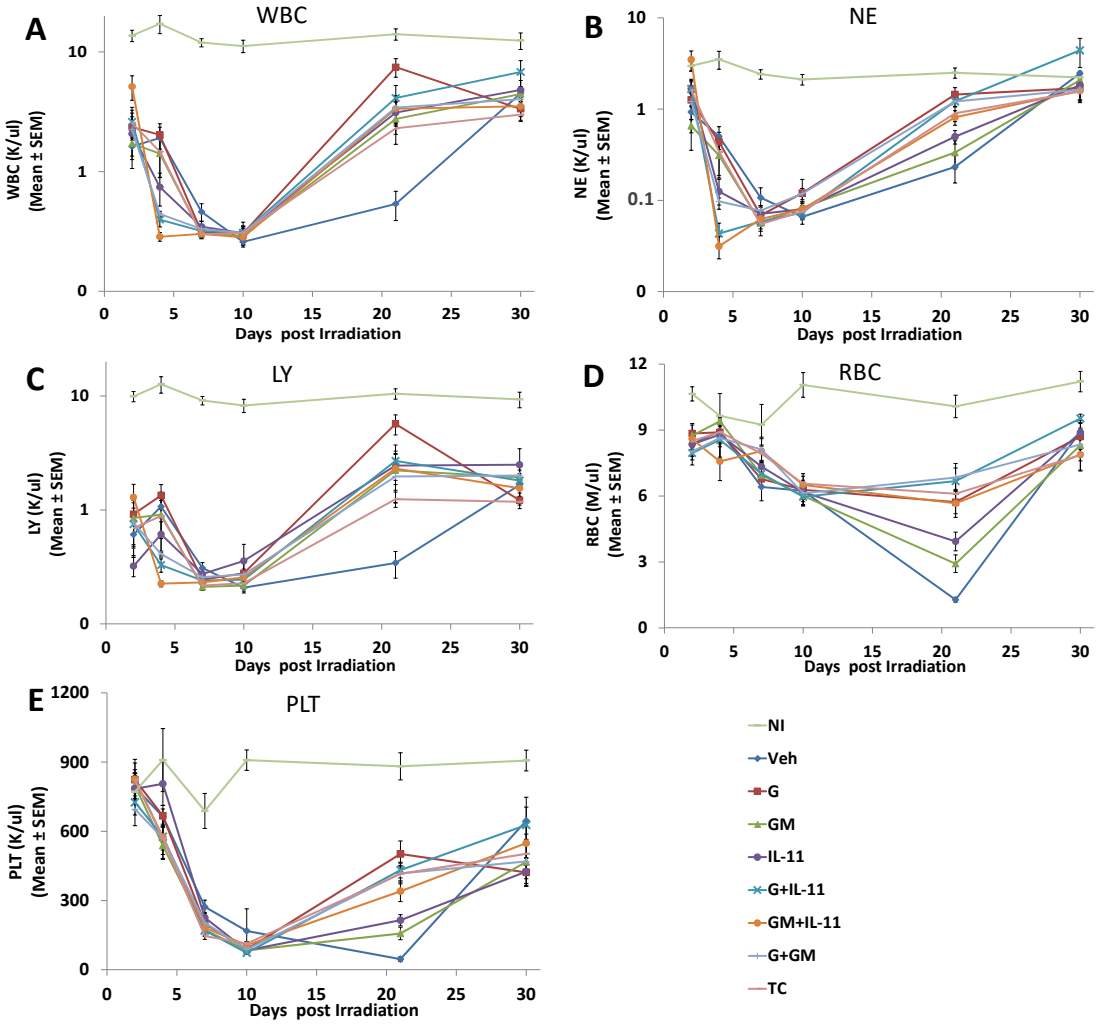
A
WBC
WBC (K/ul) (Mean ± SEM)
Days post Irradiation
B
NE
NE (K/ul) (Mean ± SEM)
Days post Irradiation
C
LY
LY (K/ul) (Mean ± SEM)
Days post Irradiation
D
RBC
RBC (M/ul) (Mean ± SEM)
Days post Irradiation
E
PLT
PLT (K/ul) (Mean ± SEM)
Days post Irradiation
NI
Veh
G
GM
IL-11
G+IL-11
GM+IL-11
G+GM
TC

**Figure 43. CBC profiles in H-ARS phase of lethal-irradiated mice treated with pegylated HGFs.**

Mice were exposed to 9.04 Gy or 9.27 Gy TBI and treated with pegylated HGFs in single, double, or TC 24 hr later. Peripheral blood CBCs were performed at different time-points as indicated in panels. n=3-21 mice in each group (panel A). P values of comparisons were summarized in Table 6-10. Sasidhar Vemula acquired the data; Tong Wu did the analyses.

**Table 6. Comparisons of WBC at different time-points of lethal-irradiated mice treated with pegylated HGFs.**

| WBC | | | | | | |
|---|---|---|---|---|---|---|
| **Treatments** | **Day2** | **Day4** | **Day7** | **Day10** | **Day21** | **Day30** |
| NI vs. Veh | <.0001 | <.0001 | <.0001 | <.0001 | <.0001 | 0.0072 |
| NI vs. G | <.0001 | <.0001 | <.0001 | <.0001 | 0.0002 | 0.0001 |
| NI vs. GM | <.0001 | <.0001 | <.0001 | <.0001 | <.0001 | 0.0001 |
| NI vs. IL-11 | <.0001 | <.0001 | <.0001 | <.0001 | <.0001 | 0.0001 |
| NI vs. G+IL-11 | <.0001 | <.0001 | <.0001 | <.0001 | <.0001 | 0.0112 |
| NI vs. GM+IL-11 | <.0001 | <.0001 | <.0001 | <.0001 | <.0001 | <.0001 |
| NI vs. G+ GM | <.0001 | <.0001 | <.0001 | <.0001 | <.0001 | <.0001 |
| NI vs. TC | <.0001 | <.0001 | <.0001 | <.0001 | <.0001 | <.0001 |
| Veh vs. G | NS | NS | NS | NS | 0.0047 | NS |
| Veh vs. IL-11 | NS | NS | NS | NS | 0.0102 | NS |
| Veh vs. G+IL-11 | NS | NS | NS | NS | 0.0062 | NS |
| Veh vs. GM+IL-11 | NS | NS | NS | NS | 0.0208 | NS |
| Veh vs. G+GM | NS | NS | NS | NS | 0.008 | NS |
| Veh vs. TC | NS | NS | NS | NS | 0.0052 | NS |
| G vs. GM+IL-11 | NS | 0.0441 | NS | NS | NS | NS |
| G vs. TC | NS | NS | NS | NS | 0.0181 | NS |
| GM vs. GM+IL-11 | NS | 0.0441 | NS | NS | NS | NS |

Numbers in the table are p values of comparisons. If a comparison has no significant difference at any time-points, it will not be shown in the table. NS: Not significant

**Table 7. Comparisons of NE at different time-points in H-ARS phase of lethal-irradiated mice treated with pegylated HGFs.**

| NE | | | | | | |
|---|---|---|---|---|---|---|
| **Treatments** | **Day2** | **Day4** | **Day7** | **Day10** | **Day21** | **Day30** |
| NI vs. Veh | 0.0386 | <.0001 | <.0001 | <.0001 | <.0001 | NS |
| NI vs. G | NS | <.0001 | <.0001 | <.0001 | 0.0295 | NS |
| NI vs. GM | 0.0109 | <.0001 | <.0001 | <.0001 | <.0001 | NS |
| NI vs. IL-11 | NS | <.0001 | <.0001 | <.0001 | <.0001 | NS |
| NI vs. G+IL-11 | NS | <.0001 | <.0001 | <.0001 | 0.0004 | NS |
| NI vs. GM+IL-11 | NS | <.0001 | <.0001 | <.0001 | <.0001 | NS |
| NI vs. G+ GM | NS | <.0001 | <.0001 | <.0001 | 0.0005 | NS |
| NI vs. TC | NS | <.0001 | <.0001 | <.0001 | <.0001 | NS |
| Veh vs. G | NS | NS | NS | NS | 0.0059 | NS |
| Veh vs. IL-11 | NS | NS | NS | NS | 0.0361 | NS |
| Veh vs. G+IL-11 | NS | NS | NS | NS | 0.0078 | NS |
| Veh vs. GM+IL-11 | NS | NS | NS | NS | 0.0203 | NS |
| Veh vs. G+GM | NS | NS | NS | NS | 0.0101 | NS |
| Veh vs. TC | NS | NS | NS | NS | 0.0063 | NS |
| G vs. GM | NS | NS | NS | NS | 0.0114 | NS |
| G vs. IL-11 | NS | NS | NS | NS | 0.0555 | NS |
| G vs. GM+IL-11 | NS | 0.0441 | NS | NS | NS | NS |
| GM vs. IL-11 | 0.0211 | NS | NS | NS | NS | NS |

| | | | | | | |
|---|---|---|---|---|---|---|
| GM vs. G+IL-11 | NS | NS | NS | NS | 0.0087 | NS |
| GM vs. GM+IL-11 | 0.0296 | 0.0441 | NS | NS | NS | NS |
| GM vs. G+GM | NS | NS | NS | NS | 0.0243 | NS |
| GM vs. TC | NS | NS | NS | NS | 0.0388 | NS |
| IL-11 vs. G+IL-11 | NS | NS | NS | NS | 0.0238 | NS |

Numbers in the table are p values of comparisons. NS: Not significant

**Table 8. Comparisons of LY at different time-points in H-ARS phase of lethal-irradiated mice treated with pegylated HGFs.**

| LY | | | | | | |
|---|---|---|---|---|---|---|
| **Treatments** | **Day2** | **Day4** | **Day7** | **Day10** | **Day21** | **Day30** |
| NI vs. Veh | <.0001 | <.0001 | <.0001 | <.0001 | <.0001 | <.0001 |
| NI vs. G | <.0001 | <.0001 | <.0001 | <.0001 | 0.0018 | <.0001 |
| NI vs. GM | <.0001 | <.0001 | <.0001 | <.0001 | <.0001 | <.0001 |
| NI vs. IL-11 | <.0001 | <.0001 | <.0001 | <.0001 | <.0001 | <.0001 |
| NI vs. G+IL-11 | <.0001 | <.0001 | <.0001 | <.0001 | <.0001 | <.0001 |
| NI vs. GM+IL-11 | <.0001 | <.0001 | <.0001 | <.0001 | <.0001 | <.0001 |
| NI vs. G+ GM | <.0001 | <.0001 | <.0001 | <.0001 | <.0001 | <.0001 |
| NI vs. TC | <.0001 | <.0001 | <.0001 | <.0001 | <.0001 | <.0001 |
| Veh vs. G | NS | NS | NS | NS | 0.0045 | NS |
| Veh vs. GM | NS | NS | NS | NS | 0.0269 | NS |
| Veh vs. IL-11 | NS | NS | NS | NS | 0.0043 | NS |
| Veh vs. G+IL-11 | NS | NS | NS | NS | 0.0101 | NS |
| Veh vs. GM+IL-11 | NS | NS | NS | NS | 0.0078 | NS |
| Veh vs. G+GM | NS | NS | NS | NS | 0.0057 | NS |
| Veh vs. TC | NS | NS | NS | NS | 0.0031 | NS |
| G vs. GM+IL-11 | NS | 0.0445 | NS | NS | NS | NS |
| G vs. TC | NS | NS | NS | NS | 0.0084 | NS |
| GM vs. GM+IL-11 | NS | 0.0445 | NS | NS | NS | NS |

Numbers in the table are p values of comparisons. NS: Not significant

**Table 9. Comparisons of RBC at different time-points in H-ARS phase of lethal-irradiated mice treated with pegylated HGFs.**

| RBC | | | | | | |
|---|---|---|---|---|---|---|
| **Treatments** | **Day2** | **Day4** | **Day7** | **Day10** | **Day21** | **Day30** |
| NI vs. Veh | NS | NS | 0.0312 | <.0001 | <.0001 | NS |
| NI vs. G | NS | NS | NS | <.0001 | <.0001 | 0.0303 |
| NI vs. GM | NS | NS | NS | <.0001 | <.0001 | 0.0093 |
| NI vs. IL-11 | NS | NS | NS | <.0001 | <.0001 | NS |
| NI vs. G+IL-11 | 0.0131 | NS | NS | <.0001 | 0.0003 | NS |
| NI vs. GM+IL-11 | NS | NS | NS | <.0001 | <.0001 | 0.0009 |
| NI vs. G+ GM | 0.0174 | NS | NS | <.0001 | 0.001 | 0.0072 |
| NI vs. TC | NS | NS | NS | <.0001 | <.0001 | 0.0009 |
| Veh vs. G | NS | NS | NS | NS | 0.0047 | NS |
| Veh vs. IL-11 | NS | NS | NS | NS | 0.0115 | NS |
| Veh vs. G+IL-11 | NS | NS | NS | NS | 0.0047 | NS |
| Veh vs. GM+IL-11 | NS | NS | NS | NS | 0.0038 | NS |
| Veh vs. G+GM | NS | NS | NS | NS | 0.006 | NS |
| Veh vs. TC | NS | NS | NS | NS | 0.0025 | NS |
| G vs. GM | NS | NS | NS | NS | 0.023 | NS |
| GM vs. G+IL-11 | NS | NS | NS | NS | 0.0045 | NS |
| GM vs. G+GM | NS | NS | NS | NS | 0.0155 | NS |
| GM vs. TC | NS | NS | NS | NS | 0.0072 | NS |

| | | | | | | |
|---|---|---|---|---|---|---|
| IL-11 vs. G+IL-11 | NS | NS | NS | NS | 0.0486 | NS |
| IL-11 vs. G+GM | NS | NS | NS | NS | 0.0473 | NS |

Numbers in the table are p values of comparisons. NS: Not significant

**Table 10. Comparisons of PLT at different time-points in H-ARS phase of lethal-irradiated mice treated with pegylated HGFs.**

| PLT | | | | | | |
|---|---|---|---|---|---|---|
| **Treatments** | **Day2** | **Day4** | **Day7** | **Day10** | **Day21** | **Day30** |
| NI vs. Veh | NS | NS | <.0001 | <.0001 | <.0001 | NS |
| NI vs. G | NS | NS | <.0001 | <.0001 | <.0001 | 0.0009 |
| NI vs. GM | NS | 0.0172 | <.0001 | <.0001 | <.0001 | 0.0059 |
| NI vs. IL-11 | NS | NS | <.0001 | <.0001 | <.0001 | 0.001 |
| NI vs. G+IL-11 | NS | 0.0481 | <.0001 | <.0001 | <.0001 | NS |
| NI vs. GM+IL-11 | NS | 0.0459 | <.0001 | <.0001 | <.0001 | 0.0356 |
| NI vs. G+ GM | NS | 0.0413 | <.0001 | <.0001 | <.0001 | 0.004 |
| NI vs. TC | NS | 0.0204 | <.0001 | <.0001 | <.0001 | 0.0104 |
| Veh vs. G | NS | NS | NS | NS | 0.0047 | NS |
| Veh vs. GM | NS | NS | NS | NS | 0.0135 | NS |
| Veh vs. IL-11 | NS | NS | NS | NS | 0.004 | NS |
| Veh vs. G+IL-11 | NS | NS | NS | NS | 0.0047 | NS |
| Veh vs. GM+IL-11 | NS | NS | NS | NS | 0.0262 | NS |
| Veh vs. G+GM | NS | NS | NS | NS | 0.006 | NS |
| Veh vs. TC | NS | NS | 0.0464 | NS | 0.0026 | NS |
| G vs. GM | NS | NS | NS | NS | 0.0016 | NS |
| G vs. IL-11 | NS | NS | NS | NS | 0.0072 | NS |
| GM vs. G+IL-11 | NS | NS | NS | NS | 0.003 | NS |

| | | | | | | |
|---|---|---|---|---|---|---|
| GM vs. G+GM | NS | NS | NS | NS | 0.0129 | NS |
| GM vs. TC | NS | NS | NS | NS | 0.0015 | NS |
| IL-11 vs. G+IL-11 | NS | NS | NS | NS | 0.0039 | NS |
| IL-11 vs. TC | NS | NS | NS | NS | 0.0034 | NS |

Numbers in the table are p values of comparisons. NS: Not significant

**Figure 44**

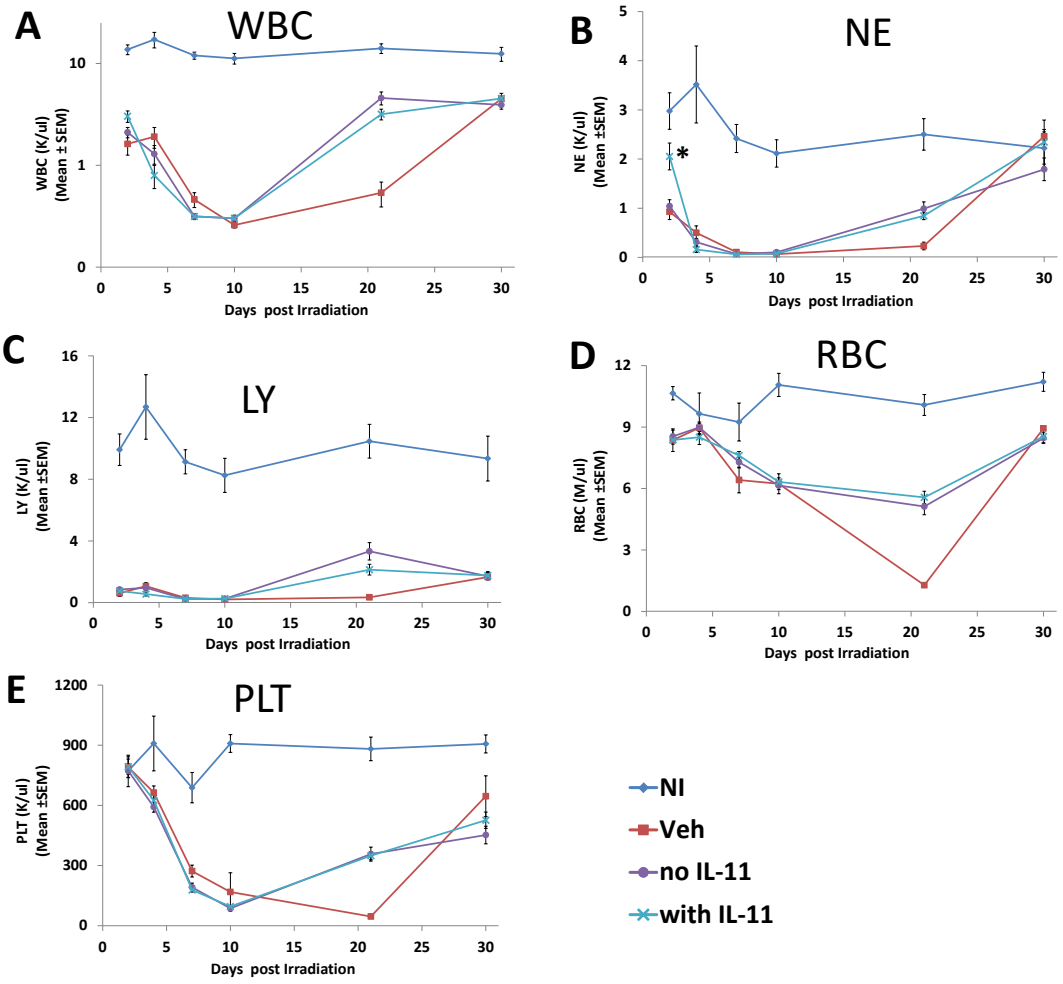
A
WBC
WBC (K/ul) (Mean ± SEM)
Days post Irradiation
B
NE
NE (K/ul) (Mean ±SEM)
*
Days post Irradiation
C
LY
LY (K/ul) (Mean ±SEM)
Days post Irradiation
D
RBC
RBC (M/ul) (Mean ±SEM)
Days post Irradiation
E
PLT
PLT (K/ul) (Mean ±SEM)
Days post Irradiation
NI
Veh
no IL-11
with IL-11

**Figure 44. CBC profiles in H-ARS phase of lethal-irradiated mice treated with "with IL-11" or "no IL-11" regimen.**

Mice in Figure 43 were re-grouped as mice received any regimens containing IL-11 were combined into "with IL-11" group and mice received regimens containing other HGFs were combined into "no IL-11" group. n=21-71 mice per time-point per group. * $p<0.05$ comparing "with IL-11" group (light blue) to "no IL-11" group (purple) at time-points as marked. Sasidhar Vemula acquired the data; Tong Wu did the analyses.

**Figure 45**

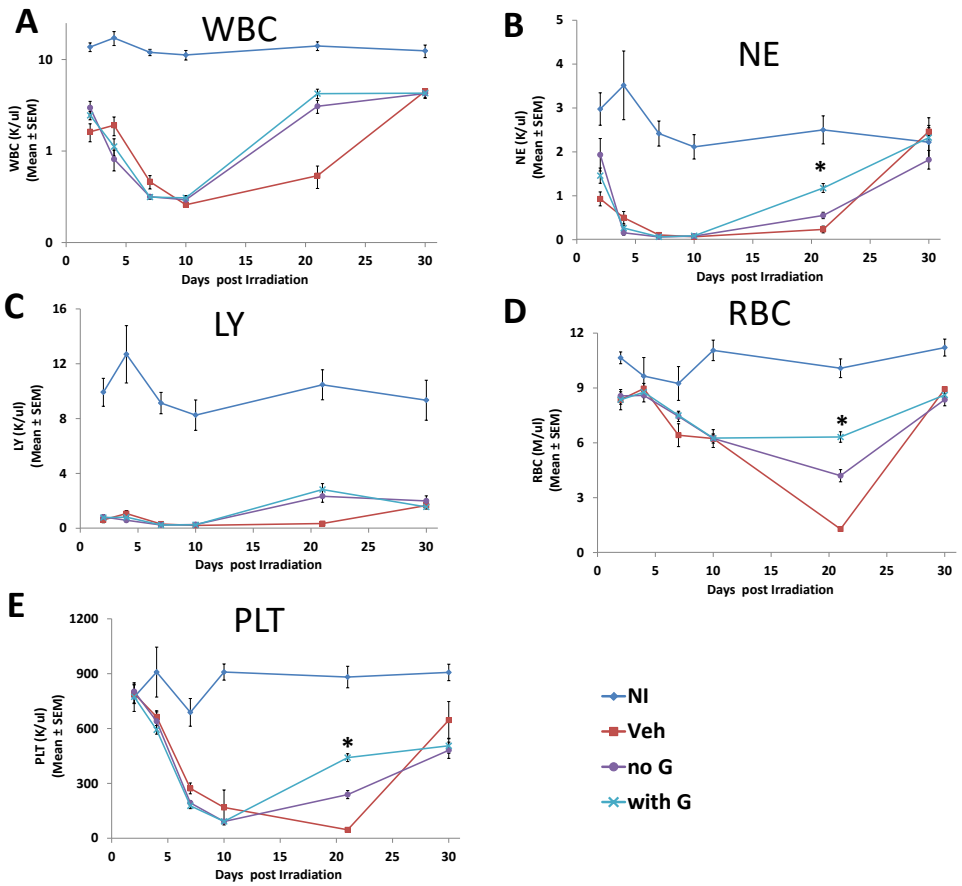
A
WBC
WBC (K/ul) (Mean ± SEM)
Days post Irradiation
B
NE
NE (K/ul) (Mean ± SEM)
Days post Irradiation
C
LY
LY (K/ul) (Mean ± SEM)
Days post Irradiation
D
RBC
RBC (M/ul) (Mean ± SEM)
Days post Irradiation
E
PLT
PLT (K/ul) (Mean ± SEM)
Days post Irradiation
NI
Veh
no G
with G

**Figure 45. CBC profiles in H-ARS phase of lethal-irradiated mice treated with "with G" or "no G" regimen.**

Mice in Figure 43 were re-grouped as the method of "with G" vs. "no G" as previously described. n=21-72 mice per time-point per group. *$p<0.05$ comparing "with G" group (light blue) to "no G" group (purple) at time-points as marked. Sasidhar Vemula acquired the data; Tong Wu did the analyses.

**Figure 46**

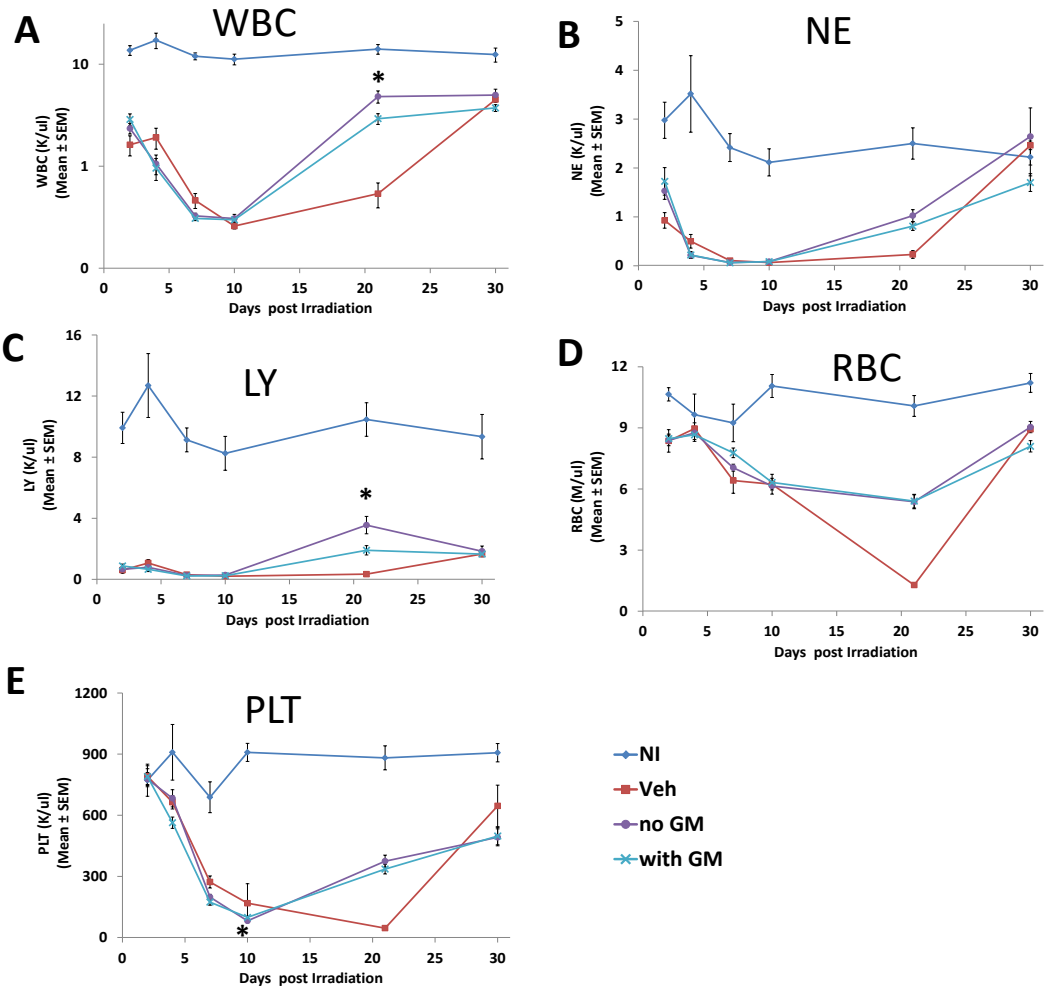
A
WBC
WBC (K/ul) (Mean ± SEM)
Days post Irradiation
B
NE
NE (K/ul) (Mean ± SEM)
Days post Irradiation
C
LY
LY (K/ul) (Mean ± SEM)
Days post Irradiation
D
RBC
RBC (M/ul) (Mean ± SEM)
Days post Irradiation
E
PLT
PLT (K/ul) (Mean ± SEM)
Days post Irradiation
NI
Veh
no GM
with GM

**Figure 46. CBC profiles in H-ARS phase of lethal-irradiated mice treated with "with GM" or "no GM" regimen.**

Mice in Figure 43 were re-grouped as the method of "with GM" vs. "no GM" as previously described. n=21-71 mice per time-point per group. * $p<0.05$ comparing "with GM" group (light blue) to "no GM" group (purple) at time-points as marked. Sasidhar Vemula acquired the data; Tong Wu did the analyses.

**Figure 47**

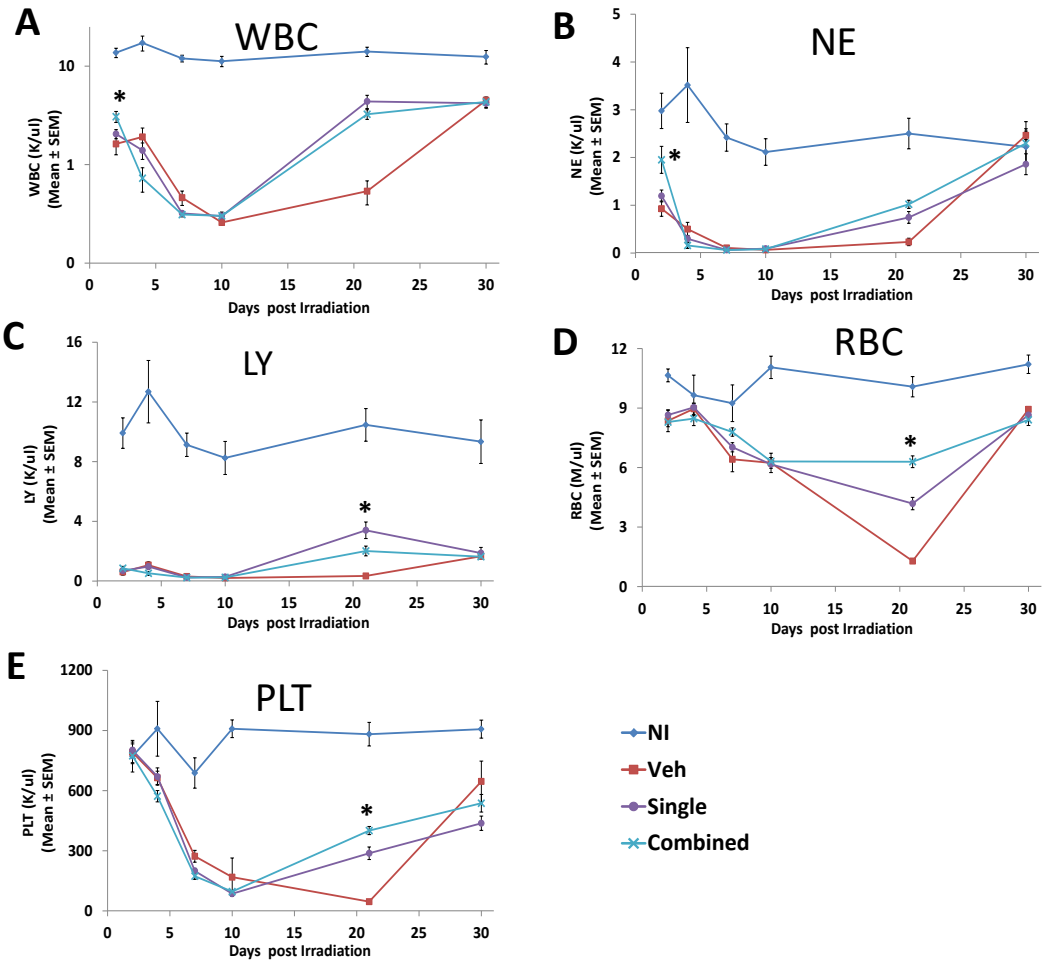
A
WBC
WBC (K/ul) (Mean ± SEM)
Days post Irradiation
B
NE
NE (K/ul) (Mean ± SEM)
Days post Irradiation
C
LY
LY (K/ul) (Mean ± SEM)
Days post Irradiation
D
RBC
RBC (M/ul) (Mean ± SEM)
Days post Irradiation
E
PLT
PLT (K/ul) (Mean ± SEM)
Days post Irradiation
NI
Veh
Single
Combined

**Figure 47. CBC profiles in H-ARS phase of lethal-irradiated mice treated with "single" or "combined" regimen.**

Mice in Figure 43 were re-grouped as the method of "single" vs. "combined" as previously described. n=21-72 mice per time-point per group. *: $p<0.05$ comparing "combined" group (light blue) to "single" group (purple) at time-points as marked. Sasidhar Vemula acquired the data; Tong Wu did the analyses.

**Figure 48**

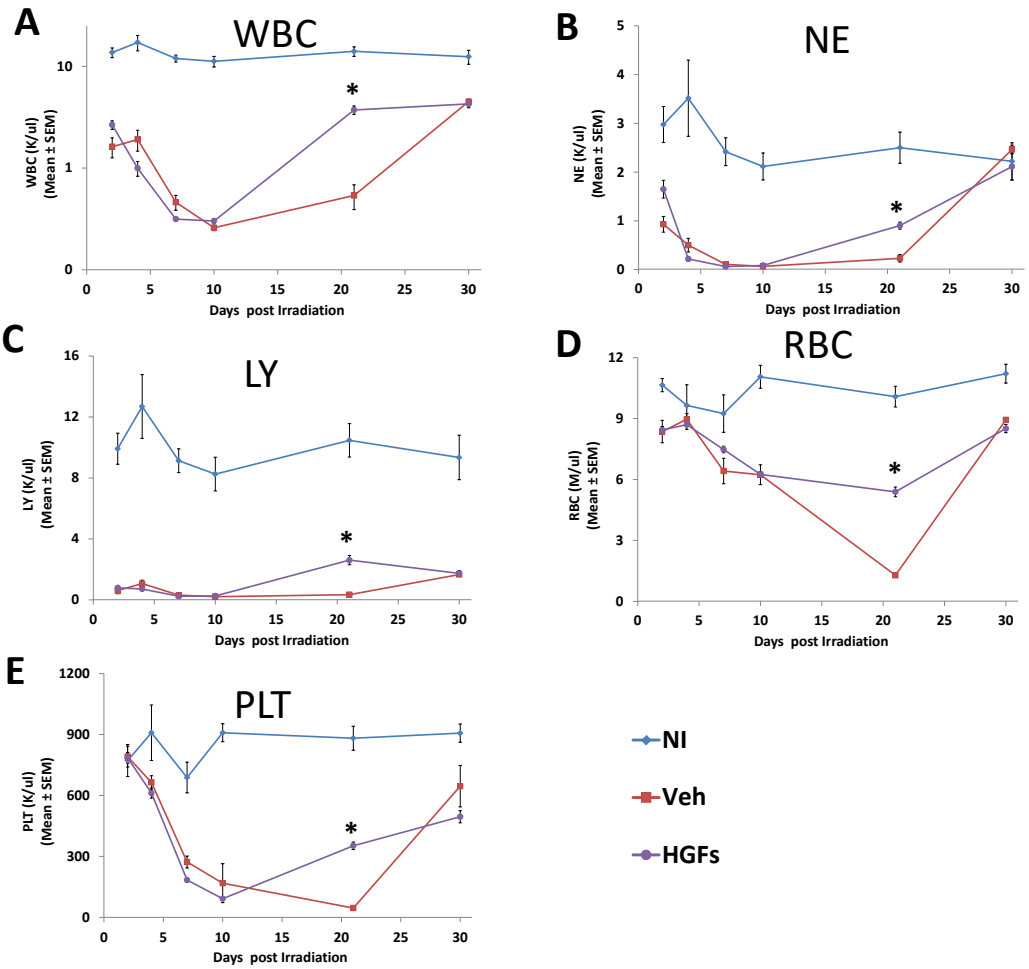
A
WBC
WBC (K/ul) (Mean ± SEM)
Days post Irradiation
B
NE
NE (K/ul) (Mean ± SEM)
Days post Irradiation
C
LY
LY (K/ul) (Mean ± SEM)
Days post Irradiation
D
RBC
RBC (M/ul) (Mean ± SEM)
Days post Irradiation
E
PLT
PLT (K/ul) (Mean ± SEM)
Days post Irradiation
NI
Veh
HGFs

**Figure 48. CBC profiles in H-ARS phase of lethal-irradiated mice treated with "HGFs" or "Veh" regimen.**

Mice in Figure 43 were re-grouped as the method of "HGFs" vs. "Veh" as previously described. n=52-121 mice per time-point per group. *$p<0.05$ comparing "HGFs" group (purple) to "Veh" group(red) at time-points as marked. Sasidhar Vemula acquired the data; Tong Wu did the analyses.

To summarize, HGF treatments do not increase WBC, NE, and LY counts at their nadirs. Instead, significant recovery of the hematopoietic system occurs around day 21 post-TBI, where HGFs increase all CBC parameters. G-CSF-containing regimens increase NE, RBC, and PLT counts at day 21; polypharmacy regimens increase WBC and NE at day 2, and increase RBC and PLT at day 21. These results support the use of HGFs in a lethal irradiation scenario, and are consistent with the increased survival of HGF-treated mice.

### 5.3.3. Peg-HGFs does not reduce peripheral blood cell apoptosis

Previous findings show that "combined" HGFs regimens treated mice had higher WBC and NE count at day 2 post-TBI and lower WBC count at day 4 than mice treated with individual HGFs, indicating that WBC and NE decrease more rapidly in mice receiving "combined" HGFs regimens (Figure 47). Comparable results were observed in the "with IL-11" vs. "no IL-11" analysis. The effect of HGF treatment on radiation-induced apoptosis was evaluated, as a potential mechanism for the observed CBC parameter changes. Peripheral blood was collected at day 2 post-TBI (24 hr post-HGFs injection). WBCs were stained with CD3 (T cells), Gr-1 (myeloid cells), Annexin-V (apoptosis marker), and 7-AAD (viability stain), and analyzed by flow cytometry. There was no statistical difference between HGFs treatment and Veh treatment; as expected, apoptosis in NI mice was lower than in IR mice, although not statistically different, in all cell types (Figure 49 A-F).

**Figure 49**

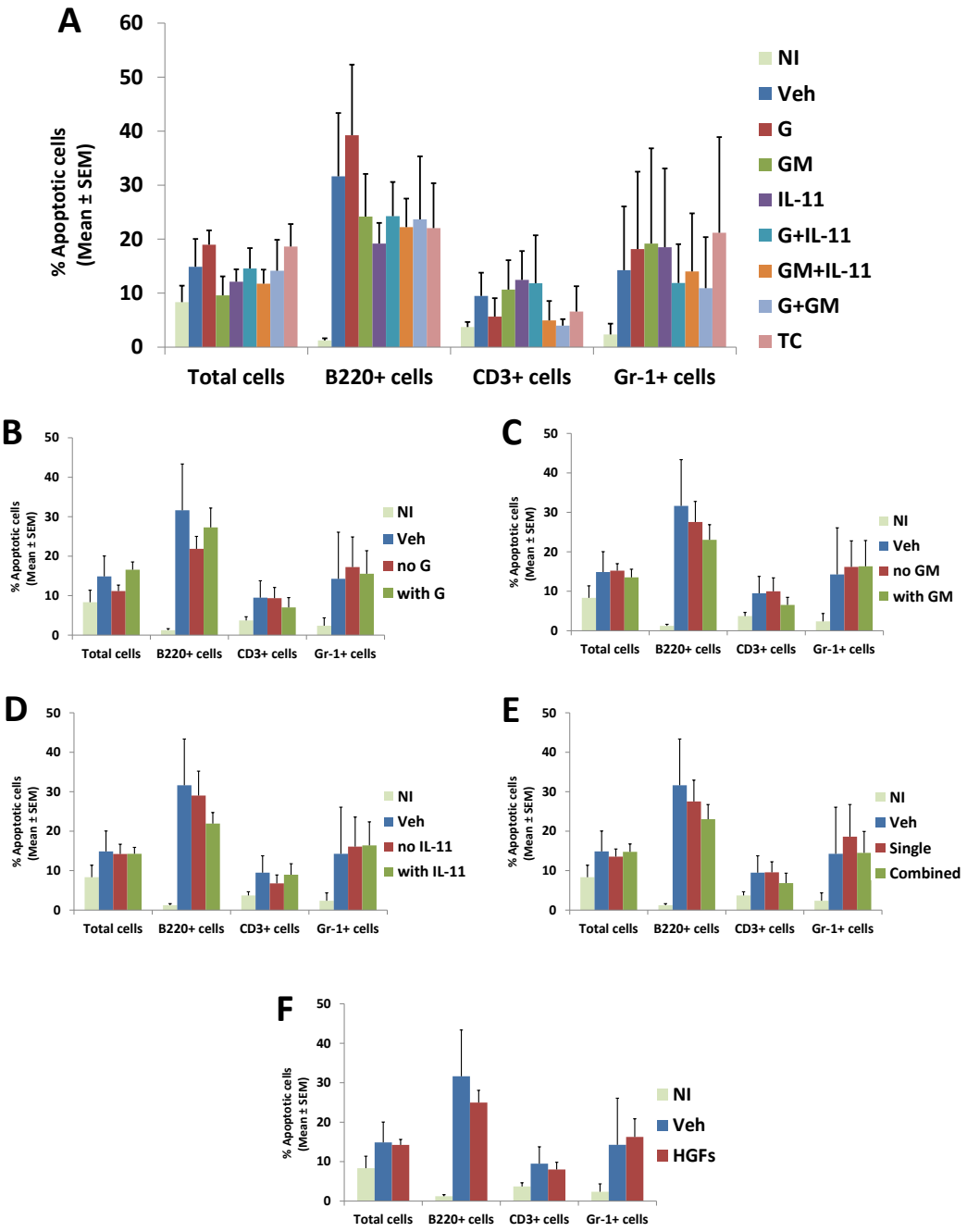
A
% Apoptotic cells (Mean ± SEM)
60
50
40
30
20
10
0
Total cells
B220+ cells
CD3+ cells
Gr-1+ cells
NI
Veh
G
GM
IL-11
G+IL-11
GM+IL-11
G+GM
TC
B
% Apoptotic cells (Mean ± SEM)
Total cells
B220+ cells
CD3+ cells
Gr-1+ cells
NI
Veh
no G
with G
C
% Apoptotic cells (Mean ± SEM)
Total cells
B220+ cells
CD3+ cells
Gr-1+ cells
NI
Veh
no GM
with GM
D
% Apoptotic cells (Mean ± SEM)
Total cells
B220+ cells
CD3+ cells
Gr-1+ cells
NI
Veh
no IL-11
with IL-11
E
% Apoptotic cells (Mean ± SEM)
Total cells
B220+ cells
CD3+ cells
Gr-1+ cells
NI
Veh
Single
Combined
F
% Apoptotic cells (Mean ± SEM)
Total cells
B220+ cells
CD3+ cells
Gr-1+ cells
NI
Veh
HGFs

**Figure 49. Apoptosis of peripheral white blood cells at day 2 post-TBI.**

Mice were exposed to 9.04 Gy TBI and injected with pegylated HGFs in single, double, or TC 24 hr later. Mice were euthanized on day 2 post-TBI and PB collected via cardiac puncture. PB cells were stained with CD3, B220, Gr-1, Annexin (apoptosis marker), and 7AAD (viability stain). Expression of Annexin-$V^+7AAD^-$ (apoptotic cells) was assessed on total white blood cells, $B220^+$ cells (B cells), $CD3^+$ cells (T cells) and $Gr\text{-}1^+$ (neutrophils) (panel A). Data were combined and analyzed in the methods as "with G" vs. "no G" (panel B), "with GM" vs. "no GM" (panel C), "with IL-11" vs. "no IL-11" (panel D), "single" vs. "combined" (panel E), "HGFs" vs. "Veh" (panel F). Bars represent mean ± SEM. n = 3-4 mice per group. P values of percentage of apoptotic cells between different groups were summarized in Table 8 (all p values > 0.05, only show the comparisons with p values <0.1). Artur Plett acquired the data; Tong Wu did the analyses.

### 5.3.4. Peg-HGFs increase HSPC count early post-TBI

To determine whether the enhanced survival and hematopoietic recovery of combined HGF regimens results from altered HSPC numbers in the bone marrow, bone marrow cellularity and HSPC numbers were analyzed up to 30 days post-TBI. Bone marrow inhibition persisted until day 21 post-TBI and recovered at day 30. At day 30, only G-CSF-treated mice had higher total bone marrow cell counts than IL-11 treated mice, there was no statistical difference between any irradiated groups and the NI control, and there was no statistical difference between any HGF-treated group and the Veh control. Up to day 21, all irradiated groups had significantly lower bone cell counts than the NI group and there was no significant difference between different irradiated groups (Figure 50 A). When analyzed in a manner similar to "with xx" vs. "no xx" in the CBC analysis, there was no statistical difference in total bone marrow cell numbers between any "with xx" and "no xx" groups at any time-points. (Figure 50 B-F). HPC numbers were slightly higher in mice receiving combined HGF regimens than in mice receiving a single HGF at day 5 and 7 post-TBI, although difference was not statistically significant (Figure 51).

In a similar study, HSC counts were phenotyped by flow cytometry post-TBI. No statistical significance in HSC ($Lin^{-}Sca^{+}CD150^{+}$) numbers was observed comparing HGF-treated groups with Veh group, or comparing different HGF-treated groups, at day 2, 7, 10 and 21 post-TBI (Figure 52). Combining all HGF-treated groups together, HSC counts were significantly increased in comparison with the Veh control at day 10 post-TBI (Figure 52 E). The differences between "single" and "combined", "with G" and "no

G", "with GM" and "no GM", "with IL-11" and "no IL-11" were minimal (Figure 52 F-I).

Competitive transplantation studies at day 5, 7, and 14 post-TBI with donor bone marrow cells from mice treated with different HGF regimens or the Veh control did not show statistical differences in chimerism rate up to 5 months post-transplantation (Figure 53 A-C). When analyzed as "HGFs" vs. "Veh", at four months post-transplantation in day-14 post-TBI transplant recipients, chimerism was significantly lower in the "HGFs" group than in the Veh control. There was no statistical difference between Veh control and "HGFs" group at any other time-points (Figure 53 D-F). When analyzed as "single" vs. "combined", the chimerism rate of "combined" group was only transiently higher than the "single" group at 1 month post-transplantation (Figure 53 I). There was no statistical difference among the "single", "combined" or Veh groups at day 5 or day 7 post-TBI (Figure 53 G & H). When analyzed in the pattern of "with G" vs. "no G" (Figure 53 J-L), "with GM" vs. "no GM" (Figure 53 M-O), and "with IL-11" vs. "no IL-11" (Figure 53 P-R), there was no significant difference between "with xx" and "no xx". In mice transplanted at day 14, both "with xx" and "no xx" groups had lower chimerism rates than Veh group.

### 5.3.5. Peg-HGFs do not extend lifespan of DEARE mice

Radiomitigator peg-HGFs successfully increased the survival rate of lethally-irradiated mice in H-ARS phase, whether the early administration can extend lifespan or alleviate DEARE symptoms in survivors is unknown. In the current study, mice surviving

**Figure 50**

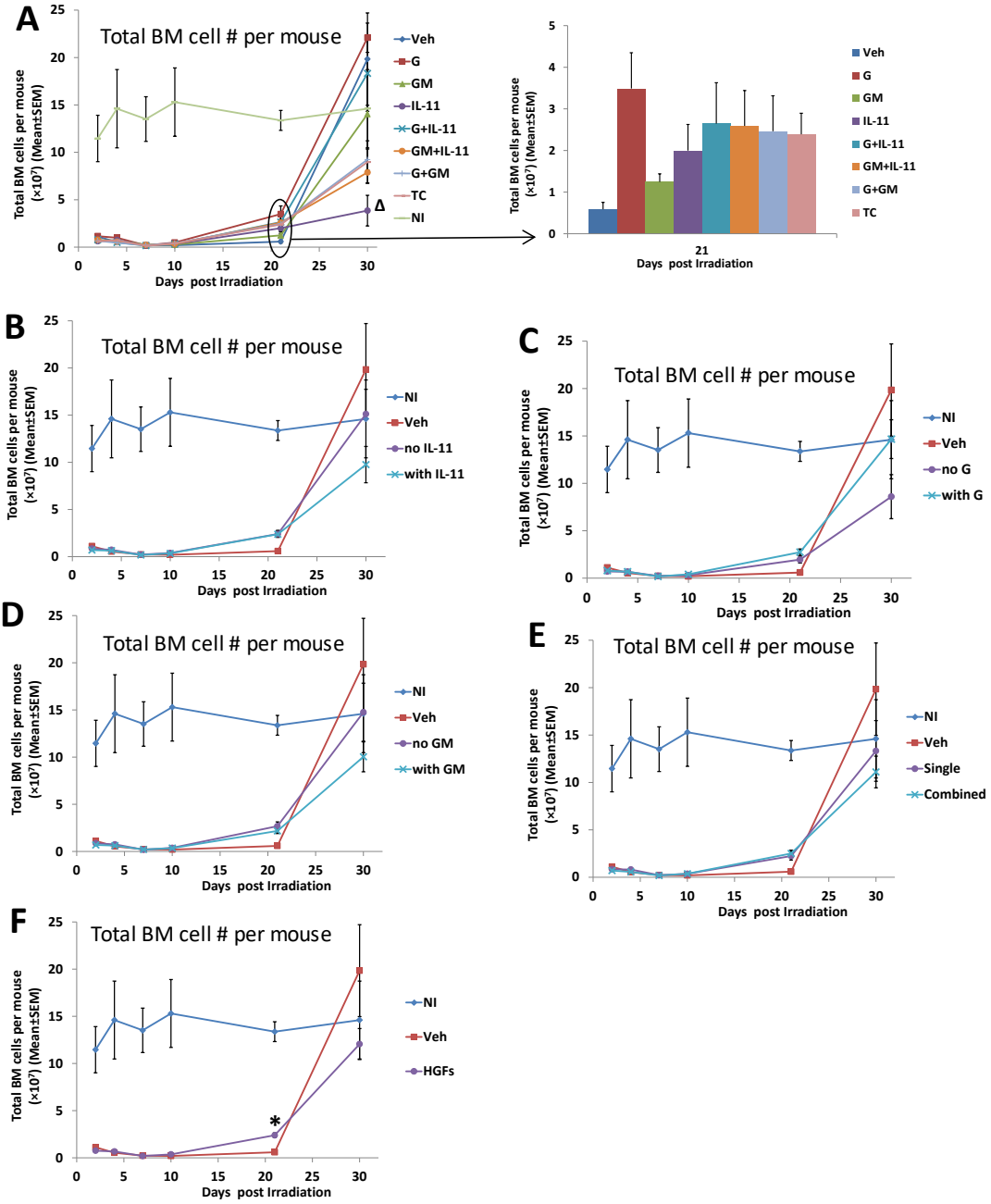
A
Total BM cell # per mouse
Total BM cells per mouse (×10⁷) (Mean±SEM)
Days post Irradiation
Veh
G
GM
IL-11
G+IL-11
GM+IL-11
G+GM
TC
NI
Δ
21
B
Total BM cell # per mouse
NI
Veh
no IL-11
with IL-11
C
Total BM cell # per mouse
NI
Veh
no G
with G
D
Total BM cell # per mouse
NI
Veh
no GM
with GM
E
Total BM cell # per mouse
NI
Veh
Single
Combined
F
Total BM cell # per mouse
NI
Veh
HGFs
*

**Figure 50. Total BM cell count in H-ARS phase of lethal-irradiated mice treated with pegylated HGFs.**

Mice were exposed to 9.04 Gy or 9.27 Gy TBI and treated with pegylated HGFs. Mice were sacrificed on day 2, 4, 7, 10, 21 and 30 post-TBI, and BM cells were flushed from femurs, tibias, pelvis, and humeri (8 bones), and counted for total BM cells per mouse (panel A, insert is the bar graph of day 21 data, no statistical difference among different irradiated groups). Data were combined and analyzed in the methods as "with IL-11" vs. "no IL-11" (panel B), "with G" vs. "no G" (panel C), "with GM" vs. "no GM" (panel D), "single" vs. "combined" (panel E), "HGFs" vs. "Veh" (panel F). Lines represent mean ± SEM. n=3-12 per group per time-point in panel A. Δ $p<0.05$ comparing IL-11 to G group in panel A. * $p<0.05$ comparing "HGFs" to "Veh" group in panel F. Artur Plett and Sasidhar Vemula acquired the data; Tong Wu did the analyses.

**Figure 51**

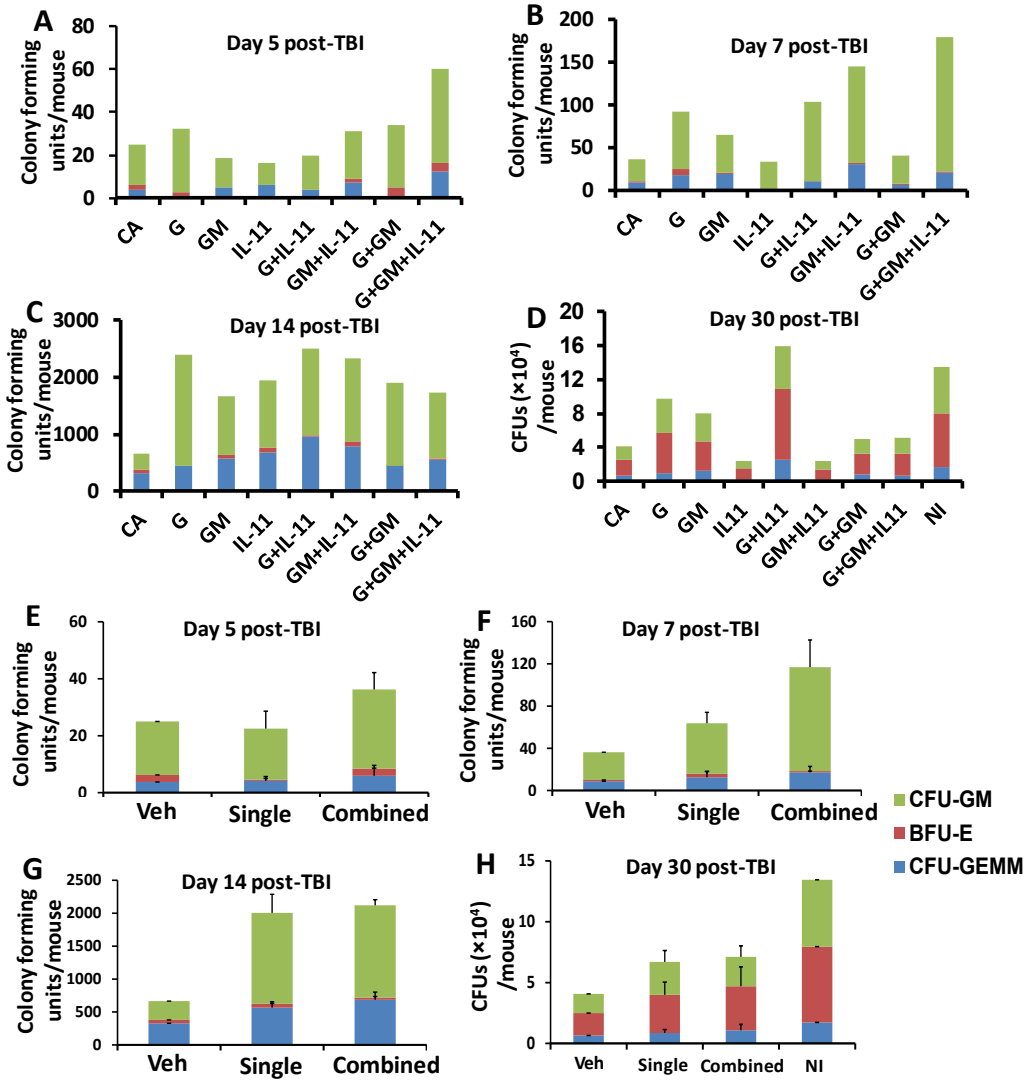
A
Day 5 post-TBI
Colony forming units/mouse
0
20
40
60
80
CA
G
GM
IL-11
G+IL-11
GM+IL-11
G+GM
G+GM+IL-11
B
Day 7 post-TBI
Colony forming units/mouse
0
50
100
150
200
CA
G
GM
IL-11
G+IL-11
GM+IL-11
G+GM
G+GM+IL-11
C
Day 14 post-TBI
Colony forming units/mouse
0
1000
2000
3000
CA
G
GM
IL-11
G+IL-11
GM+IL-11
G+GM
G+GM+IL-11
D
Day 30 post-TBI
CFUs (×10⁴) /mouse
0
4
8
12
16
20
CA
G
GM
IL11
G+IL11
GM+IL11
G+GM
G+GM+IL11
NI
E
Day 5 post-TBI
Colony forming units/mouse
0
20
40
60
Veh
Single
Combined
F
Day 7 post-TBI
Colony forming units/mouse
0
40
80
120
160
Veh
Single
Combined
CFU-GM
BFU-E
CFU-GEMM
G
Day 14 post-TBI
Colony forming units/mouse
0
500
1000
1500
2000
2500
Veh
Single
Combined
H
Day 30 post-TBI
CFUs (×10⁴) /mouse
0
5
10
15
Veh
Single
Combined
NI

**Figure 51. Recovery kinetics of HPCs in H-ARS phase of lethal-irradiated mice treated with pegylated HGFs.**

Mice were exposed to 9.27 Gy TBI and treated with pegylated HGFs as previously described. Four mice in each HGF treated group were euthanized on days 5, 7, 14 and 30 post-TBI separately and BM cells were flushed from femurs, tibias, pelvis, and humeri (8 bones). BM cells from the 4 mice were pooled and ¼ were used into colony assay. In panel A-D, n=1 in each group. Data were analyzed in method as "single" vs. "combined" (panel E-H). n=3-4 in "single" and "combined" group. Sasidhar Vemula acquired the data; Tong Wu did the analyses.

## Figure 52

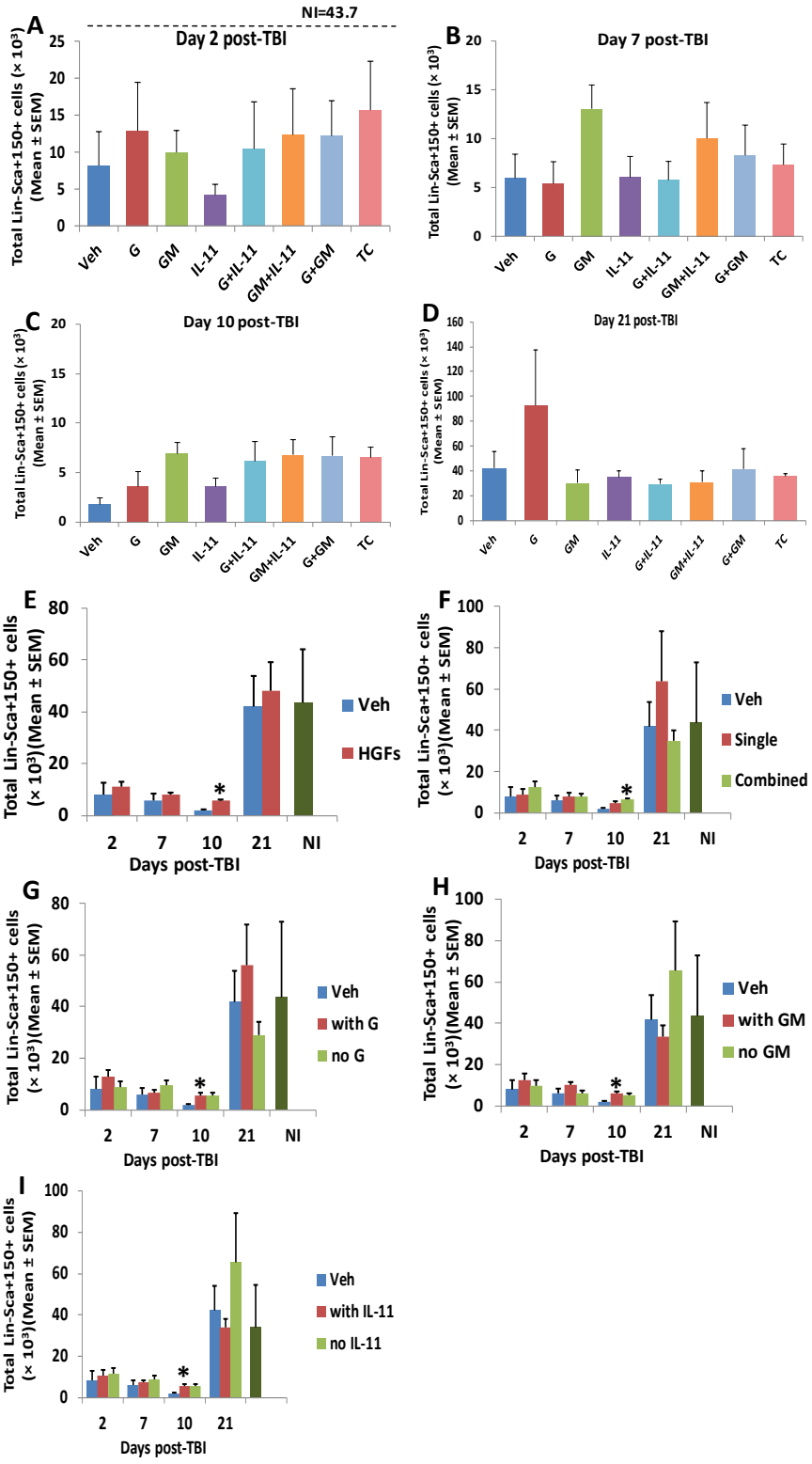
A
NI=43.7
Day 2 post-TBI
Total Lin-Sca+150+ cells (× 10³) (Mean ± SEM)
Veh
G
GM
IL-11
G+IL-11
GM+IL-11
G+GM
TC
B
Day 7 post-TBI
C
Day 10 post-TBI
D
Day 21 post-TBI
E
Total Lin-Sca+150+ cells (× 10³)(Mean ± SEM)
Veh
HGFs
2
7
10
21
NI
Days post-TBI
F
Single
Combined
G
with G
no G
H
with GM
no GM
I
with IL-11
no IL-11

**Figure 52. Recovery kinetics of hematopoietic stem cells in H-ARS phase of lethal-irradiated mice treated with pegylated HGFs.**

Mice were exposed to 9.04 Gy TBI and treated with pegylated HGFs as previously described. Mice were sacrificed on days 2, 7, 10 and 21 post-TBI. Flushed BM cells were stained with Lin markers, Sca-1 and CD150 antibodies, and then assessed by flow cytometry. The number of $Lin^{-}Sca\text{-}1^{+}CD150^{+}$ (LS $CD150^{+}$) cells per mouse were analyzed in each HGF treated group (panel A-D). Data were analyzed in methods as "HGFs" vs. "Veh" (panel E), "single" vs. "combined" (panel F), "with G" vs. "no G" (panel G), "with GM" vs. "no GM" (panel H) and "with IL-11" vs. "no IL-11" (panel I). Bars represent mean ± SEM. n=4 per group per time-point in panel A-D. *$p<0.05$ comparing to Veh group. Artur Plett acquired the data; Tong Wu did the analyses.

**Figure 53**

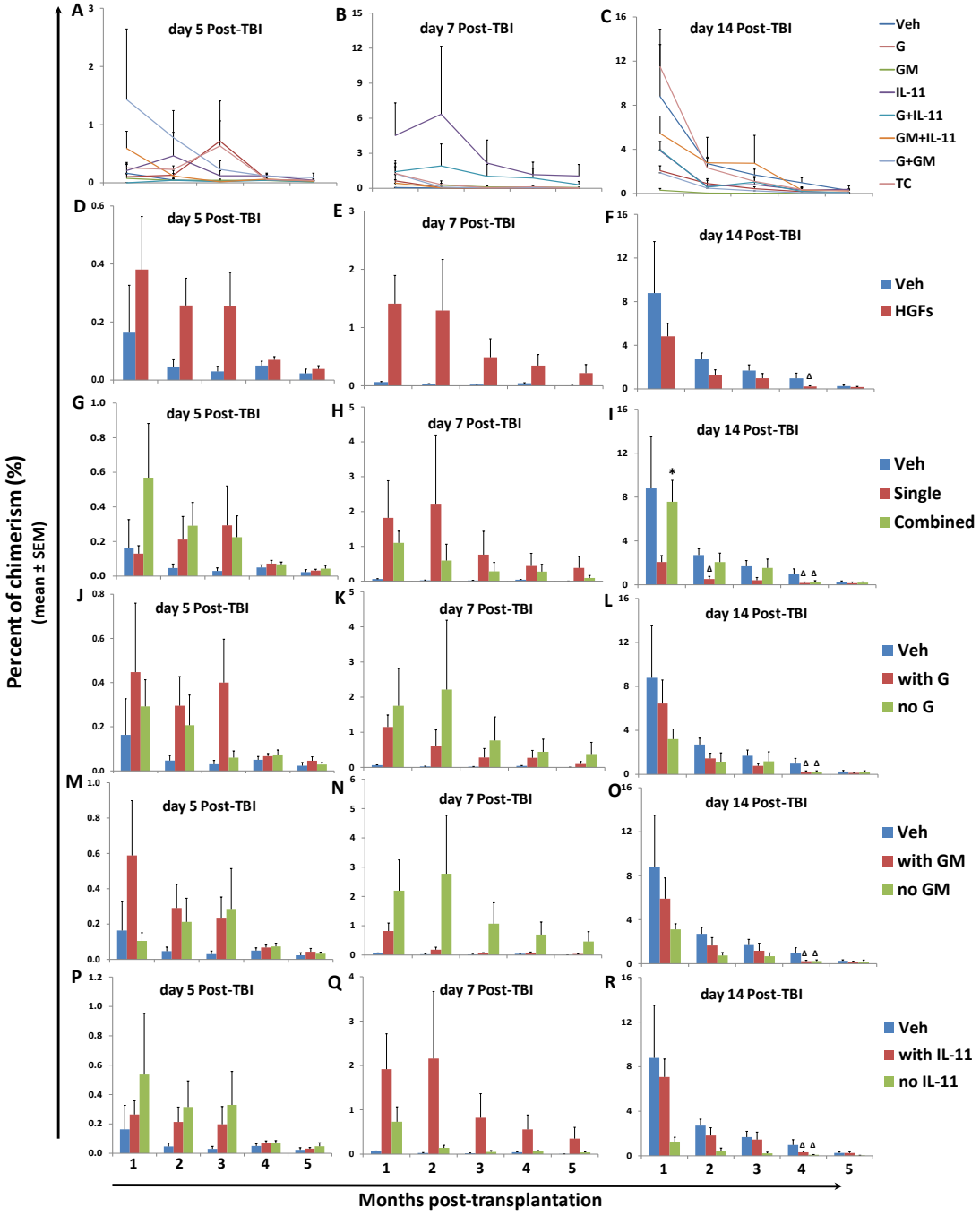
A
day 5 Post-TBI
B
day 7 Post-TBI
C
day 14 Post-TBI
Veh
G
GM
IL-11
G+IL-11
GM+IL-11
G+GM
TC
D
day 5 Post-TBI
E
day 7 Post-TBI
F
day 14 Post-TBI
Veh
HGFs
G
day 5 Post-TBI
H
day 7 Post-TBI
I
day 14 Post-TBI
Veh
Single
Combined
J
day 5 Post-TBI
K
day 7 Post-TBI
L
day 14 Post-TBI
Veh
with G
no G
M
day 5 Post-TBI
N
day 7 Post-TBI
O
day 14 Post-TBI
Veh
with GM
no GM
P
day 5 Post-TBI
Q
day 7 Post-TBI
R
day 14 Post-TBI
Veh
with IL-11
no IL-11
Percent of chimerism (%)
(mean ± SEM)
1 2 3 4 5
Months post-transplantation

**Figure 53. BM competitive transplantation for donor cells at H-ARS phase from lethal-irradiated mice treated with pegylated HGFs.**

Mice were exposed to 9.27 Gy TBI and treated with pegylated HGFs as previously described. Four mice in each HGF treated group were euthanized on day 5, 7 and 14 post-TBI and BM cells were flushed from femurs, tibias, pelvis, and humeri (8 bones). BM cells from the 4 mice were pooled and pooled sample then was split into 4 equal aliquots. Three aliquots were used for transplantation into 3 recipient mice (one aliquot per recipient, the rest one aliquot was used in colony assay as describe in Figure 51). For transplantation, the whole bone marrow fraction, regardless of the number of cells, was transplanted via the retro orbital sinus into one irradiated (5.5 + 5.5 Gy) recipient BoyJ mouse, along with $2 \times 10^5$ whole bone marrow competitor cells. Donor chimerism rates of peripheral white blood cells were tracked monthly till to 5 months post-transplantation. Data were presented as line graphs in each HGF treated group (panel A-C) and bar graphs in "HGFs" vs. "Veh" (panel D-F), "single" vs. "combined" (panel G-I), "with G" vs. "no G" (panel J-L), "with GM" vs. "no GM"(panel M-O) and "with IL-11" vs. "no IL-11" (panel P-R). Lines and bars represent mean ± SEM. n=3 per group per time-point in panel A-C. $\Delta$ $p<0.05$ comparing to Veh group. *$p<0.05$ comparing to "single" group in panel I. Artur Plett acquired the data; Tong Wu did the analyses.

the H-ARS stage (day 30 post-TBI; 4 months of age) were transferred to the RBMD study and observed until 24 months post-TBI. Mice were euthanized when severely moribund or were sacrificed at scheduled time-points for DEARE studies. Kaplan-Meier lifespan analyses were performed in SPSS. Consistent with earlier reports [310, 311], a significantly shortened lifespan was observed in Veh-treated irradiated mice in comparison with NI mice. No significant difference was observed between HGF-treated and Veh-treated groups, with the exception of the G+GM group (significantly lower than Veh group), and the differences between different HGF-treated groups were minimal (Figure 54 A and Table 11). When analyzed as "HGFs" vs. "Veh", "with IL-11" vs. "no IL-11", and "single" vs. "combined", there was no difference between "HGFs" vs. "Veh", "with IL-11" vs. "no IL-11", and "single" vs. "combined" groups (Figure 54 B-D); "no IL-11" group had significantly lower survival rate than Veh group, whereas "with IL-11"group had not (Figure 54 C).

### 5.3.6. Peg-HGFs do not alleviate body weight loss in DEARE mice

Pegylated HGFs do not increase survival rate of DEARE mice, whether HGFs at 24 hr post-TBI impact DEARE markers is still unknown. Weight loss is one of the significant markers of DEARE [40]. The body weights at 6 and 12 months post-TBI were measured. There was no statistical difference between different irradiated groups either at 6 or at 12 months post-TBI, no matter what treatments mice received (Figure 55 A). When analyzed as "HGFs" vs. "Veh", "single" vs. "combined", or "with IL-11" vs. "no IL-11", the "HGFs" and Veh mice had lower body weights than NI mice at 12 months post-TBI (Figure 55 B), but there was no difference in "single" vs. "combined" and "with

**Figure 54**

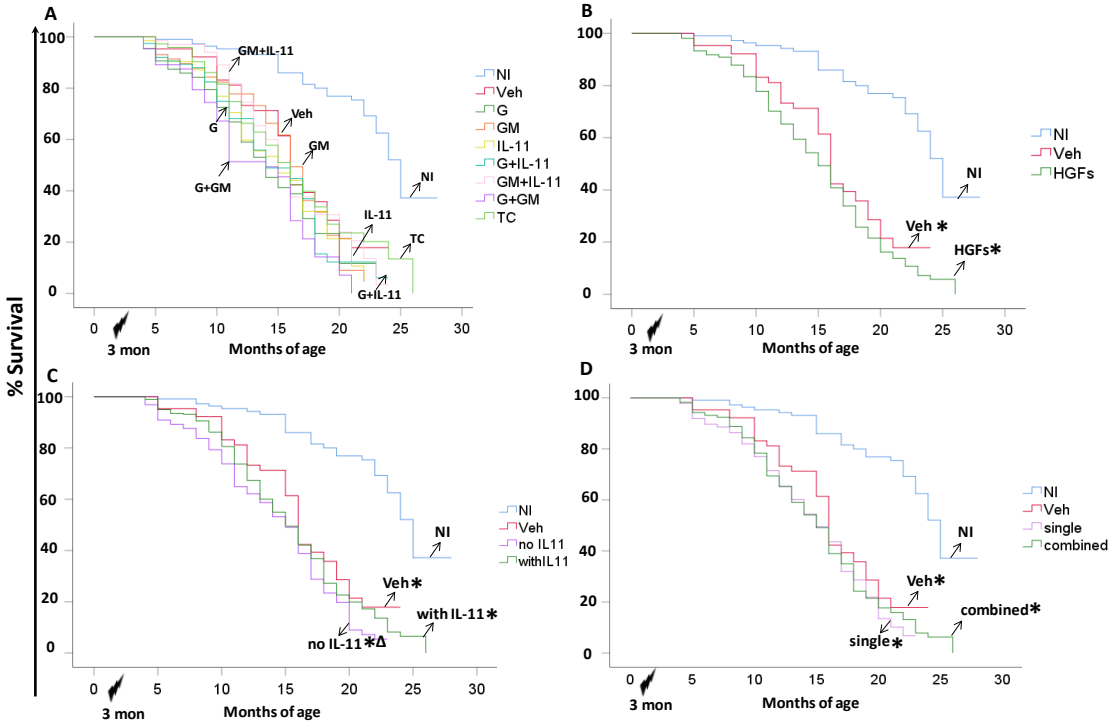
A
B
C
D
% Survival
100
80
60
40
20
0
0
5
10
15
20
25
30
3 mon
Months of age
GM+IL-11
Veh
G
GM
G+GM
NI
IL-11
TC
G+IL-11
NI
Veh
G
GM
IL-11
G+IL-11
GM+IL-11
G+GM
TC
NI
Veh
HGFs
Veh *
HGFs*
NI
Veh
no IL11
withIL11
Veh*
with IL-11*
no IL-11*Δ
NI
Veh
single
combined
Veh*
combined*
single*

**Figure 54. Long-term survival of day 30 survived mice treated with pegylated HGFs.**

Mice were exposed to 9.27 Gy TBI and treated with pegylated HGFs as previously described. Mice survived over day 30 post-TBI were transferred to RBMD study for long-term survival monitor until the end of study (24 months post-TBI). The survival mice were recorded when found dead, or were euthanized when severely moribund, or scheduled time-point sacrifices. Survival is shown as Kaplan-Meier curve. n=60-109 mice in each group (panel A). P value of comparisons for panel A were summarized in Table 11. Survival data were analyzed in the manner of "HGFs" vs. "Veh" (panel B), "with IL-11" vs. "no IL-11" (panel C), "single" vs. "combined" (panel D). "with G" vs. "no G" and "with GM" vs. "no GM" comparisons were not shown since no statistical difference between the two types of comparison. *$p<0.05$ comparing to NI group in panel B-D. $\Delta p<0.05$ comparing to Veh group in panel C. Artur Plett and Sasidhar Vemula acquired the data; Tong Wu did the analyses.

**Table 11. Comparisons of long-term survival of lethal-irradiated mice treated with pegylated HGFs.**

| Treatment | G | G+GM | G+IL-11 | GM | GM+IL-11 | IL-11 | NI | TC | Veh |
|---|---|---|---|---|---|---|---|---|---|
| G | | NS | NS | NS | NS | NS | <.0001 | NS | NS |
| G+GM | NS | | NS | 0.029 | 0.023 | NS | <.0001 | 0.033 | 0.01 |
| G+IL-11 | NS | NS | | NS | NS | NS | <.0001 | NS | NS |
| GM | NS | 0.029 | NS | | NS | NS | <.0001 | NS | NS |
| GM+IL-11 | NS | 0.023 | NS | NS | | NS | <.0001 | NS | NS |
| IL-11 | NS | NS | NS | NS | NS | | <.0001 | NS | NS |
| NI | <.0001 | <.0001 | <.0001 | <.0001 | <.0001 | <.0001 | | <.0001 | <.0001 |
| TC | NS | 0.033 | NS | NS | NS | NS | <.0001 | | NS |
| Veh | NS | 0.01 | NS | NS | NS | NS | <.0001 | NS | |

Numbers in the table are p values of comparisons. NS: Not significant

**Figure 55**

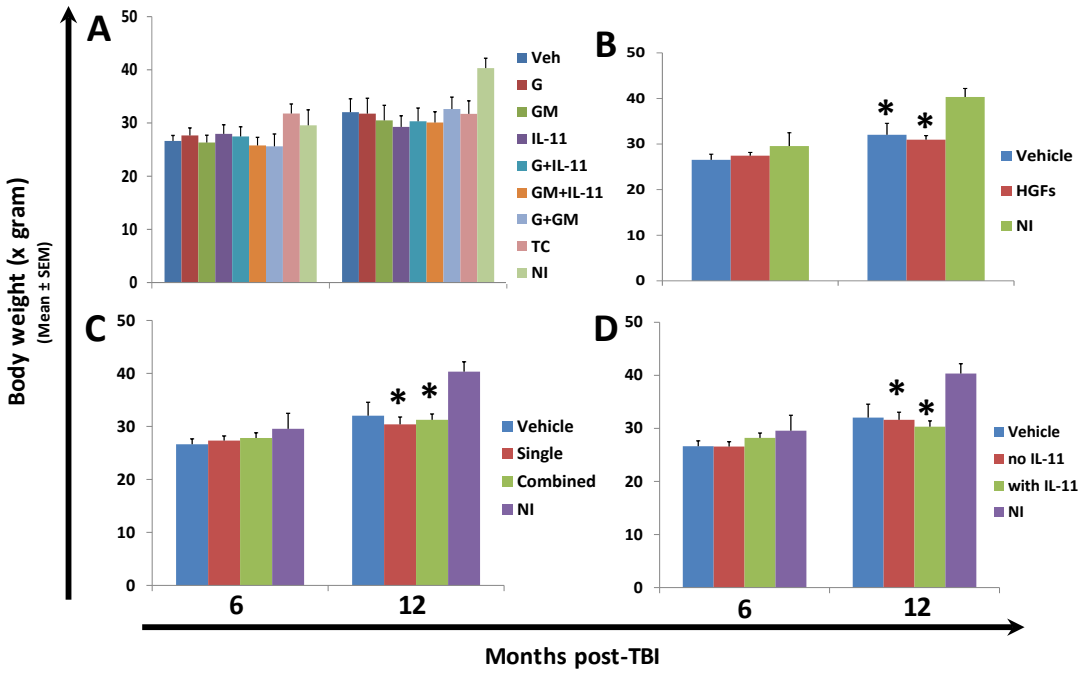
A
B
C
D
Body weight (x gram)
(Mean ± SEM)
Veh
G
GM
IL-11
G+IL-11
GM+IL-11
G+GM
TC
NI
Vehicle
HGFs
NI
Vehicle
Single
Combined
NI
Vehicle
no IL-11
with IL-11
NI
6
12
Months post-TBI

**Figure 55. Body weight in DEARE phase of lethal-irradiated mice treated with pegylated HGFs.**

Mice were exposed to 9.04 Gy TBI and treated with pegylated HGFs as previously described. Body weights were assessed at 6 and 12 months post-TBI (panel A). Data were analyzed by “HGFs” vs. “Veh” (panel B), “single” vs. “combined” (panel C), “with IL-11” vs. “no IL-11” (panel D) as previously described. Bars represent mean ± SEM. n= 5-8 mice for each group in panel A. *$p<0.05$ comparing to NI group. Artur Plett acquired the data; Tong Wu did the analyses.

IL-11" vs. "no IL-11" comparisons. (Figure 55 C & D). This indicates that HGF administration 24 hr post-TBI does not alleviate weight loss in DEARE mice.

### 5.3.7. Peg-HGFs do not reverse myeloid skewing in DEARE mice

Hematopoiesis is severely defective in DEARE mice following exposure to lethal radiation at young age [40, 147]. Dr. Orschell's laboratory has already proved that HGFs treatment at 24 hr post-TBI accelerates hematopoietic recovery at the H-ARS phase, whether it would alleviate defective long-term hematopoiesis is not clear. The CBC changes at 6 and 12 months post-TBI in the survivor mice of lethal radiation were investigated. At 12 months post-TBI, WBC, LY, and RBC were significantly decreased in most irradiated mice in comparison with age-matched NI controls. No significant difference in NE number was observed between irradiated and NI control mice at 6 or 12 months post-TBI. Myeloid skewing was apparent 12 months post-TBI in most irradiated groups, but no significant difference between HGF-treated and Veh-treated mice was observed. (Figure 56 A-G). When analyzed as "HGFs" vs. "Veh", "single" vs. "combined", or "with xx" vs. "no xx", all the significant differences were from the comparisons to NI group, there was no statistical difference between "HGFs" and "Veh", "single" and "combined", or "with xx" and "no xx" (Figure 56 H-AI).

### 5.3.8. Peg-HGFs do not increase HSC number and function in DEARE mice

While HGF treatment does not alleviate peripheral blood defects in DEARE mice, the possibility of beneficial effects in HSPC cannot be excluded. Mice were irradiated at 12 weeks LD90/30 and received HGFs treatments 24 hr post-TBI as previously

described. Survivors were sacrificed 6 and 12 months post-TBI and bone marrow cellularity, LSK cell number, and LSK $CD150^{+}CD48^{-}$ cell number were assessed by flow cytometry. There was no statistical difference between different HGF groups and Veh control (Figure 57 A-C). Consistent with the previous report, LSK and LSK $CD150^{+}CD48^{-}$ cell numbers were generally higher at 12 months post-TBI than at 6 months [40]. When analyzed as "HGFs" vs. "Veh", "single" vs. "combined", or "with xx" vs. "no xx", there was no statistical difference in these comparisons (Figure 57 D-O).

To test HSC function, transplantation studies were done at 12 months post-TBI. One hundred and fifty KSL $CD150^{+}$ cells were transplanted into the congenic recipients and recipients were sacrificed 6 months post-transplantation. The donor chimerism rates and donor-derived lineage reconstitution of peripheral blood $Gr\text{-}1^{+}$ NE, $CD8^{+}$ T cells, $CD4^{+}$ T cells, and $B220^{+}$ B cells were measured by flow cytometry. KSL $CD150^{+}$ cells from irradiated mice had significantly lower repopulation capacity than the cells from age-matched NI controls. There was no significant difference between the Veh control and HGF-treated mice (Figure 58 A) or "HGFs" vs. Veh (Figure 58 C), or "with IL-11" vs. "no IL-11" (Figure 58 E), or "single" vs. "combined" (Figure 58 G). As previously observed [147], recipients of KSL $CD150^{+}$ cells from irradiated donors exhibited imbalanced lymphoid-myeloid reconstitution. Myeloid ($Gr\text{-}1^{+}$) percentages were higher in all irradiated groups than in the NI control, explaining the myeloid skewing observed in the peripheral blood. No HGF treatment improved this HSC defect (Figure 58 B, D, F & H). HGF treatment 24 hr after TBI, therefore does not alleviate HSC deficiencies despite improving survival in the H-ARS stage.

**Figure 56**

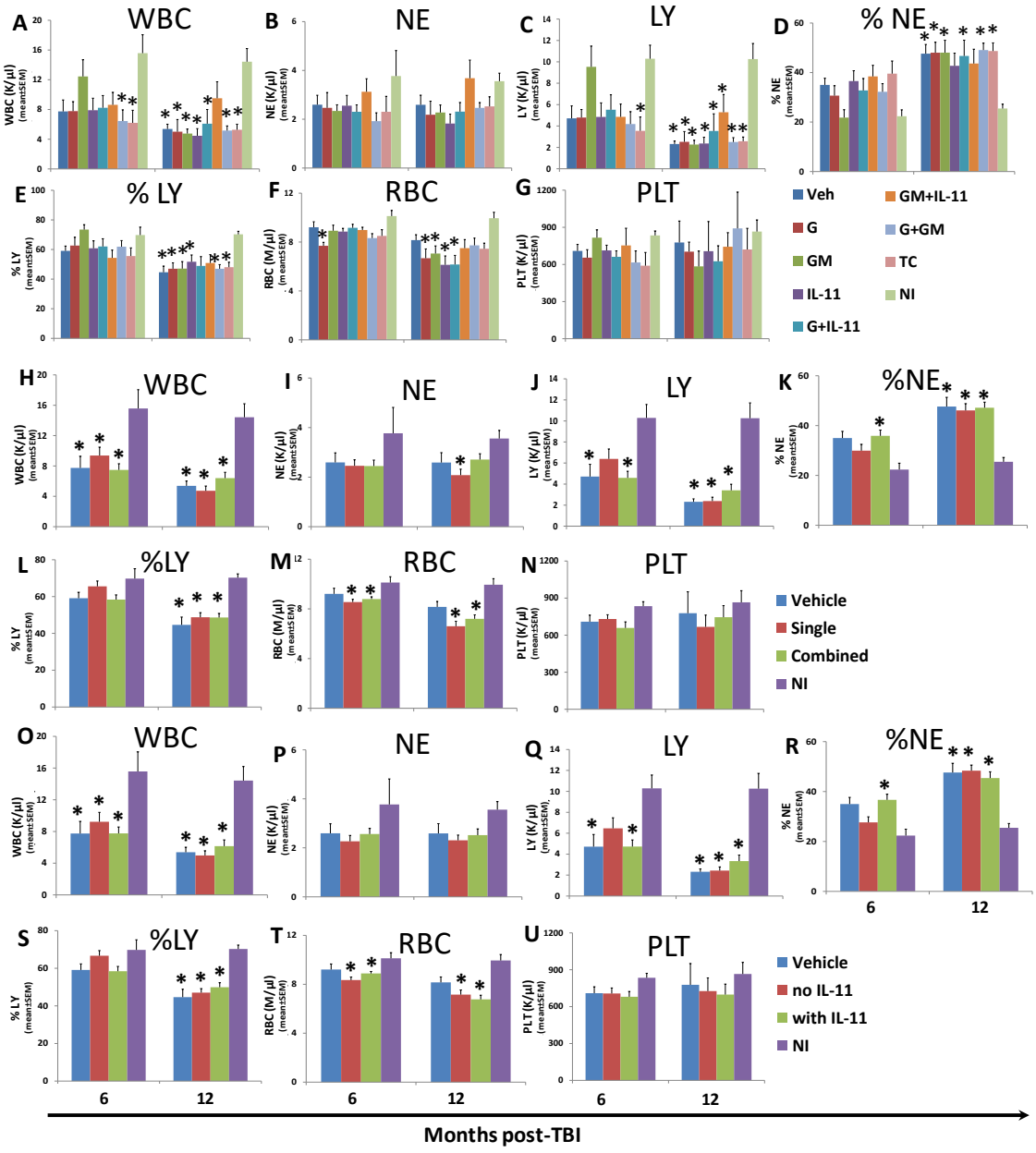
A
WBC
WBC (K/μl) (mean±SEM)
B
NE
NE (K/μl) (mean±SEM)
C
LY
LY (K/μl) (mean±SEM)
D
% NE
% NE (mean±SEM)
E
% LY
% LY (mean±SEM)
F
RBC
RBC (M/μl) (mean±SEM)
G
PLT
PLT (K/μl) (mean±SEM)
Veh
G
GM
IL-11
G+IL-11
GM+IL-11
G+GM
TC
NI
H
WBC
I
NE
J
LY
K
%NE
L
%LY
M
RBC
N
PLT
Vehicle
Single
Combined
NI
O
WBC
P
NE
Q
LY
R
%NE
S
%LY
T
RBC
U
PLT
Vehicle
no IL-11
with IL-11
NI
6
12
Months post-TBI

**Figure 56 continue**

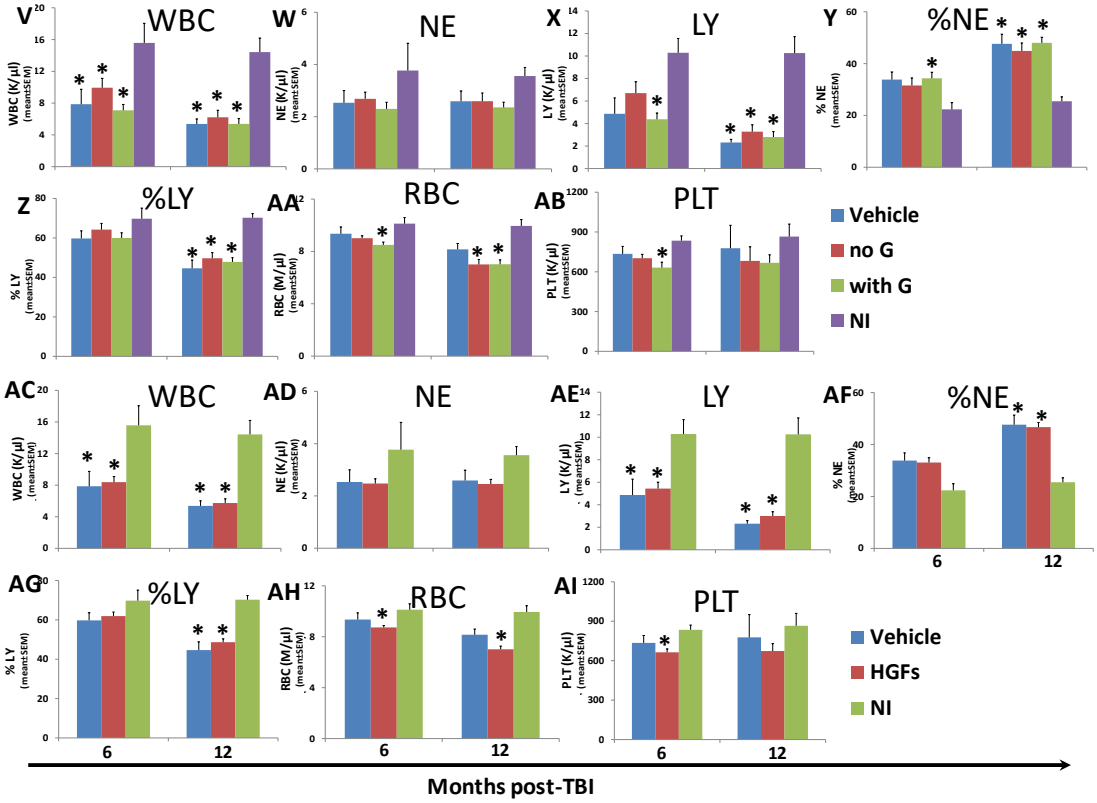

**Figure 56. CBC profiles in DEARE phase of lethal-irradiated mice treated with pegylated HGFs.**

Mice were exposed to 9.04 Gy TBI and treated with pegylated HGFs as previously described. Survived mice were tail-bled at 6 and 12 months post-TBI and assessed for CBC parameters including WBC (panel A), NE (panel B), LY (panel C), %NE (panel D), %LY (panel E), RBC (panel F), and PLT (panel G). Data were analyzed in the method as "single" vs. "combined" (panel H-N), "with IL-11" vs. "no IL-11" (panel O-U), "with G" vs. "no G" (panel V-AB), "HGFs" vs. "Veh" (panel AC-AI). Bars represent mean ± SEM. n=5-8 mice per group in panel A-G. *$p<0.05$ comparing to NI group. Artur Plett acquired the data; Tong Wu did the analyses.

**Figure 57**

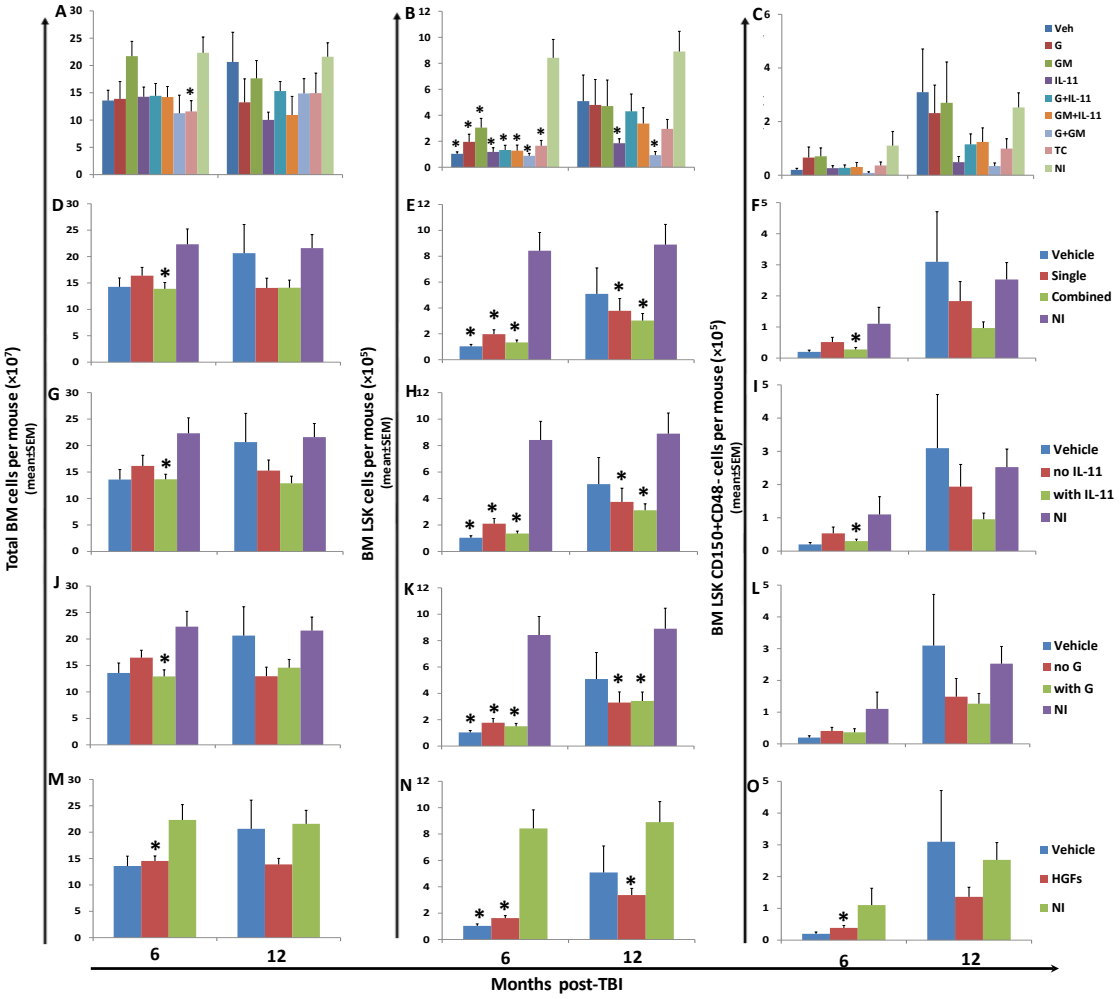
A
B
C
D
E
F
G
H
I
J
K
L
M
N
O
Total BM cells per mouse (×10⁷) (mean±SEM)
BM LSK cells per mouse (×10⁵) (mean±SEM)
BM LSK CD150+CD48- cells per mouse (×10⁵) (mean±SEM)
Veh
G
GM
IL-11
G+IL-11
GM+IL-11
G+GM
TC
NI
Vehicle
Single
Combined
NI
Vehicle
no IL-11
with IL-11
NI
Vehicle
no G
with G
NI
Vehicle
HGFs
NI
6
12
Months post-TBI

**Figure 57. BM cellularity and HSPC in DEARE phase of lethal-irradiated mice treated with pegylated HGFs.**

Mice were exposed to 9.04 Gy TBI and treated with pegylated HGFs as previously described. Mice were sacrificed at 6 and 12 months post-TBI. BM cells were flushed from pelvis, femur and tibia; red blood cells were lysed and nucleated cells were enumerated. BM cells were stained with Lin markers, c-Kit, Sca-1, CD48 and CD150 antibodies, and then assessed by flow cytometry. Cellularity and HSPC numbers were analyzed in each HGF treated group (panel A-C). Data were analyzed in the method as "single" vs. "combined" (panel D-F), "with IL-11" vs. "no IL-11" (panel G-I), "with G" vs. "no G" (panel J-L), "HGFs" vs. "Veh" (panel M-O). "with GM" vs. "no GM" plots were not shown since there was no difference between groups and the plot was similar to others. Bars represent mean ± SEM. n=5-8 per group per time-point in panel A-C. *$p<0.05$ comparing to NI group. Artur Plett acquired the data; Tong Wu did the analyses.

**Figure 58**

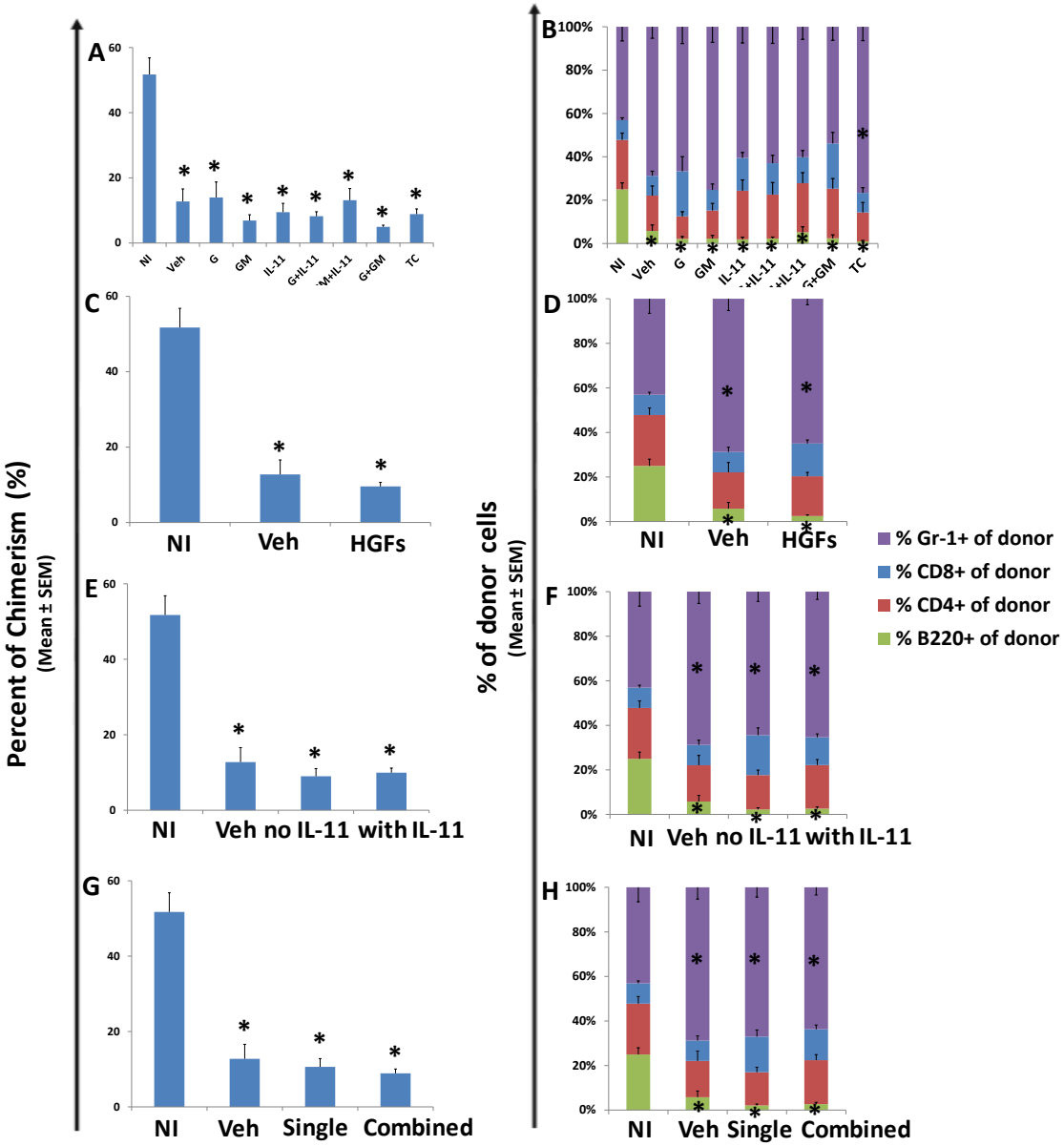
Percent of Chimerism (%)
(Mean ± SEM)
% of donor cells
(Mean ± SEM)
A
B
C
D
E
F
G
H
NI
Veh
G
GM
IL-11
G+IL-11
GM+IL-11
G+GM
TC
HGFs
Veh no IL-11
with IL-11
Single
Combined
% Gr-1+ of donor
% CD8+ of donor
% CD4+ of donor
% B220+ of donor

**Figure 58. BM competitive transplantation for donor cells at DEARE phase from lethal-irradiated mice treated with pegylated HGFs.**

Mice were exposed to 9.27 Gy TBI and treated with pegylated HGFs as previously described. Survivors were euthanized at 12 months post-TBI and $3\times10^5$ of donor whole bone marrow cells were transplanted intravenously along with $2\times10^5$ congenic competitor cells into lethal-irradiated (5.5 + 5.5 Gy) congenic recipients. Recipient mice were sacrificed at 6 months post-transplantation. The donor chimerism and lineage reconstitution were evaluated by flow cytometry as described in the Materials and Methods. Data were analyzed in each HGF treated group separately (panel A & B) and in the method as "HGFs" vs. "Veh" (panel C & D), "with IL-11" vs. "no IL-11" (panel E & F), and "single" vs. "combined" (panel G & H). Bars present as mean ± SEM. n=6-9 per group in panel A & B. *$p<0.05$ comparing to NI group. Artur Plett acquired the data; Tong Wu did the analyses.

### 5.3.9. Peg-HGFs enhance early thymic recovery post-TBI but do not alleviate thymic involution in DEARE mice

Peg-HGFs treatment 24 hr post-TBI increases LY count at day 21 (Figure 48). LY HPE is a physiological reaction to radiation-induced lymphopenia, consisting of G-CSF-driven immune reconstitution [346]. HPE is the predominant source of T cells after thymic involution [347]. The potential of HGFs treatment to promote thymic regeneration and hence boost de novo T cell generation were investigated. First, the main components of peripheral blood cells at day 21 post-TBI in selected HGFs-treated groups were assessed by flow cytometry. Consistent with previous reports, the stimulating effect of peg-G-CSF was most prominent in Gr-$1^+$ neutrophils [74, 203, 348]. Additionally, peg-G-CSF treated mice had higher $B220^+$ B cell count, $CD4^+$ and $CD8^+$ T cell counts compared with Veh-treated mice at day 21 post-TBI. Combining peg-HGFs did not further increase cell numbers (Figure 59).

Twelve w/o mice were irradiated LD90/30 and treated with peg-HGFs 24 hr post-TBI as previously described. Thymic weight and cellularity were measured at different time-points up to 12 months post-TBI. At all time-points (day 2, 7, 10, and 12 months post-TBI), thymus weight and cellularity were lower in irradiated mice in comparison with NI mice, no matter what treatments received. At day 21, peg-HGFs-treated mice had higher thymic weight and cellularity than Veh mice, although ANOVA analysis of all irradiated groups revealed no statistical difference (Figure 60 A & B). This trend was significant when combined all HGFs-treated groups together as a “HGFs” group and compared it to Veh group. The HGFs-treated mice had significantly higher thymus

weight and cellularity than the Veh-treated mice at day 21 (Figure 60 C & D). At 12 months post-TBI, the peg-HGFs-treated mice had slightly lower thymic weight and cellularity than Veh-treated mice, though the difference was not significant. When analyzed as "single" vs. "combined", "with G" vs. "no G", "with GM" vs. "no GM", and "with IL-11" vs. "no IL-11" as previously described, there was no statistical difference between any of these two groups at any time-point (Figure 60 E-L).

When analyzed the phenotype of thymocyte subpopulations, since there was no significant difference between different HGF groups at each time-point and the trends were similar to the thymus cellularity plot, for the easy of readers, the plots of each HGF comparison were not presented but only the combined analysis plots were presented as in the method of "HGFs" vs. "Veh" (Figure 61 A-H) and "single" vs. "combined" (Figure 61 I-P). The rest comparisons including "with G" vs. "no G", "with GM" vs. "no GM", and "with IL-11" vs. "no IL-11" were not presented because the similarity to the plots of "single" vs. "combined". In the plots of "HGFs" vs. "Veh" (Figure 61 A-H), DP and DN3 percentages in irradiated mice were decreased at day 2 compared to NI mice, and the percentages of $CD4^+$, $CD8^+$, DN, and DN1, DN2, and DN4 groups were relatively increased or not change. Thymi of irradiated mice began to recover with DN3 level restored to normal by day 7 and DP by day 10 respectively. No significant difference of subpopulation distribution between HGFs-treated mice and Veh-treated mice was observed at day 2, 7 or 10, consistent with the thymocyte number changes at these time-points (Figure 60 C & D). At day 21, the HGFs-treated mice had a higher percentage of DP cells than Veh-treated mice, which was significant when all HGFs-treated mice were

combined together for analysis (Figure 61 B). DN2 and DN3 followed similar trends, with no statistical difference (Figure 61 F & G). Again, at 12 months post-IR, the percentages of DP, DN2, and DN3 were lower in HGFs-treated mice than Veh mice, though the difference was not statistically significant (Figure 61 A-H). When analyzed "single" vs. "combined" as previously described, there was no statistical difference at any time-point (Figure 61 I-P). HGFs treatment therefore promotes early thymic recovery post-TBI but does not alleviate thymic involution in DEARE mice. Polypharmacy strategy does not further enhance the effect on thymic recovery.

### 5.3.10. Adding lisinopril to the TC regimen further alleviates irradiation damage

Combining all three peg-HGFs (peg-G-CSF + peg-GM-CSF + peg-IL-11, TC) results in the highest day 30 survival rate (Figure 42), and evidence suggests that ACEI is an effective radiomitigator when used alone or in combination with HGFs [93, 101, 103]. Here, radiomitigating potential of lisinopril (Liso) was evaluated on the TC-treated H-ARS mouse model. TC was administrated as previously described 24 hr post-TBI and Liso was added to drinking water (60 mg/L) from day 7-30 post-TBI. Some mice were euthanized on day 10 to evaluate bone marrow HSC content, HPC number, HSC function, and BM cytokines. Brains were examined on day 10 for petechiae as ACE inhibition is a known mitigator of brain hemorrhage post-TBI [103]. CBC parameters were analyzed at day 10 and 20. Surviving mice over day 30 were transferred to the RBMD study and monitored for long-term survival.

**Figure 59**

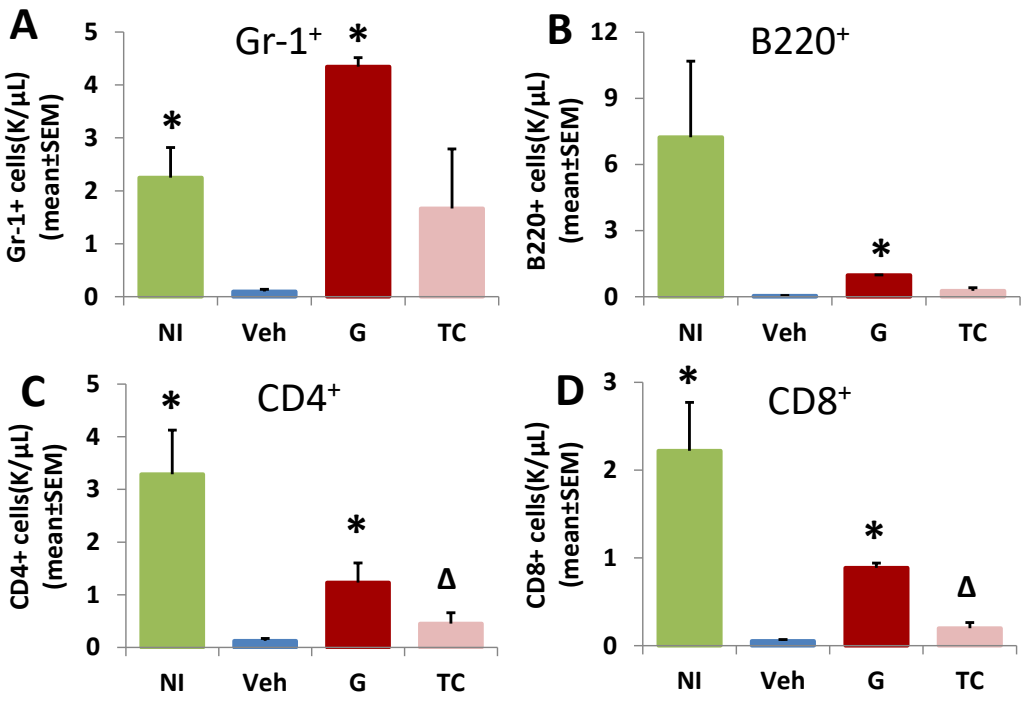
A
Gr-1+
Gr-1+ cells(K/µL) (mean±SEM)
5
4
3
2
1
0
*
*
NI
Veh
G
TC
B
B220+
B220+ cells(K/µL) (mean±SEM)
12
9
6
3
0
*
NI
Veh
G
TC
C
CD4+
CD4+ cells(K/µL) (mean±SEM)
5
4
3
2
1
0
*
*
Δ
NI
Veh
G
TC
D
CD8+
CD8+ cells(K/µL) (mean±SEM)
3
2
1
0
*
*
Δ
NI
Veh
G
TC

**Figure 59. WBC phenotype at day 21 post-TBI of mice treated with G-CSF or TC.** Mice were exposed to 8.72 Gy TBI and treated with pegylated G-CSF or TC at 24 hr post-TBI. Mice were tail-bled at day 21 post-TBI and the expression levels of Gr-1, B220, CD4 and CD8 on peripheral nucleated cells were assessed by flow cytometry. Cell number was the product of WBC number in CBC analysis at day 21 and the percentage of each population acquired by flow cytometry. Bars present mean ± SEM. n=2-4 per group. *$p<0.05$ comparing to Veh group; $\Delta p<0.05$ comparing to NI group.

**Figure 60**

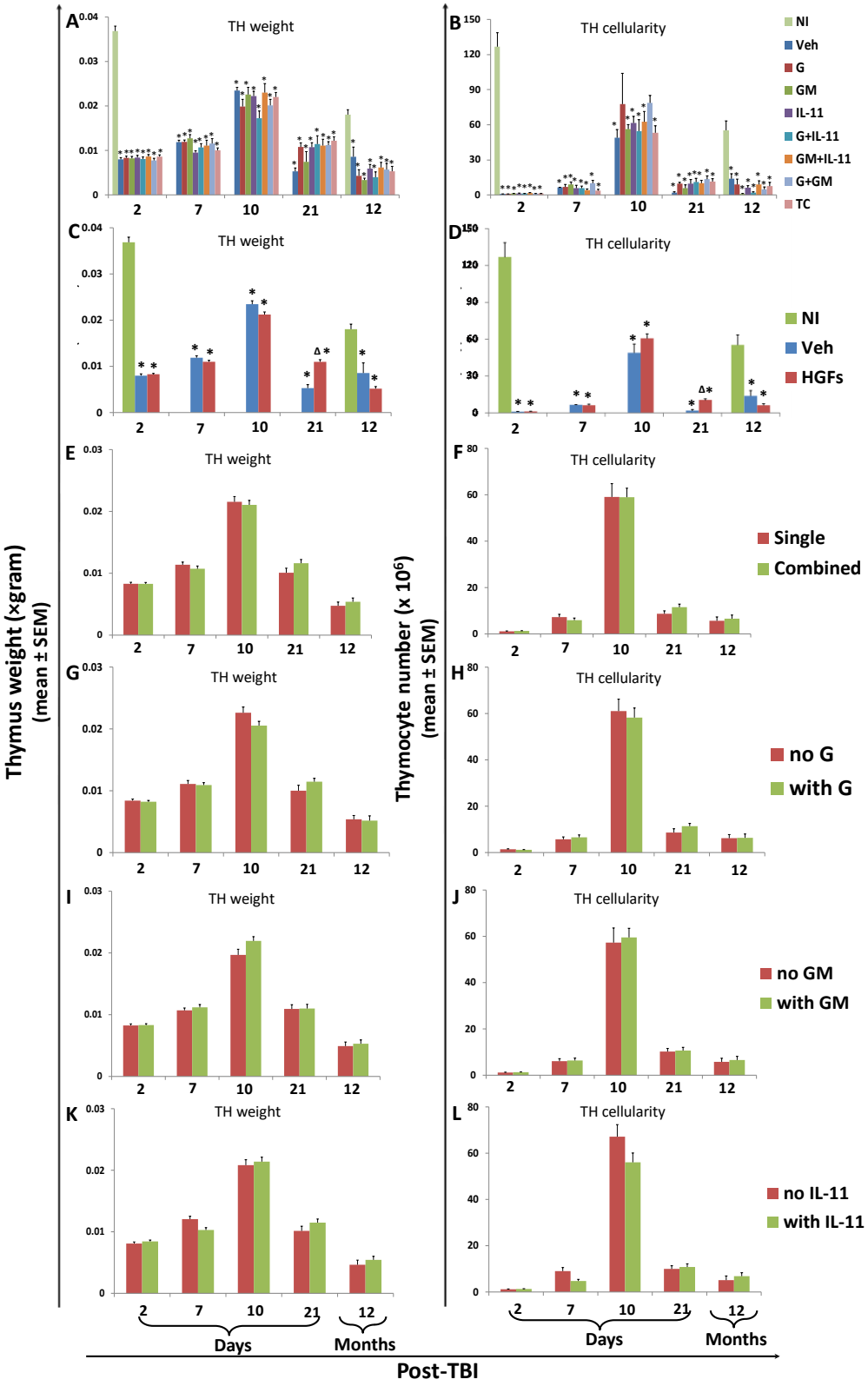
A
TH weight
B
TH cellularity
NI
Veh
G
GM
IL-11
G+IL-11
GM+IL-11
G+GM
TC
C
TH weight
D
TH cellularity
NI
Veh
HGFs
E
TH weight
F
TH cellularity
Single
Combined
G
TH weight
H
TH cellularity
no G
with G
I
TH weight
J
TH cellularity
no GM
with GM
K
TH weight
L
TH cellularity
no IL-11
with IL-11
Thymus weight (×gram)
(mean ± SEM)
Thymocyte number (x 10⁶)
(mean ± SEM)
2
7
10
21
12
Days
Months
Post-TBI

**Figure 60. Thymus weight and cellularity of lethal-irradiated mice treated with pegylated HGFs.**

Mice were exposed to 8.72, 9.04 or 9.27 Gy TBI and treated with pegylated HGFs as previously described. Thymus weight and cellularity were analyzed at day 2, 7, 10, 21 and 12 months post-TBI (panel A & B). Data were analyzed in the method as "HGFs" vs. "Veh" (panel C & D), "single" vs. "combined" (panel E & F), "with G" vs. "no G" (panel G & H), "with GM" vs. "no GM" (panel I & J) and "with IL-11" vs. "no IL-11" (panel K & L). Bars present mean ± SEM. n=3-21 per group per time-point in panel A & B. *$p<0.05$ comparing to NI group; $\Delta p<0.05$ comparing to Veh group.

**Figure 61**

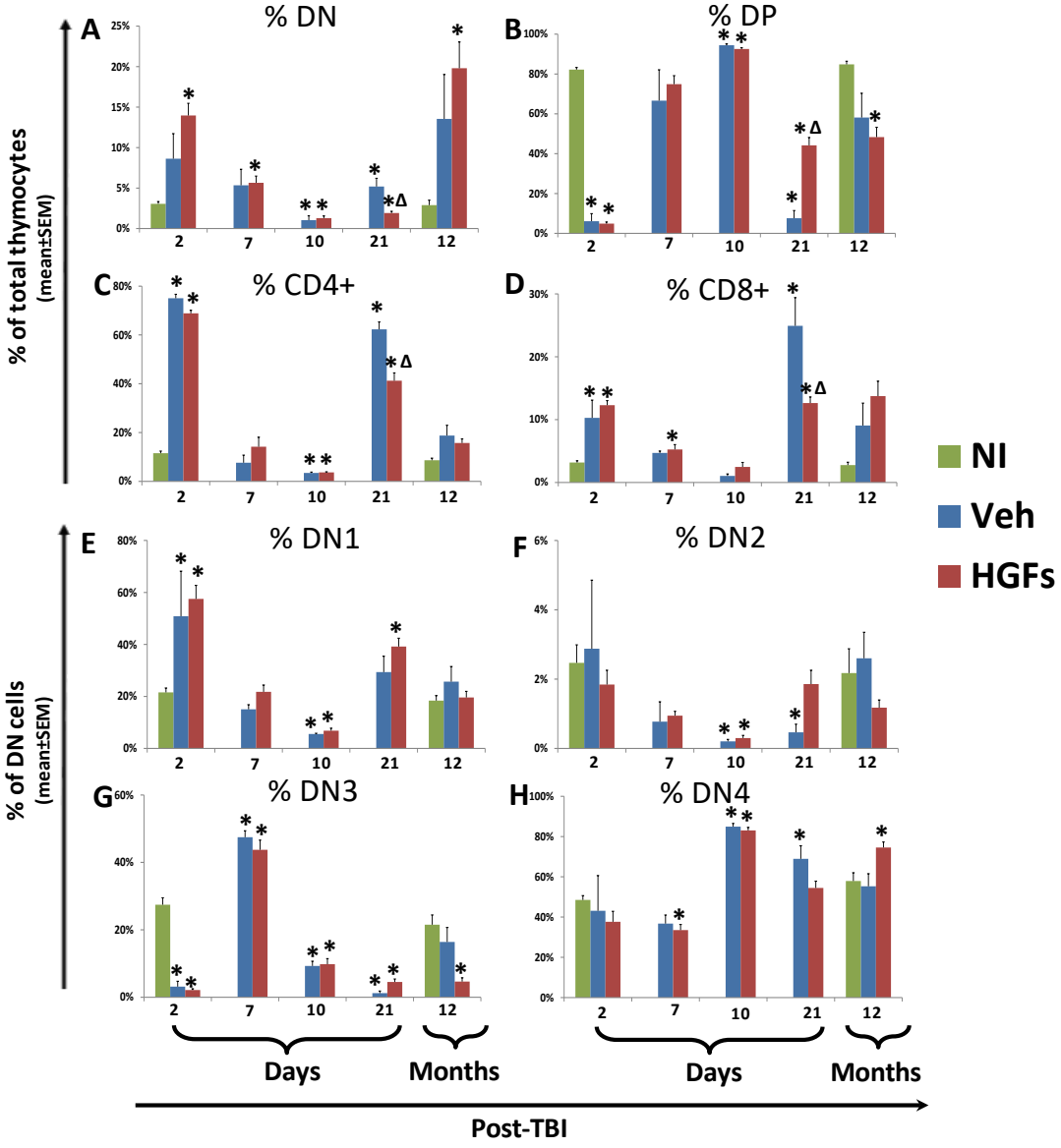
A
% DN
B
% DP
C
% CD4+
D
% CD8+
E
% DN1
F
% DN2
G
% DN3
H
% DN4
% of total thymocytes (mean±SEM)
% of DN cells (mean±SEM)
NI
Veh
HGFs
Days
Months
Post-TBI

**Figure 61 continue**

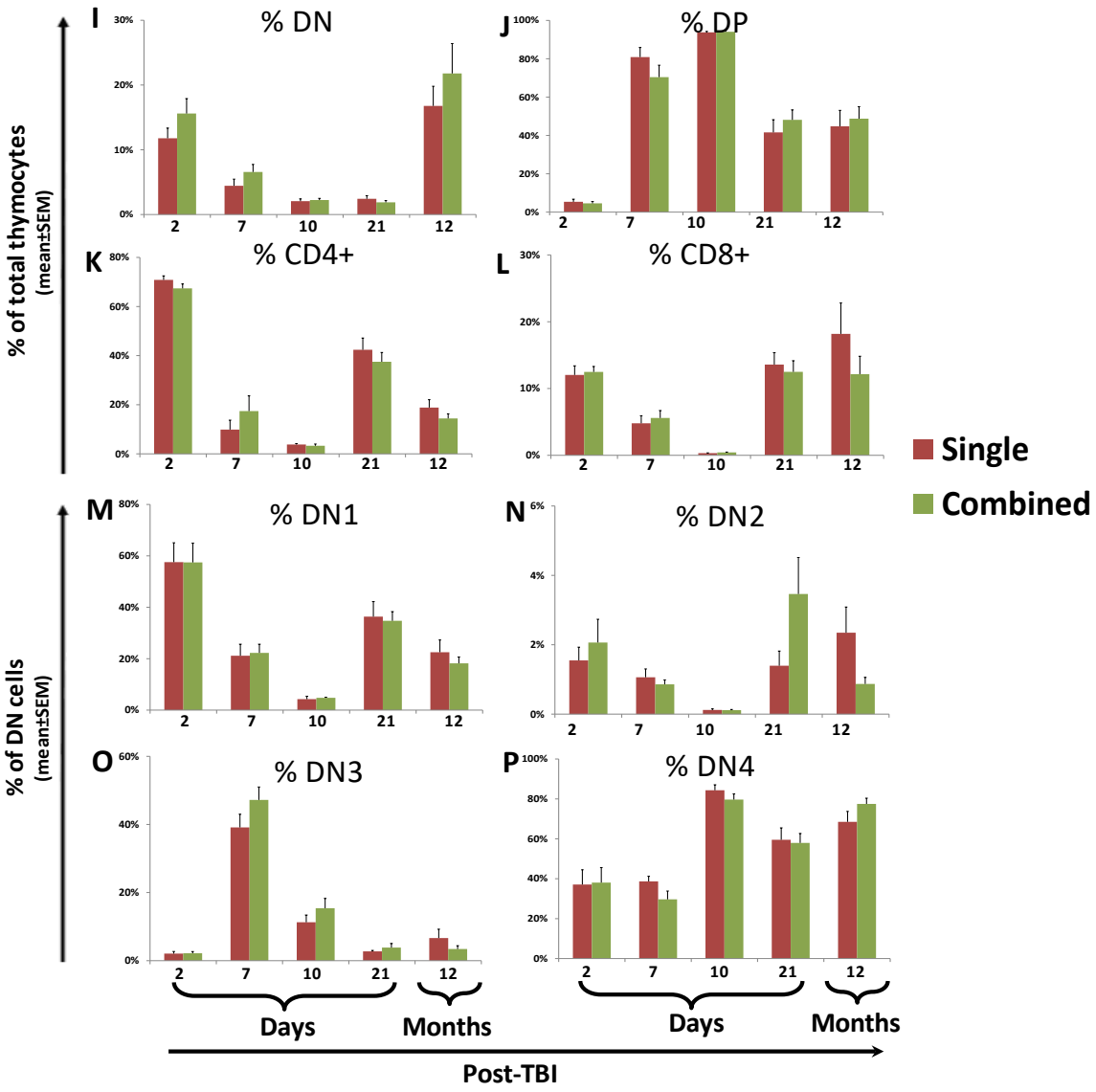

**Figure 61. Thymus subpopulation of lethal-irradiated mice treated with pegylated HGFs.**

Mice were exposed to 8.72, 9.04 or 9.27 Gy TBI and treated with pegylated HGFs as previously described. At day 2, 7, 10, 21 and 12 months post-TBI, thymocytes were stained with CD4, CD8, CD44 and CD25 antibodies and percentages of different thymocyte subpopulations were assessed by flow cytometry as described in Materials and Methods. Plots of each HGF comparison and the comparisons of "with G" vs. "no G", "with GM" vs. "no GM", and "with IL-11" vs. "no IL-11" were not presented because no significant difference was observed; and for the easy of readers, only "HGFs" vs. "Veh" (panel A-H) and "single" vs. "combined" (panel I-P) plots were presented. Bars present mean ± SEM. n=16-28 in NI group, 3-8 in Veh group, and 14-45 in HGFs group, per time-point, respectively. *$p<0.05$ comparing to NI group. $\Delta p<0.05$ comparing to Veh group.

All treatment groups [Liso, TC, and TC + lisinopril (TC+L)] significantly increased the day 30 survival rate compared with the Veh control, and this effect was most pronounced TC+L group. There was no significant difference between TC and Liso treatments alone (Figure 62 A). Interestingly, TC+L significantly increased survival rate in female mice but not in male mice (Figure 62 B & C).

Complete blood count analysis at day 20 revealed that TC+L group had higher NE numbers than TC group and Veh group only in females. Female TC+L-treated and TC-treated mice had higher RBC counts than Veh-treated mice, though the difference between TC+L and TC treatment was not significant. Male mice followed the similar trends but did not reach statistical significance (Figure 63). At day 10, there was no significant difference in total bone marrow cell number or HSC number when comparing irradiated mice to Veh mice, regardless of treatments received or gender of mice. However, cell cycle analysis revealed that female TC+L-treated mice had significantly more quiescent HSCs than males (Figure 64). The colony-forming ability of cells from TC+L-treated mice was slightly increased in comparison with cells from TC or Veh-treated mice, but this difference was not statistically significant and there were no sex differences in colony-forming ability between TC+L and TC-treated mice (Figure 65).

TC+L-treated mice had lower levels of the pro-inflammatory cytokines RANTES (in bone marrow supernatant) and IL-3 (in plasma) than Veh-treated mice. No significant difference between TC- and TC+L-treated mice, or between females and males, was observed (Figure 66). No difference in other cytokines was observed. TC+L-treated mice

had fewer petechiae in the brain than Veh-treated mice, whereas TC-treated mice were similar to Veh controls (Figure 67). Reduced brain hemorrhage in TC+L-treated mice correlates with the enhanced day 30 survival rate and is also consistent with its higher PLT level than TC-treated and Veh controls at day 10, although the difference is not statistically significant (Figure 63). The impact of TC+L on thymic recovery was also evaluated at day 10 (Figure 68). No statistically-significant differences were observed between TC, TC+L, and Veh treatment indicating that Liso is not involved in thymic recovery at day 10. The only sex difference observed was the higher percentage of DN1 in males in the Veh and TC+L groups (Figure 68).

H-ARS survivors were transferred to the RBMD study. The KM estimation of long-term survival showed no statistical difference among groups regardless of treatment, and the sex difference observed in the H-ARS study was not maintained long-term. (Figure 69). Complete blood count analysis at 6 months post-TBI showed lower WBC and LY numbers in irradiated mice but no statistical difference between Veh, TC and TC+L treated mice. No sex differences were found in CBC parameters at 6 months post-TBI (Figure 70). Cells were flushed from the bone marrow and stained for SLAM-LSK including cell cycle analysis at 6 months post-TBI. Since there was no male mouse in Veh group and only 1 female mouse in Veh group at 6 months post-TBI time-point, ANOVA test was not available; and t-test comparisons between TC and TC+L group and between male and female in the two groups was used instead. There was no significant difference in bone marrow cell number, HSC number and HSC cell cycle status between TC and TC+L groups. Male mice had higher total bone marrow cell count than female

mice in TC-treated group, and female mice had higher Lin- cells than male mice in the TC+L-treated group. There were no sex differences in HPC (LSK) and HSC (SLAM-LSK) cells (Figure 71). To assess HSC function, $0.3\times10^6$ donor cells from TC- or TC+L-treated mice were injected into each recipient with $0.2\times10^6$ competitor cells, and recipients were monitored for donor chimerism monthly up to 4 months post-transplantation. Although the average chimerism rates were higher in TC+L group than TC group, no statistically significant difference was observed when males and females were combined (Figure 72 A). Separately, however, the TC+L male mice had significantly higher donor chimerism rates than TC+L female mice, and also higher than male and female TC-treated mice. There were no sex differences in TC-treated mice (Figure 72 B).

In summary, TC+L further slightly increased day 30 survival rate than TC (not significant, Figure 62) mice and this was consistent with no significant difference between TC and TC+L groups in hematopoietic recovery markers (CBC parameters, BM cell numbers, HSC/HPC numbers, etc.). Dr. Orschell's laboratory also found a sex difference where TC+L regimen was especially effective in female population which might relate to the higher CBC parameters and less HSC in proliferation status than male mice, although the causal relationship has not been verified. Same as peg-HGFs, adding lisinopril to the mitigator regimens did not help to alleviate the DEARE effect.

## 5.4. Discussion

Impacts of different peg-HGFs regimens on survival and hematopoiesis were investigated from the H-ARS to the DEARE stage. The increased day 30

**Figure 62**

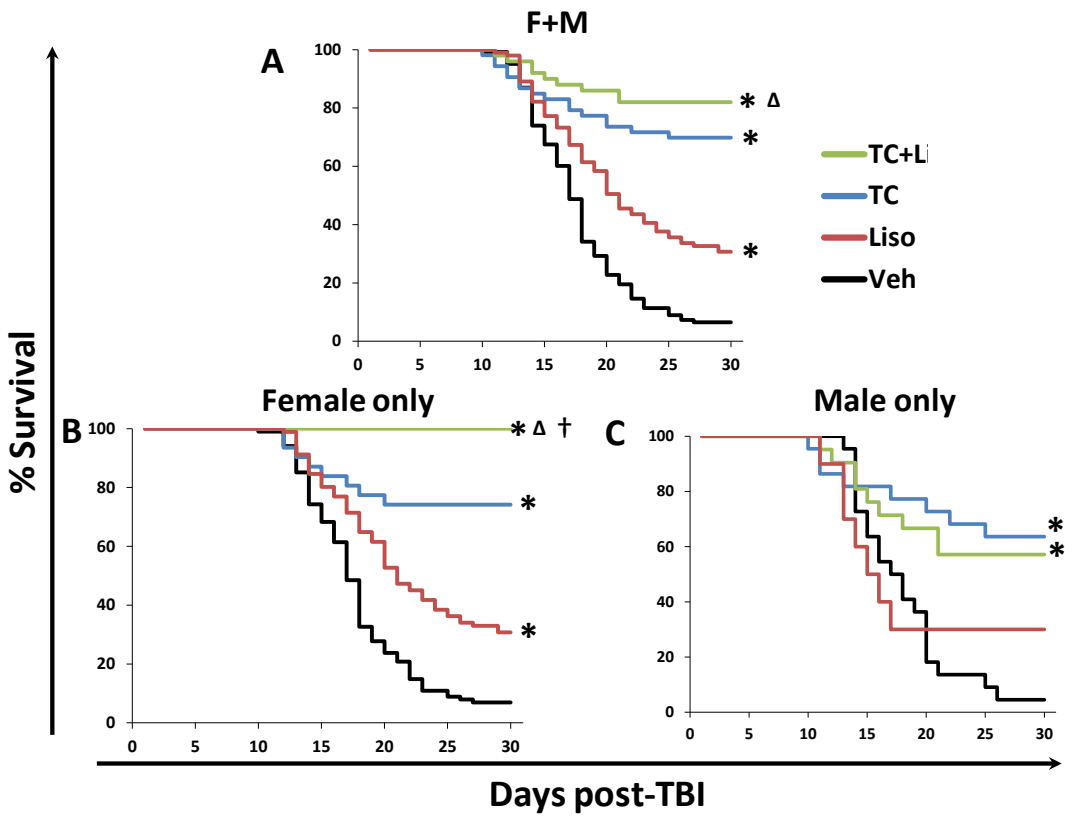

**Figure 62. Thirty-day survival of lethal-irradiated mice treated with TC, Lisinopril or TC+L.**

Mice were exposed to 9.04 Gy TBI and treated with TC or Veh 24 hr later. Lisinopril was dissolved into water for ad libitum at days 7-30 post-TBI. Thirty-day survival is shown as Kaplan-Meier curves. Total n=50-123 mice in each group (panel A). Female n=29-101 mice in each group (panel B). Male n=10-22 mice in each group (panel C). *$p<0.05$ comparing to Veh; $\Delta p<0.05$ comparing to Liso; †$p<0.05$ comparing to TC. Sasidhar Vemula and Tong Wu acquired the data; Tong Wu did the analyses.

**Figure 63**

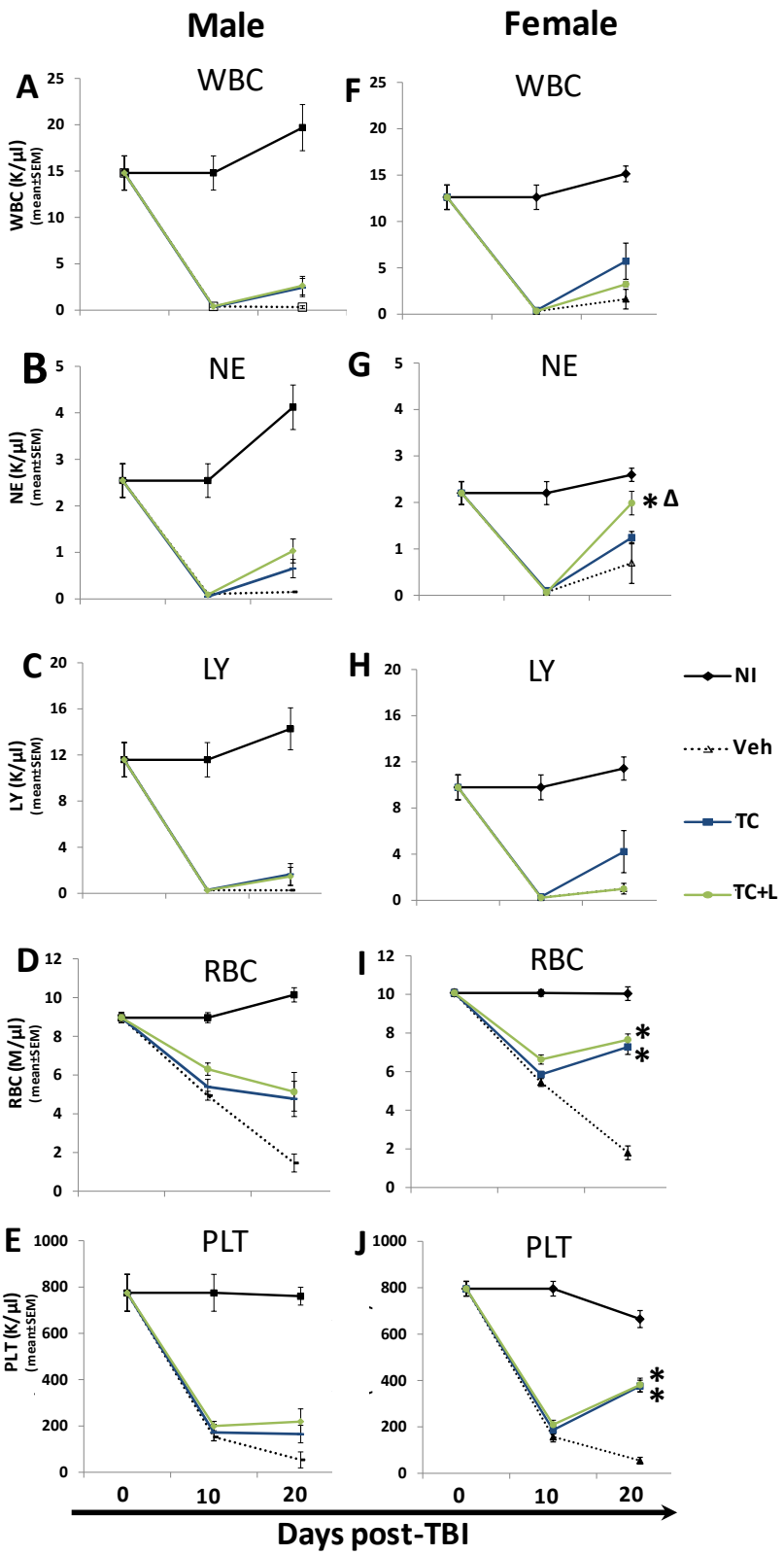
Male
Female
A
WBC
F
WBC
WBC (K/µl) (mean±SEM)
B
NE
G
NE
NE (K/µl) (mean±SEM)
* Δ
C
LY
H
LY
LY (K/µl) (mean±SEM)
NI
Veh
TC
TC+L
D
RBC
I
RBC
RBC (M/µl) (mean±SEM)
* *
E
PLT
J
PLT
PLT (K/µl) (mean±SEM)
* *
0
10
20
Days post-TBI

**Figure 63. CBC profiles in H-ARS phase of lethal-irradiated mice treated with TC or TC+L.**

Mice were exposed to 9.04 Gy TBI and treated with TC or TC+L as previously described. Mice were tail-bled on and assessed for CBC parameters were evaluated at baseline, day 10 and day 20 post-TBI. WBC (panel A & F), NE (panel B & G), LY (panel C & H), RBC (panel D & I), PLT (panel E & J) were analyzed in male (panel A-E) and female (panel F-J) separately. Lines present mean ± SEM. n=2-10 per group per gender per time-point. *$p<0.05$ comparing to Veh; $\Delta p<0.05$ comparing to TC. Sasidhar Vemula and Tong Wu acquired the data; Tong Wu did the analyses.

**Figure 64**

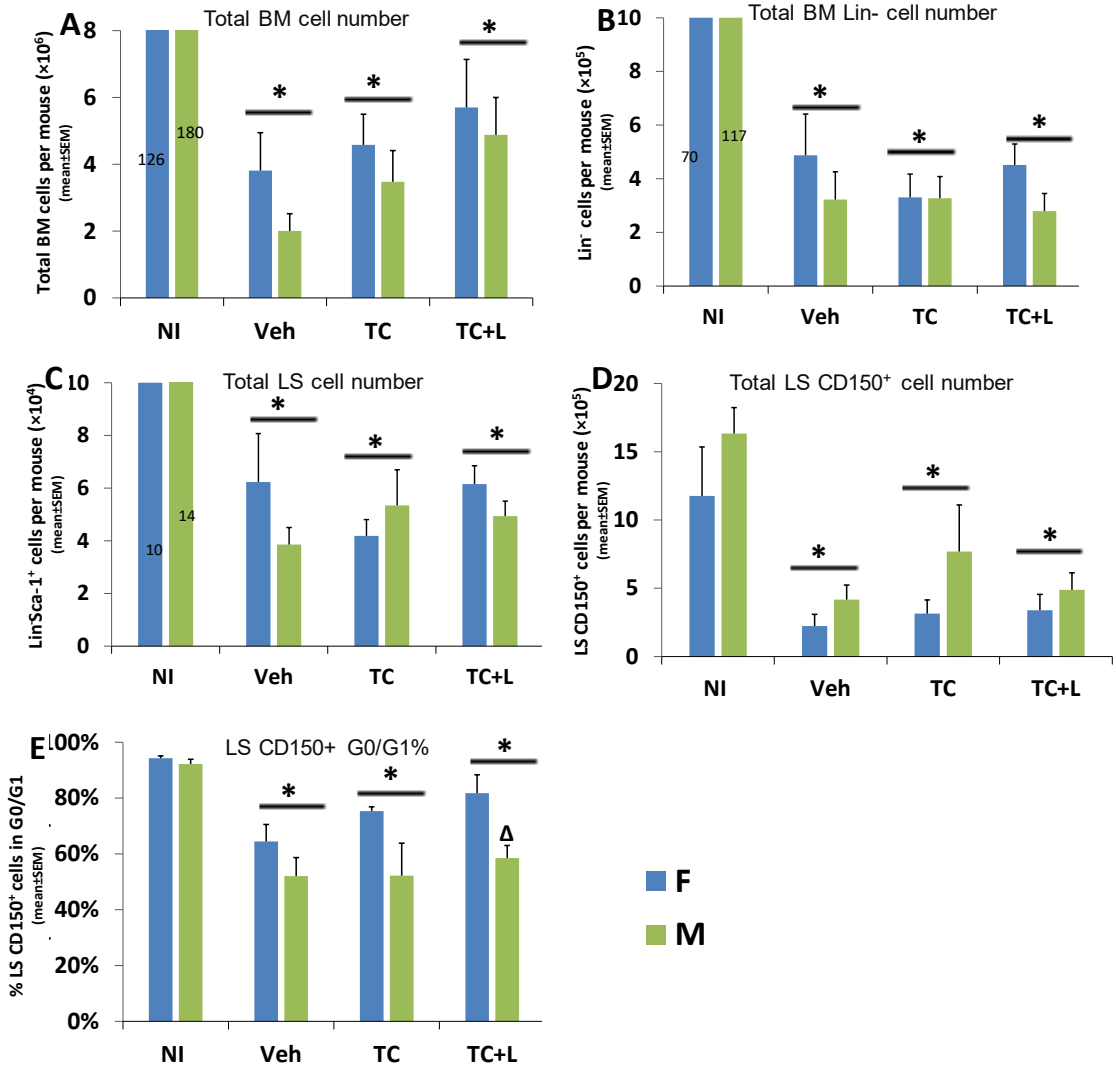
A
Total BM cell number
Total BM cells per mouse (×10⁶) (mean±SEM)
126
180
NI
Veh
TC
TC+L
B
Total BM Lin- cell number
Lin⁻ cells per mouse (×10⁵) (mean±SEM)
70
117
C
Total LS cell number
Lin⁻Sca-1⁺ cells per mouse (×10⁴) (mean±SEM)
10
14
D
Total LS CD150⁺ cell number
LS CD150⁺ cells per mouse (×10⁵) (mean±SEM)
E
LS CD150+ G0/G1%
% LS CD150⁺ cells in G0/G1 (mean±SEM)
F
M

**Figure 64. HSC number and HSC cell cycle in H-ARS phase of lethal-irradiated mice treated with TC or TC+L.**

Mice were irradiated and treated as previously described. Mice were sacrificed at day 10 post-TBI. Flushed BM cells were stained with Lin markers, Sca-1 and CD150 antibodies (panel A-D); and after fixed overnight in 1% formaldehyde, 0.042% DAPI was added for cell cycle analysis (panel E). Bars present mean ± SEM. n=5-7 per gender per group. *$p<0.05$ comparing to NI; $\Delta p<0.05$ comparing male to female.

**Figure 65**

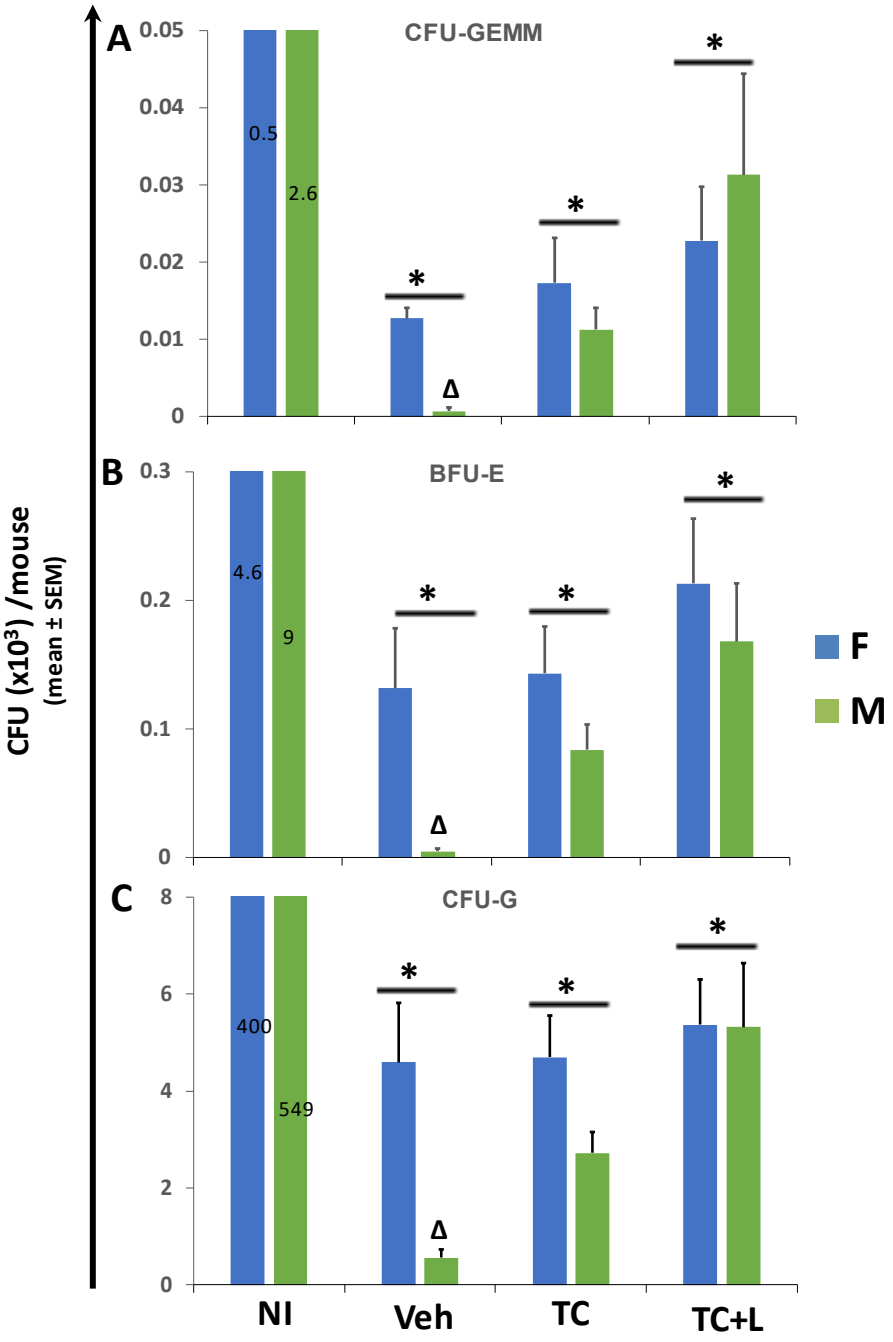
A
CFU-GEMM
0.05
0.04
0.03
0.02
0.01
0
0.5
2.6
*
*
*
Δ
B
BFU-E
0.3
0.2
0.1
0
4.6
9
*
*
*
Δ
C
CFU-G
8
6
4
2
0
400
549
*
*
*
Δ
CFU (x10³) /mouse
(mean ± SEM)
NI
Veh
TC
TC+L
F
M

**Figure 65. HPC in H-ARS phase of lethal-irradiated mice treated with TC or TC+L.** Mice were irradiated and treated as previously described. Mice were sacrificed at day 10 post-TBI and CFC assay was done as described in Materials and Methods. Bars present mean ± SEM. n=5-7 per gender per group. *$p<0.05$ comparing to NI; Δ$p<0.05$ comparing male to female.

**Figure 66**

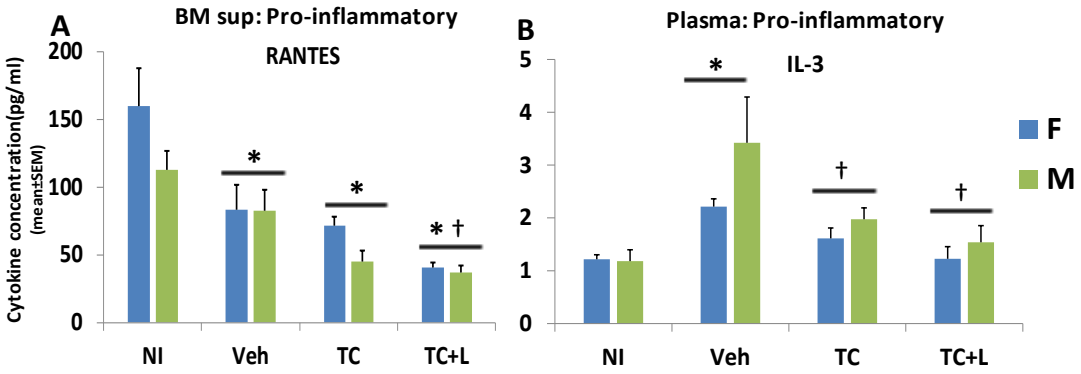
A
BM sup: Pro-inflammatory
RANTES
Cytokine concentration(pg/ml)
(mean±SEM)
200
150
100
50
0
*
*
* †
NI
Veh
TC
TC+L
B
Plasma: Pro-inflammatory
IL-3
5
4
3
2
1
0
*
†
†
NI
Veh
TC
TC+L
F
M

**Figure 66. BM and plasma cytokine in H-ARS phase of lethal-irradiated mice treated with TC or TC+L.**

Mice were irradiated and treated as previously described. Mice were sacrificed at day 10 post-TBI and plasma was obtained by cardiac puncture. BM supernatants were obtained by flushing 2 femurs and 2 tibias twice with 500 ul PBS. Cytokine detection and analysis were followed as in Materials and Methods of Chapter 3. Bars present mean ± SEM. n=4-6 per gender per group. *$p<0.05$ comparing to NI; †$p<0.05$ comparing to Veh.

**Figure 67**

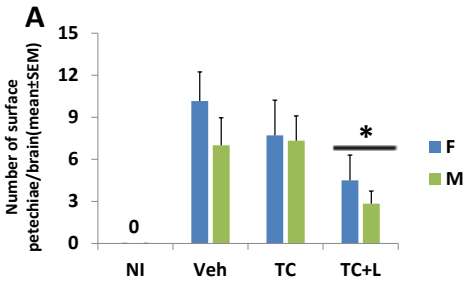
A
Number of surface petechiae/brain(mean±SEM)
15
12
9
6
3
0
0
*
F
M
NI
Veh
TC
TC+L

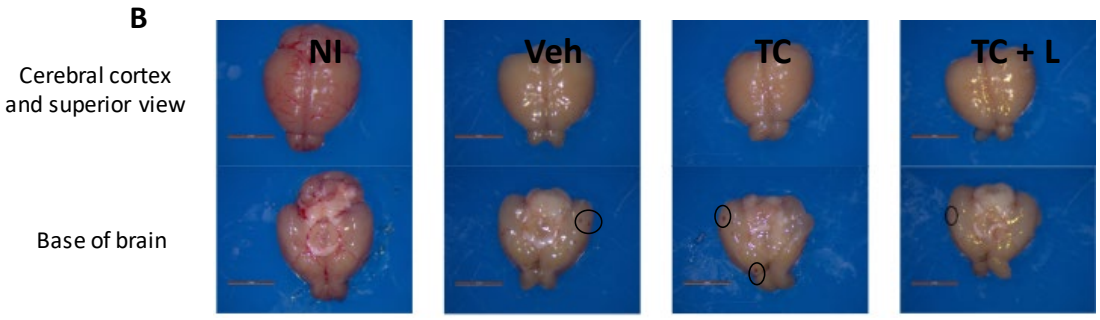
B
Cerebral cortex and superior view
Base of brain
NI
Veh
TC
TC + L

**Figure 67. Brain hemorrhages in H-ARS phase of lethal-irradiated mice treated with TC or TC+L.**

Mice were irradiated and treated as previously described. Mice were sacrificed at day 10 post-TBI and cerebrum and cerebellum were scooped out of brain and petechiae were counted macroscopically on the surface on brain. Bars present mean ± SEM. Figures in panel B were the representative brain images taken from superior and base views. The representative petechiae were circled out in black colors. n=5-7 per gender per group. *$p<0.05$ comparing to Veh.

**Figure 68**

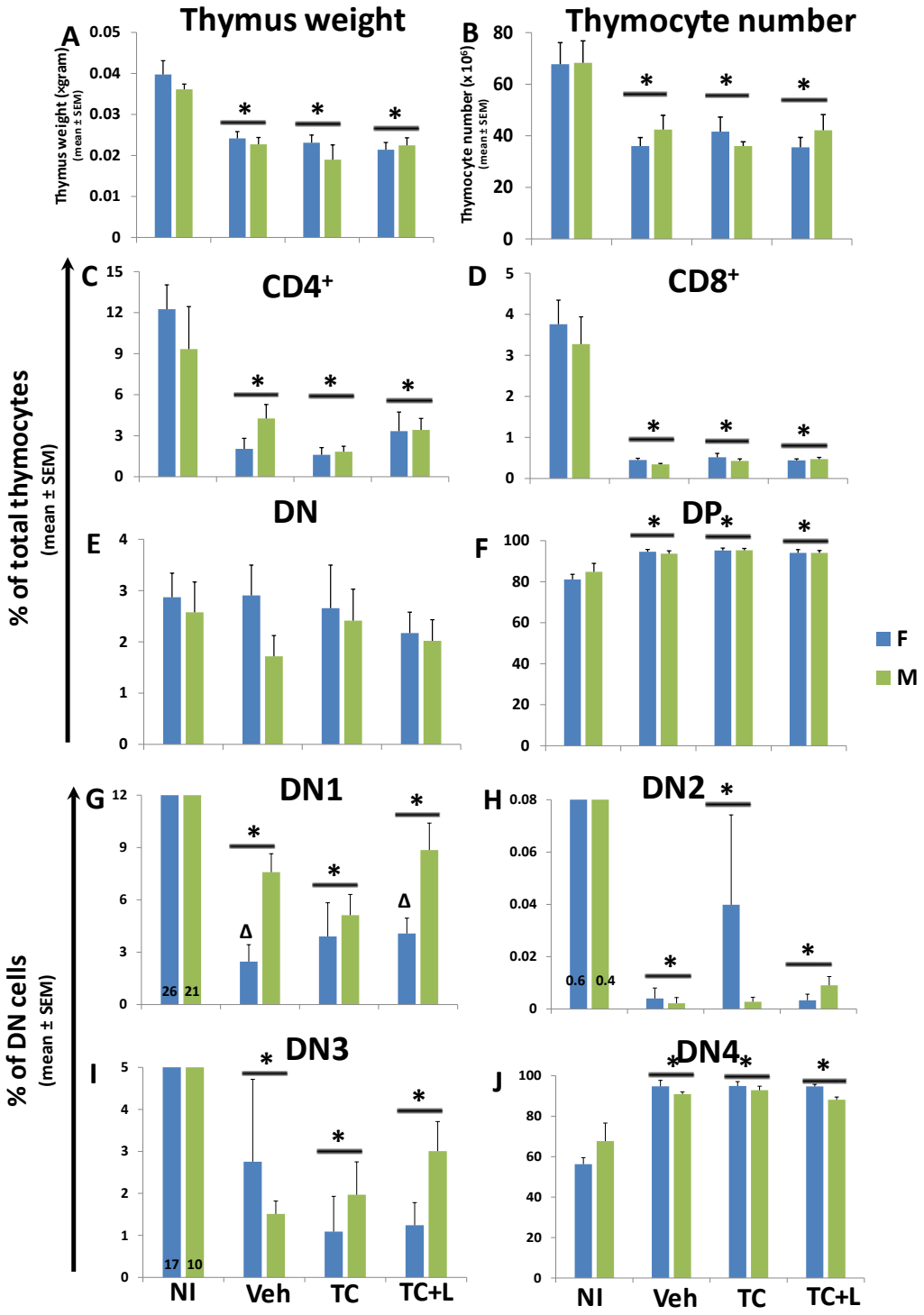
A
Thymus weight
Thymus weight (xgram) (mean ± SEM)
B
Thymocyte number
Thymocyte number (x 10⁶) (mean ± SEM)
C
CD4+
D
CD8+
% of total thymocytes (mean ± SEM)
E
DN
F
DP
F
M
G
DN1
H
DN2
% of DN cells (mean ± SEM)
I
DN3
J
DN4
26
21
0.6
0.4
17
10
NI
Veh
TC
TC+L

**Figure 68. Thymus weight, cellularity and thymocyte subpopulations in H-ARS phase of lethal-irradiated mice treated with TC or TC+L.**

Mice were irradiated and treated as previously described. Mice were sacrificed at day 10 post-TBI and the thymus weight, cellularity and thymocyte subpopulation analyses were followed as in Materials and Methods of Chapter 2. Bars present mean ± SEM. n=4-6 per gender per group. *$p<0.05$ comparing to NI; $\Delta p<0.05$ comparing male to female.

Figure 69

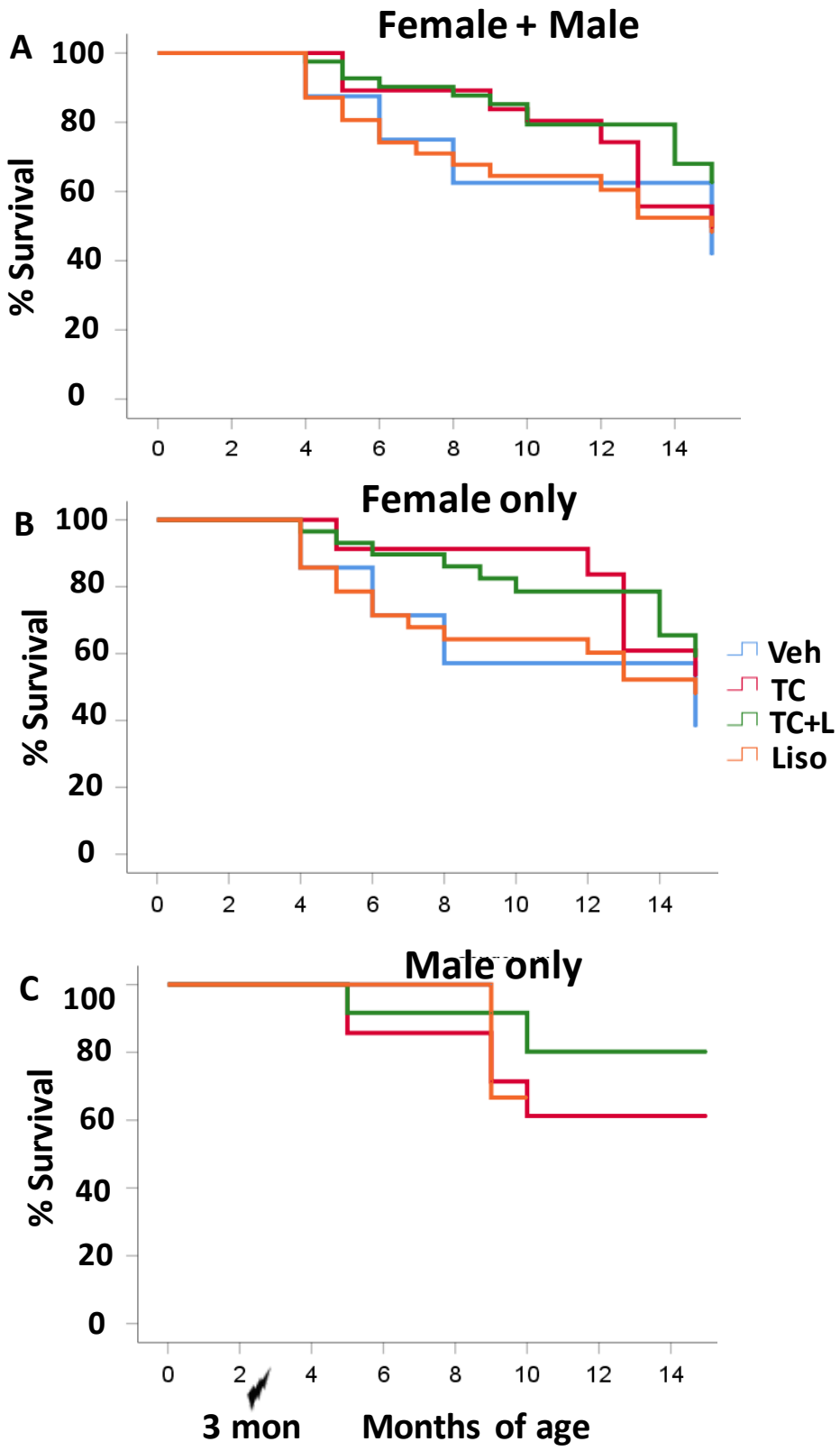
A
Female + Male
% Survival
100
80
60
40
20
0
0
2
4
6
8
10
12
14
B
Female only
% Survival
Veh
TC
TC+L
Liso
C
Male only
% Survival
3 mon
Months of age

**Figure 69. Long-term survival of day 30 survived mice treated with Liso, TC or TC+L.**

Mice were exposed to 9.27 Gy TBI and treated with Liso, TC or TC+L as previously described. Mice survived over day 30 post-TBI were transferred to RBMD study for long-term survival monitor until the end of study (15 months post-TBI). The survival mice were recorded when found dead, or were euthanized when severely moribund or scheduled time-point sacrifices. Survival is shown as Kaplan-Meier curves. Total n=8-41 mice in each group (panel A). Female n=7-29 mice in each group (panel B). Male n=1-14 mice in each group (panel C). Sasidhar Vemula and Tong Wu acquired the data; Tong Wu did the analyses.

**Figure 70**

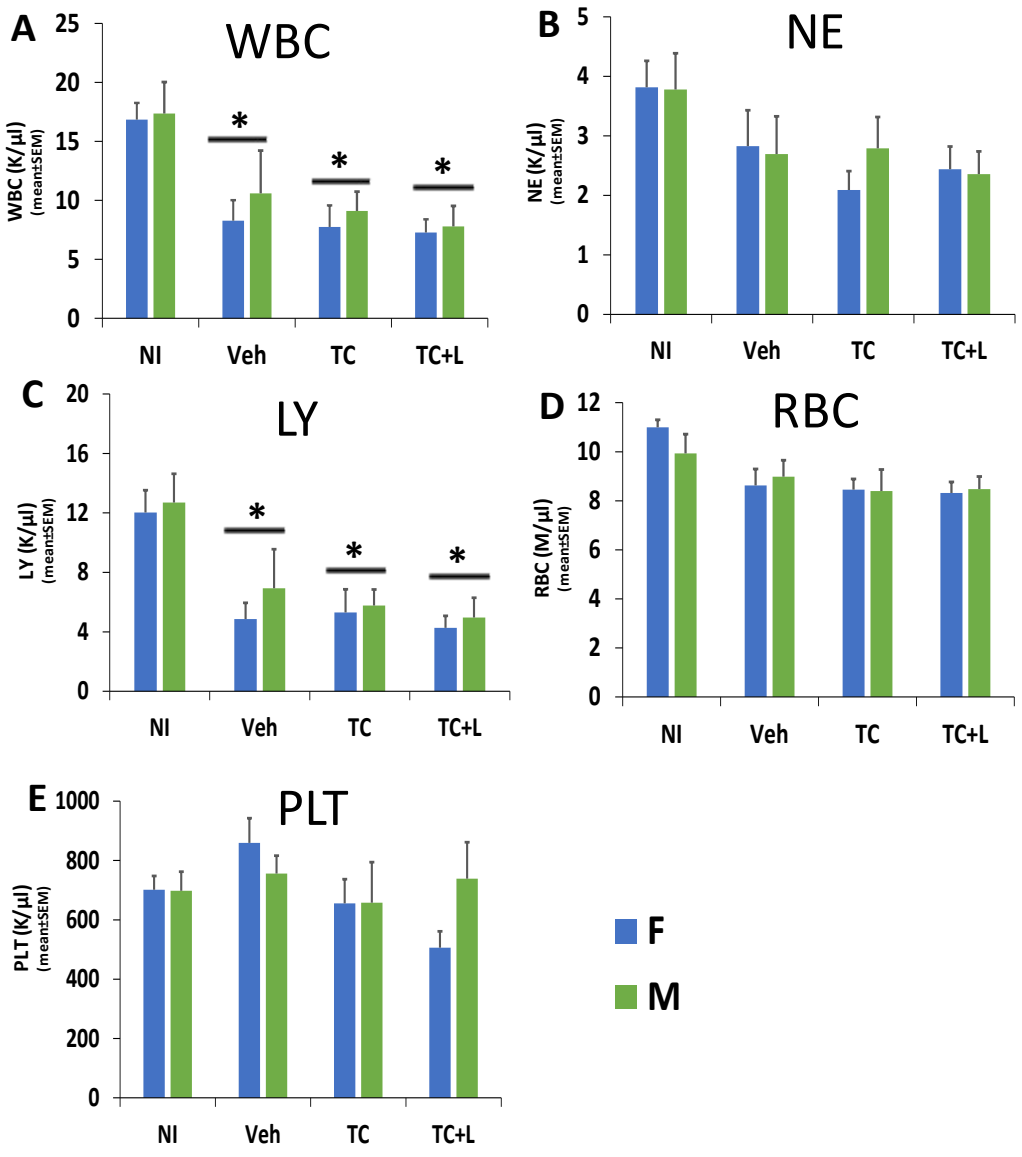
A
WBC
WBC (K/µl) (mean±SEM)
25
20
15
10
5
0
*
*
*
NI
Veh
TC
TC+L
B
NE
NE (K/µl) (mean±SEM)
5
4
3
2
1
0
NI
Veh
TC
TC+L
C
LY
LY (K/µl) (mean±SEM)
20
16
12
8
4
0
*
*
*
NI
Veh
TC
TC+L
D
RBC
RBC (M/µl) (mean±SEM)
12
10
8
6
4
2
0
NI
Veh
TC
TC+L
E
PLT
PLT (K/µl) (mean±SEM)
1000
800
600
400
200
0
NI
Veh
TC
TC+L
F
M

**Figure 70. CBC profiles in DEARE phase of lethal-irradiated mice treated with TC or TC+L.**

Mice were exposed to 9.27 Gy TBI and treated with TC or TC+L as previously described. Survivors were tail-bled at 6 months post-TBI and assessed for the WBC (panel A), NE (panel B), LY (panel C), RBC (panel D), and PLT (panel E). Bars present mean ± SEM. n= 6-10 mice per group. *$p<0.05$ comparing to NI. Sasidhar Vemula and Tong Wu acquired the data; Tong Wu did the analyses.

**Figure 71**

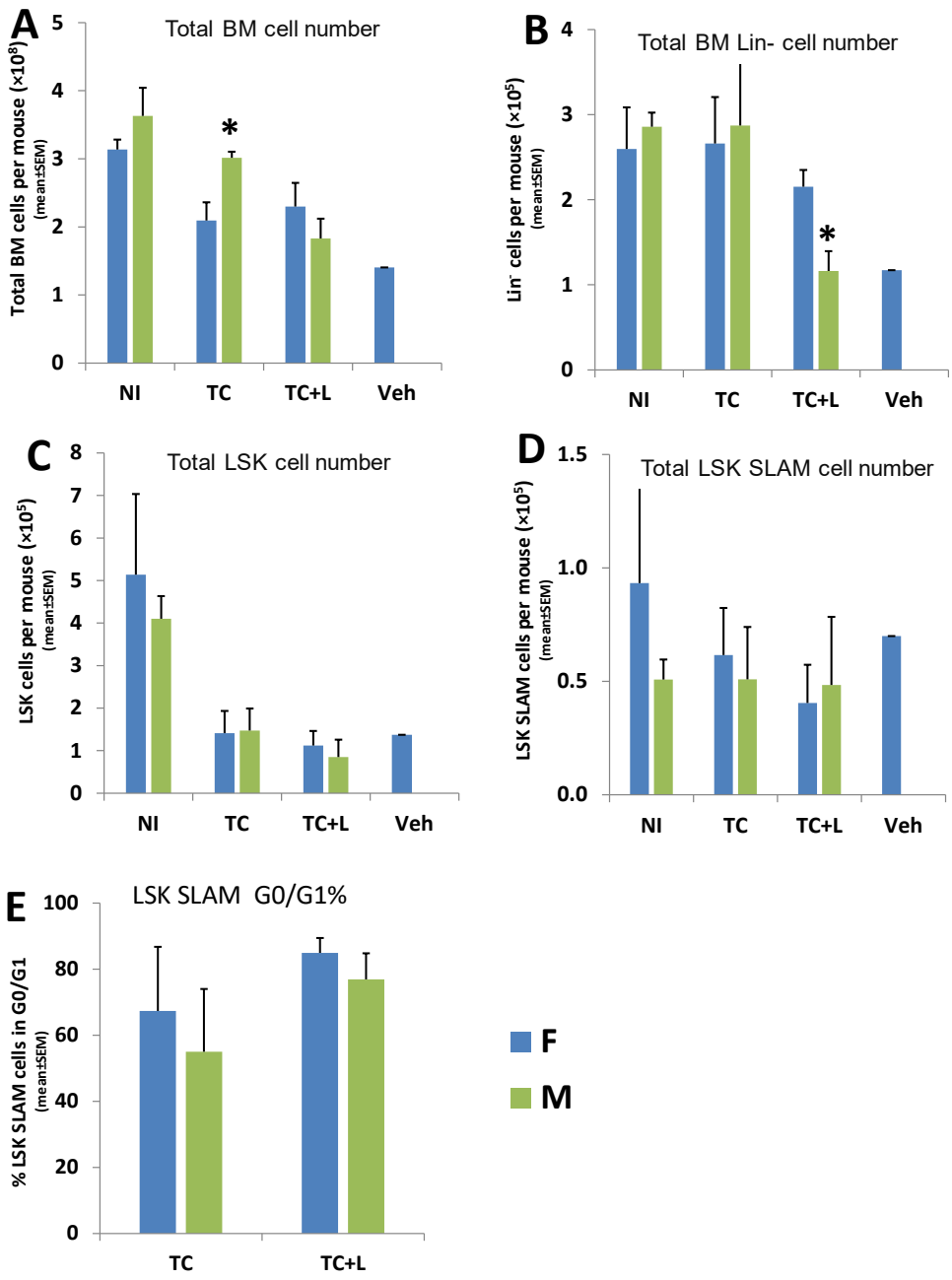
A
Total BM cell number
Total BM cells per mouse (×10⁸) (mean±SEM)
0
1
2
3
4
5
*
NI
TC
TC+L
Veh
B
Total BM Lin- cell number
Lin⁻ cells per mouse (×10⁵) (mean±SEM)
0
1
2
3
4
*
NI
TC
TC+L
Veh
C
Total LSK cell number
LSK cells per mouse (×10⁵) (mean±SEM)
0
1
2
3
4
5
6
7
8
NI
TC
TC+L
Veh
D
Total LSK SLAM cell number
LSK SLAM cells per mouse (×10⁵) (mean±SEM)
0.0
0.5
1.0
1.5
NI
TC
TC+L
Veh
E
LSK SLAM G0/G1%
% LSK SLAM cells in G0/G1 (mean±SEM)
0
20
40
60
80
100
TC
TC+L
F
M

**Figure 71. HSC number and HSC cell cycle in DEARE phase of lethal-irradiated mice treated with TC or TC+L.**

Mice were exposed to 9.27 Gy TBI and treated with TC or TC+L as previously described. Survivors were sacrificed at 6 months post-TBI. Flushed BM cells were stained with Lin markers, c-Kit, Sca-1, CD48 and CD150 antibodies for SLAM LSK analysis (panel D); and after fixed overnight in 1% formaldehyde, 0.042% DAPI was added for cell cycle analysis (panel E). Bars present mean ± SEM. n=2 per gender in NI group, only one female in Veh group, n=4-7 per gender in TC and TC+L groups. *$p<0.05$ comparing to female to male.

**Figure 72**

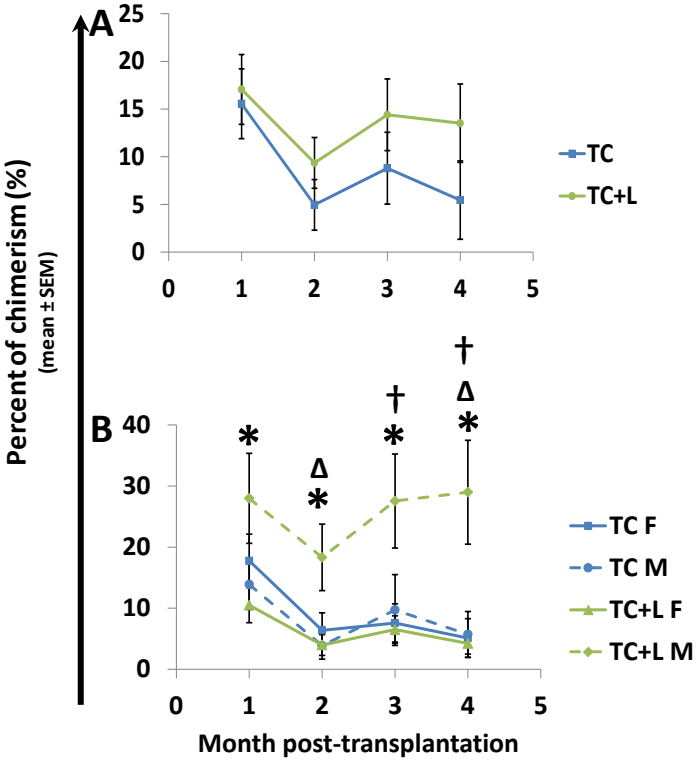
A
B
Percent of chimerism (%)
(mean ± SEM)
25
20
15
10
5
0
40
30
20
10
0
0
1
2
3
4
5
Month post-transplantation
TC
TC+L
TC F
TC M
TC+L F
TC+L M
*
Δ
†

**Figure 72. Long-term engraftment potential of BM cells in DEARE phase from lethal-irradiated mice treated with TC or TC+L.**

Mice were exposed to 9.27 Gy TBI and treated with TC or TC+L as previously described. Survivors were euthanized at 6 months post-TBI and $3\times10^5$ of donor whole BM cells were transplanted intravenously along with $2\times10^5$ competitor cells into congenic recipient. Peripheral blood was monitored for donor chimerism monthly till to 4 months post-transplantation. Data were analyzed as male + female (gender of donors) combined in each treatment group (panel A) or male and female separately (panel B). Lines present mean ± SEM. n= 9-15 recipients per group per gender. *$p<0.05$ comparing to female TC+L group; Δ$p<0.05$ comparing to male TC group; †$p<0.05$ comparing to female TC group. Sasidhar Vemula and Tong Wu acquired the data; Tong Wu did the analyses.

survival rates with single or combined peg-HGFs regimens are similar to multiple daily injections of nonpegylated HGFs [69, 349]. One injection of peg-HGFs has logistical advantage over multiple daily administrations in the chaos scenario of nuclear plant disasters and nuclear warfare and has less possibility to develop neutralizing antibodies comparing to multiple injections. Besides, the risk of spleen rupture reported in chemotherapy patient who received multiple injections of G-CSF for treatment of neutropenia [350] is less likely to happen in single dose of peg-HGF scenario; especially considering there is a portion of patients receiving HGF treatment after nuclear accident whose radiation exposure might be very low but cannot be identified because of the limitation of dosimetry methods, the risk of spleen rupture might be even higher in those immune-intact population if they receive multiple injections of HGFs.

The increased day 30 survival rate of mice treated with peg-HGFs correlates with the increased CBC parameters, including WBC, NE, RBC, and PLT, mainly at day 21 post-TBI (Figure 42 & 50). The most pronounced differences observed were between peg-HGFs-treated and Veh-treated, with few differences observed between groups treated with different combinations of peg-HGFs (Figure 44-48). The CBC analyses indicate that some peg-HGFs regimens, such as “with IL-11” and “combined” regimens increase NE level at day 2 post-TBI. The lifespan of NE is short, generally fewer than 24 hours; and the cells are constitutively committed to apoptosis after leaving the bone marrow. G-CSF and GM-CSF have been reported to delay NE apoptosis in an unirradiated scenario in vivo and in vitro by regulating the activity of caspase family proteases [351-353] and IL-11 is known to prevent intestinal crypt cell apoptosis after radiotherapy and

chemotherapy [354]. Pegylated HGFs might increase the CBC parameters at day 2 post-TBI through the protection from apoptosis. The in vivo experiment shows that irradiation increases NE and LY apoptosis at day 2 post-TBI as expected; however, peg-HGFs did not protect NE and LY from apoptosis 24h after injection, where there is no difference in the apoptotic rate between peg-HGFs-treated and Veh groups (Figure 49). There are several possible reasons for the inconsistencies between the CBC data and apoptosis study. First, RBC lysis and staining during the apoptosis study might impact WBC integrity, obscuring any anti-apoptotic effects of peg-HGFs treatment. Secondly, a protective effect may occur earlier than 24 hr, making the 24 hr post-injection (day 2 post-TBI) time-point too late to observe differences. Third, the higher NE numbers in "combined" and "with IL-11" groups may result from stronger progenitor stimulation in these groups compared with the "single" and "no IL-11" groups. However, this explanation is not supported by the lack of sustained high NE numbers at day 4 and 7.

Since mature peripheral blood cells differentiate from immature HPCs and HSCs in the BM, the HPC function was evaluated by CFU assay at different days post-TBI. Because of the scarcity of BM cells post-TBI, BM cells from four mice were pooled. Three quarters of the cells were used for the transplantation study, and the remainder for the CFU assay (Figure 51 A-D). Although statistical comparison to Veh is not available (Veh was pooled form four mice), the peg-HGFs treated groups had higher average CFU number than Veh-treated group as early as day 5 post-TBI and prominent at day 14 post-TBI (Figure 51). In another similar study to evaluate the HSC number in BM, peg-HGFs treated group had significantly higher HSC number ($LSCD150^{+}$) than Veh-treated group

at day 10 post-TBI (Figure 52 E). These results indicate that peg-HGFs stimulate the proliferation of the remaining committed hematopoietic progenitor cells after radiation exposure, whether peg-HGFs also have indirect effect on the bone marrow niche cells remains to be determined in future study.

Mice received "combined" regimens had slightly higher, but not significantly different, CFU number and HSC number than "single" regimens at early days post-TBI (Figure 51 E-H & Figure 52 F), and this hematopoietic recovery in bone marrow is consistent with the hematopoietic recovery in peripheral blood at later day (day 21) post-TBI (Figure 47), which indicates that the extra benefit in hematopoietic recovery brought from polypharmacy strategy is limited. Similar results were observed for "with IL-11" and "no IL-11" analysis. These results indicate that there is possibility that "combined" or "with IL-11" regimens have positive effects on non-hematopoietic systems, such as in gastrointestinal system [341, 355], and thus enhance the day 30 survivals in mice received these regimens (Figure 42). Future studies will investigate the broad systems/organs effects other than hematopoietic system of the peg-HGFs.

Next, transplantation study was used to evaluate the repopulation capacity of HSCs, monitoring peripheral blood chimerism for five months post-transplantation. In general, recipients had higher chimerism when transplanted at day 7 post-TBI than at 5, and higher at day 14 than days 7 and 5, meeting the expectation that HSC dysfunction gradually recovers over time following irradiation. Overall, the donor chimerism of irradiated mice was transient, no matter which treatments the donor mice received, which

indicates the loss of HSC long-term repopulating potential in irradiated mice. There were no statistically significant differences in chimerism rate between different peg-HGFs regimens (Figure 53 A-C). In order to increase the number of N in each group, all peg-HGFs-treated groups were combined into the "HGF" group and compared with Veh group. No statistical difference between these groups at any time-point in mice transplanted at day 5 or day 7 post-TBI. The average chimerism in the "HGF" group was generally lower than in the Veh group in mice transplanted 14 days post-TBI. This difference was statistically significant at four months post-transplantation (Figure 53 D-F). When "single" vs. "combined" were compared, at 1-month post day 14 transplantation study, donor cells from mice receiving "combined" regimens had significantly higher chimerism than those from mice that received "single" regimens. This trend was sustained over the subsequent months but without statistical difference (Figure 53 G-I). When analyzed in the pattern of "with G" vs. "no G" (Figure 53 J-L), "with GM" vs. "no GM" (Figure 53 M-O) and "with IL-11" vs. "no IL-11" (Figure 53 P-R), there was no significant difference comparing "with xx" to "no xx". These results indicate that peg-HGFs did not rescue the loss of HSC repopulating potential brought by radiation exposure and even exacerbate the loss at certain time-point post-TBI. Peg-HGFs likely enhance hematopoietic recovery by promoting proliferation and differentiation of short-term repopulating progenitors at early time post-TBI but at the expense of self-renewal and long-term repopulating potential of HSC, which may aggravate RBMD. This is consistent with the previous report from Li et al.[356] in which the donor receiving G-CSF treatment had lower chimerism than the donor receiving Veh treatment 1-month post-TBI. The "combined" regimen transiently increase the chimerism rate indicates that

"combined" regimen preserves the HSC short-term repopulating potential better than "single" regimen. The effect of irradiation and peg-HGFs on self-renewal capacity of stem cells need to be tested by secondary transplantation which is beyond the scope of this study.

Many studies have reported similar survival benefit of early administration of HGFs or peg-HGFs [74, 267], but long-term survival studies are rare due to prohibitive costs in long-term animal husbandry and monitoring. Most RBMD studies used sublethal radiation exposure or only monitored mice a few months post-TBI and did not use peg-HGFs as MCM [40, 357, 358]. In this study, survivors of H-ARS were transferred to RBMD study with time-point sacrifices to observe delayed effects and evaluate long-term survival. Survival analyses showed that the survival benefit of peg-HGFs treatments in H-ARS phase did not sustain in DEARE. All irradiated mice had significantly lower 2-year survival rates than NI mice, and no any peg-HGFs-treated group had significant higher survival rate than Veh-treated mice (Figure 54 A and Table 11). Combining different groups into "HGF" vs. "Veh" (Figure 54 B), "with IL-11" vs. "no IL-11" (Figure 54 C) and "single" vs. "combined" (Figure 54 D) as previously described, there was no significant difference between any of these comparisons. This result contradicts to the survival superiority of peg-HGFs in H-ARS phase, but it is consistent with the transplantation chimerism study at day 14 post-TBI (Figure 53 F) which highlighted the detrimental effect of peg-HGFs on HSC function post-TBI.

In DEARE markers studies including the body weight, CBC parameters, bone marrow HSC number and function at 6 and/or 12 months post-TBI, the results followed the similar trend in DEARE survival study, where the differences between peg-HGFs- and Veh-treated mice were minimal and there was no significant difference between "with xx" and "no xx" comparisons, or between "combined" and "single" comparison (Figure 55-58). The difference between irradiated mice and NI mice are generally more apparent in 12 months post-TBI than in 6 months post-TBI, such as body weight and myeloid skewing in peripheral blood, which reflects the "double hits" of aging and irradiation on the DEARE mice. The bone marrow LSKCD150$^{+}$ cells followed the opposite trend where the number per mouse was higher in the 12 months NI and DEARE mice than the 6 months NI and DEARE mice, respectively (Figure 57). Dr. Orschell's laboratory has previously confirmed that the LSKCD150$^{+}$ cells from irradiated survivor represent the long-term repopulating HSCs, the same as LSKCD150$^{+}$ cells from NI mice [147]. The increased CD150 on KSL population of the irradiated mice has been reported by Simonnet AJ et al. [359] and by Chua HL et al. [40, 147]. Whether the increased CD150 expression represents the enhanced long-term repopulating ability is unknown, the lack of 6 months post-TBI transplantation data makes the comparison to 12 months post-TBI transplantation impossible. There is a possibility that more LSKCD150$^{+}$ cells in DEARE mice represent a compensatory mechanism to try to maintain the increased hematopoietic demand, which is through the enhanced proliferation of HSCs, but the repopulating function of these HSCs is still defective [360-362]. From the result of 12 months post -TBI HSC phenotyping study and the result of transplantation study at the same time, peg-HGFs have limited effect on either increasing the HSC number or

enhancing long-term repopulating progenitors, comparing to the Veh-treated control. The lower levels of donor-derived lymphoid differentiation in both peg-HGFs- and Veh-treated mice than in NI mice (Figure 58) were consistent with the lower lymphocyte percentages in peripheral blood in these two groups than the NI group (Figure 56). This result indicates that the long-term immune deficiency roots in the HSCs whose multilineage differentiation ability is defective, rather than the direct effects of radiation exposure on mature lymphocytes.

DNA damage and epigenetic changes are induced by irradiation and aging, leading to downregulation of lymphoid genes and upregulation of myeloid genes, which shifts the differentiation potential of the HSC pool to the myeloid lineage. Wang et al. found that irradiation-induced G-CSF/STAT3/BATF upregulation bypasses the lymphoid differentiation checkpoint, impairs the self-renewal potential of HSCs, and depletes lymphoid-biased HSCs [363]. Potentially, BATF activation is G-CSF dependent and needs continuous stimulation with G-CSF sustain activated status and maintain HSC self-renewal inhibition [363]. Irradiation-induced apoptosis or cell cycle arrest [364] in HSCs cannot explain the myeloid skewing observed in normal aging mice and DEARE mice [363]. This model perfectly explains that LY number partially recovers at day 21 post-TBI, especially apparent in the peg-G-CSF group (Figure 45). It also raises the concern that administration of HGFs would impair HSC self-renewal and exacerbate the myeloid skewing. The transplantation study shows that a decreased chimerism rate at 4 months post-transplantation in the peg-HGFs group comparing with Veh group (Figure 53 F). This result indicates the possibility that administration of peg-HGFs as MCM rescues the

irradiated mice by inducing the differentiation of short-term repopulating progenitors and impairs the HSC long-term repopulating potential at an early time-point post-TBI, whether this impairment relates to the G-CSF/STAT3/BATF pathway needs further investigation.

The day 21 peripheral blood analysis indicated that T and B cells increase in the peg-G-CSF treated group compared to Veh group, albeit to a less extent than the increased $Gr1^+$ neutrophils (Figure 59). Adding more peg-HGFs into the regimen does not increase lymphocytes and neutrophils. The differentiation of T lymphocytes is different from B lymphocytes and neutrophils since T cells require thymic education and maturation. The atrophy of thymus is a hallmark of aging and contributes to the loss of immune function in senior mammals, including humans and mice. The involution of thymus post-TBI has been reported [186, 218, 219], but rarely discussed in an MCM scenario. In this section, the thymic involution and recovery post-TBI in H-ARS and DEARE phases, and the impact of peg-HGFs on the thymus, were investigated. Thymus is extremely sensitive to radiation, reaching the first nadir at day 2 post-TBI, followed by the first recovery peak at day 10, and then second nadir at around day 21 and second peak at around day 30-40. Subsequently, the thymus gradually involutes under the double hits of aging and irradiation (Figure 60 A & B). The first recovery results from the proliferation and expansion of radioresistant thymocytes and the second recovery is from the proliferation and expansion of ETPs which are generated de novo from HSC in bone marrow [218, 365].

Administration of peg-HGFs at 24 hr post-TBI did not change the thymic weight and cellularity at the first nadir and peak. When combining all peg-HGFs-treated groups together, the "HGFs" group had statistically higher thymus weight and cellularity than Veh group at day 21 post-TBI (Figure 60 C & D). Analysis of thymic subpopulations at day 21 reveals that the "HGF" group had a statistically higher percentage of DP cells which indicates peg-HGFs enhance the de novo thymus regeneration. Previous studies have shown that G-CSF, GM-CSF or IL-11 enhance hematopoiesis mainly by promoting the proliferation and differentiation of myeloid-megakaryoid progenitor cells [366, 367]. Current studies indicate that peg-HGFs treatment 24 hr post-TBI enhances immune recovery in both the myeloid and lymphoid lineage. Thymus-dependent de novo regeneration originated from BM-derived progenitors and thymus-independent HPE are the two ways of T cell reconstitution. The effect of peg-HGFs on HPE has not been evaluated; however, the G-CSF receptor has expression on some mature B and T lymphocytes [368, 369] and G-CSF enhances the proliferation of these cells [346, 369]. Although the expression of GM-CSF and IL-11 receptors have not been reported on the surface of peripheral lymphocytes, it is possible that GM-CSF or IL-11-taregeted cells such as monocytes have an indirect influence on lymphocyte proliferation [370, 371]. Lymphocyte recovery at day 21 following peg-HGF administration post-TBI involves both the thymus-dependent and thymus-independent T cell recovery pathways. Lymphocyte with thymus education provide a more comprehensive immune protection than lymphocyte generated from HPE. Interestingly, at 12 months post-TBI, the peg-HGFs-treated mice had lower thymic weight and cellularity than Veh group (Figure 61 J, N & O). It is consistent with the lower chimerism rate in bone marrow of peg-HGFs

group comparing with Veh control in the transplantation study (Figure 53 F). The lower thymus repopulating potential of the ETPs might be similar to the lower bone marrow repopulating potential HSCs in the irradiated mice. Further study is needed to identify whether peg-HGFs impair the homing of ETPs to thymus or impair the proliferation and differentiation of ETPs.

Except peg-HGFs, other MCMs are also investigated to see if there is space to further increase survival in H-ARS and alleviate DEARE effects. ACE is part of the classic RAS system, which converts angiotensin I to angiotensin II. ACEI is widely used in the treatment of hypertension. Recent research found that HSCs express ACE throughout the hematopoietic ontogeny from embryo to adulthood [372]. HPCs exhibit transient cell cycle arrest after two days of captopril (a classic ACEI) administration in vivo. When used as a radiomitigator instead of a radioprotectant, captopril significantly decreases radiation-induced lethality by accelerating hematopoietic recovery. The cell cycle pause leads to side effects in hypertension patients including agranulocytosis, anemia, or pancytopenia [373-375]. Based on previous findings, Liso was added to TC regimen to determine whether this new combination (TC+L) more effectively alleviates H-ARS and DEARE than TC alone. The results show that the day 30 survival rate slightly increased in the TC+L group in comparison with the TC group, and there was a sex difference in this effect. TC+L was more effective in female than in male mice (Figure 62 A-C). In the HSC cell cycle analysis at day 10 post-TBI (3 days after Liso treatment), more quiescent HSCs were present in female TC+L-treated mice than in male TC+L-treated mice; and in female mice, the percentage of HSCs in quiescent status was

slightly higher in the TC+L group than the TC and Veh group, although not statistically different (Figure 64 E). This result indicates that sex difference in cell cycle pause is a possible mechanism for the higher survival rate in female TC+L group. This is consistent with a report from Davis et al., showing an increased percentage of HSCs in quiescent status in captopril-treated female mice [103]. The transient cell cycle pause allowing more time for repair of radiation-induced DNA damage in HSCs. Cautions are needed for the interpretation of these results because there was no statistical difference in cell cycle between TC+L and TC group; and in TC group, there was similar trend of sex difference although not statistically different, which was not seen in other TC studies. The possible reasons could relate to the small size of N (5-7 mice per group) or relate to the time of sacrifice, day 10 post-TBI (3 days after Liso treatment) might be too short to observe the full effect of Liso, which also explains that why there was no significant difference between TC+L and TC groups in BM cellularity, HSC and HPC number, BM cytokines and brain petechiae studies at this time-point. Because the cell cycle arrest is transient and followed with more cells entering the G1 to G2 transition [103], it is possible that the higher neutrophil number at day 20 in the female TC+L group than TC group correlates with the earlier cell cycle pause on progenitors. In summary, there are several possible mechanisms to explain the survival benefit and the sex difference for TC+L regimen, further studies are needed to investigate other time-points after Liso treatment and increase the sample size.

In the DEARE study, TC+L group did not improve long-term survival, myeloid skewing, or HSC number (Figure 69-71). However, analysis of HSC function at DEARE

mice (6 months post-TBI) with competitive transplantation revealed that TC+L-treated male mice had significantly higher donor chimerism rate than TC+L-treated female mice and significantly higher than TC-treated mice in both genders (Figure 72). Although the long-term survival rate in TC+L-treated male mice was higher than the TC-treated male mice and was higher than TC- and TC+L-treated female mice, which is consistent with the transplantation results, the differences were not statistically significant and this might relate to the limited number of mice survived to the DEARE phase. The reason for why female TC+L-treated mice had higher day 30 survival rate than male mice in H-ARS phase, but lower long-term survival rate and HSC repopulation ability in the DEARE phase, is not clear. Further evaluation of sex hormone status at these time-points may provide insights into the observed sex difference.

To summarize, one shot of single or multiple combined peg-HGFs at 24 hr post-TBI enhances the day 30 survival rate and alleviates H-ARS, including thymus recovery, which promotes the de novo regeneration of T cells. The effects of peg-HGFs on DEARE are minimal when compared to Veh-treated mice in terms of long-term survival, body weight, myeloid skewing, HSPC number, and HSC function. Adding lisinopril from day 7 post-TBI further increases the day 30 survival rate and shows a sex difference in TC+L group. Future studies with large sample size and more mechanism studies such as sex hormone status in H-ARS and DEARE phases are needed.

# Chapter 6. Future Directions

## 6.1. Time-window and dosage-window of dmPGE2 efficacy

As described in Chapter 3, dmPGE2 administrated at -24 hr prior to irradiation does not enhance survival; whereas dmPGE2 schedules administrated within 3 hr time window prior to irradiation are all effective and -1 hr prior to irradiation conferred a little better survival than -3 hr prior to irradiation, though not statistically significantly (day 30 survival rate of 90% vs.100% respectively; Figure 21). Previous studies reported that the closer to irradiation, the more effective the dmPGE2 protection and suggested that -1 hr prior to irradiation is the time limit [134]. Current studies show the similar trend and extend the time-window to -3 hr prior to irradiation. There is a specific time-window in which dmPGE2 must be administered for a protective effect to be achieved. Since the -24 hr time-point is the only earlier time-point tested than -3 hr, whether other time-points early than -3 hr will still be effective and where is the upper limit of the time window for radioprotection are unknown. Further studies at time-points between -3 hr and -24 hr prior to irradiation would help to reveal when PGE2 signaling pathway to start and end its effects in hematopoietic system.

One dose of 35 μg or two doses of 20 μg dmPGE2 were tested in the survival studies. According to previous reports, the closer of the time-point of dmPGE2 administration to the time-point of irradiation, the lesser dmPGE2 dose is needed for providing an adequate protection. Walden TL et al. reported that 1 μg of dmPGE2 injected -5 min prior to TBI (10 Gy) results in ~90% survival [134]. The side effects of dmPGE2 injection include diarrhea and decreased ambulation, which are dose-dependent

[134], and these side effects are one of the main obstacles that prevent its wide usage. The severity and duration of these side effects with a 1 μg dmPGE2 treatment would be significantly lower than the 35 μg schedule. Investigating the potential to use this smaller dose is of importance if dmPGE2 is to be used as a radioprotectant for first responders and military personnel as they will be required to work in a radioactive material-contaminated environment and thus require treatment which is not associated with side effects that will affect their ability to work.

Another limitation of current studies is that the highest irradiation dose tested is 9.04 Gy (LD90/30) and therefore it is not known whether the dmPGE2 schedule tested render the mice capable of tolerating a higher radiation dose. In previous studies, a similar dmPGE2 regimen (40 μg at -30 min prior to TBI) increased the LD50/30 from 9.39 Gy to 16.14 Gy, with the survival curve beginning to decline after 10 Gy [134]. A probit analysis in well-defined mouse model would provide information on to how to adjust the dmPGE2 regimen according to the predicted level of radiation exposure.

As for the dmPGE2 radiomitigation, although +3 hr schedule fails to increase the survival rate and +6 hr schedule is effective and the time-window is extended to +30 hr post-TBI, whether earlier time-points than the +3 hr, especially the time-points very close to irradiation, will be effective or not, is still unknown. Although a previous study [276] indicated that dmPGE2 given immediately after irradiation could decrease the loss of functional HSPC, another survival study [134] demonstrated that mice received dmPGE2 at either 5, 15, 30, or 60 post-irradiation were all dead. This discrepancy might relate to

different mouse stain (C57BL/6 vs. CD2F1), different irradiation dose (6.5 Gy from $^{137}Cs$ vs. 10 Gy from $^{60}Co$) and different dmPGE2 dose (2 μg/g, around 40 μg per mouse vs. 10 μg per mouse). Since Walden TL et al. [134] in the survival study only used 10 μg dmPGE2, whether the result will be different if higher dosage applied, such as 35 μg, is unknown. And since in radioprotection studies, the protective effect is dmPGE2 dosage-dependent, it is reasonable to assume that radiomitigation effect might also be dosage-dependent.

In summary, further investigations into the limits of the use of dmPGE2 as a radioprotectant are required for optimizing the timing of injection, the dose of dmPGE2, and the effect of the dose of irradiation on efficacy. These studies will be beneficial curating an optimal regimen according to predicted radiation exposure, and will be meaningful to the potential recipients of dmPGE2 protection, especially to first responders and military personnel facing a radiation threat.

### 6.2. Mechanism of dmPGE2 protection

It is not known whether the protection effect of dmPGE2 is dependent on the presence of dmPGE2 at the time of irradiation, or whether non-dmPGE2 components mediate the protection effect. The metabolism of endogenous PGE2 occurs rapidly via pulmonary circulation and has a half-life of ~30 s [376]. DmPGE2 has two methyl groups at position 16, rendering it resistant to 15-hydroxy PGDH degradation [377] and extending its half-life to 20-25 min (unpublished data). Although dmPGE2 has a longer half-life than regular PGE2, the half-life of dmPGE2 is still much shorter than the

dmPGE2 radioprotectant time-window (3 hr prior to TBI). It is possible that dmPGE2 protection is not dependent on a specific lowest presence level or a threshold of dmPGE2 in bone marrow or peripheral blood. Another early study also indicate this possibility by detecting the dmPGE2 concentration in plasma, spleen and BM after injection, where they found that dmPGE2 concentrations in BM and spleen are higher in 1 hr post-injection than 5 min post-injection, whereas the -5 min dmPGE2 protection effect is better than -1 hr administration [134]. The lack of correlation between drug concentration and protection effect indicates that dmPGE2-induced activities are receptor mediated.

There are several potential mechanisms for dmPGE2 radioprotection. First, free radical scavenger is supposed to be the mechanism for protectants with sulfhydryl (thiol) group such as amifostine or glutathione [378]. However, dmPGE2 does not have sulfhydryl (thiol) group and at 30 min after injection most dmPGE2 in tissue are still in unmetabolized status, so at least it seems not a direct scavenger effect. Future study would focus on the detection of intracellular sulfhydryl containing compounds, such as glutathione, induced by the radioprotectant in a relative short time (considering the time-window for radioprotectant dmPGE2 could be as short as -5 min to -15 min prior to irradiation). Second, inhibiting cell cycling or redistributing cell cycle to late S phase could decrease the DNA damages brought by irradiation and thus increase survival. However, as described in previous chapter, the dmPGE2 suppression on HSPC proliferation is longer than 24 hr after injection but the -24 hr dmPGE2 schedule is not radioprotectant, which challenge the cell cycle inhibition theory; what's more, considering as short as -5 min prior irradiation could provide radioprotection [134], it is

almost impossible to redistribute cell cycle to late S phase in such short time. Last, changing microenvironment, such as hypoxia environment, is also a potential mechanism for radioprotectant and this is also a mechanism for radioresistant cancer cells. Although lack of direct evidence that dmPGE2 could induce hypoxia, considering one of its physiological effect is vasodilation, which means bring more oxygen to tissues, challenges this hypothesis [132]. Among all these mechanisms, the future studies focusing on accumulated intracellular sulfhydryl compounds [132] and/or elevated cAMP [379] induced by PGE2 receptor activation are promising.

Here, results suggest that EP4 agonist increases day 30 survival compared to Veh and other EP agonists (Figure 23), but the survival rate with was considerably lower than observed with dmPGE2 treatment. Although EP1, 2, and 3 agonists fail to show similar protection, it cannot be ruled out that the protective effect is mediated through a combination of all three or four agonists. In order to further verify the responsible EP receptor, future experiments need to include an EP 2+3+4 agonist combination group, or use EP agonist which hits all EP receptors (such as misoprostol), or seek a more potent EP4 agonist, or test an intensive EP4 agonist regimen.

In bone marrow, non-dmPGE2 components such as KC (Figure 25), may be regulated by dmPGE2 shortly after dmPGE2 injection. The contribution of these cytokines to the radioprotective activity of dmPGE2 will be assessed in future experiments by injecting the cytokines prior to TBI. The potential for dmPGE2 to regulate non-protein components, such as the sulfhydryl compounds as observed with

PGE2 gastric cytoprotection, cannot be ruled out [380, 381]. Considering the complexity of the role of PGE2 in normal physiological processes, it is highly possible that dmPGE2 radioprotection involves multiple molecules or pathways. The RNA sequencing and IPA analysis on the LMPP and CLP population, which under the protection of dmPGE2, would be helpful in identifying more lymphoid-related genes and reveal which differentiation stage dmPGE2 protection targets on.

### 6.3. Polypharmacy of peg-HGFs and dmPGE2

Peg-HGFs are effective radiomitigators, treatment with multiple peg-HGFs increases the survival rate following TBI (Figure 42). Although mice receiving peg-HGFs had accelerated CBC recovery at around day 20 post-TBI (Figure 48), the treatment did not ameliorate low WBC, NE, and LY counts at their nadir (day 10 post-TBI). DmPGE2 similarly increased the day 30 survival rate when used as a radioprotectant, and increased WBC and NE levels at day 10 post-TBI. DmPGE2 did not increase LY levels at day 10 post-TBI, and prolonged LY recovery until day 30 (Figure 24). DEARE mice receiving peg-HGF treatment at young age showed a trend of a more involuted thymus than Veh-treated mice (Figure 60), whereas mice receiving dmPGE2 treatment had better thymic reconstitution than Veh-treated mice (Figure 27). The lower WBC, NE, or LY post-TBI in H-ARS mice and involuted thymus in DEARE mice contribute to the higher opportunistic infection rate and death rate. A polypharmacy strategy combining dmPGE2 as radioprotectant and peg-HGFs as radiomitigator will be investigated in the future, which may further enhance hematopoiesis post-TBI. Additionally, this combined therapy may reduce the required dose of dmPGE2, alleviating the side effects associated with a

higher dose. Combining the dmPGE2 radioprotective protection of HSCs from radiation damage and peg-HGF radiomitigating promotion of HPC proliferation and differentiation may result in a beneficial synergistic effect.

### 6.4. DmPGE2 used in the scenarios of chemotherapy or radiotherapy

Patients undergoing chemotherapy or radiotherapy for malignancy or bone marrow transplantation have been successfully treated with HGFs and peg-HGFs. There are a limited number of FDA-approved radioprotectants. The only FDA-approved cytoprotectant for chemotherapy and radiotherapy is Amifostine. Although dmPGE2 as a radioprotectant greatly enhances day 30 survival, accelerates hematopoiesis recovery, and prevents myeloid skewing in DEARE mice, there is a concern that dmPGE2 may protect cancer cells and thus increase recurrence rate.

Recently, endogenous PGE2 has been shown to play an important role in tumorigenesis. COX-2, a key enzyme in the prostaglandin synthesis pathway, is overexpressed in 80-85% of adenocarcinomas [382]. Prostaglandin E synthase 2 (PTGES2), the enzyme catalyzing the final step of PGE2 synthesis, has a higher expression level in endometrial cancer tissue than in normal tissue [383]. The concentration of PGE2 is increased five-fold in breast cancer tissue compared with normal tissue [384]. The expression level of 15-hydroxyprostaglandin dehydrogenase (15-PGDH), an important enzyme responsible to the degradation of PGE2, is lower in colorectal cancer than in normal tissue [385]. Administration of a COX-2 inhibitor or EP4 antagonist inhibits cancer growth and metastasis through inhibiting

lymphangiogenesis and angiogenesis in a breast cancer mouse model [386]. Clinically, celecoxib, a selective COX-2 inhibitor, has been approved by the FDA for the treatment of familial adenomatous polyposis (FAP) [387]. Clinical trials on celecoxib or aspirin for cancer primary prevention are ongoing [388].

In addition to studies suggesting that PGE2 is a driver of cancer, a few studies indicate that it may also play an anti-cancer role. Wilson et al. reported that weekly injections of dmPGE2 for 12 weeks in APCMin$^{/+}$ mice reduced the size and number of GI adenomas in comparison with control-treated mice. Although this study's result is the opposite to other findings, it indicates that the effects on cancer cells from PGE2 are more complicated than initially thought, and the effect of exogenous vs. endogenous PGE2 might be different [389, 390].

In most PGE2 studies indicating a pro-cancer effect, the focus was on endogenous, long-lasting exposure to PGE2. A one-time injection of dmPGE2 would be metabolized quickly and thus may not drive tumorigenesis. Considering the hypovascularity and low PH in the cancer microenvironment, which is different from normal tissue, the amount of PGE2 exposure in cancer compared with in normal tissue following dmPGE2 treatment is likely to be considerably different. Since the concentration of endogenous PGE2 in the cancer microenvironment is elevated in compared with normal tissue [384], the increase brought about by a one-time dmPGE2 injection might be negligible in cancer tissue, but sufficient to provide radioprotection in normal tissue.

Future studies will therefore investigate the impact of dmPGE2 on tumorigenesis and using dmPGE2 before radiotherapy in a tumor-bearing mouse model. If dmPGE2 increases survival and boosts immune reconstitution, but does not impact the effect of radiotherapy and increase the cancer relapse rate in the long-term, it will be a strong candidate for preventing radiation effects in cancer patients.

However, the double-hit to lymphoid cells from dmPGE2 and radiotherapy may prolong the lymphoid cell inhibition period. Whether the risk for infection will increase, especially opportunistic viral infection, needs further evaluation. Additionally, the lymphocyte percentage in humans (20-30%) and mice (60-90%) is different, and the observation of initial inhibition and later recovery of lymphopoiesis in dmPGE2 injected mice might not appear in humans. A non-human primate study is necessary before progressing to human clinical trial.

REFERENCES


1. Putnam, F.W., The Atomic Bomb Casualty Commission in retrospect. Proc Natl Acad Sci U S A, 1998. 95(10): p. 5426-31.
2. Cerezo, L., Radiation accidents and incidents. What do we know about the medical management of acute radiation syndrome? Rep Pract Oncol Radiother, 2011. 16(4): p. 119-22.
3. Ozasa, K., et al., Studies of the mortality of atomic bomb survivors, Report 14, 1950-2003: an overview of cancer and noncancer diseases. Radiat Res, 2012. 177(3): p. 229-43.
4. Kamiya, K., et al., Long-term effects of radiation exposure on health. Lancet, 2015. 386(9992): p. 469-78.
5. Petryna, A., Nuclear Payouts: Knowledge and Compensation in the Chernobyl Aftermath. Anthropology Now, 2009. 1(2): p. 30-39.
6. McCall, C., Chernobyl disaster 30 years on: lessons not learned. Lancet, 2016. 387(10029): p. 1707-8.
7. Hatch, M. and E. Cardis, Somatic health effects of Chernobyl: 30 years on. Eur J Epidemiol, 2017. 32(12): p. 1047-1054.
8. Yamashita, S., et al., Lessons from Fukushima: Latest Findings of Thyroid Cancer After the Fukushima Nuclear Power Plant Accident. Thyroid, 2018. 28(1): p. 11-22.
9. Kristensen, H.M. and R.S. Norris, Global nuclear weapons inventories, 1945–2013. Bulletin of the Atomic Scientists, 2013. 69(5): p. 75-81.

10. Sovacool, B.K., A Critical Evaluation of Nuclear Power and Renewable Electricity in Asia. Journal of Contemporary Asia, 2010. 40(3): p. 369-400.
11. Christensen, D.M., C.J. Iddins, and S.L. Sugarman, Ionizing radiation injuries and illnesses. Emerg Med Clin North Am, 2014. 32(1): p. 245-65.
12. Gofman, J.W., Radiation and Human Health. 1981, San Francisco, CA, USA: Random House, Inc.
13. Christensen, D.M., et al., Management of ionizing radiation injuries and illnesses, part 1: physics, radiation protection, and radiation instrumentation. J Am Osteopath Assoc, 2014. 114(3): p. 189-99.
14. Glarum, J., D. Birou, and E. Cetaruk, 2 - Assessment of Likely Mass Casualty Events and Potential Hospital Impact, in Hospital Emergency Response Teams, J. Glarum, D. Birou, and E. Cetaruk, Editors. 2010, Butterworth-Heinemann: Boston. p. 19-83.
15. Dainiak, N., et al., The hematologist and radiation casualties. Hematology Am Soc Hematol Educ Program, 2003: p. 473-96.
16. Baljinnyam, E., et al., Effect of densely ionizing radiation on cardiomyocyte differentiation from human-induced pluripotent stem cells. Physiol Rep, 2017. 5(15).
17. Azzam, E.I., J.P. Jay-Gerin, and D. Pain, Ionizing radiation-induced metabolic oxidative stress and prolonged cell injury. Cancer Lett, 2012. 327(1-2): p. 48-60.
18. Reisz, J.A., et al., Effects of ionizing radiation on biological molecules--mechanisms of damage and emerging methods of detection. Antioxid Redox Signal, 2014. 21(2): p. 260-92.

19. Cadenas, E. and K.J. Davies, Mitochondrial free radical generation, oxidative stress, and aging. Free Radic Biol Med, 2000. 29(3-4): p. 222-30.

20. Boveris, A. and B. Chance, The mitochondrial generation of hydrogen peroxide. General properties and effect of hyperbaric oxygen. Biochem J, 1973. 134(3): p. 707-16.

21. Phaniendra, A., D.B. Jestadi, and L. Periyasamy, Free radicals: properties, sources, targets, and their implication in various diseases. Indian J Clin Biochem, 2015. 30(1): p. 11-26.

22. Cheng, X. and A.S. Ivessa, The migration of mitochondrial DNA fragments to the nucleus affects the chronological aging process of Saccharomyces cerevisiae. Aging Cell, 2010. 9(5): p. 919-23.

23. Brand, R.M., et al., Targeting Mitochondrial Oxidative Stress to Mitigate UV-Induced Skin Damage. Front Pharmacol, 2018. 9: p. 920.

24. Kalyanaraman, B., et al., Teaching the basics of reactive oxygen species and their relevance to cancer biology: Mitochondrial reactive oxygen species detection, redox signaling, and targeted therapies. Redox Biol, 2018. 15: p. 347-362.

25. Davey, K.M., et al., Mutation of DNAJC19, a human homologue of yeast inner mitochondrial membrane co-chaperones, causes DCMA syndrome, a novel autosomal recessive Barth syndrome-like condition. J Med Genet, 2006. 43(5): p. 385-93.

26. MacKenzie, J.A. and R.M. Payne, Mitochondrial protein import and human health and disease. Biochim Biophys Acta, 2007. 1772(5): p. 509-23.

27. Hall, E.J. and A.J. Giaccia, Radiobiology for the Radiologist. 7th edition ed. 2012, Philadelphia, PA, USA: Lippincott Williams & Wilkins.

28. Gaziev, A.I. and G.O. Shaikhaev, [Ionizing radiation can activate the insertion of mitochondrial DNA fragments in the nuclear genome]. Radiats Biol Radioecol, 2007. 47(6): p. 673-83.

29. Calveley, V.L., et al., Partial volume rat lung irradiation: temporal fluctuations of in-field and out-of-field DNA damage and inflammatory cytokines following irradiation. Int J Radiat Biol, 2005. 81(12): p. 887-99.

30. Najafi, M., et al., The mechanisms of radiation-induced bystander effect. J Biomed Phys Eng, 2014. 4(4): p. 163-72.

31. Bergonie, J. and L. Tribondeau, Interpretation of some results of radiotherapy and an attempt at determining a logical technique of treatment. Radiat Res, 1959. 11: p. 587-8.

32. Donnelly, E.H., et al., Acute radiation syndrome: assessment and management. South Med J, 2010. 103(6): p. 541-6.

33. López, M. and M. Martín, Medical management of the acute radiation syndrome. Reports of practical oncology and radiotherapy : journal of Greatpoland Cancer Center in Poznan and Polish Society of Radiation Oncology, 2011. 16(4): p. 138-146.

34. Seedhouse, E., Space Radiation and Astronaut Safety. 2018, Cham, Switzerland: Springer.

35. Elliott, T.B., et al., Gastrointestinal acute radiation syndrome in Gottingen minipigs (Sus scrofa domestica). Comp Med, 2014. 64(6): p. 456-63.

36. Swartz, H.M., B.B. Williams, and A.B. Flood, Overview of the principles and practice of biodosimetry. Radiation and environmental biophysics, 2014. 53(2): p. 221-232.

37. Goans, R.E., et al., Early dose assessment in criticality accidents. Health Phys, 2001. 81(4): p. 446-9.

38. Christensen, D.M., et al., Management of ionizing radiation injuries and illnesses, part 4: acute radiation syndrome. J Am Osteopath Assoc, 2014. 114(9): p. 702-11.

39. Blakely, E.A., Biological effects of cosmic radiation: deterministic and stochastic. Health Phys, 2000. 79(5): p. 495-506.

40. Chua, H.L., et al., Long-term hematopoietic stem cell damage in a murine model of the hematopoietic syndrome of the acute radiation syndrome. Health Phys, 2012. 103(4): p. 356-66.

41. Unthank, J.L., et al., Delayed Effects of Acute Radiation Exposure in a Murine Model of the H-ARS: Multiple-Organ Injury Consequent to <10 Gy Total Body Irradiation. Health Phys, 2015. 109(5): p. 511-21.

42. Chouker, A., Stress Challenges and Immunity in Space. 2020, Cham, Switzerland: Springer.

43. Yamada, M., et al., Noncancer disease incidence in atomic bomb survivors, 1958-1998. Radiat Res, 2004. 161(6): p. 622-32.

44. Hauer-Jensen, M., J.W. Denham, and H.J.N. Andreyev, Radiation enteropathy--pathogenesis, treatment and prevention. Nature reviews. Gastroenterology & hepatology, 2014. 11(8): p. 470-479.

45. Kal, H.B. and M.L. van Kempen-Harteveld, Renal dysfunction after total body irradiation: dose-effect relationship. Int J Radiat Oncol Biol Phys, 2006. 65(4): p. 1228-32.

46. Williams, J.P., C.J. Johnston, and J.N. Finkelstein, Treatment for radiation-induced pulmonary late effects: spoiled for choice or looking in the wrong direction? Current drug targets, 2010. 11(11): p. 1386-1394.

47. Movsas, B., et al., Pulmonary radiation injury. Chest, 1997. 111(4): p. 1061-76.

48. Durand, T., et al., Cognitive outcome after radiotherapy in brain tumor. Curr Opin Oncol, 2015. 27(6): p. 510-5.

49. Yamada, M.K., A link between vascular damage and cognitive deficits after whole-brain radiation therapy for cancer: A clue to other types of dementia? Drug Discov Ther, 2016. 10(2): p. 79-81.

50. Douple, E.B., et al., Long-term radiation-related health effects in a unique human population: lessons learned from the atomic bomb survivors of Hiroshima and Nagasaki. Disaster medicine and public health preparedness, 2011. 5 Suppl 1(0 1): p. S122-S133.

51. Furukawa, K., et al., Predicting future excess events in risk assessment. Risk Anal, 2009. 29(6): p. 885-99.

52. Finch, S.C., et al., Detection of Leukemia and Related Disorders, Hiroshima and Nagasaki: Research Plan. 1965, Hiroshima, Japan: Atomic Bomb Casualty Commission.

53. Preston, D.L., et al., Effect of recent changes in atomic bomb survivor dosimetry on cancer mortality risk estimates. Radiat Res, 2004. 162(4): p. 377-89.

54. Iwanaga, M., et al., Risk of myelodysplastic syndromes in people exposed to ionizing radiation: a retrospective cohort study of Nagasaki atomic bomb survivors. J Clin Oncol, 2011. 29(4): p. 428-34.

55. Preston, D.L., et al., Cancer incidence in atomic bomb survivors. Part III. Leukemia, lymphoma and multiple myeloma, 1950-1987. Radiat Res, 1994. 137(2 Suppl): p. S68-97.

56. Wang, Y., et al., Total body irradiation causes residual bone marrow injury by induction of persistent oxidative stress in murine hematopoietic stem cells. Free Radic Biol Med, 2010. 48(2): p. 348-56.

57. Wang, Y., et al., Total body irradiation selectively induces murine hematopoietic stem cell senescence. Blood, 2006. 107(1): p. 358-66.

58. Shinjo, K., et al., Granulocyte colony-stimulating factor receptor at various differentiation stages of normal and leukemic hematopoietic cells. Leuk Lymphoma, 1997. 25(1-2): p. 37-46.

59. Yu, H., et al., Deletion of Puma protects hematopoietic stem cells and confers long-term survival in response to high-dose gamma-irradiation. Blood, 2010. 115(17): p. 3472-80.

60. Tichy, A., et al., Ataxia-telangiectasia mutated kinase (ATM) as a central regulator of radiation-induced DNA damage response. Acta Medica (Hradec Kralove), 2010. 53(1): p. 13-7.

61. Ito, K. and T. Suda, Metabolic requirements for the maintenance of self-renewing stem cells. Nat Rev Mol Cell Biol, 2014. 15(4): p. 243-56.

62. Beausejour, C.M., et al., Reversal of human cellular senescence: roles of the p53 and p16 pathways. Embo j, 2003. 22(16): p. 4212-22.

63. Herranz, N. and J. Gil, Mechanisms and functions of cellular senescence. J Clin Invest, 2018. 128(4): p. 1238-1246.

64. Piccoli, C., et al., Characterization of mitochondrial and extra-mitochondrial oxygen consuming reactions in human hematopoietic stem cells. Novel evidence of the occurrence of NAD(P)H oxidase activity. J Biol Chem, 2005. 280(28): p. 26467-76.

65. Shao, L., Y. Luo, and D. Zhou, Hematopoietic stem cell injury induced by ionizing radiation. Antioxid Redox Signal, 2014. 20(9): p. 1447-62.

66. Carbonneau, C.L., et al., Ionizing radiation-induced expression of INK4a/ARF in murine bone marrow-derived stromal cell populations interferes with bone marrow homeostasis. Blood, 2012. 119(3): p. 717-26.

67. Hooper, A.T., et al., Engraftment and reconstitution of hematopoiesis is dependent on VEGFR2-mediated regeneration of sinusoidal endothelial cells. Cell Stem Cell, 2009. 4(3): p. 263-74.

68. Waselenko, J.K., et al., Medical management of the acute radiation syndrome: recommendations of the Strategic National Stockpile Radiation Working Group. Ann Intern Med, 2004. 140(12): p. 1037-51.

69. Plett, P.A., et al., Establishing a murine model of the hematopoietic syndrome of the acute radiation syndrome. Health Phys, 2012. 103(4): p. 343-55.

70. Liongue, C., et al., Granulocyte colony-stimulating factor receptor: stimulating granulopoiesis and much more. Int J Biochem Cell Biol, 2009. 41(12): p. 2372-5.

71. Panopoulos, A.D. and S.S. Watowich, Granulocyte colony-stimulating factor: molecular mechanisms of action during steady state and 'emergency' hematopoiesis. Cytokine, 2008. 42(3): p. 277-88.

72. Ruef, C. and D.L. Coleman, Granulocyte-macrophage colony-stimulating factor: pleiotropic cytokine with potential clinical usefulness. Rev Infect Dis, 1990. 12(1): p. 41-62.

73. Mehta, H.M., M. Malandra, and S.J. Corey, G-CSF and GM-CSF in Neutropenia. J Immunol, 2015. 195(4): p. 1341-9.

74. Plett, P.A., et al., PEGylated G-CSF (BBT-015), GM-CSF (BBT-007), and IL-11 (BBT-059) analogs enhance survival and hematopoietic cell recovery in a mouse model of the hematopoietic syndrome of the acute radiation syndrome. Health Phys, 2014. 106(1): p. 7-20.

75. Ventevogel, M.S. and G.D. Sempowski, Thymic rejuvenation and aging. Curr Opin Immunol, 2013. 25(4): p. 516-22.

76. van Heijst, J.W., et al., Quantitative assessment of T cell repertoire recovery after hematopoietic stem cell transplantation. Nat Med, 2013. 19(3): p. 372-7.

77. Frasca, D., et al., Hematopoietic reconstitution after lethal irradiation and bone marrow transplantation: effects of different hematopoietic cytokines on the recovery of thymus, spleen and blood cells. Bone Marrow Transplant, 2000. 25(4): p. 427-33.

78. Morrissey, P.J., et al., Administration of IL-7 to mice with cyclophosphamide-induced lymphopenia accelerates lymphocyte repopulation. J Immunol, 1991. 146(5): p. 1547-52.

79. Barata, J.T., et al., Interleukin-7 promotes survival and cell cycle progression of T-cell acute lymphoblastic leukemia cells by down-regulating the cyclin-dependent kinase inhibitor p27(kip1). Blood, 2001. 98(5): p. 1524-31.

80. Farrell, C.L., et al., Keratinocyte growth factor protects mice from chemotherapy and radiation-induced gastrointestinal injury and mortality. Cancer Res, 1998. 58(5): p. 933-9.

81. Min, D., et al., Protection from thymic epithelial cell injury by keratinocyte growth factor: a new approach to improve thymic and peripheral T-cell reconstitution after bone marrow transplantation. Blood, 2002. 99(12): p. 4592-600.

82. Mooney, C.J., et al., Selective Expression of Flt3 within the Mouse Hematopoietic Stem Cell Compartment. Int J Mol Sci, 2017. 18(5).

83. Neipp, M., et al., Effect of FLT3 ligand and granulocyte colony-stimulating factor on expansion and mobilization of facilitating cells and hematopoietic stem cells in mice: kinetics and repopulating potential. Blood, 1998. 92(9): p. 3177-88.

84. Streeter, P.R., et al., Progenipoietins: biological characterization of a family of dual agonists of fetal liver tyrosine kinase-3 and the granulocyte colony-stimulating factor receptor. Exp Hematol, 2001. 29(1): p. 41-50.

85. Streeter, P.R., L.Z. Dudley, and W.H. Fleming, Activation of the G-CSF and Flt-3 receptors protects hematopoietic stem cells from lethal irradiation. Exp Hematol, 2003. 31(11): p. 1119-25.

86. Herodin, F., et al., Short-term injection of antiapoptotic cytokine combinations soon after lethal gamma -irradiation promotes survival. Blood, 2003. 101(7): p. 2609-16.

87. Schmieder, R.E., et al., Renin-angiotensin system and cardiovascular risk. Lancet, 2007. 369(9568): p. 1208-19.

88. Paul, M., A. Poyan Mehr, and R. Kreutz, Physiology of local renin-angiotensin systems. Physiol Rev, 2006. 86(3): p. 747-803.

89. Yusuf, S., et al., Effects of an angiotensin-converting-enzyme inhibitor, ramipril, on cardiovascular events in high-risk patients. N Engl J Med, 2000. 342(3): p. 145-53.

90. Chappell, M.C., Biochemical evaluation of the renin-angiotensin system: the good, bad, and absolute? Am J Physiol Heart Circ Physiol, 2016. 310(2): p. H137-52.

91. Rodgers, K.E., et al., Effect of angiotensin II on hematopoietic progenitor cell proliferation. Stem Cells, 2000. 18(4): p. 287-94.

92. Mrug, M., et al., Angiotensin II stimulates proliferation of normal early erythroid progenitors. J Clin Invest, 1997. 100(9): p. 2310-4.

93. Ellefson, D.D., et al., Synergistic effects of co-administration of angiotensin 1-7 and Neupogen on hematopoietic recovery in mice. Cancer Chemother Pharmacol, 2004. 53(1): p. 15-24.

94. Durik, M., B. Seva Pessoa, and A.J. Roks, The renin-angiotensin system, bone marrow and progenitor cells. Clin Sci (Lond), 2012. 123(4): p. 205-23.

95. Barshishat-Kupper, M., et al., Captopril modulates hypoxia-inducible factors and erythropoietin responses in a murine model of total body irradiation. Exp Hematol, 2011. 39(3): p. 293-304.

96. Rodgers, K.E. and G.S. Dizerega, Contribution of the Local RAS to Hematopoietic Function: A Novel Therapeutic Target. Front Endocrinol (Lausanne), 2013. 4: p. 157.

97. Griffing, G.T. and J.C. Melby, Enalapril (MK-421) and the white cell count and haematocrit. Lancet, 1982. 1(8285): p. 1361.

98. Marathias, K.P., et al., Hematocrit-lowering effect following inactivation of renin-angiotensin system with angiotensin converting enzyme inhibitors and angiotensin receptor blockers. Curr Top Med Chem, 2004. 4(4): p. 483-6.

99. Charrier, S., et al., Inhibition of angiotensin I-converting enzyme induces radioprotection by preserving murine hematopoietic short-term reconstituting cells. Blood, 2004. 104(4): p. 978-85.

100. Day, R.M., et al., Enhanced hematopoietic protection from radiation by the combination of genistein and captopril. Int Immunopharmacol, 2013. 15(2): p. 348-56.

101. McCart, E.A., et al., Delayed Captopril Administration Mitigates Hematopoietic Injury in a Murine Model of Total Body Irradiation. Sci Rep, 2019. 9(1): p. 2198.

102. Conti, S., P. Cassis, and A. Benigni, Aging and the renin-angiotensin system. Hypertension, 2012. 60(4): p. 878-83.

103. Davis, T.A., et al., Timing of captopril administration determines radiation protection or radiation sensitization in a murine model of total body irradiation. Exp Hematol, 2010. 38(4): p. 270-81.

104. Azizi, M., et al., Acute angiotensin-converting enzyme inhibition increases the plasma level of the natural stem cell regulator N-acetyl-seryl-aspartyl-lysyl-proline. J Clin Invest, 1996. 97(3): p. 839-44.

105. Rousseau-Plasse, A., et al., Lisinopril, an angiotensin I-converting enzyme inhibitor, prevents entry of murine hematopoietic stem cells into the cell cycle after irradiation in vivo. Exp Hematol, 1998. 26(11): p. 1074-9.

106. Moulder, J.E. and E.P. Cohen, Future strategies for mitigation and treatment of chronic radiation-induced normal tissue injury. Semin Radiat Oncol, 2007. 17(2): p. 141-8.

107. Fish, B.L., et al., Combined Hydration and Antibiotics with Lisinopril to Mitigate Acute and Delayed High-dose Radiation Injuries to Multiple Organs. Health Phys, 2016. 111(5): p. 410-9.

108. Harizi, H., J.B. Corcuff, and N. Gualde, Arachidonic-acid-derived eicosanoids: roles in biology and immunopathology. Trends Mol Med, 2008. 14(10): p. 461-9.

109. Ricciotti, E. and G.A. FitzGerald, Prostaglandins and inflammation. Arterioscler Thromb Vasc Biol, 2011. 31(5): p. 986-1000.

110. Smyth, E.M., et al., Prostanoids in health and disease. J Lipid Res, 2009. 50 Suppl: p. S423-8.

111. Nasrallah, R., R. Hassouneh, and R.L. Hebert, PGE2, Kidney Disease, and Cardiovascular Risk: Beyond Hypertension and Diabetes. J Am Soc Nephrol, 2016. 27(3): p. 666-76.

112. Norregaard, R., T.H. Kwon, and J. Frokiaer, Physiology and pathophysiology of cyclooxygenase-2 and prostaglandin E2 in the kidney. Kidney Res Clin Pract, 2015. 34(4): p. 194-200.

113. Claria, J., Cyclooxygenase-2 biology. Curr Pharm Des, 2003. 9(27): p. 2177-90.

114. Gomez, I., et al., The role of prostaglandin E2 in human vascular inflammation. Prostaglandins Leukot Essent Fatty Acids, 2013. 89(2-3): p. 55-63.

115. Kalinski, P., Regulation of immune responses by prostaglandin E2. J Immunol, 2012. 188(1): p. 21-8.

116. Markovič, T., et al., Structural features of subtype-selective EP receptor modulators. Drug Discov Today, 2017. 22(1): p. 57-71.

117. Dey, I., M. Lejeune, and K. Chadee, Prostaglandin E2 receptor distribution and function in the gastrointestinal tract. Br J Pharmacol, 2006. 149(6): p. 611-23.

118. Markovic, T., et al., Structural features of subtype-selective EP receptor modulators. Drug Discov Today, 2017. 22(1): p. 57-71.

119. Nishigaki, N., M. Negishi, and A. Ichikawa, Two Gs-coupled prostaglandin E receptor subtypes, EP2 and EP4, differ in desensitization and sensitivity to the metabolic inactivation of the agonist. Mol Pharmacol, 1996. 50(4): p. 1031-7.

120. Bilson, H.A., D.L. Mitchell, and B. Ashby, Human prostaglandin EP3 receptor isoforms show different agonist-induced internalization patterns. FEBS Lett, 2004. 572(1-3): p. 271-5.

121. Pelus, L.M., H.E. Broxmeyer, and M.A. Moore, Regulation of human myelopoiesis by prostaglandin E and lactoferrin. Cell Tissue Kinet, 1981. 14(5): p. 515-26.

122. Pelus, L.M., et al., Regulation of macrophage and granulocyte proliferation. Specificities of prostaglandin E and lactoferrin. J Exp Med, 1979. 150(2): p. 277-92.

123. Gentile, P., D. Byer, and L.M. Pelus, In vivo modulation of murine myelopoiesis following intravenous administration of prostaglandin E2. Blood, 1983. 62(5): p. 1100-7.

124. Lu, L., et al., Prostaglandin E acts at two levels to enhance colony formation in vitro by erythroid (BFU-E) progenitor cells. Exp Hematol, 1987. 15(7): p. 765-71.

125. Lu, L., L.M. Pelus, and H.E. Broxmeyer, Modulation of the expression of HLA-DR (Ia) antigens and the proliferation of human erythroid (BFU-E) and multipotential (CFU-GEMM) progenitor cells by prostaglandin E. Exp Hematol, 1984. 12(9): p. 741-8.

126. Lu, L., et al., Enhancement of the proliferation of human marrow erythroid (BFU-E) progenitor cells by prostaglandin E requires the participation of OKT8-positive T lymphocytes and is associated with the density expression of major histocompatibility complex class II antigens on BFU-E. Blood, 1986. 68(1): p. 126-33.

127. North, T.E., et al., Prostaglandin E2 regulates vertebrate haematopoietic stem cell homeostasis. Nature, 2007. 447(7147): p. 1007-11.

128. Hoggatt, J., et al., Prostaglandin E2 enhances hematopoietic stem cell homing, survival, and proliferation. Blood, 2009. 113(22): p. 5444-55.

129. Frisch, B.J., et al., In vivo prostaglandin E2 treatment alters the bone marrow microenvironment and preferentially expands short-term hematopoietic stem cells. Blood, 2009. 114(19): p. 4054-63.

130. Pelus, L.M. and J. Hoggatt, Pleiotropic effects of prostaglandin E2 in hematopoiesis; prostaglandin E2 and other eicosanoids regulate hematopoietic stem and progenitor cell function. Prostaglandins Other Lipid Mediat, 2011. 96(1-4): p. 3-9.

131. Hoggatt, J., et al., Differential stem- and progenitor-cell trafficking by prostaglandin E2. Nature, 2013. 495(7441): p. 365-9.

132. Hanson, W.R. and C. Thomas, 16, 16-dimethyl prostaglandin E2 increases survival of murine intestinal stem cells when given before photon radiation. Radiat Res, 1983. 96(2): p. 393-8.

133. Hanson, W.R. and D.J. Grdina, Radiation-induced DNA single-strand breaks in the intestinal mucosal cells of mice treated with the radioprotectors WR-2721 or 16-16 dimethyl prostaglandin E2. Int J Radiat Biol Relat Stud Phys Chem Med, 1987. 52(1): p. 67-76.

134. Walden, T.L., Jr., M. Patchen, and S.L. Snyder, 16,16-Dimethyl prostaglandin E2 increases survival in mice following irradiation. Radiat Res, 1987. 109(3): p. 440-8.

135. Hoggatt, J., et al., Recovery from hematopoietic injury by modulating prostaglandin E(2) signaling post-irradiation. Blood Cells Mol Dis, 2013. 50(3): p. 147-53.

136. Jacobson, L.O., et al., The role of the spleen in radiation injury and recovery. J Lab Clin Med, 1950. 35(5): p. 746-70.

137. Till, J.E. and C.E. Mc, A direct measurement of the radiation sensitivity of normal mouse bone marrow cells. Radiat Res, 1961. 14: p. 213-22.

138. Becker, A.J., C.E. Mc, and J.E. Till, Cytological demonstration of the clonal nature of spleen colonies derived from transplanted mouse marrow cells. Nature, 1963. 197: p. 452-4.

139. Bradley, T.R. and D. Metcalf, The growth of mouse bone marrow cells in vitro. Aust J Exp Biol Med Sci, 1966. 44(3): p. 287-99.

140. Stephenson, J.R., et al., Induction of colonies of hemoglobin-synthesizing cells by erythropoietin in vitro. Proc Natl Acad Sci U S A, 1971. 68(7): p. 1542-6.

141. Iscove, N.N. and F. Sieber, Erythroid progenitors in mouse bone marrow detected by macroscopic colony formation in culture. Exp Hematol, 1975. 3(1): p. 32-43.

142. Johnson, G.R. and D. Metcalf, Pure and mixed erythroid colony formation in vitro stimulated by spleen conditioned medium with no detectable erythropoietin. Proc Natl Acad Sci U S A, 1977. 74(9): p. 3879-82.

143. Whitlock, C.A., D. Robertson, and O.N. Witte, Murine B cell lymphopoiesis in long term culture. J Immunol Methods, 1984. 67(2): p. 353-69.

144. Reya, T., et al., Stem cells, cancer, and cancer stem cells. Nature, 2001. 414(6859): p. 105-11.

145. Harrison, D.E., Competitive repopulation: a new assay for long-term stem cell functional capacity. Blood, 1980. 55(1): p. 77-81.

146. Harrison, D.E., et al., Primitive hemopoietic stem cells: direct assay of most productive populations by competitive repopulation with simple binomial, correlation and covariance calculations. Exp Hematol, 1993. 21(2): p. 206-19.

147. Chua, H.L., et al., Lifelong Residual bone Marrow Damage in Murine Survivors of the Hematopoietic Acute Radiation Syndrome (H-ARS): A Compilation of Studies Comprising the Indiana University Experience. Health Phys, 2019. 116(4): p. 546-557.

148. Benveniste, P., et al., Intermediate-term hematopoietic stem cells with extended but time-limited reconstitution potential. Cell Stem Cell, 2010. 6(1): p. 48-58.

149. Osawa, M., et al., Long-term lymphohematopoietic reconstitution by a single CD34-low/negative hematopoietic stem cell. Science, 1996. 273(5272): p. 242-5.

150. Morita, Y., H. Ema, and H. Nakauchi, Heterogeneity and hierarchy within the most primitive hematopoietic stem cell compartment. J Exp Med, 2010. 207(6): p. 1173-82.

151. Challen, G.A., et al., Mouse hematopoietic stem cell identification and analysis. Cytometry A, 2009. 75(1): p. 14-24.

152. Akashi, K., et al., A clonogenic common myeloid progenitor that gives rise to all myeloid lineages. Nature, 2000. 404(6774): p. 193-7.

153. Kondo, M., I.L. Weissman, and K. Akashi, Identification of clonogenic common lymphoid progenitors in mouse bone marrow. Cell, 1997. 91(5): p. 661-72.

154. Karsunky, H., et al., Flk2+ common lymphoid progenitors possess equivalent differentiation potential for the B and T lineages. Blood, 2008. 111(12): p. 5562-70.

155. Kiel, M.J., et al., SLAM family receptors distinguish hematopoietic stem and progenitor cells and reveal endothelial niches for stem cells. Cell, 2005. 121(7): p. 1109-21.

156. Oguro, H., L. Ding, and S.J. Morrison, SLAM family markers resolve functionally distinct subpopulations of hematopoietic stem cells and multipotent progenitors. Cell Stem Cell, 2013. 13(1): p. 102-16.

157. Adolfsson, J., et al., Upregulation of Flt3 expression within the bone marrow Lin(-)Sca1(+)c-kit(+) stem cell compartment is accompanied by loss of self-renewal capacity. Immunity, 2001. 15(4): p. 659-69.

158. Adolfsson, J., et al., Identification of Flt3+ lympho-myeloid stem cells lacking erythro-megakaryocytic potential a revised road map for adult blood lineage commitment. Cell, 2005. 121(2): p. 295-306.

159. Mackarehtschian, K., et al., Targeted disruption of the flk2/flt3 gene leads to deficiencies in primitive hematopoietic progenitors. Immunity, 1995. 3(1): p. 147-61.

160. Lyman, S.D. and S.E. Jacobsen, c-kit ligand and Flt3 ligand: stem/progenitor cell factors with overlapping yet distinct activities. Blood, 1998. 91(4): p. 1101-34.

161. McKenna, H.J., et al., Mice lacking flt3 ligand have deficient hematopoiesis affecting hematopoietic progenitor cells, dendritic cells, and natural killer cells. Blood, 2000. 95(11): p. 3489-97.

162. Sitnicka, E., et al., Key role of flt3 ligand in regulation of the common lymphoid progenitor but not in maintenance of the hematopoietic stem cell pool. Immunity, 2002. 17(4): p. 463-72.

163. Zriwil, A., et al., Direct role of FLT3 in regulation of early lymphoid progenitors. Br J Haematol, 2018. 183(4): p. 588-600.

164. Beaudin, A.E., S.W. Boyer, and E.C. Forsberg, Flk2/Flt3 promotes both myeloid and lymphoid development by expanding non-self-renewing multipotent hematopoietic progenitor cells. Exp Hematol, 2014. 42(3): p. 218-229.e4.

165. Laurenti, E. and B. Gottgens, From haematopoietic stem cells to complex differentiation landscapes. Nature, 2018. 553(7689): p. 418-426.

166. Gorgens, A., et al., Revision of the human hematopoietic tree: granulocyte subtypes derive from distinct hematopoietic lineages. Cell Rep, 2013. 3(5): p. 1539-52.

167. Drissen, R., et al., Distinct myeloid progenitor-differentiation pathways identified through single-cell RNA sequencing. Nat Immunol, 2016. 17(6): p. 666-676.

168. Zheng, S., et al., Molecular transitions in early progenitors during human cord blood hematopoiesis. Mol Syst Biol, 2018. 14(3): p. e8041.

169. Pellin, D., et al., A comprehensive single cell transcriptional landscape of human hematopoietic progenitors. Nat Commun, 2019. 10(1): p. 2395.

170. Pietras, E.M., et al., Functionally Distinct Subsets of Lineage-Biased Multipotent Progenitors Control Blood Production in Normal and Regenerative Conditions. Cell Stem Cell, 2015. 17(1): p. 35-46.

171. Sanjuan-Pla, A., et al., Platelet-biased stem cells reside at the apex of the haematopoietic stem-cell hierarchy. Nature, 2013. 502(7470): p. 232-6.

172. Muller-Sieburg, C.E., et al., Myeloid-biased hematopoietic stem cells have extensive self-renewal capacity but generate diminished lymphoid progeny with impaired IL-7 responsiveness. Blood, 2004. 103(11): p. 4111-8.

173. Yamamoto, R., et al., Clonal analysis unveils self-renewing lineage-restricted progenitors generated directly from hematopoietic stem cells. Cell, 2013. 154(5): p. 1112-1126.

174. Velten, L., et al., Human haematopoietic stem cell lineage commitment is a continuous process. Nat Cell Biol, 2017. 19(4): p. 271-281.

175. Buenrostro, J.D., et al., Integrated Single-Cell Analysis Maps the Continuous Regulatory Landscape of Human Hematopoietic Differentiation. Cell, 2018. 173(6): p. 1535-1548.e16.

176. Karamitros, D., et al., Single-cell analysis reveals the continuum of human lympho-myeloid progenitor cells. Nat Immunol, 2018. 19(1): p. 85-97.

177. Dzhagalov, I. and H. Phee, How to find your way through the thymus: a practical guide for aspiring T cells. Cell Mol Life Sci, 2012. 69(5): p. 663-82.

178. Zlotoff, D.A. and A. Bhandoola, Hematopoietic progenitor migration to the adult thymus. Ann N Y Acad Sci, 2011. 1217: p. 122-38.

179. Germain, R.N., T-cell development and the CD4-CD8 lineage decision. Nat Rev Immunol, 2002. 2(5): p. 309-22.

180. Dembic, Z., H. von Boehmer, and M. Steinmetz, The role of T-cell receptor alpha and beta genes in MHC-restricted antigen recognition. Immunol Today, 1986. 7(10): p. 308-11.

181. Davis, M.M. and P.J. Bjorkman, T-cell antigen receptor genes and T-cell recognition. Nature, 1988. 334(6181): p. 395-402.

182. Krogsgaard, M. and M.M. Davis, How T cells 'see' antigen. Nat Immunol, 2005. 6(3): p. 239-45.

183. Radtke, F., H.R. MacDonald, and F. Tacchini-Cottier, Regulation of innate and adaptive immunity by Notch. Nat Rev Immunol, 2013. 13(6): p. 427-37.

184. Baldwin, T.A., et al., The timing of TCR alpha expression critically influences T cell development and selection. J Exp Med, 2005. 202(1): p. 111-21.

185. Singer, A., S. Adoro, and J.H. Park, Lineage fate and intense debate: myths, models and mechanisms of CD4- versus CD8-lineage choice. Nat Rev Immunol, 2008. 8(10): p. 788-801.

186. Rezzani, R., et al., Thymus and aging: morphological, radiological, and functional overview. Age (Dordr), 2014. 36(1): p. 313-51.

187. Fink, P.J., The biology of recent thymic emigrants. Annu Rev Immunol, 2013. 31: p. 31-50.

188. Tanchot, C., et al., Conversion of naive T cells to a memory-like phenotype in lymphopenic hosts is not related to a homeostatic mechanism that fills the peripheral naive T cell pool. J Immunol, 2002. 168(10): p. 5042-6.

189. Bosco, N., et al., Auto-reconstitution of the T-cell compartment by radioresistant hematopoietic cells following lethal irradiation and bone marrow transplantation. Exp Hematol, 2010. 38(3): p. 222-232.e2.

190. Mueller, S.N., et al., Memory T cell subsets, migration patterns, and tissue residence. Annu Rev Immunol, 2013. 31: p. 137-61.

191. Kaech, S.M., Celebrating diversity in memory T cells. J Immunol, 2014. 192(3): p. 837-9.

192. Gray, D.H., et al., Developmental kinetics, turnover, and stimulatory capacity of thymic epithelial cells. Blood, 2006. 108(12): p. 3777-85.

193. Seach, N., M. Hammett, and A. Chidgey, Isolation, characterization, and reaggregate culture of thymic epithelial cells. Methods Mol Biol, 2013. 945: p. 251-72.

194. Zlotoff, D.A., et al., Delivery of progenitors to the thymus limits T-lineage reconstitution after bone marrow transplantation. Blood, 2011. 118(7): p. 1962-70.

195. Lai, A.Y. and M. Kondo, Identification of a bone marrow precursor of the earliest thymocytes in adult mouse. Proc Natl Acad Sci U S A, 2007. 104(15): p. 6311-6.

196. Saran, N., et al., Multiple extrathymic precursors contribute to T-cell development with different kinetics. Blood, 2010. 115(6): p. 1137-44.

197. Schwarz, B.A., et al., Selective thymus settling regulated by cytokine and chemokine receptors. J Immunol, 2007. 178(4): p. 2008-17.

198. Shi, Y. and M. Zhu, Medullary thymic epithelial cells, the indispensable player in central tolerance. Sci China Life Sci, 2013. 56(5): p. 392-8.

199. Aifantis, I., E. Raetz, and S. Buonamici, Molecular pathogenesis of T-cell leukaemia and lymphoma. Nat Rev Immunol, 2008. 8(5): p. 380-90.

200. Singh, V.K. and T.M. Seed, Pharmacological management of ionizing radiation injuries: current and prospective agents and targeted organ systems. Expert Opin Pharmacother, 2020. 21(3): p. 317-337.

201. Chua, H.L., et al., Survival efficacy of the pegylated G-CSF Maxy-G34 and Neulasta in a mouse model of lethal H-ARS, and residual bone marrow damage in treated survivors. Health Physics, 2014. 106(1): p. 21-38.

202. Hankey, K.G., et al., Pegfilgrastim Improves Survival of Lethally Irradiated Nonhuman Primates. Radiat Res, 2015. 183(6): p. 643-55.

203. Farese, A.M., et al., Filgrastim improves survival in lethally irradiated nonhuman primates. Radiat Res, 2013. 179(1): p. 89-100.

204. Satyamitra, M., et al., Impact of Abbreviated Filgrastim Schedule on Survival and Hematopoietic Recovery after Irradiation in Four Mouse Strains with Different Radiosensitivity. Radiat Res, 2017. 187(6): p. 659-671.

205. Sasaki, H., K. Kodama, and M. Yamada, A review of forty-five years study of Hiroshima and Nagasaki atomic bomb survivors. Aging. J Radiat Res, 1991. 32 Suppl: p. 310-26.

206. Bhatia, S., et al., Breast cancer and other second neoplasms after childhood Hodgkin's disease. N Engl J Med, 1996. 334(12): p. 745-51.

207. Denkinger, M.D., et al., HSC Aging and Senescent Immune Remodeling. Trends Immunol, 2015. 36(12): p. 815-824.

208. Unthank, J.L., et al., Cardiac and Renal Delayed Effects of Acute Radiation Exposure: Organ Differences in Vasculopathy, Inflammation, Senescence and Oxidative Balance. Radiat Res, 2019. 191(5): p. 383-397.

209. Shakhov, A.N., et al., Prevention and mitigation of acute radiation syndrome in mice by synthetic lipopeptide agonists of Toll-like receptor 2 (TLR2). PLoS One, 2012. 7(3): p. e33044.

210. Plett, P.A., et al., The H-ARS Dose Response Relationship (DRR): Validation and Variables. Health Phys, 2015. 109(5): p. 391-8.

211. Plett, P.A., et al., PEGylated G-CSF (BBT-015), GM-CSF (BBT-007), and IL-11 (BBT-059) analogs enhance survival and hematopoietic cell recovery in a mouse model of the Hematopoietic Syndrome of the Acute Radiation Syndrome. Health Physics, 2014. 106(1): p. 7-20.

212. Jones, J.W., et al., Effect of gender on biomarker response in a mouse model of the hematopoietic acute radiation syndrome. Health Physics, 2019. 116(4): p. 484-502.

213. Garrett, J., et al., Characterization and Etiology of Swollen Muzzles in Irradiated Mice. Radiation Research, 2019. 191(1): p. 31-42.

214. Garrett, J., et al., Subcutaneous wounding postirradiation reduces radiation lethality in mice. Radiat Res, 2014. 181(6): p. 578-83.

215. Dynlacht, J.R., et al., Further Characterization of the Mitigation of Radiation Lethality by Protective Wounding. Radiation Research, 2017. 187(6): p. 732-742.

216. Vogel, B., et al., Determination of collagen content within picrosirius red stained paraffin-embedded tissue sections using fluorescence microscopy. MethodsX, 2015. 2: p. 124-34.

217. Patchen, M.L., Amifostine plus granulocyte colony-stimulating factor therapy enhances recovery from supralethal radiation exposures: preclinical experience in animals models. Eur J Cancer, 1995. 31A Suppl 1: p. S17-21.

218. Takada, A., et al., Biphasic pattern of thymus regeneration after whole-body irradiation. J Exp Med, 1969. 129(3): p. 445-57.

219. Huiskamp, R., J.A.G. Davids, and O. Vos, Short- and Long-Term Effects of Whole-Body Irradiation with Fission Neutrons or X Rays on the Thymus in CBA Mice. Radiation Research, 1983. 95(2): p. 370-381.

220. Guo, D., et al., Age and sex differences in microRNAs expression during the process of thymus aging. Acta Biochimica et Biophysica Sinica, 2017. 49(5): p. 409-419.

221. Gui, J., et al., MCL1 increases primitive thymocyte viability in female mice and promotes thymic expansion into adulthood. International Immunology, 2011. 23(10): p. 647-659.

222. Sempowski, G.D., et al., T cell receptor excision circle assessment of thymopoiesis in aging mice. Mol Immunol, 2002. 38(11): p. 841-8.

223. Aspinall, R. and D. Andrew, Gender-related differences in the rates of age associated thymic atrophy. Dev Immunol, 2001. 8(2): p. 95-106.

224. Xiao, J., et al., The non-canonical Wnt pathway negatively regulates dendritic cell differentiation by inhibiting the expansion of Flt3(+) lymphocyte-primed multipotent precursors. Cell Mol Immunol, 2016. 13(5): p. 593-604.

225. Grover, A., et al., Single-cell RNA sequencing reveals molecular and functional platelet bias of aged haematopoietic stem cells. Nat Commun, 2016. 7: p. 11075.

226. Rossi, D.J., et al., Cell intrinsic alterations underlie hematopoietic stem cell aging. Proceedings of the National Academy of Sciences of the United States of America, 2005. 102(26): p. 9194-9199.

227. Rube, C.E., et al., Accumulation of DNA damage in hematopoietic stem and progenitor cells during human aging. PLoS One, 2011. 6(3): p. e17487.

228. Kim, M., H.-B. Moon, and G.J. Spangrude, Major Age-Related Changes Of Mouse Hematopoietic Stem/Progenitor Cells. Annals of the New York Academy of Sciences, 2003. 996(1): p. 195-208.

229. Kamminga, L.M., et al., Impaired hematopoietic stem cell functioning after serial transplantation and during normal aging. Stem Cells, 2005. 23(1): p. 82-92.

230. Behrens, A., et al., Impact of genomic damage and ageing on stem cell function. Nat Cell Biol, 2014. 16(3): p. 201-7.

231. Rossi, D.J., et al., Deficiencies in DNA damage repair limit the function of haematopoietic stem cells with age. Nature, 2007. 447(7145): p. 725-729.

232. Morrison, S.J., et al., The aging of hematopoietic stem cells. Nature Medicine, 1996. 2(9): p. 1011-1016.

233. Nijnik, A., et al., DNA repair is limiting for haematopoietic stem cells during ageing. Nature, 2007. 447(7145): p. 686-90.

234. Snoeck, H.W., Aging of the hematopoietic system. Curr Opin Hematol, 2013. 20(4): p. 355-61.

235. Trowell, O.A., The sensitivity of lymphocytes to ionising radiation. J Pathol Bacteriol, 1952. 64(4): p. 687-704.

236. Kusunoki, Y. and T. Hayashi, Long-lasting alterations of the immune system by ionizing radiation exposure: implications for disease development among atomic bomb survivors. Int J Radiat Biol, 2008. 84(1): p. 1-14.

237. Farese, A.M., et al., Lymphoid and Myeloid Recovery in Rhesus Macaques Following Total Body X-Irradiation. Health Phys, 2015. 109(5): p. 414-26.

238. Li, C.R., S. Santoso, and D.D. Lo, Quantitative analysis of T cell homeostatic proliferation. Cell Immunol, 2007. 250(1-2): p. 40-54.

239. Min, B.H., Spontaneous T Cell Proliferation: A Physiologic Process to Create and Maintain Homeostatic Balance and Diversity of the Immune System. Front. Immunol., 2018. 19: p. 547.

240. Kadish, J.L. and R.S. Basch, Hematopoietic thymocyte precursors. I. Assay and kinetics of the appearance of progeny. J Exp Med, 1976. 143(5): p. 1082-99.

241. Hiesche, K.D. and L. Revesz, Effect of cortisone and X-irradiation on cellular depletion and regeneration in the thymus of mice: experimental discrimination between thymus lymphocyte precursors in the bone marrow and in the thymus. Pathol Res Pract, 1979. 164(2): p. 157-66.

242. Harris, J.E. and C.E. Ford, CELLULAR TRAFFIC OF THE THYMUS: EXPERIMENTS WITH CHROMOSOME MARKERS. EVIDENCE THAT THE THYMUS PLAYS AN INSTRUCTIONAL PART. Nature, 1964. 201: p. 884-5.

243. Dukor, P., et al., Regeneration of thymus grafts. I. Histological and cytological aspects. Transplantation, 1965. 3(5): p. 639-68.

244. Blomgren, H. and L. Revesz, Cellular composition of mouse thymus after x-ray exposure. Exp Cell Res, 1968. 51(1): p. 92-104.

245. Coggle, J.E., The absence of late effects of radiation on the cellularity of the mouse thymus. Int J Radiat Biol Relat Stud Phys Chem Med, 1981. 40(2): p. 229-32.

246. Zhang, P., et al., Increased Expression of Connective Tissue Growth Factor (CTGF) in Multiple Organs After Exposure of Non-Human Primates (NHP) to Lethal Doses of Radiation. Health Phys, 2015. 109(5): p. 374-90.

247. Hernández, L., et al., Aging and radiation: bad companions. Aging Cell, 2015. 14(2): p. 153-161.

248. Pinchuk, L.M. and N.M. Filipov, Differential effects of age on circulating and splenic leukocyte populations in C57BL/6 and BALB/c male mice. Immun Ageing, 2008. 5: p. 1.

249. Youm, Y.H., et al., Prolongevity hormone FGF21 protects against immune senescence by delaying age-related thymic involution. Proc Natl Acad Sci U S A, 2016. 113(4): p. 1026-31.

250. Kajioka, E.H., et al., Immunologic variables in male and female C57BL/6 mice from two sources. Comp Med, 2000. 50(3): p. 288-91.

251. Pido-Lopez, J., N. Imami, and R. Aspinall, Both age and gender affect thymic output: more recent thymic migrants in females than males as they age. Clin Exp Immunol, 2001. 125(3): p. 409-13.

252. Dooley, J. and A. Liston, Molecular control over thymic involution: from cytokines and microRNA to aging and adipose tissue. Eur J Immunol, 2012. 42(5): p. 1073-9.

253. Noguchi, M., et al., Interleukin-2 receptor gamma chain mutation results in X-linked severe combined immunodeficiency in humans. Cell, 1993. 73(1): p. 147-57.

254. Gui, J., et al., Thymus Size and Age-related Thymic Involution: Early Programming, Sexual Dimorphism, Progenitors and Stroma. Aging Dis, 2012. 3(3): p. 280-90.

255. Libert, C., L. Dejager, and I. Pinheiro, The X chromosome in immune functions: when a chromosome makes the difference. Nat Rev Immunol, 2010. 10(8): p. 594-604.

256. Pogribny, I., et al., Fractionated low-dose radiation exposure leads to accumulation of DNA damage and profound alterations in DNA and histone methylation in the murine thymus. Mol Cancer Res, 2005. 3(10): p. 553-61.

257. Prasanna, P.G., et al., Radioprotectors and Radiomitigators for Improving Radiation Therapy: The Small Business Innovation Research (SBIR) Gateway for Accelerating Clinical Translation. Radiat Res, 2015. 184(3): p. 235-48.

258. Singh, V.K., et al., Medical countermeasures for unwanted CBRN exposures: part II radiological and nuclear threats with review of recent countermeasure patents. Expert Opin Ther Pat, 2016. 26(12): p. 1399-1408.

259. Glover, D., et al., Clinical trials of WR-2721 prior to alkylating agent chemotherapy and radiotherapy. Pharmacol Ther, 1988. 39(1-3): p. 3-7.

260. Hoggatt, J. and L.M. Pelus, Eicosanoid regulation of hematopoiesis and hematopoietic stem and progenitor trafficking. Leukemia, 2010. 24(12): p. 1993-2002.

261. Lisowska, B., D. Kosson, and K. Domaracka, Lights and shadows of NSAIDs in bone healing: the role of prostaglandins in bone metabolism. Drug Des Devel Ther, 2018. 12: p. 1753-1758.

262. Yang, T. and Y. Du, Distinct roles of central and peripheral prostaglandin E2 and EP subtypes in blood pressure regulation. Am J Hypertens, 2012. 25(10): p. 1042-9.

263. Martinez-Colon, G.J. and B.B. Moore, Prostaglandin E2 as a Regulator of Immunity to Pathogens. Pharmacol Ther, 2018. 185: p. 135-146.

264. Kawahara, K., et al., Prostaglandin E2-induced inflammation: Relevance of prostaglandin E receptors. Biochim Biophys Acta, 2015. 1851(4): p. 414-21.

265. Hanson, W.R., Radiation protection of murine intestine by WR-2721, 16,16-dimethyl prostaglandin E2, and the combination of both agents. Radiat Res, 1987. 111(2): p. 361-73.

266. Dutta, S. and P. Sengupta, Men and mice: Relating their ages. Life Sci, 2016. 152: p. 244-8.

267. Chua, H.L., et al., Survival efficacy of the PEGylated G-CSFs Maxy-G34 and neulasta in a mouse model of lethal H-ARS, and residual bone marrow damage in treated survivors. Health Phys, 2014. 106(1): p. 21-38.

268. Singh, P., et al., Blockade of prostaglandin E2 signaling through EP1 and EP3 receptors attenuates Flt3L-dependent dendritic cell development from hematopoietic progenitor cells. Blood, 2012. 119(7): p. 1671-82.

269. Singh, P., et al., Survivin Is Required for Mouse and Human Bone Marrow Mesenchymal Stromal Cell Function. Stem Cells, 2018. 36(1): p. 123-129.

270. Singh, V.K. and V.S. Yadav, Role of cytokines and growth factors in radioprotection. Exp Mol Pathol, 2005. 78(2): p. 156-69.

271. Mirantes, C., E. Passegué, and E.M. Pietras, Pro-inflammatory cytokines: emerging players regulating HSC function in normal and diseased hematopoiesis. Exp Cell Res, 2014. 329(2): p. 248-54.

272. Metcalf, D., Hematopoietic cytokines. Blood, 2008. 111(2): p. 485-91.

273. Feher, I. and J. Gidali, Prostaglandin E2 as stimulator of haemopoietic stem cell proliferation. Nature, 1974. 247(5442): p. 550-1.

274. Gidali, J. and I. Feher, The effect of E type prostaglandins on the proliferation of haemopoietic stem cells in vivo. Cell Tissue Kinet, 1977. 10(4): p. 365-73.

275. Pelus, L.M., Modulation of myelopoiesis by prostaglandin E2: Demonstration of a novel mechanism of action in vivo. Immunologic Research, 1989. 8(3): p. 176-184.

276. Porter, R.L., et al., Prostaglandin E2 increases hematopoietic stem cell survival and accelerates hematopoietic recovery after radiation injury. Stem Cells, 2013. 31(2): p. 372-83.

277. Akkinapally, S., et al., Prostaglandin E1 for maintaining ductal patency in neonates with ductal-dependent cardiac lesions. Cochrane Database Syst Rev, 2018. 2: p. Cd011417.

278. Hagedorn, E.J., et al., Getting more for your marrow: boosting hematopoietic stem cell numbers with PGE2. Exp Cell Res, 2014. 329(2): p. 220-6.

279. Yokoyama, U., et al., The prostanoid EP4 receptor and its signaling pathway. Pharmacol Rev, 2013. 65(3): p. 1010-52.

280. O'Callaghan, G. and A. Houston, Prostaglandin E2 and the EP receptors in malignancy: possible therapeutic targets? Br J Pharmacol, 2015. 172(22): p. 5239-50.

281. Ikushima, Y.M., et al., Prostaglandin E(2) regulates murine hematopoietic stem/progenitor cells directly via EP4 receptor and indirectly through mesenchymal progenitor cells. Blood, 2013. 121(11): p. 1995-2007.

282. Smith, J.N. and L.M. Calvi, Regulatory Interactions in the Bone Marrow Microenvironment. IBMS Bonekey, 2011. 8(2): p. 96-111.

283. Sawant, K.V., et al., Chemokine CXCL1 mediated neutrophil recruitment: Role of glycosaminoglycan interactions. Sci Rep, 2016. 6: p. 33123.

284. King, A.G., et al., Identification of unique truncated KC/GRO beta chemokines with potent hematopoietic and anti-infective activities. J Immunol, 2000. 164(7): p. 3774-82.

285. Slordal, L., et al., Radioprotection by murine and human tumor-necrosis factor: dose-dependent effects on hematopoiesis in the mouse. Eur J Haematol, 1989. 43(5): p. 428-34.

286. Pruijt, J.F., et al., Leukemia inhibitory factor induces in vivo expansion of bone marrow progenitor cells that accelerate hematopoietic reconstitution but do not enhance radioprotection in lethally irradiated mice. Stem Cells, 1997. 15(1): p. 50-5.

287. Gomez-Roman, N., RBIO-01. RADIATION RESPONSES OF 2D AND 3D GLIOBLASTOMA CELLS: A NOVEL, 3D-SPECIFIC RADIOPROTECTIVE ROLE OF VEGF/Akt SIGNALING THROUGH FUNCTIONAL ACTIVATION OF NHEJ. Neuro-Oncology, 2016. 18(suppl_6): p. vi172-vi172.

288. Basile, L.A., et al., Multilineage hematopoietic recovery with concomitant antitumor effects using low dose Interleukin-12 in myelosuppressed tumor-bearing mice. J Transl Med, 2008. 6: p. 26.

289. Chen, T., et al., IL-12 facilitates both the recovery of endogenous hematopoiesis and the engraftment of stem cells after ionizing radiation. Exp Hematol, 2007. 35(2): p. 203-13.

290. Legue, F., et al., IL-6 a key cytokine in in vitro and in vivo response of Sertoli cells to external gamma irradiation. Cytokine, 2001. 16(6): p. 232-8.

291. Neta, R., et al., Role of interleukin 6 (IL-6) in protection from lethal irradiation and in endocrine responses to IL-1 and tumor necrosis factor. J Exp Med, 1992. 175(3): p. 689-94.

292. Keller, J.R., J.M. Gooya, and F.W. Ruscetti, Direct synergistic effects of leukemia inhibitory factor on hematopoietic progenitor cell growth: comparison with other hematopoietins that use the gp130 receptor subunit. Blood, 1996. 88(3): p. 863-9.

293. Sonoda, Y., Interleukin-4--a dual regulatory factor in hematopoiesis. Leuk Lymphoma, 1994. 14(3-4): p. 231-40.

294. Fischer, K.D. and D.K. Agrawal, Hematopoietic stem and progenitor cells in inflammation and allergy. Front Immunol, 2013. 4: p. 428.

295. Wang, J., et al., Enhanced mobilization of hematopoietic progenitor cells by mouse MIP-2 and granulocyte colony-stimulating factor in mice. J Leukoc Biol, 1997. 62(4): p. 503-9.

296. Broxmeyer, H.E., et al., Synergistic inhibition in vivo of bone marrow myeloid progenitors by myelosuppressive chemokines and chemokine-accelerated recovery of progenitors after treatment of mice with Ara-C. Exp Hematol, 2006. 34(8): p. 1069-77.

297. Chung, S.W., et al., The comparative effects of cyclosporin A and 16,16 dimethyl prostaglandin E2 on the allogeneic induction of monocyte/macrophage procoagulant activity and the cytokines macrophage procoagulant inducing factor and interleukin-2. Immunology, 1991. 74(4): p. 670-6.

298. Bottero, V., S. Withoff, and I.M. Verma, NF-kappaB and the regulation of hematopoiesis. Cell Death Differ, 2006. 13(5): p. 785-97.

299. Dikov, M.M., et al., Vascular endothelial growth factor effects on nuclear factor-kappaB activation in hematopoietic progenitor cells. Cancer Res, 2001. 61(5): p. 2015-21.

300. Maca, R.D., The effects of prostaglandins on the proliferation of cultured human T lymphocytes. Immunopharmacology, 1983. 6(4): p. 267-77.

301. Sreeramkumar, V., M. Fresno, and N. Cuesta, Prostaglandin E2 and T cells: friends or foes? Immunol Cell Biol, 2012. 90(6): p. 579-86.

302. Mary, D., et al., Regulation of interleukin 2 synthesis by cAMP in human T cells. J Immunol, 1987. 139(4): p. 1179-84.

303. Mohtashami, M., et al., Induction of T-cell development by Delta-like 4-expressing fibroblasts. Int Immunol, 2013. 25(10): p. 601-11.

304. Schmitt, T.M. and J.C. Zuniga-Pflucker, Induction of T cell development from hematopoietic progenitor cells by delta-like-1 in vitro. Immunity, 2002. 17(6): p. 749-56.

305. Zuniga-Pflucker, J.C., T-cell development made simple. Nat Rev Immunol, 2004. 4(1): p. 67-72.

306. Plett, P.A., S.M. Frankovitz, and C.M. Orschell-Traycoff, In vivo trafficking, cell cycle activity, and engraftment potential of phenotypically defined primitive hematopoietic cells after transplantation into irradiated or nonirradiated recipients. Blood, 2002. 100(10): p. 3545-52.

307. Plett, P.A., S.M. Frankovitz, and C.M. Orschell, Distribution of marrow repopulating cells between bone marrow and spleen early after transplantation. Blood, 2003. 102(6): p. 2285-91.

308. Xing, Y. and K.A. Hogquist, Isolation, identification, and purification of murine thymic epithelial cells. J Vis Exp, 2014(90): p. e51780.

309. Gazit, R., et al., Fgd5 identifies hematopoietic stem cells in the murine bone marrow. J Exp Med, 2014. 211(7): p. 1315-31.

310. Thomson, J.F., et al., Life shortening in mice exposed to fission neutrons and gamma rays I. Single and short-term fractionated exposures. Radiat Res, 1981. 86(3): p. 559-72.

311. Upton, A.C., M.L. Randolph, and J.W. Conklin, Late effects of fast neutrons and gamma rays in mice as influenced by the dose rate of irradiation: life shortening. Radiat Res, 1967. 32(3): p. 493-509.

312. Hoggatt, J., et al., Bleeding the laboratory mouse: Not all methods are equal. Exp Hematol, 2016. 44(2): p. 132-137.e1.

313. Sckisel, G.D., et al., Differential phenotypes of memory CD4 and CD8 T cells in the spleen and peripheral tissues following immunostimulatory therapy. J Immunother Cancer, 2017. 5: p. 33.

314. den Braber, I., et al., Maintenance of peripheral naive T cells is sustained by thymus output in mice but not humans. Immunity, 2012. 36(2): p. 288-97.

315. Yanes, R.E., et al., Lymphocyte generation and population homeostasis throughout life. Semin Hematol, 2017. 54(1): p. 33-38.

316. Doulatov, S., et al., Hematopoiesis: a human perspective. Cell Stem Cell, 2012. 10(2): p. 120-36.

317. Hoggatt, J., et al., Prostaglandin E2 enhances long-term repopulation but does not permanently alter inherent stem cell competitiveness. Blood, 2013. 122(17): p. 2997-3000.

318. Robertson, P., et al., CXCR4 and CCR5 mediate homing of primitive bone marrow-derived hematopoietic cells to the postnatal thymus. Exp Hematol, 2006. 34(3): p. 308-19.

319. Rivina, L., M.J. Davoren, and R.H. Schiestl, Mouse models for radiation-induced cancers. Mutagenesis, 2016. 31(5): p. 491-509.

320. Morse, H.C., 3rd, et al., Bethesda proposals for classification of lymphoid neoplasms in mice. Blood, 2002. 100(1): p. 246-58.

321. Utsuyama, M. and K. Hirokawa, Radiation-induced-thymic lymphoma occurs in young, but not in old mice. Exp Mol Pathol, 2003. 74(3): p. 319-25.

322. Ward, J.M., Lymphomas and leukemias in mice. Exp Toxicol Pathol, 2006. 57(5-6): p. 377-81.

323. Breyer, R.M., et al., Prostanoid receptors: subtypes and signaling. Annu Rev Pharmacol Toxicol, 2001. 41: p. 661-90.

324. Anderson, G. and Y. Takahama, Thymic epithelial cells: working class heroes for T cell development and repertoire selection. Trends Immunol, 2012. 33(6): p. 256-63.

325. Nitta, T. and H. Suzuki, Thymic stromal cell subsets for T cell development. Cell Mol Life Sci, 2016. 73(5): p. 1021-37.

326. Majumdar, S. and D. Nandi, Thymic Atrophy: Experimental Studies and Therapeutic Interventions. Scand J Immunol, 2018. 87(1): p. 4-14.

327. Pica, F., et al., Prostaglandin E2 induces apoptosis in resting immature and mature human lymphocytes: a c-Myc-dependent and Bcl-2-independent associated pathway. J Pharmacol Exp Ther, 1996. 277(3): p. 1793-800.

328. Konya, V., et al., E-type prostanoid receptor 4 (EP4) in disease and therapy. Pharmacol Ther, 2013. 138(3): p. 485-502.

329. Rossi, D.J., D. Bryder, and I.L. Weissman, Hematopoietic stem cell aging: mechanism and consequence. Exp Gerontol, 2007. 42(5): p. 385-90.

330. Mastino, A., et al., Correlation between induction of lymphocyte apoptosis and prostaglandin E2 production by macrophages infected with HIV. Cell Immunol, 1993. 152(1): p. 120-30.

331. Chouaib, S., et al., Prostaglandin E2 acts at two distinct pathways of T lymphocyte activation: inhibition of interleukin 2 production and down-regulation of transferrin receptor expression. J Immunol, 1985. 135(2): p. 1172-9.

332. Tsapogas, P., et al., The Cytokine Flt3-Ligand in Normal and Malignant Hematopoiesis. Int J Mol Sci, 2017. 18(6).

333. Sitnicka, E., et al., Critical role of FLT3 ligand in IL-7 receptor independent T lymphopoiesis and regulation of lymphoid-primed multipotent progenitors. Blood, 2007. 110(8): p. 2955-64.

334. Wang, Q., et al., Stage-specific roles for Zmiz1 in Notch-dependent steps of early T-cell development. Blood, 2018. 132(12): p. 1279-1292.

335. Zaldumbide, A., et al., The role of the Ets2 transcription factor in the proliferation, maturation, and survival of mouse thymocytes. J Immunol, 2002. 169(9): p. 4873-81.

336. Ceredig, R. and A.G. Rolink, The key role of IL-7 in lymphopoiesis. Semin Immunol, 2012. 24(3): p. 159-64.

337. Ma, A., R. Koka, and P. Burkett, Diverse functions of IL-2, IL-15, and IL-7 in lymphoid homeostasis. Annu Rev Immunol, 2006. 24: p. 657-79.

338. Kohn, L.A., et al., Human lymphoid development in the absence of common gamma-chain receptor signaling. J Immunol, 2014. 192(11): p. 5050-8.

339. Moroni, M., et al., Accelerated hematopoietic syndrome after radiation doses bridging hematopoietic (H-ARS) and gastrointestinal (GI-ARS) acute radiation syndrome: early hematological changes and systemic inflammatory response syndrome in minipig. Int J Radiat Biol, 2014. 90(5): p. 363-72.

340. Hauer-Jensen, M., Toward development of interleukin-11 as a medical countermeasure for use in radiological/nuclear emergencies. Dig Dis Sci, 2014. 59(7): p. 1349-51.

341. Yang, L., et al., The protective role of interleukin-11 against neutron radiation injury in mouse intestines via MEK/ERK and PI3K/Akt dependent pathways. Dig Dis Sci, 2014. 59(7): p. 1406-14.

342. Demetri, G.D., Targeted approaches for the treatment of thrombocytopenia. Oncologist, 2001. 6 Suppl 5: p. 15-23.

343. Maier, R., V. Ganu, and M. Lotz, Interleukin-11, an inducible cytokine in human articular chondrocytes and synoviocytes, stimulates the production of the tissue inhibitor of metalloproteinases. J Biol Chem, 1993. 268(29): p. 21527-32.

344. Kaye, J.A., The clinical development of recombinant human interleukin 11 (NEUMEGA rhIL-11 growth factor). Stem Cells, 1996. 14 Suppl 1: p. 256-60.

345. Lee, H.T., et al., Interleukin-11 protects against renal ischemia and reperfusion injury. Am J Physiol Renal Physiol, 2012. 303(8): p. F1216-24.

346. Zhao, H., et al., Effects of recombinant human granulocyte colony-stimulating factor on central and peripheral T lymphocyte reconstitution after sublethal irradiation in mice. J Radiat Res, 2013. 54(1): p. 83-91.

347. Moxham, V.F., et al., Homeostatic proliferation of lymphocytes results in augmented memory-like function and accelerated allograft rejection. J Immunol, 2008. 180(6): p. 3910-8.

348. Singh, V.K., V.L. Newman, and T.M. Seed, Colony-stimulating factors for the treatment of the hematopoietic component of the acute radiation syndrome (H-ARS): a review. Cytokine, 2015. 71(1): p. 22-37.

349. MacVittie, T.J., et al., Therapeutic use of recombinant human G-CSF (rhG-CSF) in a canine model of sublethal and lethal whole-body irradiation. Int J Radiat Biol, 1990. 57(4): p. 723-36.

350. Masood, N., et al., Splenic rupture, secondary to G-CSF use for chemotherapy induced neutropenia: a case report and review of literature. Cases J, 2008. 1(1): p. 418.

351. van Raam, B.J., et al., Granulocyte colony-stimulating factor delays neutrophil apoptosis by inhibition of calpains upstream of caspase-3. Blood, 2008. 112(5): p. 2046-54.

352. Klein, J.B., et al., Granulocyte-macrophage colony-stimulating factor delays neutrophil constitutive apoptosis through phosphoinositide 3-kinase and extracellular signal-regulated kinase pathways. J Immunol, 2000. 164(8): p. 4286-91.

353. Kobayashi, S.D., et al., Spontaneous neutrophil apoptosis and regulation of cell survival by granulocyte macrophage-colony stimulating factor. J Leukoc Biol, 2005. 78(6): p. 1408-18.

354. Orazi, A., et al., Interleukin-11 prevents apoptosis and accelerates recovery of small intestinal mucosa in mice treated with combined chemotherapy and radiation. Lab Invest, 1996. 75(1): p. 33-42.

355. Booth, C. and C.S. Potten, Effects of IL-11 on the growth of intestinal epithelial cells in vitro. Cell Prolif, 1995. 28(11): p. 581-94.

356. Li, C., et al., Granulocyte colony-stimulating factor exacerbates hematopoietic stem cell injury after irradiation. Cell Biosci, 2015. 5: p. 65.

357. Botnick, L.E., E.C. Hannon, and S. Hellman, A long lasting proliferative defect in the hematopoietic stem cell compartment following cytotoxic agents. Int J Radiat Oncol Biol Phys, 1979. 5(9): p. 1621-5.

358. Hellman, S. and L.E. Botnick, Stem cell depletion: an explanation of the late effects of cytotoxins. Int J Radiat Oncol Biol Phys, 1977. 2(1-2): p. 181-4.

359. Simonnet, A.J., et al., Phenotypic and functional changes induced in hematopoietic stem/progenitor cells after gamma-ray radiation exposure. Stem Cells, 2009. 27(6): p. 1400-9.

360. Testa, N.G., J.H. Hendry, and G. Molineux, Long-term bone marrow damage in experimental systems and in patients after radiation or chemotherapy. Anticancer Res, 1985. 5(1): p. 101-10.

361. Mauch, P., et al., Hematopoietic stem cell compartment: acute and late effects of radiation therapy and chemotherapy. Int J Radiat Oncol Biol Phys, 1995. 31(5): p. 1319-39.

362. Mauch, P., M. Rosenblatt, and S. Hellman, Permanent loss in stem cell self renewal capacity following stress to the marrow. Blood, 1988. 72(4): p. 1193-6.

363. Wang, J., et al., A differentiation checkpoint limits hematopoietic stem cell self-renewal in response to DNA damage. Cell, 2012. 148(5): p. 1001-14.

364. d'Adda di Fagagna, F., et al., A DNA damage checkpoint response in telomere-initiated senescence. Nature, 2003. 426(6963): p. 194-8.

365. Kadish, J.L. and R.S. Basch, Thymic regeneration after lethal irradiation evidence for an intra-thymic radioresistant T cell precursor. J Immunol, 1975. 114(1 Pt 2): p. 452-8.

366. Tanikawa, S., et al., Effects of recombinant human granulocyte colony-stimulating factor on the hematologic recovery and survival of irradiated mice. Blood, 1990. 76(3): p. 445-9.

367. Goldman, S.J., Preclinical biology of interleukin 11: a multifunctional hematopoietic cytokine with potent thrombopoietic activity. Stem Cells, 1995. 13(5): p. 462-71.

368. Franzke, A., et al., G-CSF as immune regulator in T cells expressing the G-CSF receptor: implications for transplantation and autoimmune diseases. Blood, 2003. 102(2): p. 734-9.

369. Morikawa, K., et al., Characterization of granulocyte colony-stimulating factor receptor expressed on human lymphocytes. Br J Haematol, 2002. 118(1): p. 296-304.

370. Prevost, J.M., et al., Granulocyte-macrophage colony-stimulating factor (GM-CSF) and inflammatory stimuli up-regulate secretion of the soluble GM-CSF receptor in human monocytes: evidence for ectodomain shedding of the cell surface GM-CSF receptor alpha subunit. J Immunol, 2002. 169(10): p. 5679-88.

371. Akdis, M., et al., Interleukins (from IL-1 to IL-38), interferons, transforming growth factor beta, and TNF-alpha: Receptors, functions, and roles in diseases. J Allergy Clin Immunol, 2016. 138(4): p. 984-1010.

372. Bernstein, K.E., et al., A modern understanding of the traditional and nontraditional biological functions of angiotensin-converting enzyme. Pharmacol Rev, 2013. 65(1): p. 1-46.

373. van Brummelen, P., et al., Captopril-associated agranulocytosis. Lancet, 1980. 1(8160): p. 150.

374. Strair, R.K., et al., Reversible captopril-associated bone marrow aplasia. Can Med Assoc J, 1985. 132(4): p. 320-2.

375. Safar, M.E., Fatal bone-marrow suppression associated with captopril. Br Med J (Clin Res Ed), 1981. 283(6294): p. 791-2.

376. Kozak, K.R., et al., Metabolism of prostaglandin glycerol esters and prostaglandin ethanolamides in vitro and in vivo. J Biol Chem, 2001. 276(40): p. 36993-8.

377. Stone, C.D., et al., Prostaglandin E2 inhibits in vitro and in vivo lymphocyte responses in allogeneic transplantation. Ann Thorac Surg, 1990. 49(6): p. 927-30; discussion 931.

378. Hospers, G.A., E.A. Eisenhauer, and E.G. de Vries, The sulfhydryl containing compounds WR-2721 and glutathione as radio- and chemoprotective agents. A review, indications for use and prospects. Br J Cancer, 1999. 80(5-6): p. 629-38.

379. Hanson, W.R. and E.J. Ainsworth, 16,16-Dimethyl prostaglandin E2 induces radioprotection in murine intestinal and hematopoietic stem cells. Radiat Res, 1985. 103(2): p. 196-203.

380. Miller, T.A., et al., Nonprotein sulfhydryl compounds in canine gastric mucosa: effects of PGE2 and ethanol. Am J Physiol, 1985. 249(1 Pt 1): p. G137-44.

381. Szabo, S., J.S. Trier, and P.W. Frankel, Sulfhydryl compounds may mediate gastric cytoprotection. Science, 1981. 214(4517): p. 200-2.

382. Williams, C.S., M. Mann, and R.N. DuBois, The role of cyclooxygenases in inflammation, cancer, and development. Oncogene, 1999. 18(55): p. 7908-16.

383. Ke, J., et al., Prostaglandin E2 (PGE2) promotes proliferation and invasion by enhancing SUMO-1 activity via EP4 receptor in endometrial cancer. Tumour Biol, 2016. 37(9): p. 12203-12211.

384. O'Flaherty, J.T., et al., Fatty acid metabolites in rapidly proliferating breast cancer. PLoS One, 2013. 8(5): p. e63076.

385. Yan, M., et al., 15-Hydroxyprostaglandin dehydrogenase, a COX-2 oncogene antagonist, is a TGF-beta-induced suppressor of human gastrointestinal cancers. Proc Natl Acad Sci U S A, 2004. 101(50): p. 17468-73.

386. Xin, X., et al., Targeting COX-2 and EP4 to control tumor growth, angiogenesis, lymphangiogenesis and metastasis to the lungs and lymph nodes in a breast cancer model. Lab Invest, 2012. 92(8): p. 1115-28.

387. Steinbach, G., et al., The effect of celecoxib, a cyclooxygenase-2 inhibitor, in familial adenomatous polyposis. N Engl J Med, 2000. 342(26): p. 1946-52.

388. Wu, Q., et al., Long-term aspirin use for cancer primary prevention: A protocol for updated systematic review and subgroup meta-analysis of randomized clinical trials. Medicine (Baltimore), 2019. 98(39): p. e17382.

389. Wilson, J.W. and C.S. Potten, The effect of exogenous prostaglandin administration on tumor size and yield in Min/+ mice. Cancer Res, 2000. 60(16): p. 4645-53.

390. Nakanishi, M. and D.W. Rosenberg, Multifaceted roles of PGE2 in inflammation and cancer. Semin Immunopathol, 2013. 35(2): p. 123-37.

CURRICULUM VITAE

**Tong Wu**

## Education

| | | |
|---|---|---|
| 2005 | **B.S.** Clinical Medicine<br>Tianjin Medical University | Tianjin, China |
| 2008 | **M.S.** Hematology/Oncology<br>Peking Union Medical College | Tianjin, China |
| 2020 | **Ph.D.** Anatomy, Cell Biology & Physiology<br>Indiana University | Indianapolis, IN |

## Professional Experience

2008-2010 **Residency/Staff**; Jiangxi Provincial Cancer Institute & Cancer Hospital

- Performed primary patient care under the supervision of attending physicians, attended clinical rounds and provided patient education.

2010-2013 **Attending Physician**; Jiangxi Provincial Cancer Institute & Cancer Hospital

- Appropriately diagnosed and treated hematologic diseases and other solid tumors.
- Involved in clinical trials in new therapeutics to complications of chemotherapy/radiotherapy with patients suffered from hematological or solid malignancies.

| | |
|---|---|
| 2014-present | **Research Assistant**; Indiana University School of Medicine<br>• Participated in projects involving in developing and evaluating new medical countermeasures against lethal radiation in a well-defined mouse model. |

## Honors and Certificates

| | |
|---|---|
| 2001-2004 | Tianjin Medical University Scholarship; Tianjin Medical University |
| 2014 | IBMG Program Fellowship; Indiana University School of Medicine |
| 2015 | Achievement Multiparameter Flow; Flocyte Associates Training Program |
| 2015 | Scholars In Training; Radiation Research Society |
| 2017 | Abstract Achievement Award; American Society of Hematology |
| 2017 | Graduate Student Travel Grants; Indiana University School of Medicine |
| 2017-2019 | Excellence in Reviewing; Spandidos Publications |
| 2019 | Jumpstart to Teaching; IUPUI |

## Publications

[1] Wu T, Plett PA, Chua HL, Jacobsen M, Sandusky GE, MacVittie TJ, Orschell CM. Immune reconstitution and thymic involution in the acute and delayed hematopoietic radiation syndromes. Health Phys. Submitted.

[2] Wu T, Plett PA, Chua HL, Pelus LM, and Orschell CM. Prostaglandin E2 promotes recovery of thymus in survivors of the hematopoietic acute radiation syndrome (H-ARS). Blood.2017; 130:1008 (poster).

[3] Koh B, Hufford MM, Pham D, Olson MR, Wu T, Jabeen R, Sun X, Kaplan MH. The ETS family transcription factors Etv5 and PU.1 function in parallel to promote Th9 cell development. J Immunol. 2016;197:2465-72. PMID: 27496971.

[4] Plett PA, Sampson CH, Chua HL, Jackson W, Vemula S, Sellamuthu R, Fisher A, Feng H, Wu T, MacVittie TJ, Orschell CM. The H-ARS Dose Response Relationship (DRR): validation and variables. Health Phys. 2015;109:391-8. PMID: 26425900.

[5] Wu T, Vemula S, Plett PA, Chua HL, Sampson CH, Fisher A, Feng H, Sellamuthu R, Cox GN, and Orschell CM. Pegylated hematopoietic growth factors and effects on long-term immune reconstitution in a murine model of residual bone marrow damage (RBMD). 61st Annual Meeting of the Radiation Research Society, September 19-22, 2015 (poster).

[6] Shuang YR, Li YP, Wu T, Peng ZQ, Yang GM, Huang Y, Yi K, Chen JX, Wu YH. (2013). Clinical manual of lymphoma. Nanchang: Jiangxi Science and Technology Publishing House.

[7] Wu T, Li ZJ, Qiu LG. Complications of chronic lymphocytic leukemia: analysis of 203 cases in China. Leuk Res. 2010; 34: e64-5. PMID: 19699521.

[8] Wu T, Li ZJ, Wang YF, Qiu LG. Applicability of different clinical staging systems in chronic lymphocytic leukemia for Chinese patients. Journal of Leukemia & Lymphoma. 2010; 3:136-9.

[9] Wu T, Li ZJ, Qiu LG. Advancement about hematological autoimmune complications in chronic lymphocytic leukemia (Review). Journal of Leukemia & Lymphoma. 2010; 19: 246-9.

[10] Wu T, Shuang YR. Recent advances in prognosis and treatment of peripheral T-Cell lymphoma, not otherwise specified (Review). The Practical Journal of Cancer. 2010; 25: 100-3.

[11] Wu T, Li ZJ, Wang YF, Zhao YZ, Qi JY, Qian LS, Qiu LG. Prognostic factor analysis in 203 patients with chronic lymphocytic leukemia. Zhonghua Xue Ye Xue Za Zhi. 2009; 30:435-9. PMID: 19954591.

[12] Wu T, Li ZJ, Wang YF, Zhao YZ, Qian LS, Qiu LG. Autoimmune cytopenia as a complication in patients with chronic lymphocytic leukemia: report of 7 cases and literature review. Journal of Clinical Hematology. 2009; 5: 491-2.

[13] Li ZJ, Wu T, Qiu LG, Li YN. Clinical analysis and diagnosis of mantle cell lymphoma presented as lympho-proliferative disease. Journal of Clinical Hematology. 2009; 5: 225-8.

[14] Wu T, Li ZJ, Qiu LG. Research progress in chronic lymphocytic leukemia and its secondary cancers (Review). Journal of Clinical Hematology. 2009; 22:629-31.

[15] Wu T, Wang YF, Qiu LG. Pathophysiological research advances in immunologic lung injury after allogeneic stem cell transplantation (Review). International Journal of Blood Transfusion and Hematology. 2008; 31: 343-6.

[16] Wu T, Wang YF, Qiu LG. Research progress in diagnosis and treatment of immunologic lung injury after allogeneic stem cell transplantation (Review). Chinese Journal of Organ Transplantation. 2008; 5:317-9.

[17] Li ZJ, Qiu LG, Wu T, Wang YF, Zou DH, Zhao YZ, Qi JY, Yang RC, Qian LS. The clinical and laboratory features of 263 cases of chronic lymphocytic leukemia. Zhonghua Xue Ye Xue Za Zhi. 2008; 29:300-3. PMID: 18844065.

[18] Wang YF, Deng SH, Wu T, Xu Y, Zou DH, Wang Y, Zhao YZ, Qiu LG. Outcome of bortezomib plus chemotherapy with or without stem cell transplantation for treatment of multiple myeloma. Zhonghua Xue Ye Xue Za Zhi. 2008; 29:397-400. PMID: 19031743.

[19] Hao M, Li SD, Wu T, Meng HX, Li CH, Xu Y, Qiu LG. Influence of mesenchymal stem cells on UCB CD34+ cell expansion and characteristics. Zhongguo Shi Yan Xue Ye Xue Za Zhi. 2008; 16:1403-7. PMID: 19099653.